DOCTOR OF PHILOSOPHY

Behaviour of epoxy filled flat-face joints in concrete for wave energy converters

Khosravi, Noushin

Award date:
2018

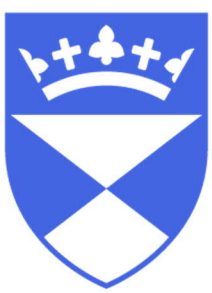

University of Dundee

Behaviour of epoxy filled flat-face joints in concrete for wave energy converters

Noushin Khosravi

A thesis presented in application for the Degree of Doctor of Philosophy
Division of Civil Engineering
University of Dundee
2018

DECLARATION

I hereby declare that I am the author of this thesis, that the work of which it is a record has been composed by me, and it has not been previously presented for a higher degree.

Noushin Khosravi

CERTIFICATE

This is to certify that **Noushin Khosravi** has carried out her research under my supervision and that she has fulfilled the conditions of Ordinance 14 of the University of Dundee, so that she is qualified to submit this thesis in application for the Degree of Doctor of Philosophy.

Prof. M R Jones CEng, MICE

Director of Concrete Technology Unit

University of Dundee

PUBLICATIONS

Newlands, M., Khosravi, N. D., Jones, M. R. Chernin, L., *Mechanical Performance of Statically Loaded Flat Face Epoxy Bonded Concrete Joints, RILEM Material and Structures, (2018),51:49.*

Newlands, M. D., Jones, M. R., Khosravi, N., *Concrete in the marine environment*, CONCRETE Engineering International, Vol. 48, Issue 10, pp. 54–55.

Khosravi, N., Barker, L., O'Donoghue, V., Benzie, J., Newlands, M. D. and Jones, M. R. *Use of Concrete as the Primary Construction Material for the Pelamis Wave Energy Converter*, 1st International conference on Renewable Energies Offshore, 24-26 November 2014, Lisbon, Portugal.

ACKNOWLEDGEMENT

I would like to express my sincere gratitude to my supervisors Professor Rod Jones and Dr Moray Newlands for guiding and supporting me through every step of the way. Their technical advice, vast knowledge, and endless encouragement contributed to successful completion of this thesis.

Many thanks must be given to Mr Jon Benzie for giving me the opportunity to work with Pelamis wave power Ltd. His technical insight provided the foundation for conducting this research.

Special thanks are extended to Dr Leon Chernin, Dr Laszlo Csetenyi, Mr Alan Tough, Dr Judith Halliday and Mrs Lorna Newlands for their support through various stages of the research and checking my written work. Also, I would like to thank CTU technician Mr Christopher Walker for his constant help through the experimental and the laboratory testing.

All staff at BIHE must also be acknowledged, especially Dr Peyman Misaghi, for their efforts to educate Bahá'í students in Iran. Higher education was not possible for me without their faithful services and sacrifices.

I must thank my friends and colleagues within the university and elsewhere, especially Dr Kezban Ozlutas for her true friendship and emotional support. Special thanks must go to Tommaso Bizzotto for his constant care, hours of technical discussion and patience.

Finally, I would like to thank my family for their infinite love, encouragement, and support through the tough times. It is to my parents that this thesis is dedicated.

ABSTRACT

The need and demand for renewable energy is widely understood but there has been equally vociferous opposition to the capital and operational costs of these technologies. While wind energy has developed extensively in the offshore environment over the past decade, problems with intermittent generation means that more reliable technologies are necessary. Of these wave power is particularly attractive as it can be reliably predicted. Although wave energy convertors (WEC) have existed for decades none has achieved significant commercial adoption. Wave energy is diffuse, and this means WECs must be both large and used in arrays. Existing types have generally been constructed in steel and this has proven too expensive.

The need for cost reduction and rapid construction of WECs has stimulated interest in structural concrete. However, while marine concrete is well established, WEC will require joints and there is limited data regarding the performance and behaviour of epoxy bond lines in concrete structural elements exposed to the marine environment. In particular, there is a need to understand the macro and micro mechanical behavior of jointed systems under static and cyclic loading in seawater salt solution and under cycles of wetting and drying.

Therefore, this research was aimed at undertaking an extensive experimental programme to determine how concrete elements joined by epoxy bond lines function. The work required innovative testing rigs to be designed and constructed and novel monitoring techniques to be developed. The experimental programme was divided into three main phases.

Phase I addressed the macro scale performance of epoxy bonded concrete under shear/compression, flexure, and torsion. The failure mode and the joint strength were found to be sensitive to the experimental setup, the thickness of the joint, surface preparation, the mechanical properties of the epoxy and concrete, and the exposure to seawater. Digital Image Correlation (DIC) analysis showed that the presence of joints did not interrupt the flow of strain in specimens. Regarding epoxy bonded concrete to steel, the effects of anti-corrosion paint and applying the fresh epoxy concrete directly on the steel plates were assessed. The results indicate failure mode change and strength reduction by normal anti-corrosion paint and double shear strength by direct fresh epoxy concrete application. However, fresh epoxy concrete joint degrades faster and makes an unfortunate better path for water and chloride penetration.

Phase II focused on the durability of epoxy bonded concrete in seawater. A prototype was made in accordance with one of the famous WECs and evaluated after two years of exposure in the marine environment. This assessment highlighted the deficiency of onsite standard monitoring methods to pick up the defects within the joints. The performance of this assembly was also dependent on the presence of the post tensioning. Furthermore, the water penetration and ion diffusion testing of laboratory samples showed that full immersion leads to higher water penetration while cycles of wetting and drying lead to higher chloride diffusion in the bond line and direct application of fresh epoxy concrete on a hard concrete can have negative durability consequences.

Phase III comprised a number of post tensioned epoxy bonded concrete samples with varying loading conditions in under cyclic wetting and drying exposure with artificial seawater solution. The focus has been on three different stress distribution zones (cracked concrete, joints, and un-cracked concrete) under no loading, sustained loading, and cyclic loading. No load and sustained load conditions showed very similar behaviour, but the damage evolved considerably in cyclically loaded samples. Reduced stiffness of the beams was observed in all cases. There was also a shift of crack propagation from the middle of the epoxy layer to the bond line under cyclic loading. Chloride diffusion and water penetration, which were originally one of the main concerns of the bonded system, did not progress at the interface of concrete and epoxy, and the diffusion rate was not affected by the state of loading.

Overall, the results demonstrated the interconnectivity and complexity of numerous variables involved in assuring the performance of epoxy bonded concrete in the marine environment. Although the initial mechanical strength of the system may look acceptable, the problem of initial defects, residual stresses, substrate sliding, and also the hydrolysis or plasticization in presence of water should be addressed. It is also very important to consider fatigue and extreme loading conditions together with the environmental effects in designing the bonded systems. Finally, issues are identified that require further investigation to ensure acceptable performance of epoxy bonded concrete during its service life in the marine environment especially in the absence of post tensioning.

Table of Contents

Declaration i

Certificate ii

Publications iii

Acknowledgement iv

Abstract v

List of figures xiii

List of tables xix

List of equations xxi

1. Introduction 1

1.1. Research background 2

1.2. Aims and objectives 3

1.3. Scope 4

1.4. Outline of the thesis 5

2. Literature review 7

2.1. Introduction 7

2.2. History of floating concrete structures 7

2.2.1. Advantages of concrete over steel for offshore structures 9

2.2.2. Aspects of investigation for a floating marine structure 9

2.3. Bonded post-tensioned concrete as the main construction method of WECs 13

2.4. Definition of Structural adhesive 15

2.5. Global deformation and strength of the joints 16

2.5.1. Role of shear keys and comparison between dry and epoxy joints 16

2.5.2. Factors influencing the joint strength 20

2.5.3. Design models for bonded concrete 24

2.5.4. Performance of epoxy bonded concrete to plate 28

2.6. Meso/micro mechanical behaviour of the joints 33

2.6.1. Durability of epoxy bonded concrete to concrete 33

2.6.2. Durability of epoxy bonded concrete to plate 35

2.6.3. Durability of epoxy bonded plate to plate 39
2.7. Performance of concrete under cyclic loading 40
2.7.1. S-N curves 42
2.7.2. Fatigue damage accumulation 43
2.7.3. Fatigue design 44
2.7.4. Summary of factors influencing cyclic loading testing of concrete 45
2.8. Performance of the joints under cyclic loading 47
2.8.1. Plate bonded joints under cyclic loading in the aerospace industry 47
2.8.2. Bonded joints under cyclic loading for civil engineering applications 48
2.8.3. Meso/micro mechanical behaviour of the joints under cyclic loading 51
2.8.4. Effect of loading type and crack width on chloride induced corrosion 51
2.9. Conclusions 53
3. Experimental program, materials and test methods 55
3.1. Introduction 55
3.2. Phase I: Static macro scale mechanical performance of epoxy bonded concrete 56
3.2.1. Phase I: Part 1: Mechanical testing of epoxy bonded concrete to concrete 56
3.2.1. Phase I: Part 2: Shear testing of epoxy bonded concrete to steel 58
3.3. Phase II: Static meso/micro scale behaviour of epoxy bonded concrete 60
3.3.1. Phase II: Part 1: Prototype development and testing 60
3.3.2. Phase II: Part 2: Durability testing of bonded concrete to concrete 61
3.4. Phase III: Cyclic loading meso/micro scale behaviour of epoxy bonded concrete 63
3.5. Material properties, concrete design and specimen preparation 64
3.5.1. Cement 64
3.5.2. Aggregate 64
3.5.3. Water 64
3.5.4. Admixtures 64
3.5.5. Artificial seawater salt 65
3.5.6. Epoxy adhesive properties 65
3.5.7. Anti-corrosion paint 65

3.5.8. Concrete mix 67
3.5.9. Mixing, curing and preparation 68
3.6. Phase I test methods: Static macro scale mechanical performance of epoxy bonded concrete 69
3.6.1. Strain monitoring of jointed specimens using Digital Image Correlation (DIC).....69
3.6.2. Jointed sections shear capacity test methods 70
3.6.3. Shear testing of the jointed sections after cyclic wetting and drying.....72
3.6.4. Shear testing of the jointed sections with induced defect.....73
3.6.5. Jointed section tensile capacity test methods.....75
3.6.6. Jointed sections torsion test method.....77
3.6.7. Shear capacity of bonded concrete to steel: Push out test method.....79
3.6.8. Shear capacity of bonded concrete to steel: Double lap shear test method 81
3.7. Phase II test methods: Static meso/micro scale behaviour of epoxy bonded concrete 84
3.7.1. Scaled (1:11) prototype development following the Pelamis WEC concept.....84
3.7.2. Schmidt rebound hammer test 87
3.7.3. Chloride analysis: $AgNO_3$ spray (colorimetric method) 88
3.7.4. Computed Tomography (CT) scanning.....88
3.7.5. Water penetration test method 89
3.7.6. Initial Surface Absorption Test (ISAT) method 89
3.7.2. CEN TS 12390-11 test method.....90
3.7.3. Chloride migration test method 90
3.7.4. NT Build 492 test method 91
3.7.5. Multi Regime (MR) test for jointed samples 93
3.7.6. Scanning Electron Microscope (SEM).....94
3.7.7. Tensile testing of bulk epoxy.....94
3.8. Phase III test methods: Cyclic loading meso/micro scale behaviour of epoxy bonded concrete 96
3.8.1. Samples size and configuration 98
3.8.2. Stress analysis.....100
3.8.3. Post tensioning method 103

3.8.4. Preloading and cracking 104
3.8.5. No load and sustained load application 105
3.8.6. Actuator setting and cyclic loading pattern 105
3.8.7. Installation 108
3.8.8. Monitoring methods 110
3.9. Summary of All test methods 111
4. Mechanical strength and deformation of epoxy joints 113
4.1. Introduction 113
4.2. Modes of failure 113
4.3. Shear capacity of jointed concrete sections 114
4.3.2. Failure modes in shear tests 114
4.3.3. Calculated shear strength of the jointed sections 116
4.3.4. Effect of cyclic wetting and drying on shear capacity of the joints 117
4.3.5. Surface shear strain of the epoxy bonded sections 117
4.3.6. Effect of induced defect on shear capacity of the joints 118
4.4. Tensile capacity of jointed concrete sections 119
4.4.2. Tensile strength of the jointed sections 120
4.4.3. Surface tensile strain of the epoxy bonded sections 122
4.5. Torsional capacity of jointed sections 123
4.5.2. Torsional strength 124
4.5.3. Surface shear strain of the epoxy bonded sections under torsion 126
4.5.4. Failure of circular sections in torsion 128
4.6. Shear capacity of bonded concrete to steel: Effect of Anti-corrosion paint 129
4.7. Shear capacity of bonded concrete to steel: Effect of fresh concrete bond 131
4.8. Conclusions 134
5. Prototype development and durability behaviour of joints 137
5.1. Introduction 137
5.2. Prototype floatation and assessment 137
5.2.1. Base line assessment and commissioning of the prototype in the tank 138

5.2.2. Assessment of the prototype after 12 months floating in seawater salt solution tank 139

5.2.3. Final evaluation after of the prototype after floating in the west coast of Scotland139

5.2.4. UPV survey 142

5.2.5. Rebound hammer survey 145

5.2.6. Coring and destructive testing 146

5.2.7. CT-scan analysis of the joints after 24 months exposure 147

5.2.8. Chloride analysis of the cored samples using $AgNO_3$ spray 148

5.2.9. Chloride analysis of the cored samples using X-Ray Fluorescence (XRF) 149

5.2.10. Chloride analysis of the cored samples using acid soluble titration and chloride profiling 151

5.3. Durability performance of epoxy bonded concrete to concrete 152

5.3.1. Water penetration depth in epoxy bonded concrete 152

5.3.2. Initial surface absorption of epoxy bonded concrete 154

5.3.3. Natural chloride diffusion in epoxy bonded concrete 154

5.3.4. Accelerated chloride diffusion in epoxy bonded concrete 157

5.4. Bulk epoxy analysis 158

5.4.1. SEM and EDX of the bulk epoxy 158

5.4.2. Effect of moisture on tensile capacity of the bulk epoxy 159

5.5. Conclusions 160

6. Chloride ingress in bonded concrete under combined environmental actions and mechanical loads 162

6.1. Introduction 162

6.2. Pre-cracking and fracture energy of the composite 163

6.3. No load condition: Deformation and meso/micro structural changes 166

6.4. Sustained load condition: Deformation and meso/micro structural changes 168

6.5. Cyclic load condition: Deformation and meso/micro structural changes 170

6.6. Growth of the major crack under various loading conditions 174

6.7. Void analysis of three stress zones 174

6.8. Chloride ingress under various loading conditions 180

6.9. Chloride induced corrosion under various loading conditions 183
6.10. UPV measurements under various loading conditions 184
6.11. Zone 1:Cracked side: Key observations and possible theoretical explanations 185
6.12. Zone 2: Epoxy layer: Key observations and possible theoretical explanations 187
6.12.1. Low workability and initial defects 188
6.12.2. Insufficient mixing and initial defects 188
6.12.3. Constraint shrinkage and initial defects 188
6.12.4. Thermosetting resins and residual stresses 188
6.12.5. Applied post tensioning and Poisson ratio effect 189
6.12.6. Fracture behaviour of epoxy 189
6.12.7. Coupled effect of moisture and loading 192
6.13. Zone 3: Body of concrete: Key observations and possible theoretical explanations .. 194
6.14. Conclusions 195
7. Over all Conclusions, comparison of the results with the available data, and recommendations 196
7.1. Introduction 196
7.2. Summary of over all conclusions based on the tested variables in each Phase 196
7.3. Origins of uncertainty in the results 201
7.3.1. Workmanship faults 201
7.3.2. Low workability of the epoxies 201
7.3.3. Presence of the residual stresses 201
7.3.4. Load eccentricities, stress concentration at the edges, and dependency on the shape and size of samples 201
7.4. Suggestions for improving the test methods 202
7.5. Comparison of the results to the available guidance and data 203
7.5.1. Estimating the ultimate strength of epoxy bonded concrete to concrete 203
7.5.2. Estimating ultimate shear capacity of epoxy bonded concrete to steel 205
7.5.3. Effect of humidity on the ultimate strength of epoxy bonded concrete 206
7.5.4. Static water penetration and chloride ingress through the joints 206
7.5.5. Performance of epoxy bonded concrete under cyclic loading 208

7.5.6. Mechanical loading and chloride ingress in epoxy bonded concrete 209
7.6. Main areas of concern and recommendations for further research 209
7.6.1. Presence of defects in epoxy layer 210
7.6.2. Performance of epoxy bonded concrete in humid environment 210
7.6.3. Importance of post tensioning in the reliable performance of epoxy bonded concrete 210
7.6.4. Waves and significant water penetration through the joint 211
7.6.5. Extensive crack propagation in the epoxy layer under cyclic loading 211
7.6.6. Cracking adjacent to the joint and chloride induced corrosion in the cracked surface under cyclic loading 211
8. References 212
Appendix A 222
Appendix B 224

LIST OF FIGURES

Figure 1.1. Schematic presentation of epoxy filled flat-face joint and the critical unreinforced area 1
Figure 1.2. Pelamis Wave Energy Converter (WEC) 2
Figure 2.1. One of The world's first pre-stressed concrete barges launched in 1964 (Pérez Fernández and Lamas Pardo, 2013). 8
Figure 2.2. The curved bottom of the vessel for LPG by match cast segmental construction (Gerwick, 1999). 12
Figure 2.3. Range of behavior of fully pre-stressed concrete (FPC) to partially pre-stressed concrete (PPC), with various ratios of pre-stressing (φ) and normal reinforced concrete(RC) for elements with the same ultimate limit capacity (Karayannis and Chalioris, 2013). 14
Figure 2.4. Typical structural joints in bridge construction (Rombach, 2002) 14
Figure 2.5. Basic structure of epoxy resin (Boyle, 2001), R refers to any group of molecule with attached carbon atom 16
Figure 2.6. Comparison between joints with multiple key, single key and no key (Koseki and Breen, 1983) 17
Figure 2.7. Shear test arrangement and the crack pattern at ultimate failure load for flat-face epoxy joint (Koseki and Breen, 1983) 18
Figure 2.8. Experimental set up for post-tensioned shear key joint (Rombach, 2002) 19
Figure 2.9. Experimental and numerical results showing more ductile behavior of dry joint versus brittle but stronger performance of epoxy joint (Rombach, 2002) 19
Figure 2.10. Parameters of the roughness profile (CEB-FIP, 2012) 21
Figure 2.11. Different adhesive thickness versus average and interface stress (bonded plate to plate) (Gleich, 2002) 23
Figure 2.12. Bond strength by different test methods (a) low surface roughness (b) high surface roughness (Momayez et al., 2005). 24
Figure 2.13. Comparison between the models for predicting shear capacity of jointed sections (Rombach, 2002). 26
Figure 2.14. Shear resisting area in new proposed model by Rombach (2002) 27
Figure 2.15. Typical testing set up for FRP plate bonded to concrete and important parameters : bond length (L_{frp}) , height of free concrete edge (h_c), ,loading offset (δ) (Yao et al., 2005) 29
Figure 2.16. Typical fracture plane for bonded plate to concrete (Lu et al., 2005). 29
Figure 2.17. Typical failure modes of bonded plate to concrete (CEB-FIP, 2012) 29
Figure 2.18. Bond strength reduction after one month of immersion in water (Frigione et al., 2006) 34
Figure 2.19. Four point bending test set up for measuring interface fracture toughness (Lau and Büyüköztürk, 2010) 34
Figure 2.20. (a) Failure mode in dry condition, (b) interface de-bonding after 4 weeks of exposure (Lau and Büyüköztürk, 2010) 35
Figure 2.21. Residual fracture toughness of bonded FRP to concrete after wetting and drying cycles (Tuakta and Büyüköztürk, 2011b) 36
Figure 2.22. Bond strength reduction after 2 years immersion in water (Benzarti et al., 2011) 36

Figure 2.23. Initial and final peel stress after 14 years of exposure in humid environment (Nishizaki and Kato, 2011)..... 37
Figure 2.24. Mechanism of weakening of epoxy bond concrete in humid environment (Büyüköztürk et al., 2011). 38
Figure 2.25. Concrete deterioration under fatigue loading (ω: dimensionless index representing the number of acoustic events) ((Sakata and Ohtsu, 1997) 41
Figure 2.26. Changes of longitudinal modulus and residual strains during fatigue loading (Torrenti et al., 2010) 41
Figure 2.27. Fatigue strength of concrete (ACI Committee 215R-74, 1997)..... 43
Figure 2.28. Crack growth during torsional fatigue loading (Subramaniam and Shah, 2003)..... 46
Figure 2.29. Fatigue test set up considering possibility of cracking of the interface (Randl, 2013)..... 48
Figure 2.30. Fatigue test results for cracked interface, reinforcement passing through the joint (Randl, 2013), HPW: high pressure water jet for surface roughening..... 49
Figure 2.31. Failure of concrete adjacent to the epoxy joint under seismic loading, without any crossing reinforcement (Megally et al., 2002)..... 50
Figure 3.1. The main Phases of the research project 55
Figure 3.2. Main aspects of the research program in Phase I: Part 1: Mechanical testing of epoxy bonded concrete to concrete 56
Figure 3.3. Main variables in Phase I: Part 2: Shear testing of epoxy bonded concrete to steel..... 58
Figure 3.4. Main aspect of research in Phase II: Part 1: Scaled (1:11) WEC prototype development and testing..... 60
Figure 3.5. Main variables in Phase II: Part 2: Durability testing of bonded concrete to concrete..... 61
Figure 3.6. The important parameters of Phase III: Cyclic loading meso/micro scale behaviour of epoxy bonded concrete..... 63
Figure 3.7. Internal and external mould for casting the concrete segments by pre-cast manufacturer..... 68
Figure 3.8. Digital Image Correlation (DIC) set up for strain monitoring 69
Figure 3.9. Slant shear test set up..... 71
Figure 3.10. Bi-surface shear test a) set up 1 and b) set up 2. (Shear strain is monitored in this test, and the flexural stress is negligible)..... 72
Figure 3.11. Schematic presentation of the tank for producing cyclic wetting and drying..... 73
Figure 3.12. Location of defects in jointed specimens..... 75
Figure 3.13. Location of UPV tests for a) horizontal tests b) vertical tests (along joint testing) 75
Figure 3.14. Modified split cylinder test set up 76
Figure 3.15. Modified flexural test setup 76
Figure 3.16. Dimensions of square specimen for torsion test..... 77
Figure 3.17. Torsion test: mould preparation for rectangular sections..... 77
Figure 3.18. Torsion test: preparation of circular sections 78
Figure 3.19. Torsion test setup 79
Figure 3.20. Push out test sample size 80
Figure 3.21. Push out test set up..... 81

Figure 3.22. Double lap shear test: mould details 82
Figure 3.23. Fresh concrete casting with epoxy for double lap shear test 83
Figure 3.24. Double lap shear test set up 83
Figure 3.25. Schematic presentation of scaled prototype in accordance with Pelamis WEC 84
Figure 3.26. Dundee prototype assembling procedure 87
Figure 3.27. ISAT test equipment (Mehta and Monteiro, 2006) 90
Figure 3.28. Direction of joint in migration test 91
Figure 3.29. NT build 492 set up (NT BUILD 492, 1999) 92
Figure 3.30. Multi Regime (MR) equipment (Castellote et al., 2001) 93
Figure 3.31. Measuring conductivity and voltage in Multi Regime testing 93
Figure 3.32. ASTM D 638 specimen dimension for Type I (rigid and semi rigid plastic) 95
Figure 3.33. Aluminium mould for casting epoxy according to ASTM D 638 (2014) 95
Figure 3.34. Bulk epoxy tensile test 96
Figure 3.35. Four point bending test according to BS EN 12390-5 (2009d) 97
Figure 3.36. Mould, 6 mm rebar, and connection wire 98
Figure 3.37. Loading position and constituting element of the beams in Phase III 99
Figure 3.38. Schematic stress diagram of the critical area (assuming un-cracked section) (a) At the beginning of each cycle, (b) At the highest applied cyclic load 100
Figure 3.39. Tensile test of M10 and monitoring the strain in the middle 200 mm of the bar using DEMEC 103
Figure 3.40. Relationship between strain of the bar and loading 104
Figure 3.41. The induced saw cut and first loading to induce the major crack 105
Figure 3.42. Actuator features for loading (2.5 mm lead) provided by LC automation ltd. 106
Figure 3.43. ROBO Cylinder RCP2-RA10C loading options-showing the position of Lead 2.5 (Load control by using push option was used for the main loading stage) 106
Figure 3.44. Schematic demonstration of the loading cycles –Load control at loading step 3. 108
Figure 3.45. The actuator and installation of the frame in the tank 109
Figure 3.46. The cyclic wetting and drying tank and applying the load with the steel fork attached to the actuator 109
Figure 3.47. CT scanning set up achieving 78 μm resolution 110
Figure 4.1. Possible modes of failure 113
Figure 4.2. Failure modes observed in slant and bi-surface shear tests 115
Figure 4.3. Percentile occurrence of different failure modes in slant shear (SS) and bi-surface shear (BS) tests 115
Figure 4.4. Shear strength obtained from the slant (SS) and bi-surface (BiS) shear tests 116
Figure 4.5. Surface shear strain γ_{xy} distribution for (a) the slant and (b) bi-surface shear tests 118
Figure 4.6. Failure modes observed (a), (b) and (c) modified flexural test, (c), (d), and (f) split cylinder test 119
Figure 4.7. Percentile occurrence of different failure modes in the split cylinder and modified flexural tests 120

Figure 4.8. Ultimate tensile stress considering various epoxies, surface preparation and joint thickness 121
Figure 4.9. Effect of the joint thickness on joint tensile strength, compared to joint with 2 mm thickness ……...122
Figure 4.10. Surface strain ε_{xx} distribution for (a) the split cylinder and (b) flexural tests, both tests with 3 mm sandblasted epoxy B joint..... 123
Figure 4.11. Failure modes observed in the torsion tests..... 124
Figure 4.12. Torsional stress vs. rotational deflection..... 125
Figure 4.13. Surface shear strain γ_{xy} distribution during cohesive failure of specimen T6 in torsion..... 127
Figure 4.14. Surface shear strain γ_{xy} distribution during joint failure of specimen T7 in torsion..... 128
Figure 4.15. Ultimate shear stress in push out test with different steel protection methods..... 129
Figure 4.16. Failure mode in push out test without any paint on the steel..... 130
Figure 4.17. Failure mode in push out test with the normal anti-corrosion paint on the steel 130
Figure 4.18. Failure mode in push out test with the epoxy anti-corrosion paint on steel..... 130
Figure 4.19. Stress-slip graphs for “No paint “specimens in the push out test 131
Figure 4.20. Failure mode of bonded hard concrete to steel..... 132
Figure 4.21. Failure mode of bonded fresh concrete to steel..... 132
Figure 4.22. Ultimate shear stress in double lap test with different jointing techniques 133
Figure 4.23. CT scan of a standard cube, fresh concrete-epoxy bond..... 133
Figure 5.1. Geographic milestones of the prototype development and testing (the wave data were extracted from atlas of UK marine renewable energy resources cited by Venugopal and Nemalidinne (2015)) 138
Figure 5.2. Successful floatation of the scaled prototype (1:11), submerged to 55% in 1 M artificial seawater salt solution tank at Pelamis ltd. 139
Figure 5.3. Open plan of the prototype and major damages according to visual inspection (unit mm). 140
Figure 5.4. Damaged parts of the prototype (Visual inspection)..... 141
Figure 5.5. UPV horizontal evaluation with 200 mm distance between transducers..... 142
Figure 5.6. UPV vertical evaluation with 100 mm distance between transducers..... 143
Figure 5.7. Rebound hammer number (for 45^0 measurements)..... 145
Figure 5.8. Prototype coring and testing plan including the sample numbers..... 146
Figure 5.9. Coring of the prototype using the saw..... 146
Figure 5.10. CT scan analysis of the cores from the prototype..... 147
Figure 5.11. Large internal defect in the joint, sample No. 42..... 148
Figure 5.12. Average water penetration depth (mm) of the jointed concrete samples with two different concrete mixes, construction methods and exposure conditions..... 152
Figure 5.13. Typical shape of water ingress through hard-hard concrete bond 153
Figure 5.14. Rare case of water ingress through hard-hard concrete bond..... 153
Figure 5.15. Shape of water ingress through hard-fresh concrete bond 154
Figure 5.16. Average diffusion coefficient according to CEN TS 12390-11(2010) method 155
Figure 5.17. Chloride ingress depth through bonded concrete by spraying 0.1 M of $AgNO_3$ after 3 months of exposure..... 156

Figure 5.18. Poor jointing technique and high chloride ingress around the epoxy layer 156
Figure 5.19. Typical shape of chloride ingress through hard-hard concrete bond 157
Figure 5.20. Typical shape of chloride ingress through fresh-hard concrete bond..... 157
Figure 5.21. Accelerated chloride migration tests (epoxy A) 158
Figure 5.22. EDX and SEM analysis of bulk epoxy A, B and C 159
Figure 5.23. Tensile test of epoxy B according to ASTM D638 (2014)..... 160
Figure 6.1. Schematic moment distribution along the beam after cracking ..... **Error! Bookmark not defined.**
Figure 6.2. Pre-cracking of the samples with various post-tensioning level 164
Figure 6.3. CT-scan images from middle section of sample A (No load condition)..... 166
Figure 6.4. Initial and final loading of sample A (No load condition)..... 167
Figure 6.5. CT scan images from middle section of sample B (No load condition)..... 168
Figure 6.6. CT-scan images from middle section of sample C (Sustained load condition)..... 168
Figure 6.7. 3D reconstruction from CT-scan images of sample D (Sustained load condition) 169
Figure 6.8. Initial and final loading of sample E (Cyclic load condition)..... 170
Figure 6.9. 3D reconstruction from CT-scan images of two separate parts of sample E (Cyclic loaded condition), Note: this is not the full beam 171
Figure 6.10. CT-scan images from middle section of sample E (Cyclic load condition) 171
Figure 6.11. CT-scan image of separated part of sample E (the area with lower applied moment and higher shear stress). Note: it is not the full half beam 172
Figure 6.12. Initial and final loading of sample F (Cyclic load condition)..... 173
Figure 6.13. CT-scan images from middle section of sample F (Cyclic loaded condition)..... 173
Figure 6.14. Final condition of the major crack under Sustained and Cyclic load..... 174
Figure 6.15. Plan for void analysis using VG studio max 2.2 software..... 175
Figure 6.16. Example of void analysis of sample A (No load condition)..... 176
Figure 6.17. Example of void analysis of sample D (Sustained load condition)..... 177
Figure 6.18. Example of void analysis of sample E (Cyclic load condition)..... 178
Figure 6.19. Percentage of void increase immediately after pre-cracking and after 3 months exposure compared to the initial scan..... 179
Figure 6.20. Percentage of void increase after 3 months exposure compared to the initial scan 180
Figure 6.21. Comparison of chloride penetration depth in various loading conditions..... 181
Figure 6.22. $AgNO_3$ spraying for determining chloride penetration depth for No load and sustained load condition 182
Figure 6.23. $AgNO_3$ spraying for determining chloride ingress depth for sample E (Cyclic load condition) 182
Figure 6.24. Chloride induced corrosion under cyclic loading (sample E)..... 183
Figure 6.25. White material on the cracked surface of cyclically loaded sample E..... 184
Figure 6.26. UPV configuration and possible pulse path 184
Figure 6.27. Summary of the key observations for zone 1: cracked side under various loading conditions 185

Figure 6.28. Difference of the fracture process zone in metals and concrete (Bažant, 2002) 186
Figure 6.29. Summary of the key observations for zone 2: epoxy layer under various loading conditions 187
Figure 6.31. SEM image of epoxy B 190
Figure 6.32. SEM images of fracture surfaces as weight % of filler 191
Figure 6.33. Crack deflection of epoxies with nano-composite filler (Guo, 2012) 191
Figure 6.34. Fracture energy reduction of epoxy B during humid environment supplied by the manufacturer 193
Figure 6.35. Summary of the key observations for zone 3: body of concrete under various loading conditions 194
Figure 7.1. Main conclusions according to the main features of Phase I: Part 1: Mechanical testing of epoxy bonded concrete to concrete 197
Figure 7.2. Main conclusions according to the main variables in Phase I: Part 2: Shear testing of epoxy bonded concrete to steel 198
Figure 7.3. Main conclusions of Phase II: Part 1: Prototype development 198
Figure 7.4. Main conclusions according to the main variables in Phase II: Part 2: Durability testing of bonded concrete to concrete 199
Figure 7.5. Main conclusions according to the main aspects of Phase III: Cyclic loading meso/micro scale behavior of epoxy bonded concrete 200

LIST OF TABLES

Table 2-1. Example of the load cases for a floating structure in the North Sea (Private communication with Pelamis Wave Power Ltd.) 11
Table 2-2. Roughness coefficient for various surface preparations (Randl, 2013) 22
Table 2-3. Comparison of various jointing techniques (Gleich, 2002) 28
Table 2-4. Limit of cumulative damage ratio DNV-OS-C502 (2010) 44
Table 2-5. C1 values according to the exposure condition DNV-OS-C502 (2010) 45
Table 2-6. Usual K values for jointed sections (R=0.1, frequency=5 Hz) (Broughton et al., 2007) 47
Table 3-1. Phase I: Part 1: Summary of mechanical testing of epoxy bonded concrete to concrete (concrete Mix 1 in Table 3.9) 57
Table 3-2. Summary of experimental programme in Phase I: Part 2: Shear testing of epoxy bonded concrete to steel (concrete Mix 1 in Table 3.9) 59
Table 3-3. Dundee prototype, summary of testing procedure in Phase II: Part 1: Scaled (1:11) WEC prototype (concrete Mix 2 in Table 3.9) 61
Table 3-4. Summary of experimental programme of Phase II: Part 2 (all the joints had 3 mm thickness and the surfaces were sand blasted) 62
Table 3-5. Summary of the experimental programme in Phase III: Cyclic loading meso/micro scale behaviour of epoxy bonded concrete 64
Table 3-6. Average composition of seawater salt (Mehta, 2002) 65
Table 3-7. Epoxy adhesive general characteristics, based on manufacturer data sheet 66
Table 3-8. Epoxy adhesive mechanical characteristics, based on manufacturer data sheet 66
Table 3-9. Test concrete mix proportions and selected properties 67
Table 3-10. Concrete mix assigned for various Phases of the project 67
Table 3-11. Shear force in the joint in the bi-surface shear test for two different set up 72
Table 3-12. General guidelines for concrete quality based on UPV (IAEA, 2002) 74
Table 3-13. Parts details of the scaled porotype 84
Table 3-14. ASTM D 638 specimen dimension Type I (rigid and semi rigid plastic) 95
Table 3-15 Details of the beams in Phase III 99
Table 3-16. Approximate self-weight of the sample 101
Table 3-17. Loading programme using Robo cylinder actuator 107
Table 3-18. Interpretation of Half –cell potential measurements (Gu and Beaudoin, 1998) 111
Table 3-19. Summary of test/monitoring methods in all Phases of the project 112
Table 4-1. Effect of simulated seawater exposure on shear strength 117
Table 4-2. Effect of induced defect on horizontal and vertical UPV 118
Table 4-3. Torsional test results 126
Table 5-1. Results of baseline assessment of the prototype 139
Table 5-2. Minimum lateral path for UPV (Bungey and Millard, 2010) 144
Table 5-3. Typical bulk oxide of Portland cement (Hewlett, 2001) 149
Table 5-4. XRF analysis of the cored samples 150
Table 5-5. Chloride analysis using acid soluble titration and comparison with XRF 151

Table 5-6. ISAT 1881-208 results 154
Table 6-1. Post tensioned beams testing schedule 162
Table 6-2. Mode I fracture toughness and energy release rate for the post-tensioned epoxy bonded concrete samples 165
Table 7-1. Comparison of the results to BE EN 1504-4 (2004a), requirements for acceptable performance of epoxy bonded concrete to concrete 204
Table 7-2. General comment about concrete permeability/absorption/diffusion (The Concrete Society, 2008) 207
Table 7-3. Comparison of the results with The Concrete Society (2008)'s general comments on permeability/absorption/diffusion of concrete 208
Table 7-4. Expected number of resisting loading cycles of the beams according to DNV-OS-C502 (2010) 209

LIST OF EQUATIONS

Equation 2.1 (CEB-FIP, 2012) 20
Equation 2.2 (CEB-FIP, 2012) 21
Equation 2.3 (CEB-FIP, 2012) 21
Equation 2.4 (CEB-FIP, 2012) 25
Equation 2.5 (CEB-FIP, 2012) 26
Equation 2.6 (Rombach, 2002) 27
Equation 2.7 (Chen and Teng, 2001) 30
Equation 2.8 (Chen and Teng, 2001) 30
Equation 2.9 (Chen and Teng, 2001) 30
Equation 2.10 (Chen and Teng, 2001) 30
Equation 2.11 (Volkersen (1938) analysis Cited by Barnes and Mays (2001)) 30
Equation 2.12 (Volkersen (1938) analysis cited by Barnes and Mays (2001)) 31
Equation 2.13 (Volkersen (1938) analysis cited by Barnes and Mays (2001)) 31
Equation 2.14 (Tuakta and Büyüköztürk, 2011a) 38
Equation 2.15 (Torrenti et al., 2010) 42
Equation 2.16 (Torrenti et al., 2010) 43
Equation 2.17 (Torrenti et al., 2010) 43
Equation 2.18(Torrenti et al., 2010) 44
Equation 2.19 DNV-OS-C502 (2010) 45
Equation 2.20 (Broughton, 1999) 47
Equation 3.1 70
Equation 3.2 70
Equation 3.3 (ACI-ASCE Committee 445, 2013) 78
Equation 3.4 (ACI-ASCE Committee 445, 2013) 78
Equation 3.5 85
Equation 3.6 85
Equation 3.7 85
Equation 3.8 85
Equation 3.9 85
Equation 3.10 86
Equation 3.11 86
Equation 3.12 86
Equation 3.13 89
Equation 3.14 (NT BUILD 492, 1999) 92
Equation 3.15(Castellote et al., 2001) 94
Equation 3.16 (Castellote et al., 2001) 94
Equation 3.17 101
Equation 3.18 101
Equation 3.19 101

Equation 3.20 101
Equation 3.21 101
Equation 3.22 102
Equation 3.23 102
Equation 3.24 102
Equation 3.25 102
Equation 5.1(Bungey and Millard, 2010) 144
Equation 6.1 164
Equation 6.2 (Tada et al., 1973) 164
Equation 6.3 (Tada et al., 1973) 165
Equation 6.4 (Tada et al., 1973) 165
Equation 6.5, Euro Code 2 (2004b) 165
Equation 7.1 (CEB-FIP, 2012) 205
Equation 7.2 DNV-OS-C502 (2010) 208

1. INTRODUCTION

The production of renewable energy has become one of the most important political, economic, environmental, and technical issues around the globe. Renewable energy can be generated from various sources, such as wind, tidal, wave and solar. Wave energy is currently one of the least developed of the offshore renewable technologies but has significant potential if a cost-effective method for exploiting the resource can be developed.

Existing Wave Energy Converters (WECs) have been constructed in steel and this has been very expensive. Reduction in capital costs through use of alternative primary structural materials like concrete is vitally important to enable WECs to compete with other renewable sources such as offshore wind energy. Development of structural concrete is suitable for volume production in order to reduce costs through economies of scale as well.

Among various concrete construction methods, segmental precast construction with epoxy filled flat-face joints offers tremendous potential as the cheapest and fastest manufacturing method of WECs. However, while marine concrete is well developed there is a lack of understanding regarding behaviour of joints as main structural element in the harsh marine environments. Jointing two concrete segments with epoxy leads to a critical unreinforced area (see Figure 1.1). This configuration can be accompanied with post-tensioning by considering the additional manufacturing cost and maintenance requirements. The macro and micro mechanical and durability performance of the epoxy filled joint and the critical unreinforced area are not adequately analysed in seawater and under various types of loading. While the feasibility studies that have been carried out to date have indicated that the use of concrete offers benefits over steel for floating offshore structures, they have also highlighted similar areas of concern that need to be investigated further (Pelamis Wave Power, 2013).

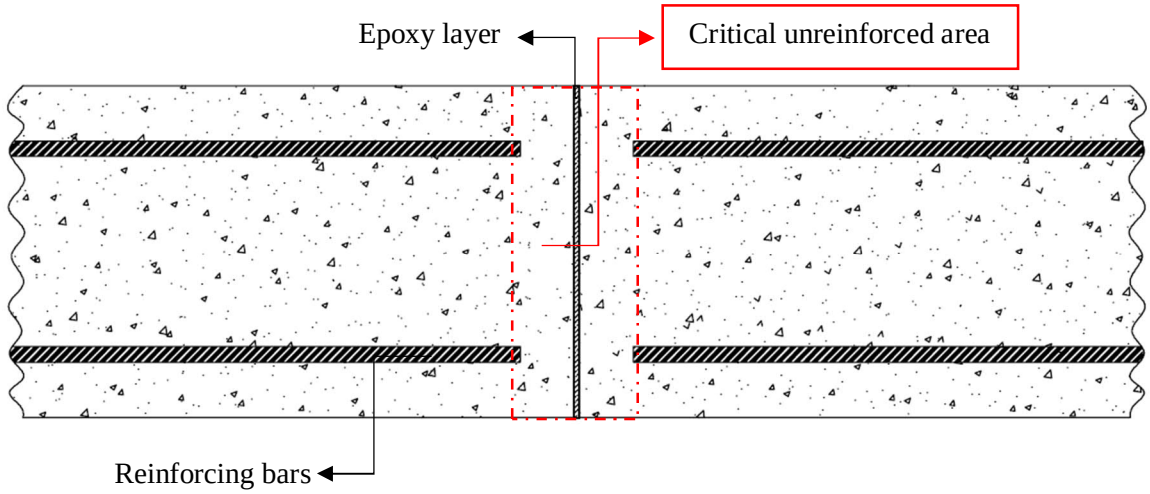

Figure 1.1. Schematic presentation of epoxy filled flat-face joint and the critical unreinforced area

Throughout this thesis, reliability of flat-face epoxy bonded concrete for use in offshore WECs will be challenged. The undertaken research aims to comprehensively assess numerous interconnected variables affecting mechanical and durability performance of the joint. Including the combined effect of cyclic loading and exposure under cycles of wetting and drying in seawater will allow for an improved understanding of this composite system in the marine environment. The findings are also likely to have implications on primary areas of uncertainty for designing flat-face epoxy filled joints in floating concrete structures.

1.1. RESEARCH BACKGROUND

The current research program started with a Knowledge Transfer Partnership (KTP) program between the University of Dundee and Pelamis Wave Power Ltd. aimed at reducing the cost of manufacturing by using concrete as the main structural material for the WEC. The Pelamis WEC was a floating offshore device that could convert ocean wave energy into electricity (see Figure 1.2). It was a semi-submerged, articulated structure composed of multiple cylindrical sections linked by hinged joints. Motion of the hinged joints was restrained by hydraulic cylinders that pump fluid into high-pressure accumulators, which smooth out the irregular wave-by-wave absorbed energy.

Figure 1.2. Pelamis Wave Energy Converter (WEC)

Five tubes were made of steel, but initial studies carried out by Pelamis Wave Power Ltd. and some external third parties highlighted the potential for using concrete as the primary structural material for the tubes. Preliminary designs predicted that changing from steel to concrete could result in around a 50% cost reduction for the main tube element, representing a 10% reduction in total cost of producing each machine. Moreover, the next generation machine was supposed to have a greater power capture, as it was larger with a non-circular cross section. It was anticipated that this cross section would be easier to volume manufacture in concrete than in steel. Over all, Pelamis Wave Power Ltd. wished to investigate concrete use for the following reasons:

- Cost: Replacement of high-value steel fabrication with cheaper materials
- Manufacturing: Faster production of sections for assembly.
- Flexibility: Design of non-uniform section shapes and increase in machine scale

Although Pelamis Wave Power Ltd. went into administration in November 2014, the concept of developing a floating concrete structure for the renewable energy sector is still vital. For example, Albatern Ltd. is another manufacturer of floating wave structures seeking to use concrete as a primary material. The size and function of the Albatern wave converter is different to Pelamis, but the challenges in making it from concrete are quite similar. Additionally, there is also potential for using concrete for floating wind structures that offers the same benefits of fast and cheap construction.

An investigation into using concrete as the primary material for a floating structure should include construction methods, materials and durability, evaluation of loads, design approaches, towing and installation, and maintenance (ACI Committee 357, 2010); but the main focus of this project is on segmental construction and addressing challenges faced regarding static and dynamic mechanical and durability performance of jointed concrete systems.

There are many different construction methods available for offshore concrete structures. For example, slip or jump forming, where the structure is cast as a continuous member. These construction methods are favourable due to reducing the number of joints throughout the structure, since it is the joints which tend to be the point of weakness and produce nonlinearity for transferring stresses across the sections. Instead the initial capital cost for slip forming is high and careful planning of the logistics and materials are required. Besides, acquiring a very good surface finish can be challenging due to adjusting the friction between the form work and fresh properties of concrete. Therefore, the current study focused on the cheapest and probably fastest option, which is the flat-face epoxy bonded concrete sections. Th post-tensioned precast segmental construction has been widely used for constructing large bridges. However, there are not many precedents of using them for offshore floating structures.

1.2. AIMS AND OBJECTIVES

The overall aim of this research is to assess the performance of flat-face epoxy bonded concrete exposed to the North Sea environment, and to highlight the challenges involved in mechanical and durability design of this configuration. To accomplish this, reviewing the literature, several experimental programmes, making prototypes and numerical modelling are required. It is hoped that the findings will contribute to the development of a cheap and fast construction for the renewable energy sector.

The specific objectives of this research are:

i) To comprehensively review the important variables affecting global deformation and strength of the epoxy bonded concrete.

ii) To understand role of the epoxy layer in transferring the stresses between two concrete segments.

iii) To evaluate the factors influencing the failure modes and the shear capacity of epoxy bonded concrete to steel.

iv) To understand challenges involved in buoyancy calculations, casting, construction, quality control and maintenance of a segmented floating concrete structure following Pelamis WEC concept.

v) To assess durability issues of epoxy filled joints after exposure to seawater.

vi) To develop a multipurpose test setup for evaluating epoxy bonded concrete under simultaneous effect of cyclic loading and cyclic wetting and drying in artificial seawater salt solution.

vii) To compare the effect of static and cyclic loading on damage evolution in the critical unreinforced area of the bonded post-tensioned concrete.

1.3. SCOPE

The research was focused on a comprehensive assessment of the behaviour of flat-face epoxy filled concrete joint under structural and environmental loads potentially met during its use in floating offshore renewable structures. A floating structure is a dynamic structure, designed to move and respond when subject to wave loading. As such it is different to most of the other offshore concrete structures such as oil and gas platforms, which are designed as large, mostly static structures which some respond to static waves. A floating structure will be subjected to significant cyclic and static loading throughout the design life and the effect of this on the concrete and epoxy joints mechanical and durability performance needs careful assessment. Therefore, the research program was undertaken in three main phases looking at performance of the composite joint at different scales, under various combined loading and exposure conditions.

Phase I focused on mechanical aspects of concrete jointed with epoxy under static loading. Macro scale global deformation and strength of the joints under shear, tension and torsion were assessed considering numerous interconnect variables affecting the epoxy bond. Moreover, the mechanical behaviour of bonded concrete to steel was evaluated considering the presence of steel plates as the end section of a WEC.

Phase II was related to static meso/micro behaviour of epoxy bonded concrete. A prototype was made based on the Pelamis WEC concept, and its long-term behaviour in the sea was monitored. Various chloride migration and water penetration tests were conducted on epoxy-bonded concrete under laboratory condition as well.

Phase III assessed the performance of flat-face epoxy bonded concrete under simultaneous mechanical loading and exposure under cycles of wetting and drying. The effect of extreme cyclic loading on chloride ingress and water penetration through the bond line between the concrete and epoxy was evaluated. The extent of damage in concrete, epoxy and interface was also monitored.

1.4. OUTLINE OF THE THESIS

The thesis is a consecutive progression through literature review, experimental programme and design, implementation, and results presentation to conclusions on performance of epoxy bonded concrete in the marine environment.

Chapter 2 Literature review critically reviews the available literature on the macro, meso and micro scale mechanical and durability performance of epoxy bonded concrete under static and cyclic loading conditions. The flat face epoxy bonding of concrete to concrete or to steel plates is the focus of this investigation. The role of shear keys in epoxy bonded concrete segments is challenged and the main factors affecting joint strength are considered. The effect of humidity on the bond property is reviewed, and the deficiencies in current guidelines in different practice codes regarding designing epoxy bonded concrete for the marine environment are highlighted. The review summarizes the performance of concrete under fatigue loading and shows the lack of understanding in performance of epoxy bonded concrete under cyclic loading. The simultaneous effect of cyclic loading and exposure to the marine environment is also challenged.

Chapter 3 Experimental program, materials and test methods sets forth the research programme in three main phases in relation to the scope of the project. The methodology, applied test setups, materials, and specimen preparation procedures are explained in detail.

Chapter 4 Mechanical strength and deformation of epoxy joint reports the results obtained in macro scale global deformation testing and strength measurements of epoxy bonded concrete to concrete and to steel. Investigations are carried out into the effects of substrate preparation, joint thickness, epoxy type, exposure under cycles of wetting and drying and presence of defects on ultimate failure strength of epoxy bonded concrete to concrete. The shear/compression, tension and torsion testing were conducted to assess these parameters and monitor the stress transfer between two concrete segments. In the case of epoxy bonded concrete to steel, shear capacity of the assembly is assessed considering the effect of anti-corrosion paint on the plate and applying fresh concrete with epoxy on the plate.

Chapter 5 Prototype development and durability behavior presents the observed behaviour of the small scale prototype according to Pelamis concept after two years of exposure. It also assesses the extent of water and chloride ingress through the joints under two exposure conditions and with different concrete mixes. The durability challenges of two different construction methods of bonding hard concrete to hard concrete and jointing hard concrete to fresh concrete at the same time with epoxy, are highlighted.

Chapter 6 Chloride ingress in bonded concrete under combined environmental actions and mechanical loads investigates performance of the epoxy bonded post-tensioned concrete under simultaneous effect of cyclic loading and exposure to regular cycles of wetting and drying in artificial

seawater salt solution. The observed behaviour from a novel test set up is presented, and possible theoretical explanations are drawn from them. Finally, the main areas of concern regarding epoxy bonded joints in the marine environment are identified.

Chapter 7 Over all Conclusions, comparison of the results with the available data, and recommendations presents summary of conclusions from each phase and draws overall conclusions from the work. The results of the research are compared to the available codes and data. The extent of potential durability and mechanical performance of the epoxy bonded concrete in the marine environment are explained, and a number of recommendations for further research programmes are set up.

2. LITERATURE REVIEW

2.1. INTRODUCTION

This Chapter provides a review of the key aspects in developing a floating segmental concrete structure, focusing on mechanical and durability performance of epoxy bonded concrete. The literature is categorized based on multi-scale assessment of epoxy bonded concrete under static and cyclic loading. Therefore, macro scale behavior of the joints regarding global deformation and strength, along with meso/micro scale performance considering durability, cracking, permeability and coupled effect of mechanical loading and exposure in the marine environment are covered in the following sections.

The topic of this project is very wide and includes a vast range of studies from aerospace applications to structural retrofitting. However, most of the existing knowledge is not directly applicable to bonded concrete in a floating WEC due to differences in bond line thicknesses, substrate materials, joint geometry, failure mechanisms, loading types, and environmental conditions.

Due to the widespread use of concrete in a marine environment, and several successful preceding of offshore concrete structures, the durability and mechanical performance of pure concrete is just briefly mentioned while the need for studying flat-face epoxy jointed systems in a marine environment is highlighted throughout the literature.

In contribution to the overall aim of this research project, a review of available codes and standards, library and accredited web resources, research within the industry, and experiments carried out by others of a similar nature have been conducted and are reported in this chapter.

2.2. HISTORY OF FLOATING CONCRETE STRUCTURES

There is a long history of use of concrete for offshore structures, which can be categorized into two main types, Gravity Based Structures (GBS) and floating structures (Pérez Fernández and Lamas Pardo, 2013). The first gravity based concrete oil platform was installed in the Gulf of Mexico in 1950, and thousands of similar small concrete structures were subsequently constructed. However, construction of the gravity-based structure The Ekofisk Tank in 1973 in the North Sea is considered a significant milestone in concrete offshore structure history, and this led to more than 40 such offshore structures being cited in the North Sea. Within floating structures, there are various applications and subdivisions like ships and barges, industrial plant ships, floating piers and docks, floating bridges, immersed tunnels, and navigation structures (ACI Committee 357, 2010).

Historically, the use of concrete as a structural material in the marine environment dates to ancient Roman and Greece, but the first recorded floating reinforced concrete vessel was built by Lambot in 1848. This boat was simply made by using a sand-cement mortar on an iron mesh framework, and the remains of the vessel is now in a museum in France (Nawy, 2008).

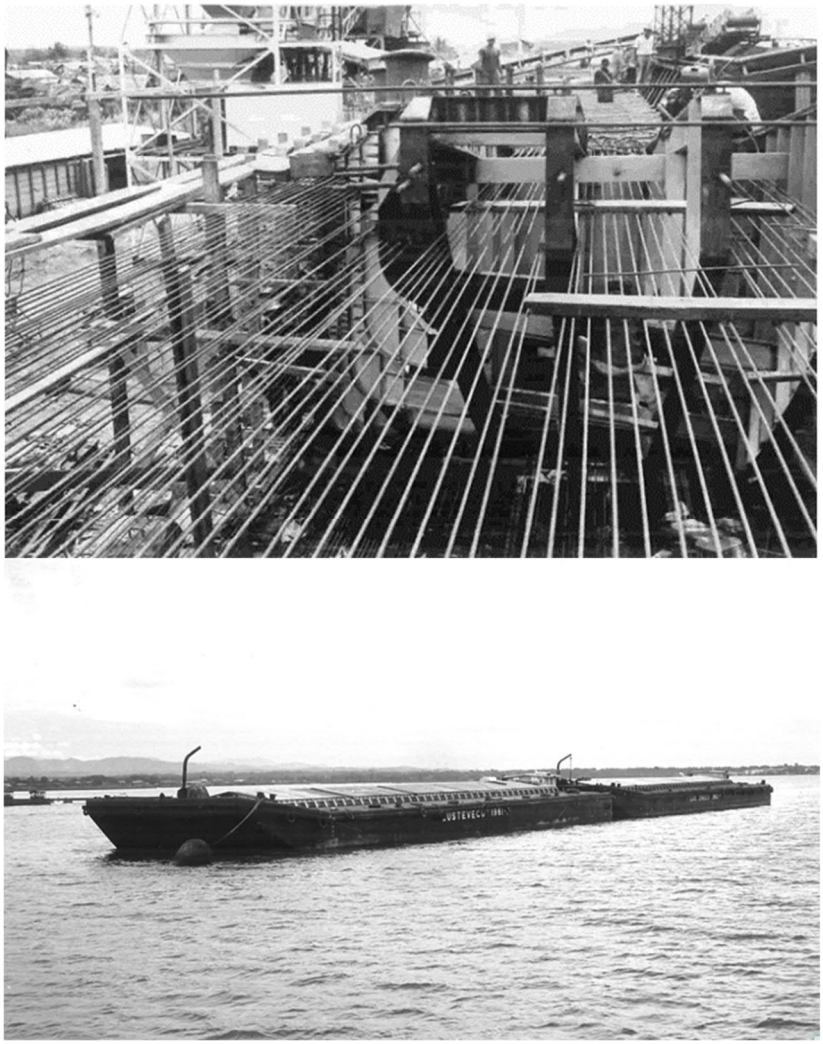

Figure 2.1. One of The world's first pre-stressed concrete barges launched in 1964 (Pérez Fernández and Lamas Pardo, 2013).

The first self-propelled reinforced concrete vessel was M.S. Namsenfjord, built by N.K. Fougner in Norway in 1917. Following this, a shortage of steel during World Wars I and II resulted in the continued construction and development of concrete ships. For example, the U.S.A manufactured 12 reinforced concrete ships in 1918. These vessels were built with light-weight concrete using expanding clay and shale aggregates, with a density of 1760 kg/m^3, strength of 28 MPa and a dead weight of up to 7500 tons. Construction of concrete vessels, barges and large floating dry docks continued throughout World War II, with two further prestressed concrete ships being constructed during this period (ACI Committee 357, 2010).

One of the more recent large offshore concrete structures to be constructed was the Liquefied Natural Gas terminal (LNG) Adriatic. This was built in Algeciras in 2007 and was the world's first offshore gas terminal. (Pérez Fernández and Lamas Pardo, 2013).

2.2.1. Advantages of concrete over steel for offshore structures

As discussed in the previous section, the use of concrete in the marine environment has a long history, and the material is considered to have the following advantages:

- Concrete exhibits good properties against corrosion, especially when compared to steel, provided that the mix design and detailing takes into account the specific challenges of the marine environment. This eliminates the need for surface coatings and reduces maintenance requirements over the life cycle of the structure.
- Concrete is a high rigidity material and is well suited to resisting hydrostatic and bending compression forces.
- The cost of concrete is less reliant on global markets compared to steel, as concrete can be easily produced locally and does not need to be imported. This also has the added benefit of producing local jobs.

Specific advantages for the Pelamis or any other floating wave or wind structure are as follows:

- The weight of the concrete reduces the need for ballast in the structure.
- Reinforced concrete is generally considered to have good fatigue properties which are important in a structure subject to cyclic loading such as the Pelamis.
- Optimization of device geometry and increased power are achievable due to the flexibility of shape possible with concrete
- Cost reviews highlight that concrete tubes are likely to offer cost savings over steel, especially when looking at volume manufacture of intricate non-circular cross sections.

2.2.2. Aspects of investigation for a floating marine structure

Using concrete as the primary material for a floating structure requires knowledge from a variety of different disciplines. The main aspects for investigation are discussed in the following sections, however the focus of the current project is epoxy bonded concrete and all these major investigations should be conducted for joints as well.

2.2.2.1. Material and durability

The North Sea environment is considered to be a harsh climate due to the following: 35 g/l salinity, surface temperature of 5-17 ºC; wave heights of 25-30 m and wind velocity in excess of 45 m/s (Helland et al., 2010). Mehta (2002) categorized deterioration factors of the marine environment into the physical, like surface wearing and cracking, and the chemical, like reactions leading to expansin of materials. All potential deterioration parameters should be checked in the context of the specific conditions of the North Sea, but most durability studies focus on chloride-induced corrosion as the main cause of damage. Ahn and Reddy (2001) claimed that corrosion of reinforcing steel should be considered as the most important parameter in assessing durability of concrete, because corrosion

causes expansion, cracking and spalling of cover along with structural failure due to loss of bond between concrete and steel. Zhao et al. (2011) also noted that expansive corrosion products gradually produce tensile stresses. Once the tensile stress is greater than the concrete tensile capacity, cracks at the concrete surface initiate and propagate. These cracks can provide a suitable path for ingress of more chloride and other harmful agents. Therefore, concrete cracking is usually considered as the serviceability limit for design. BS 8500-1 (2015a) explained exposure classes for chloride induced corrosion environments. A floating marine structure can be considered as XS3 due to cycles of wetting and drying that may occur for the structure.

2.2.2.2. Water tightness

Concrete does not have good tensile properties and will crack when subject to tensile strain. Excessive cracking can cause corrosion of the rebar, as mentioned previously and could result in leaking of the structure if cracks are allowed to form through its thickness. Therefore, it is important to maintain crack formation within acceptable limits. Longitudinal post-tensioning steel can ensure that the structure is always in compression, and longitudinal bending, and hoop reinforcement should be used to resist the tendency of the cross section to deform under external hydrostatic pressures. However, it will not be possible to eliminate tensile stresses entirely in the circumferential direction, and therefore careful reinforcement detailing will be required to ensure that crack formation is be kept to a minimum. Preliminary costing studies for Pelamis have shown that supplying and fixing the required reinforcement is a significant proportion of the manufacturing cost. Therefore, one of the main focusses for the design work should be how to optimize the tube cross section so that the minimal amount of rebar is required while keeping overall crack widths within the specified design limits. Options that could be considered for reducing the amount of reinforcement used include the potential addition of fibres within the concrete mix to reduce non-structural cracking, or the provision of waterproof linings in order to reduce the risk associated with water leakage via through-thickness cracks (Khosravi et al., 2015).

2.2.2.3. Evaluation of loads

Identification, definition, and determination of the various loads which affect the floating structure in a marine environment are essential for design purposes. The load evaluation process determines the value of the live loads, accidental loads, and environmental loads which are applied to the structure during the life of the structure. These loads include, amongst others, the hydrostatic, axial, moment, and torsional loads that the machine needs to resist. There are also the construction loads, towing and installation loads for a certain device e.g. Pelamis machine. Table 2-1 represents a sample of load cases on the Pelamis machine. A very high value of torsion is specific to Pelamis or any floating structure with such a configuration (Khosravi et al., 2015).

Table 2-1. Example of the load cases for a floating structure in the North Sea (Private communication with Pelamis Wave Power Ltd.)

Load case	Load value
Heave Bending Moment (Nm)	8.86E+06
Tube Draping Bending Moment (Nm)	2.66E+07
Tube Torque (Nm)	1.50E+07
Axial Surge (N)	3.50E+06
Heave Shear (N)	3.50E+06
Sway Shear (N)	3.50E+06
Hydrostatic Pressure (N/m^2)	1.00E+05

2.2.2.4. Design

The conceptual design phase of the floating concrete structure should consider hydrostatic and hydrodynamic loads and hydrostatic stability. This phase considers various main factors and come up with a simple prototype to give a better understanding of the structure (Wang and Wang, 2014). The detailed design phase should be conducted according to the established design codes, such as the DNV OS C502 (2010) for offshore concrete structures, and BS 6349 (2013b) for maritime structures, for identifying the appropriate design philosophy. It should be noted that while the codes provide a starting point for design, they were primarily developed for the oil and gas industry and are applicable for structures which are subjected to very different forces than the dynamic WEC machine. Therefore, there may be areas in the design where it is appropriate to deviate from the current code specifications. Moreover, typical reinforcement content for a land-based structure is 300-400 kg/m^3, but for minimizing hydrodynamic loads the floating structure should be made slender with very high reinforcement content, as high as 1000 kg/m^3. Therefore, the construction, planning and design should be very much integrated (Wang and Wang, 2014).

2.2.2.5. Construction

There are many different construction methods used for offshore concrete structures. One of these approaches is the use of post-tensioned precast segmental construction similar to the method used for constructing large bridges. These different precast construction methods may be accompanied by some cast in-situ components. For example, Figure 2.2 shows the precast construction for the internal hull of N'Kossa FPSO - Liquid Petroleum Gas (LPG), where the exterior walls were all cast in place. Precast segmental construction is assumed to be the simplest construction method and likely to be the cheaper option.

Figure 2.2. The curved bottom of the vessel for LPG by match cast segmental construction (Gerwick, 1999).

There are alternative methods such as slip or jump forming, where the structure is cast as a continuous member. These types of construction methods reduce the number of joints throughout the structure. Many marine structures like gravity based oil platforms are constructed by slip forming The North Sea platform Gullfaks C, built in 1987, is the largest slip form constructed platform to date (Fossa et al., 2008). Slip forming needs a higher initial capital cost and achieving good surface finish is challenging with this method.

As well as conventional mixes and designs, steel fibre concrete mixes are sometimes used to reduce the tensile cracking, and self-consolidating concrete (SCC) also has potential when there is congested steel reinforcement (Gerwick, 1999).

Stability, maneuverability, and strength of the machine during towing will need to be evaluated as part of the design process, and a suitable technique which will ensure the safe and economical movement of the WEC should be developed. The tow route, water depth and environmental and weather conditions are the most important factors to consider in this regard (ACI Committee 357, 2010). Surveys, periodic inspections and proper installation of sensors are required to ensure the performance of the structure during its service life. Causes of deterioration should be identified in order to plan for assessment of the amount and possible location of the damage. Finally, a plan for repair approach following the inspection will be required.

2.3. BONDED POST-TENSIONED CONCRETE AS THE MAIN CONSTRUCTION METHOD OF WECS

Precast segmental construction can be considered as one of the fastest and cheapest construction options for a floating WEC. Post-tensioned concrete has been widely used in bridge construction mostly based on AASHTO 89 Guide Specifications for Design and Construction of Segmental Concrete Bridges (1989). There is guidelines available for key aspects of prestressed or post-tensioned structures regarding moment distribution, serviceability limit states, creep and loss of post-tensioning and construction issues. Typically, all concrete structures, except water retaining structures, are designed based on ultimate limit state (collapse, buckling, accidental damage) and then serviceability checks will be considered, but pre-stressed concrete is designed based on serviceability limit state (deflection, cracking, durability, vibration, fatigue, fire) and then ultimate limit state checks are conducted (Mosley et al., 2012).

Although it is assumed that post-tensioned concrete will be designed based on serviceability limit state and no cracking is permitted, it is realistic to consider some extent of cracking especially in partially prestressed concrete (concrete elements with combination of conventional reinforcement and pre-stressed tendons). Figure 2.3 shows the provision of cracking and deformation under bending for various percentages of pre-stressing. Normal reinforced concrete is based on cracking of concrete even under self-weight which leads to more ductile behavior. Fully pre-stressed concrete will show more brittle failure due to absence of cracking zone, while partially pre-stressed concrete can experience cracking under dead load and, depending on the ratio of pre-stressing, can show more plastic behavior. However, design criteria and crack width for partially pre-stressed concrete is not as well established as for conventional concrete (Karayannis and Chalioris, 2013). Therefore, some cracking can potentially occur in segmental construction of floating concrete structure due to extreme loading condition or in extended service life in a marine environment does not seem wrong. Accordingly, the assessment of chloride penetration in cracked sections under various loads becomes important.

Another important aspect of post-tensioned concrete for the marine environment is the durability and mechanical performance of joints, thus being the main topic of the current research program various possible joint configurations for precast, post-tensioned concrete segments have been developed. Figure 2.4 shows some examples of joints which have been used in bridge construction, but not all of them are appropriate for a floating marine structure regarding sealing issues or difficulties in the offshore installation processes.

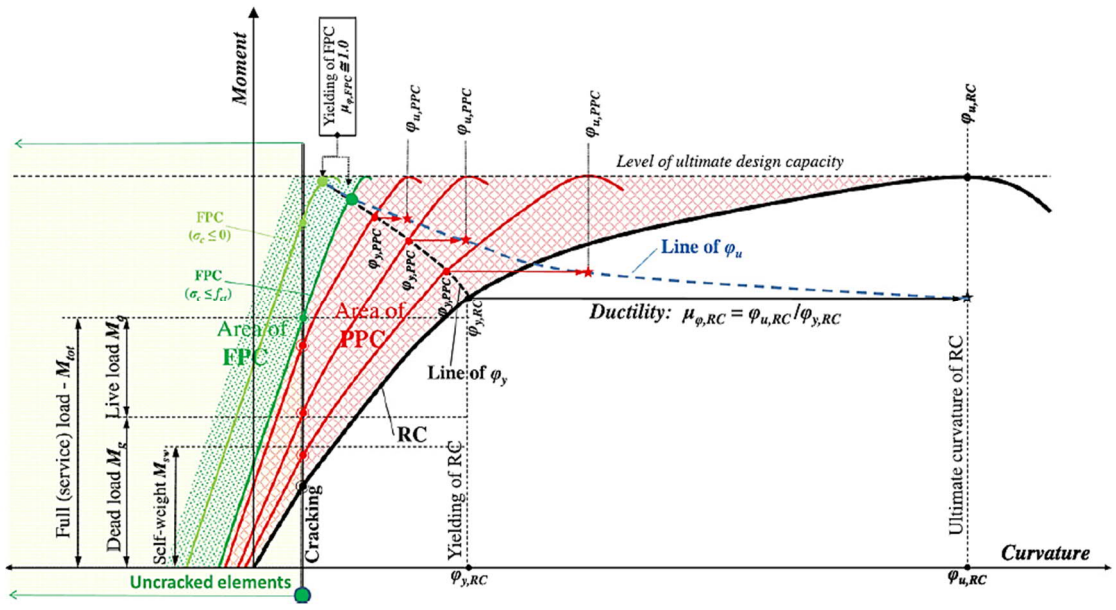

Figure 2.3. Range of behavior of fully pre-stressed concrete (FPC) to partially pre-stressed concrete (PPC), with various ratios of pre-stressing (φ) and normal reinforced concrete(RC) for elements with the same ultimate limit capacity (Karayannis and Chalioris, 2013).

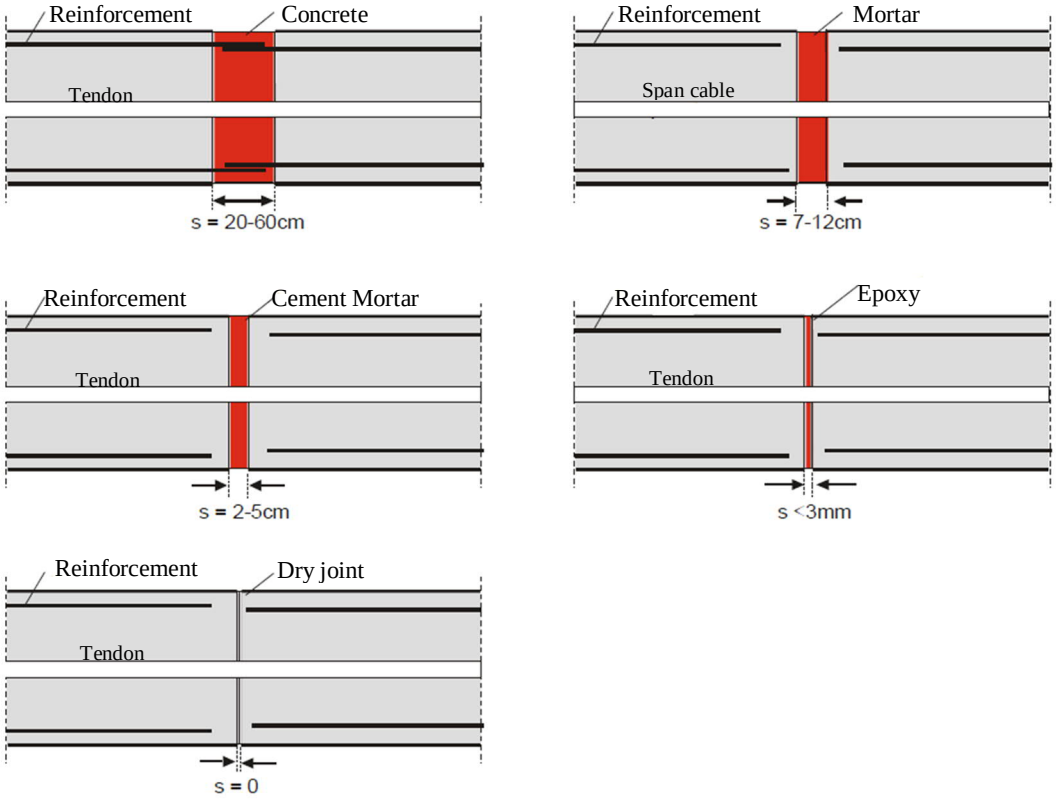

Figure 2.4. Typical structural joints in bridge construction (Rombach, 2002)

Resins have been widely used in the aerospace industry for bonding thin sheets of metal due to their superior strength, corrosion resistance and good fatigue performance (Gleich, 2002); but there are not enough precedents of using resins as the structural element in civil engineering. They are mostly used in segmental match cast bridge construction as the sealing material for proper durability performance (The Concrete Society, 2010), or for repair and strengthening of the concrete with externally bonded steel or fiber plates (Barnes and Mays, 2001). Moreton (1981) mentioned four main reasons for using epoxy in bridge construction which are applicable to floating concrete structures as well:

1) Acts as lubricant for locating mating surfaces during construction.
2) Water tightness and sealing of the joints
3) Transfers the stresses between concrete segments after fully cured
4) Corrects alignment errors, if required

The water tightness and stress transfer are the focus of this project. Therefore, the following sections focus on reviewing available knowledge about the bonded concrete performance in static and cyclic loading states and considers the global deformation strength behavior as well meso/micro mechanical performance.

2.4. DEFINITION OF STRUCTURAL ADHESIVE

ASTM D 907 (2015b) defines an adhesive as a material that can keep together substances by surface attachment. The two surfaces are called adherends. Between adhesive and adherents (interface), the forces of attraction hold the materials to each other. These forces of attraction can be mechanical interlocking or chemical bonds due to physical interactions. Therefore, it is important that the bond strength does not just depend on the bulk characteristics of the adhesive and adherends.

Any adhesive that can join two rigid materials, bear/transfer loads, and is durable over long periods is a structural adhesive. Structural adhesives can have different chemical categories like epoxy, phenolic, acrylic, cyanoacrylate , and urethane (Hartshorn, 2012). However, epoxies became one of the most common ones since the 1940s and are used in segmental construction, so the focus of this study is on epoxies as the structural adhesive.

Epoxy resin is a thermosetting reactive polymer with basic molecular combination of one oxygen and two carbon atoms (see Figure 2.5). One the main raw component of most commercially available epoxy resins is epicholorohydrin. This molecular base can change widely and lead to several types of epoxies. The epoxy resins can react with a large number of hardener chemicals or curatives, like amines and anhydrides. Considering the various combinations of curatives, there can be an infinite number of epoxies with different characteristics (Boyle, 2001). Epoxies are normally characterized based on glass transition temperature (T_g), mechanical performance, stability, viscosity at room

temperature, curing time, chemical resistance, and substrate type which all depends on the epoxy resin formulation.

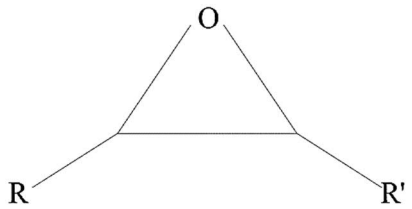

Figure 2.5. Basic structure of epoxy resin (Boyle, 2001), R refers to any group of molecule with attached carbon atom

Epoxies have many advantages compared to bolted or welded joints mainly due to high fatigue resistance, low manufacturing cost, and sealing and thermal or electrical insulation properties, but they have some limitations. For example, they should not be designed for peel and cleavage stress. They also have high surface preparation requirements, and are susceptible to damage in hostile environments, or at elevated temperatures. Moreover, there are no easy non-destructive methods available for monitoring the quality of bonded sections. Hartshorn (2012) also asserts that designing structural adhesive joints is still a great challenge due to shortage of information about performance of joints, and especially behaviour of joints in hostile environments and under cyclic loading. Although there had been a substantial number of tests to compare the performances, they still cannot provide a realistic framework for design. Therefore, physical testing is still an important goal for future studies in this regard.

2.5. GLOBAL DEFORMATION AND STRENGTH OF THE JOINTS

This section looks at macro scale global deformation and strength of bonded concrete to concrete or bonded concrete to plate under static loading. The effective factors influencing failure behavior are discussed and available design models are presented and compared in the case of dry and epoxy joints.

2.5.1. Role of shear keys and comparison between dry and epoxy joints

There are many examples of the use of shear keys in construction of bridges for jointing concrete segments. Dry shear key joints particularly have been widely used and there are many studies evaluating their performance. The current project may be criticized about using flat face jointed system while the literature review shows that the shear keys do not play an important role in transferring the stresses between sections. In bridge construction, shear keys are required for alignment of the sections and transferring stress only during erection, but they do not provide shear transfer in permanent conditions, so they should always be under compression in order to avoid cracking of unreinforced concrete adjacent to the joint (Hewson, 2003).

Generally, it is assumed that the epoxy bonded joints and concrete act monolithic in shear if they are always under at least 1.5 MPa compression (Hewson, 2003). In contrast, Moreton (1981) said that if the joint is bonded and cured perfectly, the recommendation of at least 1.5 MPa compression is not necessary and the behavior will be monolithic anyway. However, a minimum 0.3 MPa compression on the joints during the whole period of curing is advised. Although scattered results in his experiment assumed to be due to defects in time of gluing raise doubts about this conclusion.

Koseki and Breen (1983) tested shear transfer and ultimate strength of different post-tensioned dry and epoxy joints (no key, single large key, multiple key). The results showed that presence of keys makes a great difference in dry joints, but all types of epoxy joints behave monolithically and have full strength. No substantial slip can be seen for epoxied joints until the failure stage. The comparison can be seen in Figure 2.6, and Figure 2.7 shows the typical ultimate failure cracking in a flat- face joint with epoxy. Rombach (2004) also showed that the epoxy joints fail in less than 0.3 to 0.5 mm vertical deflection. Shear keys with gaps more than this value will not take any load, and their presence does not make any difference. All glued joints fail in concrete close to epoxy but still they have a higher load capacity compared to dry joints.

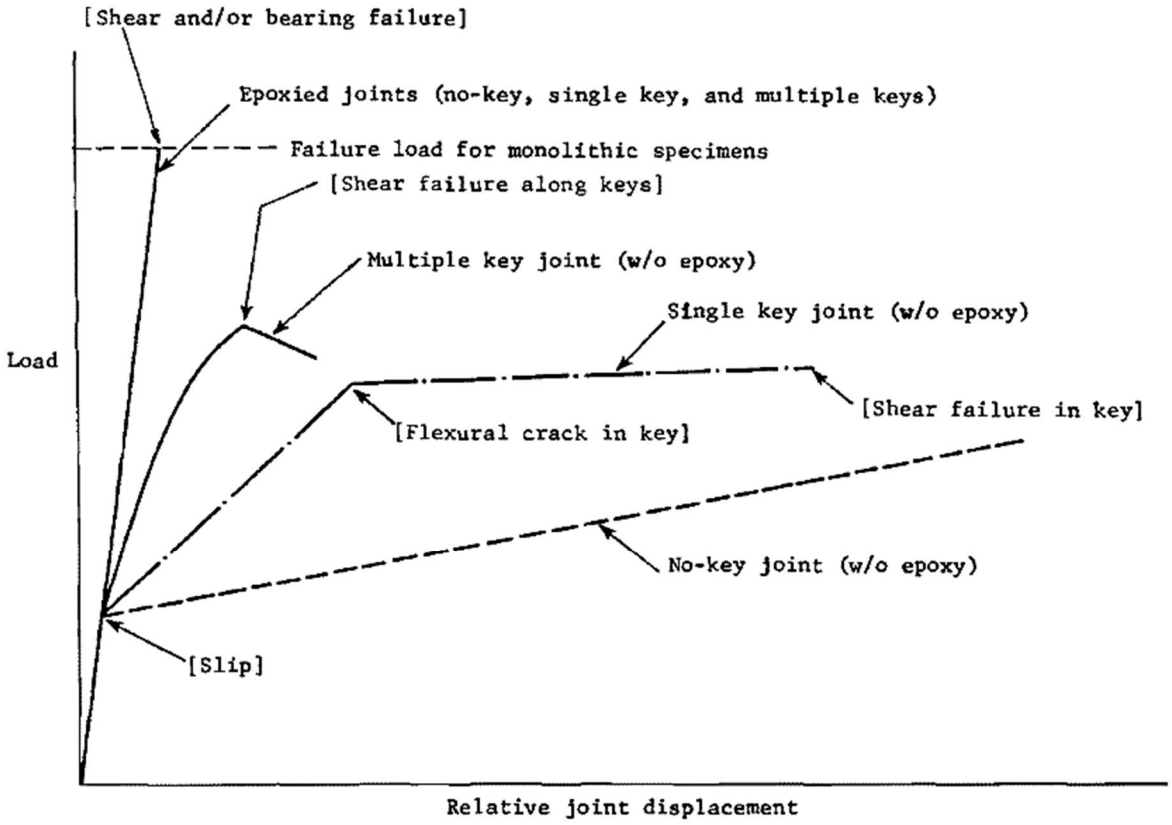

Figure 2.6. Comparison between joints with multiple key, single key and no key (Koseki and Breen, 1983)

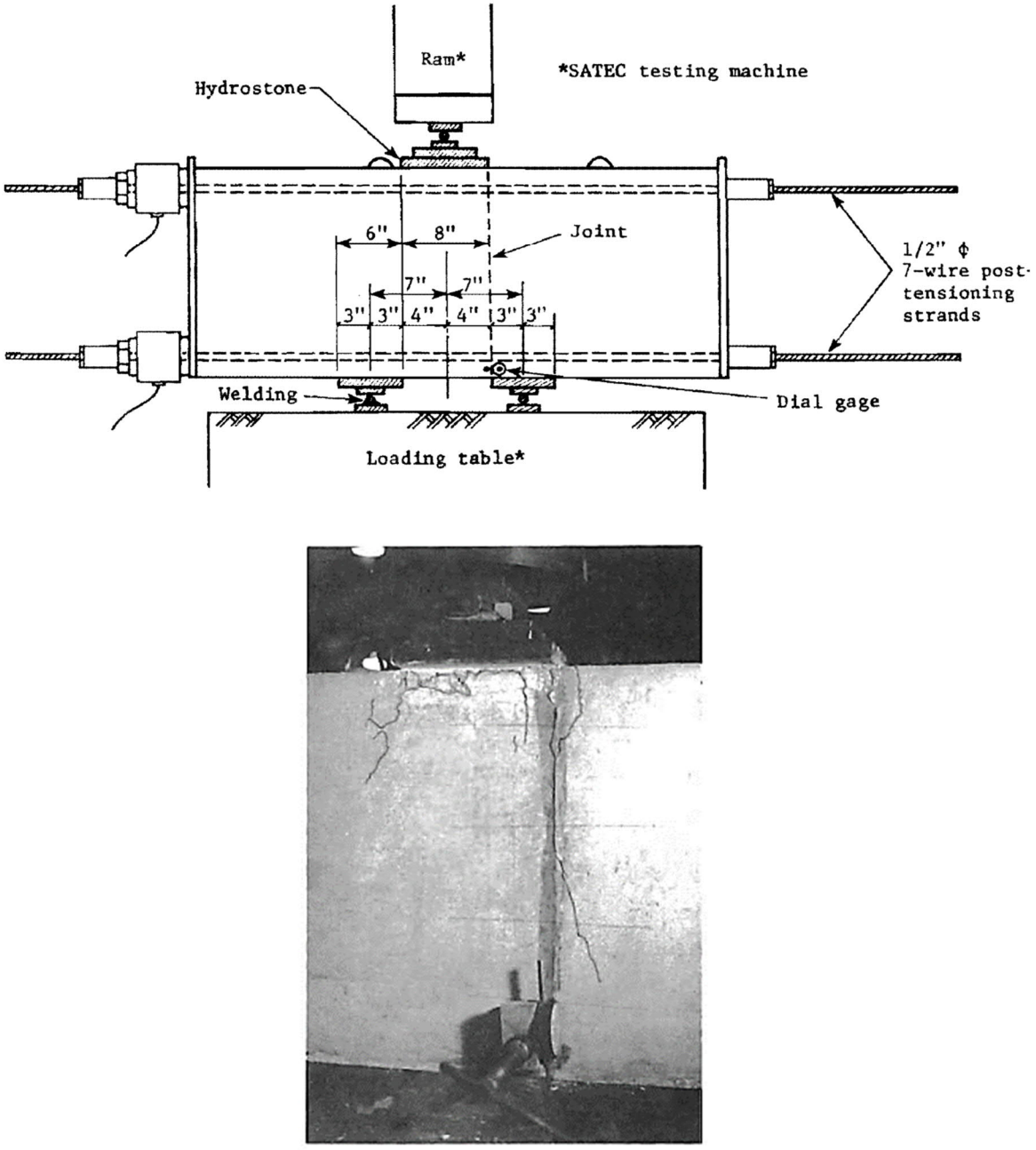

Figure 2.7. Shear test arrangement and the crack pattern at ultimate failure load for flat-face epoxy joint (Koseki and Breen, 1983)

Turmo et al. (2006) used hooked end steel fibre reinforced concrete and tested dry shear key joints under service and ultimate load. The results revealed that steel fibre reinforcement does not increase shear capacity of bonded concrete. High local shear or flexure stresses in the keys can cause various range of cracking of keys. The level of compression and capacity of each key are effective factors in cracking patterns before failure.

Although it seems that the presence of shear keys does not play any role in shear transfer in epoxy bonded concrete, Rombach (2002) numerical investigation on dry joints showed that shear keys play

an important role in torsion and plain joints are insufficient in torsion. However, it still does not mean that flat face joints with epoxy will not be sufficient, because the ductility and strength of epoxy joints are completely different compared to dry joints. Therefore, it is not reasonable to use the dry joints results for epoxy jointed system. Rombach (2002) also conducted an experimental study on post-tensioned jointed systems shown in Figure 2.8 and Figure 2.9, and the results obviously show that epoxy joints are much more brittle, although stronger.

A vast number of researches are available on dry jointed sections, although the results cannot be used in the case of epoxy joints. The behavior of dry joints can be completely different from epoxy joints because the dry joint can open and it is substantially ductile (Deeprasertwong and Leung, 1994). Moreover, the role of shear keys in epoxy joints under special loading conditions, like torsion, is not clear but as mentioned before, epoxy joints even without any keys are stronger than dry joints with keys.

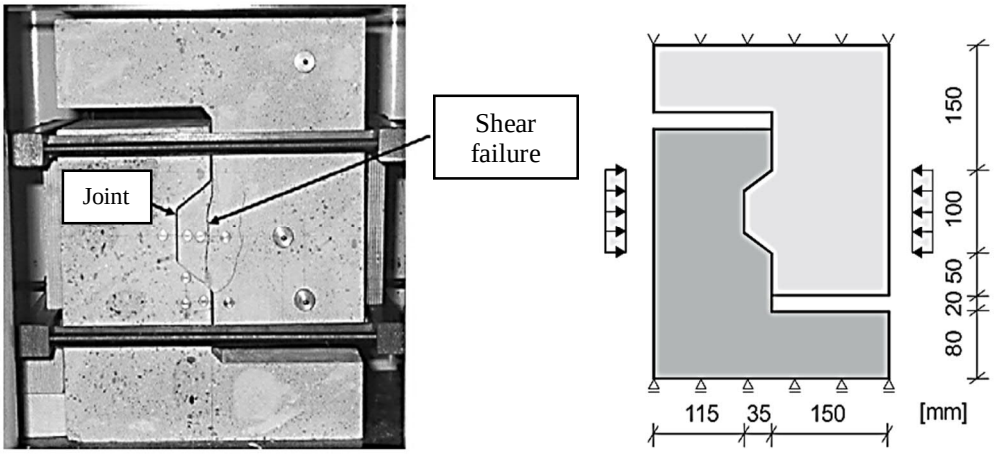

Figure 2.8. Experimental set up for post-tensioned shear key joint (Rombach, 2002)

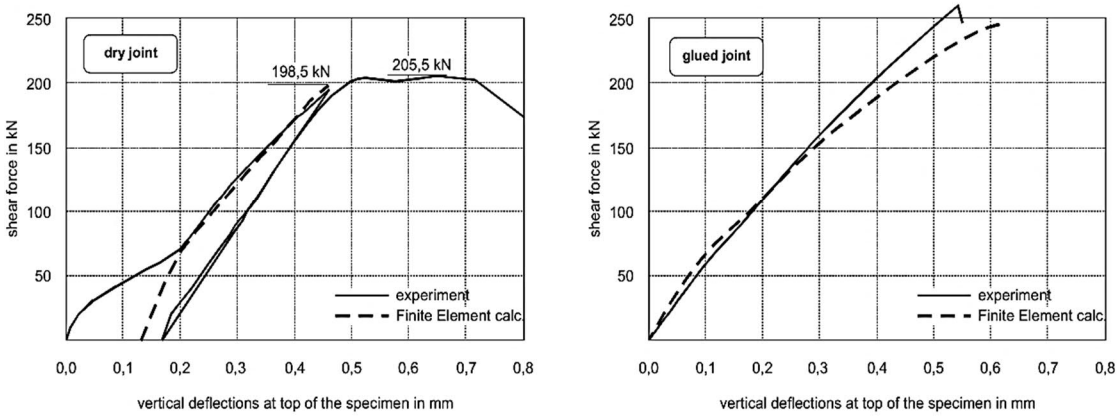

Figure 2.9. Experimental and numerical results showing more ductile behavior of dry joint versus brittle but stronger performance of epoxy joint (Rombach, 2002)

2.5.2. Factors influencing the joint strength

There are many variables affecting the structural performance of jointed concrete sections, such as surface roughness, cleaning of surface, curing condition, concrete strength and quality, stiffness of different layers, eccentricity of force, joint thickness, and workmanship faults especially in big manufacturing sites. Different test methods can also show different bond strength. For example, Momayez et al. (2005) conducted a series of shear tests which showed the bond strengths from some tests up to eight times larger than others. Substantial experimental programmes have been conducted since 1960, but still it is difficult to comment certainly on the mechanical performance of jointed systems because it is difficult to clearly understand the shear stress distribution in the joint. The tests are very dependent on the sample size due to transferring of shear stresses to the edge zone, which has constrain forces (CEB-FIP, 2012). There are also many environmental factors like humidity and temperature. These parameters will be discussed in the durability section of this chapter.

There is also the problem of manufacturing defects. Ultrasonic Pulse Velocity (UPV) can be the best method for detection of defects but the majority of studies are focused on the evaluation and quality of concrete, not on the adhesion strength of multilayer systems, such as between epoxy and a concrete substrate (Czarnecki et al., 2006).

2.5.2.1. Surface roughness

Assessing bond strength of fresh concrete overlays bonded to hardened concrete has shown that the quality of the bond is linked to the surface roughness (Santos and Júlio, 2013, Garbacz et al., 2005, Santos and Julio, 2007). Therefore, the use of various surface preparation techniques in an attempt to improve the bond strength of concrete overlays is common throughout the construction industry. Typical techniques include wire brushing and sandblasting.

As bonding agents are introduced, the relationship between surface roughness and bond strength is unclear. Garbacz et al. (2005) , Júlio et al. (2005) and Santos et al. (2012) concluded that the application of a bond coat unified the adhesion level, negating the influence of surface roughness especially in cases of bonding hardened concrete to hardened concrete.

Abu-Tair et al. (2000) tried to define roughness parameters and CEB-FIP (2012) introduced roughness characteristics based on surface profile. Figure 2.10, Equation 2.1, Equation 2.2, and Equation 2.3 present the equations for calculating roughness parameters. The typical roughness values are also suggested for the shear design calculations in Table 2-2.

$$R_a = \frac{1}{l} \cdot \int_0^l |y(x) - \bar{y}| \, . \, dx \approx \frac{1}{n} \sum_{i=1}^{n} |y_i - \bar{y}|$$

Equation 2.1 (CEB-FIP, 2012)

$$\bar{y} = \frac{1}{l} . \int_0^l y(x) \, . dx \approx \frac{1}{n} \sum_{i=1}^{n} y_i$$

Equation 2.2 (CEB-FIP, 2012)

$$R_z = \frac{1}{5} . \sum_{i=1}^{5} R_{zi}$$

Equation 2.3 (CEB-FIP, 2012)

Ra: Mean roughness

Rz: Average of maximum valley to peak

x: Assessment length

y(x): Profile height at position x

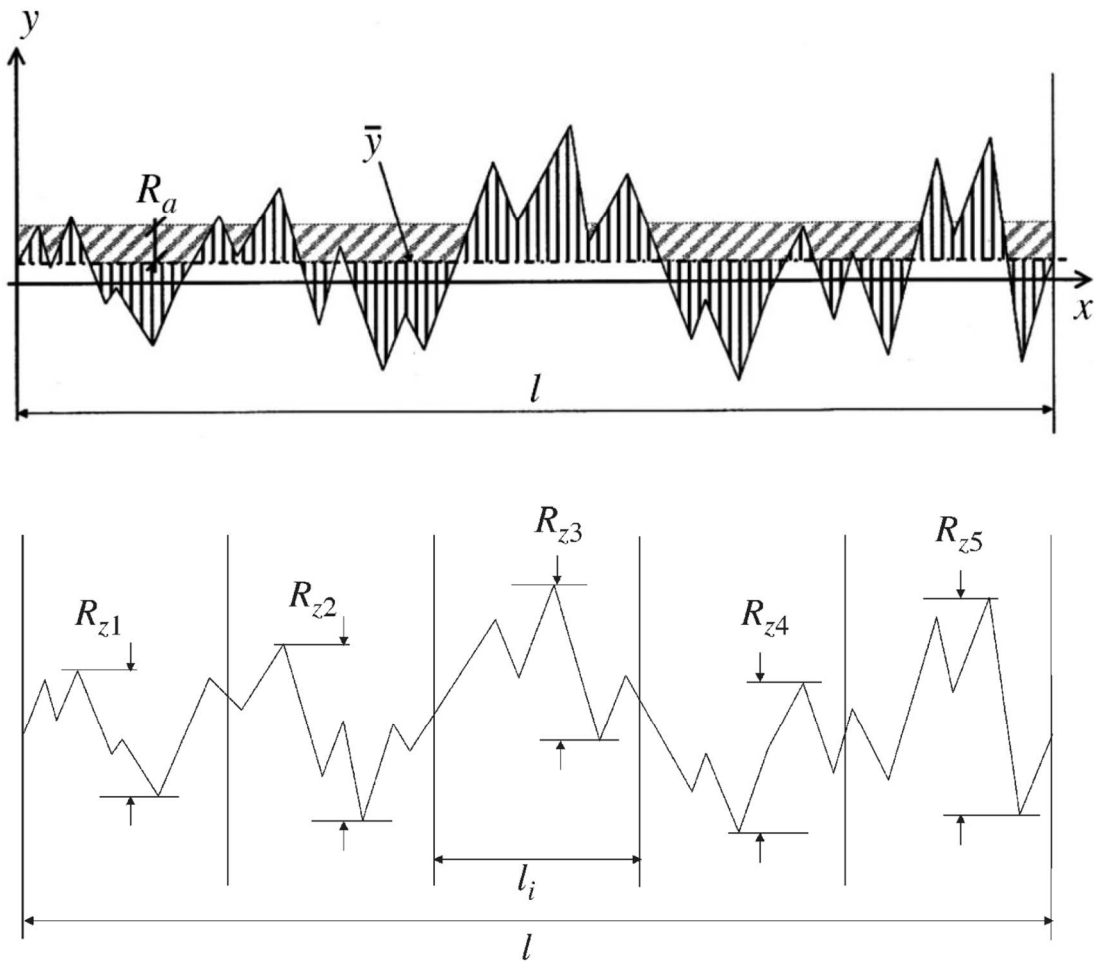

Figure 2.10. Parameters of the roughness profile (CEB-FIP, 2012)

Table 2-2. Roughness coefficient for various surface preparations (Randl, 2013)

Category	c_a
Very smooth (e.g cast against steel framework)	0.025
Smooth (e.g. untreated slightly roughened)	0.20
Rough (e.g. sandblasted, high-pressure water blasted etc.)	0.40
Very Rough (e.g. high-pressure water blasted, indented)	0.50

2.5.2.2. Bond line thickness

As previously stated, the addition of bonding agents at the interface has a profound effect on the relationship between surface roughness and bond strength. However, the influence of the bonding agent is also of interest in relation to the differential stiffness between the bonding agent and the concrete layers; and the influence of thickness on the behavior of the joint and ultimate strength. Regarding the thickness of the adhesive layer, existing data is very scarce. Studies of Derewonko et al. (2008), Frigione et al. (2006) and Da Silva et al. (2009) showed sensitivity of bond strength to thickness of the adhesive in thin joints (0.5 mm- 2 mm), which is not normally the case with structural adhesives. The typical thickness of epoxy adhesive in segmental construction is shown in Figure 2.4. Hewson (2003) , Koseki and Breen (1983) and epoxy suppliers also advise 2-3 mm as the thickness of the joints in segmental construction.

In the case of bonded plate to plate, Gleich (2002) cited studies like Adams and Peppiatt (1974) which showed the reduction of bond strength by increasing bond line thickness. Adams and Peppiatt (1974) believed that this phenomenon was related to increased porosity from air voids and micro cracking caused in the curing process in thicker joints.

On the other hand , Gleich (2002) focused on the importance of interface stresses on predicting the effect of bond line thickness. The study explains how theoretical models use average stress lines of the joint to predict the behavior of the joint, while maximum stress occurs at the edges. The result of their FE analysis showed that both peel and shear stress decrease with increase in joint thickness. Figure 2.11 shows how the average stress decreases while the interfacial stress increases.

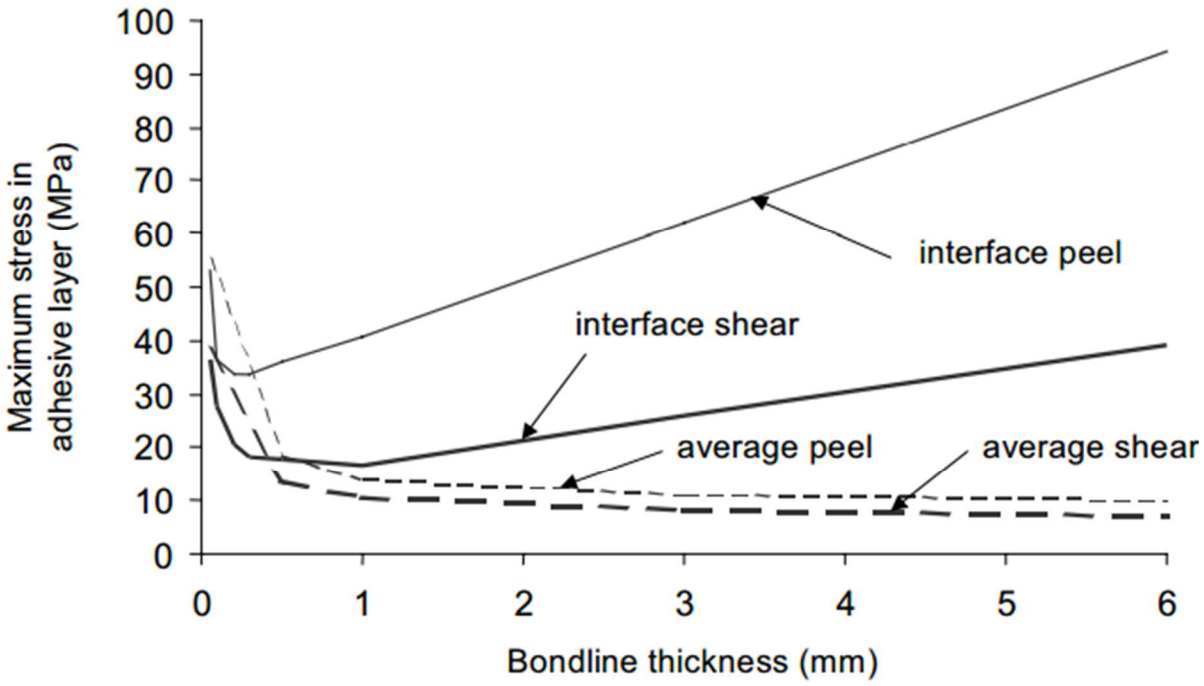

Figure 2.11. Different adhesive thickness versus average and interface stress (bonded plate to plate) (Gleich, 2002)

2.5.2.3. Test methods for measuring ultimate strength of the joint

Slant shear test BS EN 12615 (1999) is the only standard test specifically designed for bonded concrete. All the requirements of bond strength in BS EN 1504-4 (2004a) for structural bonding are based on slant shear, 6 MPa being the required shear strength for slant shear in this code. Compression forces are involved in this test method so it cannot be considered as the pure shear test, which is why Momayez et al. (2005) devised the Bi-surface shear method. This method seems to present shear at the interface.

Other studies like Abu-Tair et al. (1996) and (2000), Bonaldo et al. (2005), Santos and Julio (2007), (2011) and (2012), Tayeh et al. (2012) and many others with all sorts of splitting, pull off and slant shear tests showed that bond strength is very much dependant on the test method and the results can be very scattered . The failure modes can also change from adhesive failure to cohesive or mixed failure. For example, Figure 2.12 shows one of the comparisons between tests methods with two levels of surface roughness and different types of mortar mix acting as bonding agents with average 3 mm thickness. The coefficient of variations for this set of tests is between 6.3-15.8.

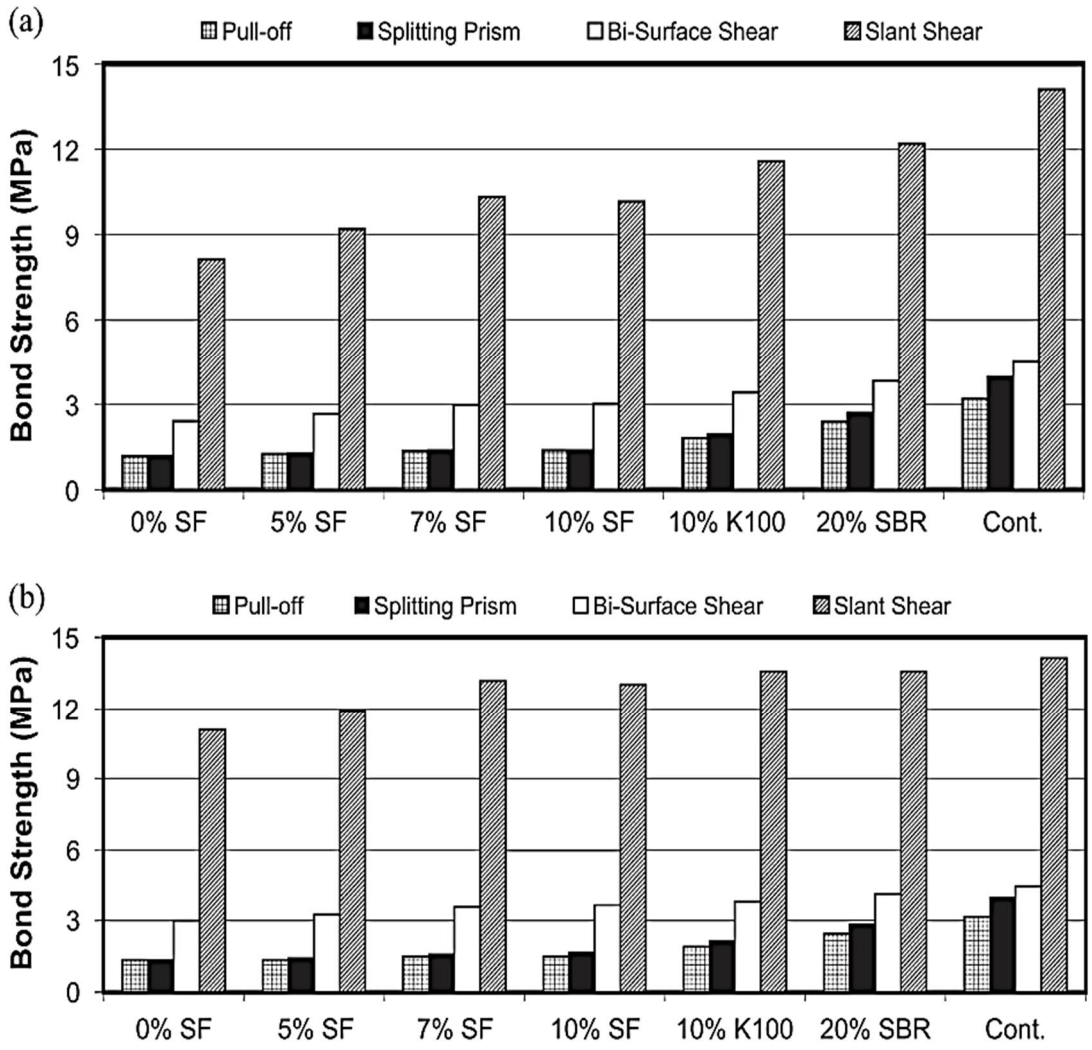

Figure 2.12. Bond strength by different test methods (a) low surface roughness (b) high surface roughness (Momayez et al., 2005).

SF: Silica Fume, K: polymer adhesive, SBR: Styrene Butadiene Resin, Cont: Continuous sample

2.5.3. Design models for bonded concrete

Shear friction theory is used in design codes for concrete cast at different times and express shear at interface by considering the effect of shear reinforcement going through both concrete and joint (dowel action). It is criticised that recommendations are based on small specimens with one shear keys and parameters like different stiffness and shrinkage of the layers are not considered (Santos and Júlio, 2014).

Equation 2.4 presents the main parameters involved in shear performance based on CEB-FIP (2012) as one of the most comprehensive models in this field. Mechanical interlocking, friction due to compression forces and dowel action of reinforcement are considered as the main factors in shear resistance. It should be mentioned that Equation 2.4 only applies for concrete cast at different times and does not apply for any other situation.

$$\tau_u = \underbrace{\tau_a}_{\text{Adhesion interlock, } \tau_a = c_a f_{ctd}} + \underbrace{\mu\left(\rho k_1 f_y + \sigma_n\right)}_{\text{Shear friction}} + \underbrace{k_2 \rho \sqrt{f_y f_{cc}}}_{\text{Dowel action}} \leq \beta_c . \nu . f_{cc}$$

Equation 2.4 (CEB-FIP, 2012)

τ_u: Ultimate shear resistance of interface

τ_a: Adhesion interlock

c_a: Roughness coefficient (Table 2-2)

μ: friction Coefficient (smooth: 0.5-0.7, slightly roughened: 0.8-1.0 and very rough: 1.1-1.4)

ρ: The ratio of reinforcement

*k_1: Coefficient of efficiency for tensile force that can be activated in the reinforcement

σ_n: Compressive stress due to external normal force

*k_2: Coefficient for flexural resistance of reinforcement

*$\boldsymbol{\beta}_c$: Coefficient allowing for angle of diagonal concrete strut

*ν: Reduction factor for strength of diagonal concrete strut

f_{cc}: Concrete 28 days compressive strength

f_{ctd}: Tensile strength of the new concrete layer

**Values of these parameters are mentioned in CEB-FIP (2012), they are not detailed here because shear friction and dowel action are not the concept of this study*

The German code only allows frictional forces to be considered in segmental bridge design processes. It also does not take into account shear keys, and only allows epoxy joints to be used. Therefore, the design shear force (V_u) for segmental bridges can be summarized to Equation 2.5 as A_T is the only effective shear area.

$$V_u = \mu . \sigma_n . A_T$$

Equation 2.5 (CEB-FIP, 2012)

A mentioned before, most of the segmental bridges were designed based on AASHTO 89 (1989). Rombach (2002) compared CEB-FIP (2012), AASHTO 89 (1989) and his new proposed model in Figure 2.13.

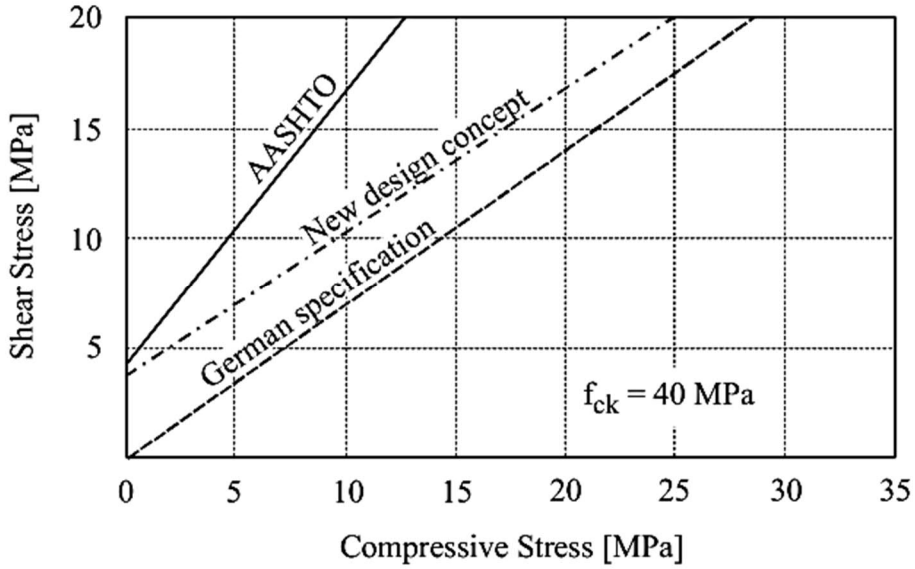

Figure 2.13. Comparison between the models for predicting shear capacity of jointed sections (Rombach, 2002).

AASHTO 89 (1989) considered friction of plain surfaces as well as shear capacity of shear keys, while the German code ignored the load bearing of shear keys, but assumed a greater contact area and only allowed epoxy joints. Rombach (2002) suggests that the AASHTO design model is not appropriate for high compressive stresses in ultimate loading and that load capacity of joints are overestimated. He proposes a new design model as shown in Equation 2.6, which is slightly different to AASHTO regarding consideration of the frictional area, and is more conservative. It should be noted that none of these models consider complicated behaviour of concrete close to failure load. In the case of glued joints, the new model just considers frictional resistance by A_{joint}. The glued joints can increase shear capacity by around 20%, but this cannot be guaranteed due to typical low quality of joints in construction sites.

$$V_u = \frac{1}{\gamma_f}(\mu.\sigma_n.A_{joint} + f.f_{ck}.A_{key})$$

Equation 2.6 (Rombach, 2002)

γ_f =2: Safety coefficient

μ=0.65: Coefficient of friction

σ_n: Compressive stress due to external normal force

$f_{ck:}$ Concrete compressive strength

f=0.14: Factor for the indentation of the joint

A_{key} and A_{joint}: key and joint shear area can be seen in Figure 2.14

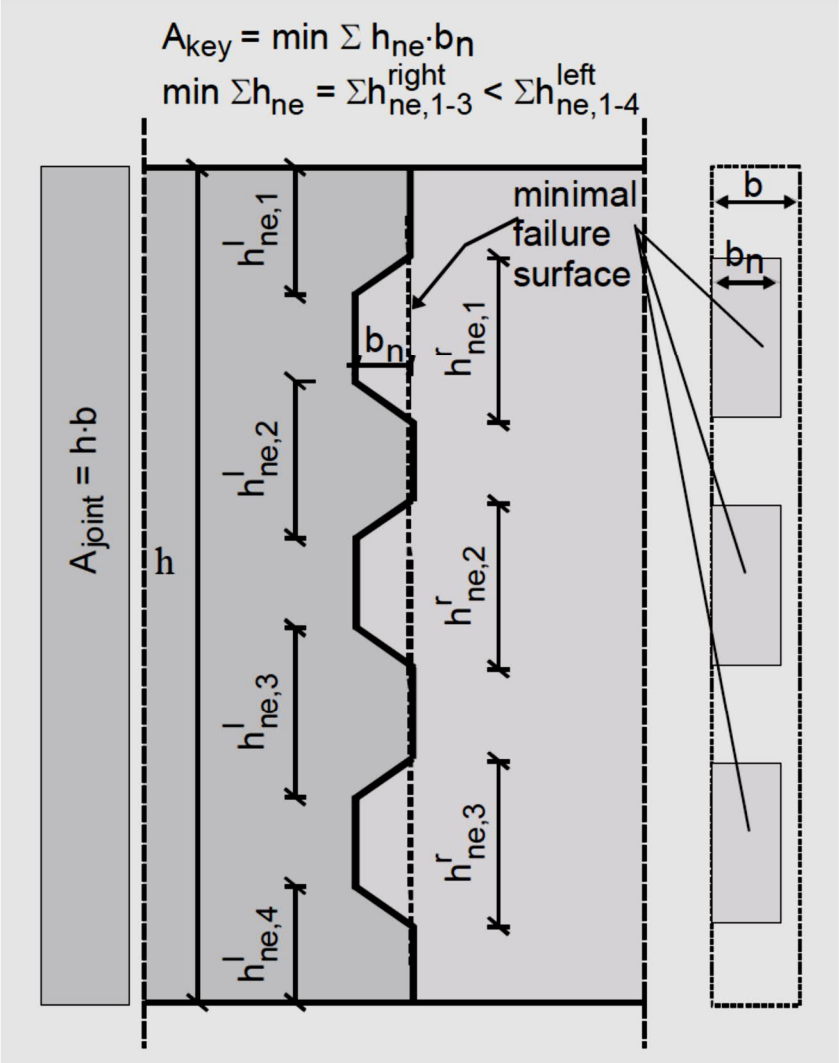

Figure 2.14. Shear resisting area in new proposed model by Rombach (2002)

2.5.4. Performance of epoxy bonded concrete to plate

There are various techniques available for jointing concrete to steel. Table 2-3 shows that bonded joints can be considered as one of the best methods for attaching two materials dues to fatigue and corrosion resistance, but it is not the best choice regarding non-destructive inspection and resistance to the environmental effects. Epoxy bonded plates to concrete is the focus of this study, and this section reviews failure modes, effective factors, and available models of bonded concrete to plates.

Table 2-3. Comparison of various jointing techniques (Gleich, 2002)

Jointing method	Bonded	Bolted	Welded	Bonded and bolted
Surface preparation required	Extensive	Little	Little	Extensive
Joining of dissimilar materials	Good	Limited	Poor	Good
Added weight to structure	Low	High	Moderate	Moderate
Fatigue resistance	High	Poor	Moderate	Moderate
Corrosion resistance	High	Poor	Moderate	Moderate
Inspection by NDT*	Very limited	Adequate	Adequate	Limited
Ease of disassembly	Difficult	Easy	Difficult	Difficult
Production cost	Medium	Low	Low	High
Resistance to environment	Poor	Poor	Moderate	Moderate
Production time	Slow	Fast	Moderate	Slow

*Non-Destructive Test

2.5.4.1. Testing and failure modes of bonded plate to concrete

Connecting steel and Fibre Reinforced Polymer (FRP) plates to concrete have been practiced for strengthening beams and columns. There are a vast number of experimental programs on many effective variables specifically optimum bond length and corresponding ultimate load capacity of the composite. The most easy and typical testing set up can be seen in Figure 2.15 (Yao et al., 2005). Accordingly, bond length (L_{frp}), height of free concrete edge (h_c), loading offset (δ), concrete strength, FRP to concrete width ratio are normally considered as the main effective factors on the performance of the system. Figure 2.16 shows the typical fracture plane in this kind of testing.

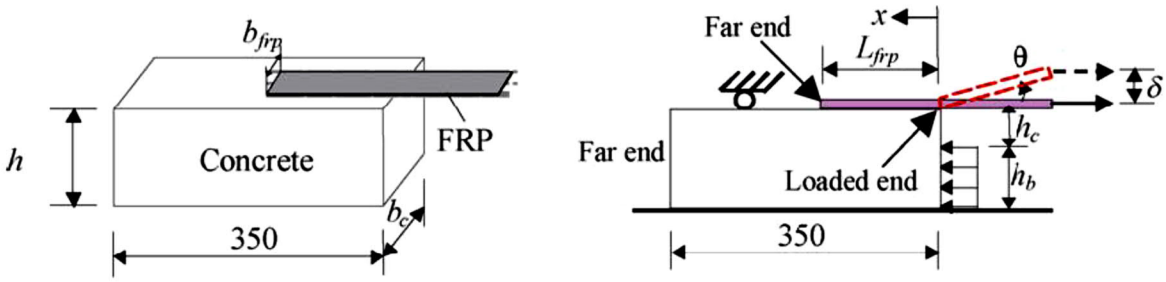

a) Perspective b) Elevation

Figure 2.15. Typical testing set up for FRP plate bonded to concrete and important parameters : bond length (L_{frp}) , height of free concrete edge (h_c), ,loading offset (δ) (Yao et al., 2005)

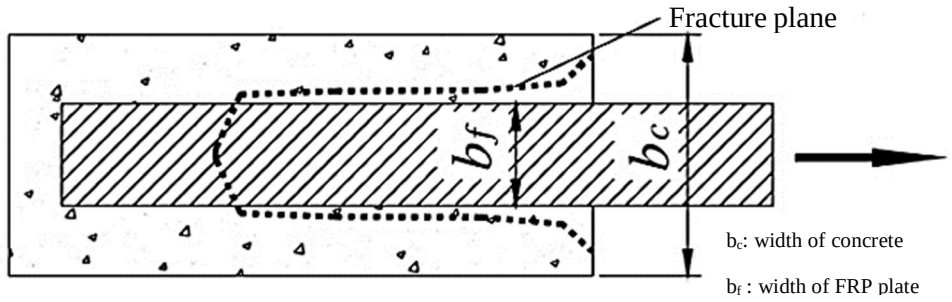

Figure 2.16. Typical fracture plane for bonded plate to concrete (Lu et al., 2005).

CEB-FIP (2012) also categorizes the failures in two main types as end de-bonding and intermediate crack deboning. Figure 2.17 shows typical crack propagation for these two types of failure. Toutanji and Ortiz (2001) also observed the same near surface failure of concrete with various surface preparation and FRP type.

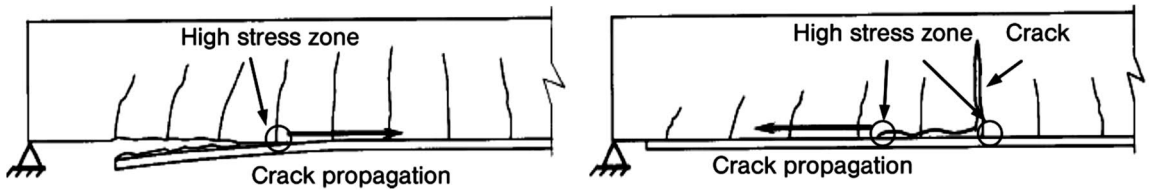

a) Typical end de-bonding failure b) Typical intermediate crack de-bonding

Figure 2.17. Typical failure modes of bonded plate to concrete (CEB-FIP, 2012)

2.5.4.2. Modelling bonded plates to concrete

There are also many studies on modelling the ultimate load capacity and anchorage length of the bonded plates. One of the most cited models is Chen and Teng (2001) model (Lu et al., 2005). This model is presented in Equation 2.7 to Equation 2.10. This model match well to the available experimental data, but it does not take into account adhesive properties. These models are based on nonlinear fracture mechanics approach and by considering a triangular shear stress distribution in the

bond. It means that the behaviour of the bond after the cracking is also considered by reducing the stress and increasing the deformation.

$$P_u = \alpha\beta_w\beta_l L_e b_{frp}\sqrt{f_c'}$$

Equation 2.7 (Chen and Teng, 2001)

P_u: Ultimate load (N)

f'_c: Compressive strength of concrete

α: Best fit value α=0.427

β_w and β_l: Dimensionless coefficient related to concrete to FRP width ratio and bond length

$$\beta_w = \sqrt{\frac{2 - \frac{b_{frp}}{b_c}}{1 + \frac{b_{frp}}{b_c}}}$$

Equation 2.8 (Chen and Teng, 2001)

$$\beta_l = \begin{cases} 1.0 & if\ L_{frp} \geq L_e \\ sin\frac{\pi}{2}\frac{L_{frp}}{L_e} & if\ L_{frp} < L_e \end{cases}$$

Equation 2.9 (Chen and Teng, 2001)

L_e: Effective bond length

$$L_e = \sqrt{\frac{E_{frp}t_{frp}}{\sqrt{f_c'}}}$$

Equation 2.10 (Chen and Teng, 2001)

On the other hand , there are analytical models like Volkersen (1938) analysis cited by Barnes and Mays (2001), and Bizindavyi and Neale (1999) based on linear elastic stress analysis for calculating the shear stress in the bond layer. These formulas consider the effect of adhesive and its thickness. This formula can be used only in elastic range and are not valid after occurring of the first cracks. Volkersen (1938) analysis cited by Barnes and Mays (2001) are presented here as an example.

$$\tau(x) = \omega\frac{P(l)}{b}\frac{\cosh(\omega x)}{\sinh(\omega l)}$$

Equation 2.11 (Volkersen (1938) analysis Cited by Barnes and Mays (2001))

τ: Shear stress

l: Bond length

x: Distance from loading point

P: Load

b: Width of adhesive layer

ω: A constant

$$\omega^2 = \frac{G}{a}\left(\frac{1}{E_s t} + \frac{1}{E_c h}\right)$$

Equation 2.12 (Volkersen (1938) analysis cited by Barnes and Mays (2001))

G: Shear modulus for adhesive

$$G = \frac{E}{2(1+\nu)}$$

Equation 2.13 (Volkersen (1938) analysis cited by Barnes and Mays (2001))

a: Thickness of adhesive layer

E_s: Modules of elasticity of steel

E_c: Modulus of elasticity of concrete

h: Thickness of concrete

t: Thickness of steel plate

2.5.4.3. Effect of the plate stiffness and adhesive thickness on bonded plate to concrete

Equation 2.10 means that there is an optimum bond length, and any further increase of bond length does not have any effect on bond strength. This formula is in line with Eskandarian et al. (2006) quasi-static fracture tests on double-cantilever-beam specimens for measuring energy release rate for different substrate materials. They showed that stiffer and thicker substrate will lead to lower energy release rates, which means that higher bond length is required for stiffer material. Specifically, on bonded steel to concrete, Barnes and Mays (2001) focused on bond length and effect of steel stiffness and adhesive and steel thickness on shear transformation, and observed concentration of stresses on loaded end and distribution of stresses up to 155 mm length of the bond. They suggested an increase in adhesive and plate thickness in order to reduce peak stresses.

Regarding the ultimate shear strength, Si Larbi et al. (2007) conducted push out tests with 100 mm anchorage and FE modeling with different joint thicknesses and surface roughness. They calculated average ultimate strength of steel bonded to concrete as 5.5 MPa. Moreover, they observed that adhesives show high stiffness (4-15 times more than shear studs) but the strength is comparable.

The current research considers using bonded concrete to steel for a WEC and there are various types of loading like tension and torsion applied on the joint simultaneously. Si Larbi et al. (2009) highlighted the importance of considering the simultaneous effect of shear and tension on bond strength, since the failure mode and strength can change in the case of biaxial loading. In the case of torsion, CEB-FIP (2012) presents a model of FRP strengthened concrete, but only in the case of concrete wrapping and it cannot be used in other sorts of strengthening. Dehghani and Fadaee (2014) conducted a reliability analysis and showed the importance of loading rate and plate stiffness in torsion.

In conclusion, there are many studies on concrete strengthening with bonded FRP or steel and most of the main effective parameters are extensively reviewed, but their applicability to floating offshore structures is questioned because they do not consider the bonded plates as the main structural element, and the simultaneous effect of different loading types especially torsion is not sufficiently studied. Moreover, there are some very practical questions that need to be answered for constructing a WEC with a steel end plate. For example, the effect of anti-corrosion paint on the bonding capacity and applying fresh concrete with epoxy on concrete.

2.6. MESO/MICRO MECHANICAL BEHAVIOUR OF THE JOINTS

This section looks at durability of bonded concrete by considering the effect of humidity and temperature. Durability of polymers, epoxies and water diffusion in bulk epoxy are studied by Popineau et al. (2005) and Leger et al. (2010) , but they cannot be useful in the case of bonded concrete because the major challenge is the interface not bulk epoxy. Moreover, concrete is more porous and has a higher diffusion rate than bulk epoxy. Hence, this section concentrates on epoxy bonded materials.

2.6.1. Durability of epoxy bonded concrete to concrete

Accelerated chloride, gas and permeability testing of bonded fresh concrete to high performance concrete by Tayeh et al. (2012) showed very low permeably and intact or micro cracking of composite sections. However, there was no epoxy involved in their experiment and this low permeability (for example water permeability coefficient of $3\text{-}6\times10^{-11}$m/s) of the composite can be attributed to high performance concrete rather than the bond. Çolak et al. (2009) tested freeze-thawing, temperature and corrosive environment ($MgCl_2$, $MgSO_4$) and the effect of surface moisture using the wedge test. The results showed that freeze and thaw up to 40 ^oC does not have any significant effect while higher temperatures can decrease the strength of the joint by softening of the epoxy. Corrosive environments affect bulk concrete strength but not the joint interface. Applying epoxy in conditions of saturated concrete causes interface failure and high levels of moisture can affect strength. It is also interesting that an increase in adhesive thickness leads to reduction of strength especially at higher temperatures. Frigione et al. (2006) undertook flexural testing using three types of epoxy, and also slant shear tests after one-month immersion in water. The adhesive showed reduction of glass transition temperature (T_g) and stiffness. The bond strength decreased by 30% after one month of immersion, as can be seen in Figure 2.18, and the performance of joint degraded with increasing thickness.

Lau and Büyüköztürk (2010) used sandwich beam specimens as illustrated in Figure 2.19. After a rather short period of moisture and temperature ($23\ ^0$ C and $50\ ^0$C) conditioning (4 weeks) the failure mode changed from failure in body of concrete to interface failure (see Figure 2.20). Fracture toughness in humid environment for Mode I (tension) reduced from 14 (J/m^2) to 4(J/m^2) for 23^0 C and from 12 (J/m^2) to 3(J/m^2) for $50\ ^0$C.

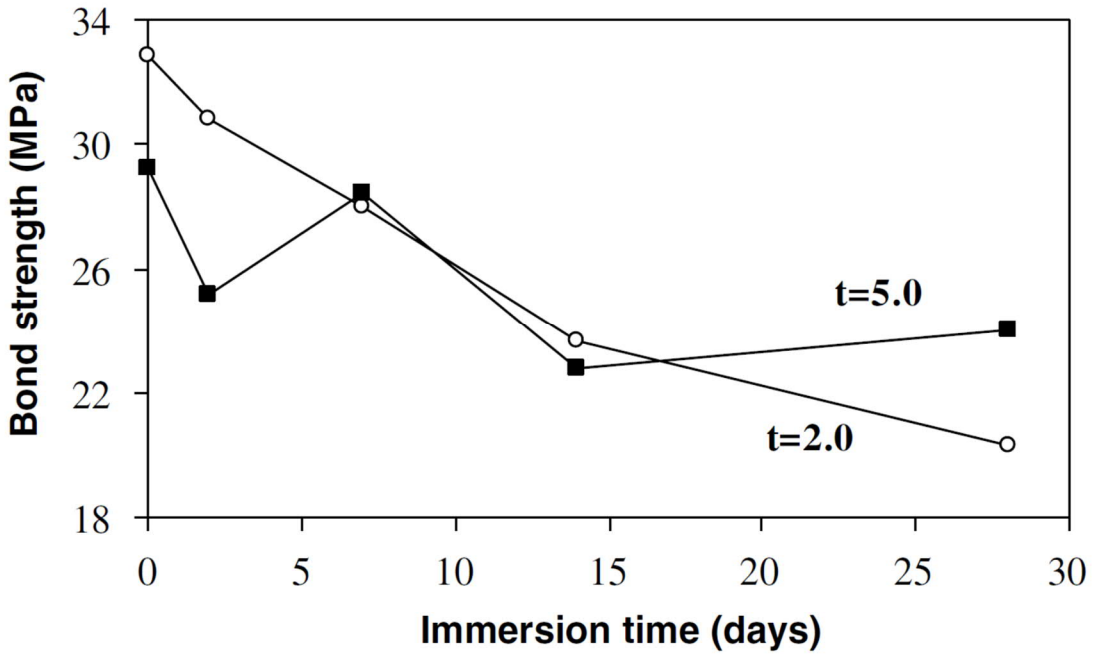

Figure 2.18. Bond strength reduction after one month of immersion in water (Frigione et al., 2006)

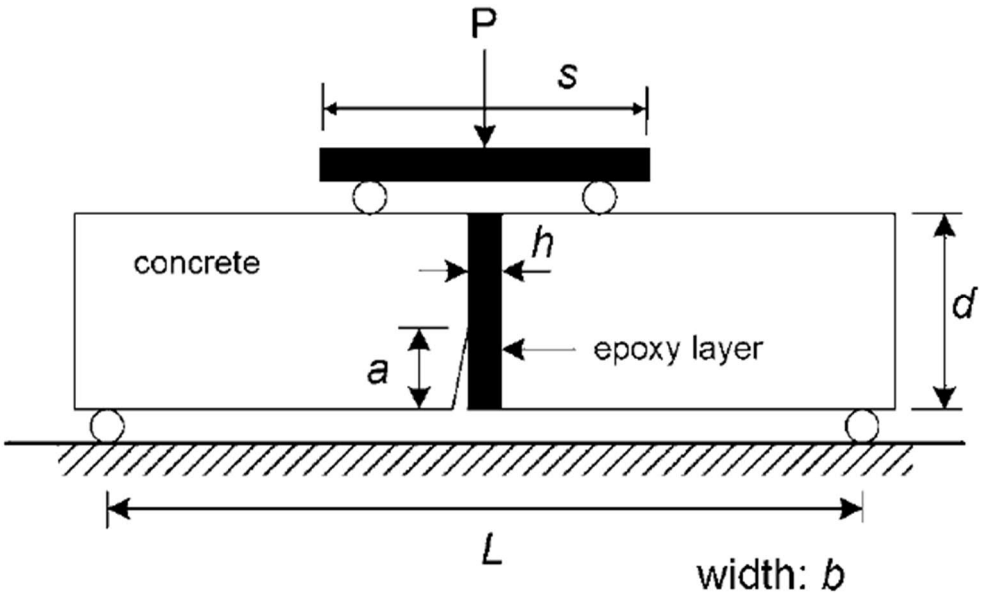

Figure 2.19. Four point bending test set up for measuring interface fracture toughness (Lau and Büyüköztürk, 2010)

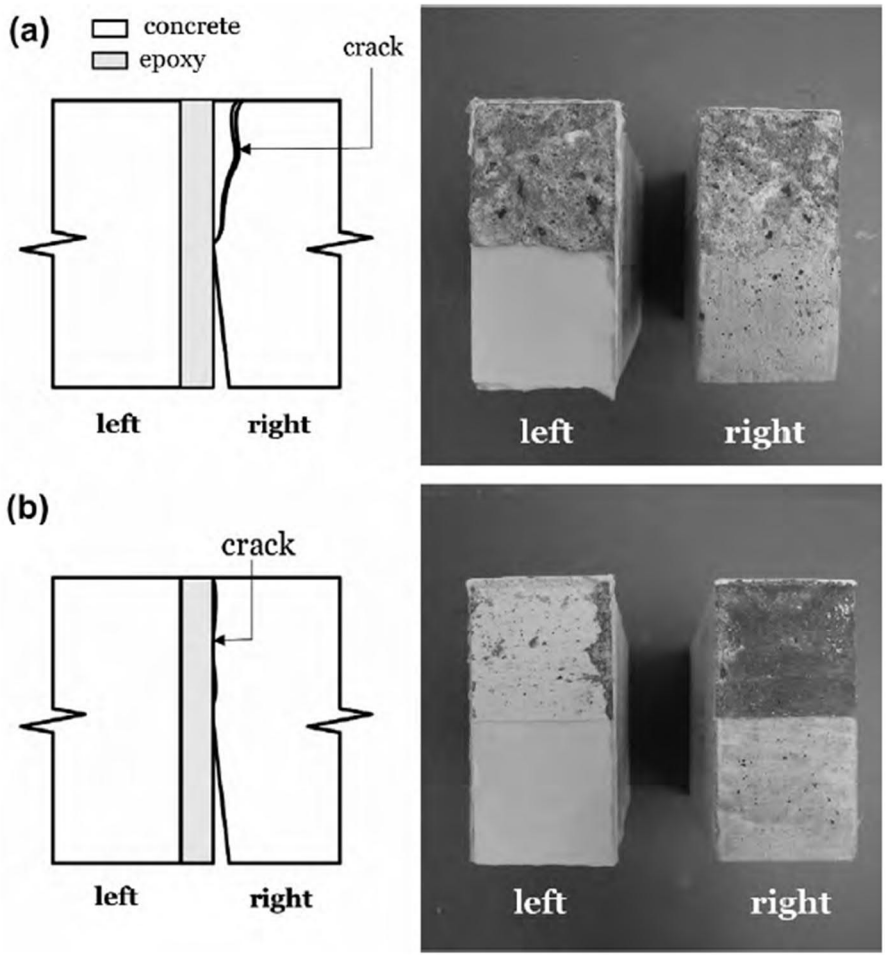

Figure 2.20. (a) Failure mode in dry condition, (b) interface de-bonding after 4 weeks of exposure (Lau and Büyüköztürk, 2010)

The number of studies on durability of bonded concrete to concrete is very limited and they show the negative effect of moisture and high temperature on ultimate strength of epoxy, but there is no certain value of strength reduction and the reason for this degradation is not clear. There is also no study on simultaneous effect of loading and environmental factors.

2.6.2. Durability of epoxy bonded concrete to plate

Tuakta and Büyüköztürk (2011b) tested the residual fracture toughness of bonded FRP to concrete after wetting and drying cycles and found that the degradation of strength reached a certain value: the bond strength cannot decrease after reaching this asymptotic fracture toughness value. Figure 2.21 shows the results of their testing under various temperature and exposure periods. They also concluded that this strength loss is irreversible. However, the testing period sounds very short for making such a conclusion.

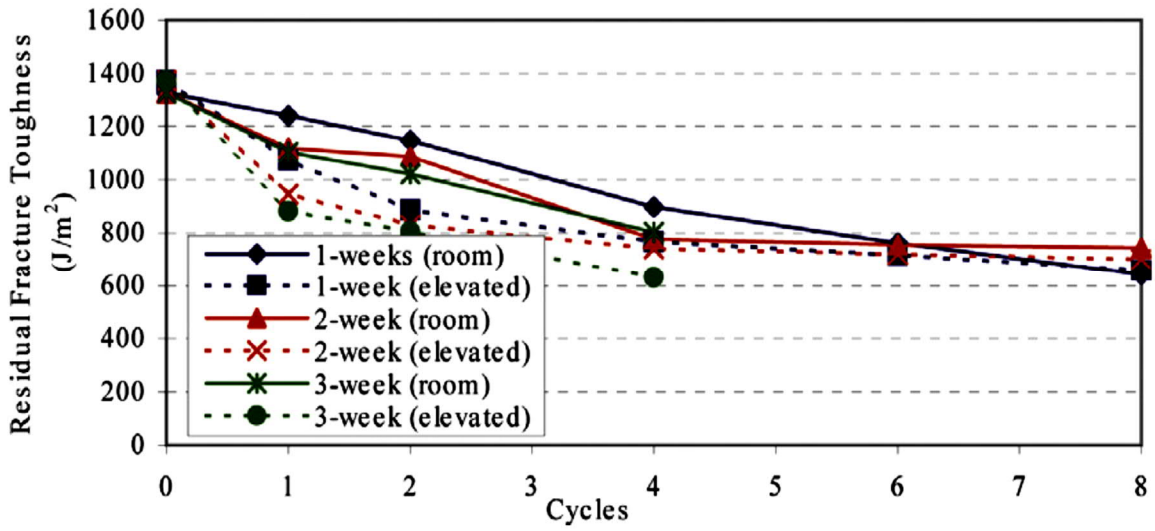

Figure 2.21. Residual fracture toughness of bonded FRP to concrete after wetting and drying cycles (Tuakta and Büyüköztürk, 2011b)

Benzarti et al. (2011) experimental program also showed that increased humidity caused bond strength reduction up to 58% after almost 2 years (see Figure 2.22) and caused more interface and mix failure. Surface preparations had slight positive effect on ultimate strength. Strength reduction and plasticization of bulk epoxy was observed as well. It seems that the main cause of strength reduction was diffusion of moisture in the first layers of concrete or interface.

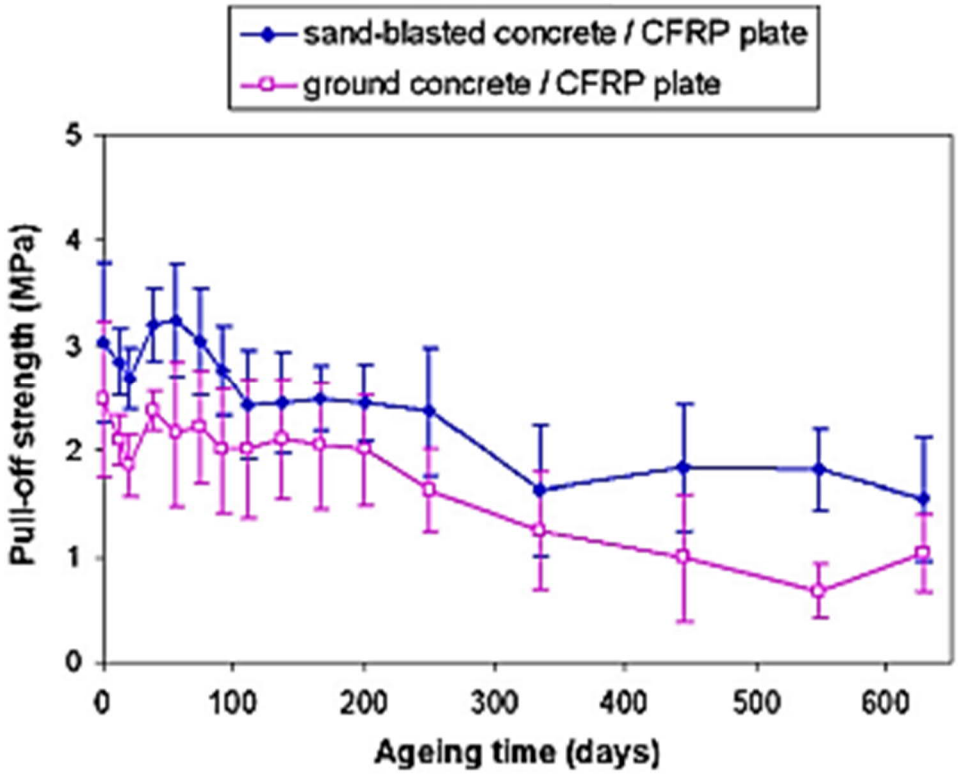

Figure 2.22. Bond strength reduction after 2 years immersion in water (Benzarti et al., 2011)

Regarding longer durability, Nishizaki and Kato (2011) conducted 14 years of outdoor exposure and 6 month immersion tests for carbon fibre sheets glued to concrete, using peel and pull off tests to evaluate the performance after the exposure. The failure modes for pull off test were consistent (failure in the body of concrete) at all times. Peel test had various failure modes and the strength reduced as (see in Figure 2.23). Considering the peel test, it seems to be difficult to conclude anything certain about the bond because the failure modes have been very scattered.

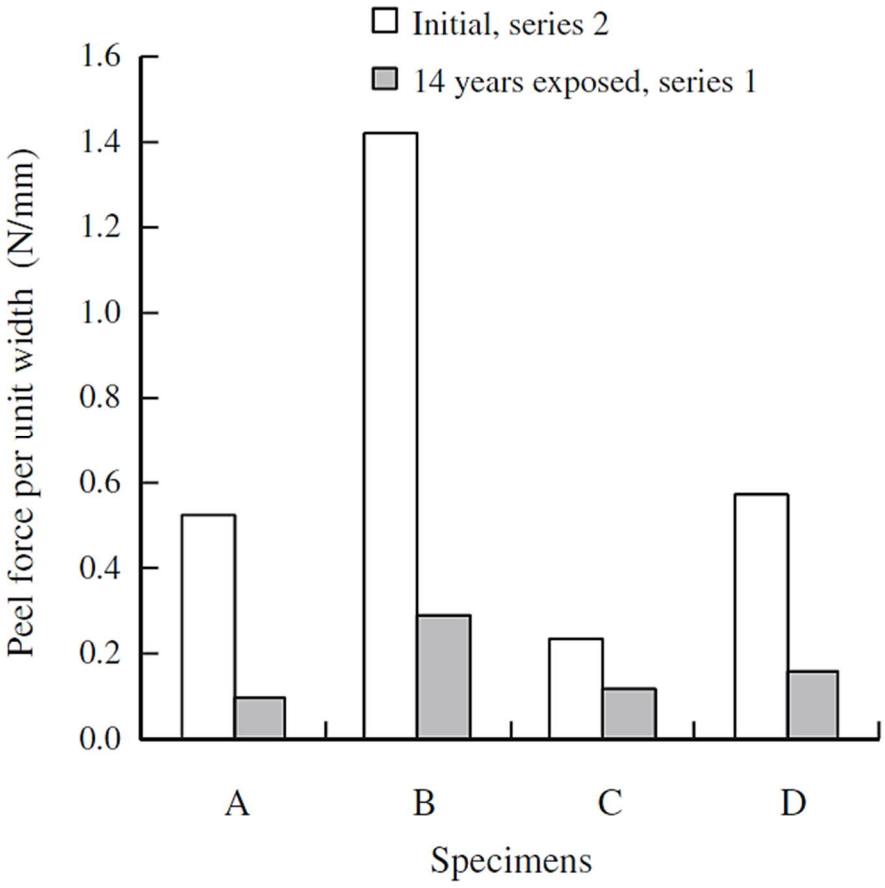

Figure 2.23. Initial and final peel stress after 14 years of exposure in humid environment (Nishizaki and Kato, 2011)

Büyüköztürk et al. (2011) used molecular dynamic techniques to simulate interface de-bonding and explain the reason behind interface degradation in the presence of water using the atomistic approach. As can be seen in Figure 2.24 , the reaction between water molecules and epoxy leads to a weakening of the interface. On the other hand, toughening and plasticization of the first layer of concrete with epoxy and water does not let the initial crack continue through concrete so it propagates at the interface.

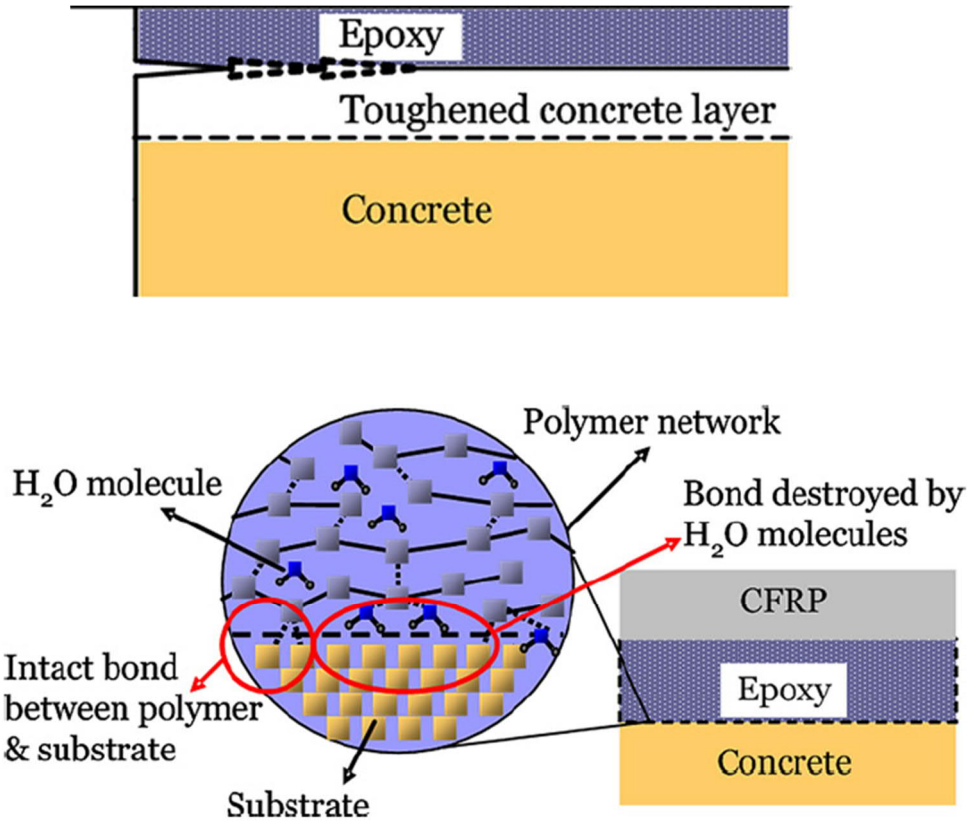

Figure 2.24. Mechanism of weakening of epoxy bond concrete in humid environment (Büyüköztürk et al., 2011).

Tuakta and Büyüköztürk (2011a) proposed a model for predicting the long-term performance of bonded FRP-concrete based on the peel and shear result after cyclic wetting and drying. The longest duration of exposure was 3 weeks. The model predicted the residual fracture toughness according to interface moisture, Equation 2.14 where A and b should be obtained with moisture conditioning tests. They modelled interface moisture for finding the threshold moisture contents (C/C_{th}) with finite element method using Fick's law of diffusion. Accordingly, they modelled the number of wet and drying cycles required for fracture toughness to reach asymptotic value having no further reduction afterward.

$$\Gamma = Ae^{-b\left(\frac{c}{c_{th}}\right)}$$

Equation 2.14 (Tuakta and Büyüköztürk, 2011a)

Tuakta and Büyüköztürk (2011a) is not comprehensive, since they suggested values of A and b for just certain types of epoxies used in their tests, and they do not describe the characteristics of the epoxy. The model also does not consider the effect of stress coupled diffusion while most of the structural bonded concrete sections may be both under loading and wetting-drying conditions.

2.6.2.1. Effect of sustained load coupled with moisture on bonded plate to concrete

Tuakta and Büyüköztürk (2011a) evaluated the effect of sustained load coupled with moisture diffusion. They observed that only certain levels of sustained load can be effective in accelerating degradation of interface and moisture diffusion. There is only a quick increase in deflection at the beginning of loading, but for low level of loading there will be no obvious change while the higher loadings can cause higher deflection and creep crack propagation. However, they admit further research is required in this regard to find a correlation between the effects of stressed coupled diffusion.

Finally, considering the substantial effect of moisture on bonded concrete, Lau (2012) suggested considering 50% reduction in design capacity, use of water proofing spray, and avoiding to use epoxy bonded concrete as the main load carrying structure in a humid environment.

2.6.3. Durability of epoxy bonded plate to plate

The same effect of moisture on epoxy bonded systems has been observed in the case of bonded concrete to plate and more research is available in this regard. For example, Roy et al. (2000) conducted testing after exposure in sea water at 25 ^{0}C and 40 ^{0}C. Aging processes are the same at 25 ^{0}C and 40 ^{0}C, but the aging rate is 10 times higher at 40 degrees. They suggested that the main cause of damage was adhesive swelling.

There are some studies like Knox and Cowling (2000) and Broughton and Mera (1999) on the effect of temperature and humidity on jointed systems and they have shown that hostile environment can cause plasticization and strength reduction of the resins. Bowditch (1996) suggested that plasticization can have a positive effect by reducing residual stresses following curing, but degrading of the interface negate the benefit from plasticisation.

Degradation of bulk epoxy cannot be considered as the main factor for durability performance of the joint. Gledhill and Kinloch (1974) conducted a study on instability of adhesive joints in hostile environments and observed losses in joint strength are caused by adverse effects of water on the interface rather than the bulk adhesive. Furthermore, Bordes et al. (2009) did a study on predicting long term strength of the epoxy joint for steel aged in sea water. The results also suggested that the changes to the joint can be due to plasticization, swelling, or hydrolysis of the epoxy.

2.7. PERFORMANCE OF CONCRETE UNDER CYCLIC LOADING

To have a good understanding of fatigue strength of jointed concrete, it seems essential to review the available knowledge on pure concrete first and then assess and compare the performance of joints based on that. Fatigue strength of concrete is influenced by many factors like type and level of loading, frequency, shape and eccentricity of loading, environmental conditions and material properties.

Regarding material properties, the parameters like aggregates and water cement ratio that affect static strength influence fatigue strength as well (Ahmed et al., 1999). Comparing micro cracking networks under fatigue and static loading shows that the nature of cracking is the same but the fractures under fatigue are better spread and larger in number. Fatigue micro cracking generally develops around the aggregates and cement matrix, which is similar to static loading and they are parallel to compression loading and perpendicular to the tensile loading (Zhang, 1998).

Torrenti et al. (2010) mentioned various methods like acoustic emission, heat dissipation, deformation measurements and volumetric strain to monitor concrete deterioration under fatigue loading. Accordingly, Sakata and Ohtsu (1997) is cited as an example to present the evolution of concrete deterioration using acoustic emission under fatigue loading in three main stages (first 5 to 10% of the total cycles, 80 to 90% of the total cycles and the rest of cycles to failure) shown in Figure 2.25.

In the same manner, evolution of micro cracking causes a decrease of modulus of elasticity and progress of the irrecoverable strain. Figure 2.26 shows these changes corresponding to three main phases that mentioned before. It is assumed that the intact fraction of the concrete sample is resisting the stresses and failure happens when the residual intact area is not enough to resist the applied load (Alliche and Frangois, 1992).

ACI Committee 215R-74 (1997) refers to fatigue strength of concrete in a very simple and vague way. This report claims that fatigue strength of concrete under various loading types like compression, tension, or flexure can be considered as 55% of static strength.

A general statement for fatigue strength of concrete under compression load is Aas-Jakobsen's formula (Equation 2.15), and valid for a range of frequencies from 0.1 to 150 Hz, for stress of up to 80% of static strength, and for 2×10^6 number of cycles. If the stress level is higher, the frequency will become the dominant factor, fewer cycles are required for failure, and the strength expression does not follow this equation.

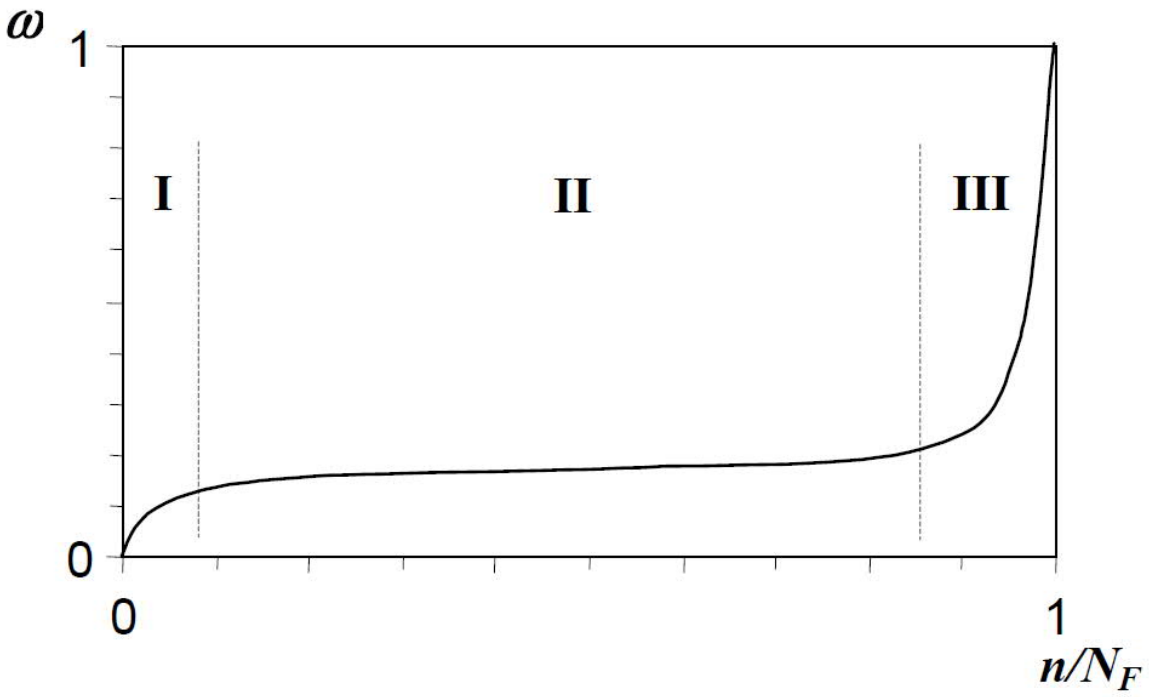

Figure 2.25. Concrete deterioration under fatigue loading (ω: dimensionless index representing the number of acoustic events) ((Sakata and Ohtsu, 1997)

Phase I: (first 5 to 10% of the total cycles): rapid progress of deterioration.

Phase II: (80 to 90% of the total cycles): main part of fatigue life, stabilized rate of deterioration.

Phase III: (the rest of cycles to failure): deterioration acceleration leading to final failure.

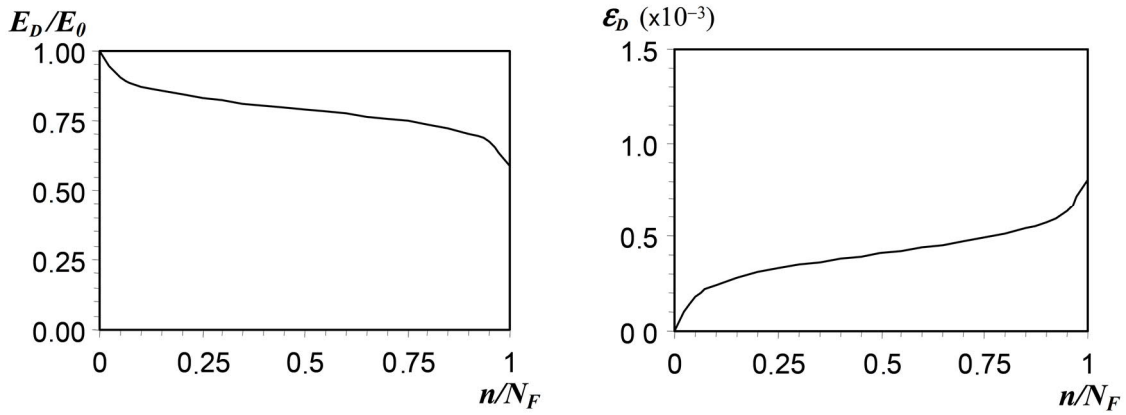

Figure 2.26. Changes of longitudinal modulus and residual strains during fatigue loading (Torrenti et al., 2010)

$$\sigma_{max} / f_c = 1 - \beta(1 - R) \log N_F$$

Equation 2.15 (Torrenti et al., 2010)

σ_{max}: Maximum stress during cycles

σ_{min}: Minimum stress during cycles

f_c: Static strength

$R = \sigma_{min} / \sigma_{max}$: loading ratio

β: material constant, normally 0.0685

N_F: number of cycles to failure

It should be mentioned that fatigue test results are scattered, and it is not precise to present the fatigue strength as an average single value. It is recommended to use probabilistic approaches and present fatigue testing results by Gaussian distribution (Torrenti et al., 2010) . Therefore, the fatigue curve derived from 50% of failure probability is normally used (ACI Committee 215R-74, 1997).

2.7.1. S-N curves

The model of S-N curves was produced to show the fatigue behaviour of materials in a simple, dimensionless way which is neutralized from the properties that influence concrete strength. Wohler curve is used to show the stress versus number of cycles (σ-Nf). There are 3 main types of fatigue that can be introduced, based on the number of cycles:

- Low cycle fatigue: $N_F \leq 10^3$ c
- Large cycle fatigue: $10^3 \leq N_F \leq 10^7$ c
- Very large cycle fatigue: 10^7 c $\leq N_F$

Figure 2.27 shows typical S-N curves for concrete which is S versus logarithmic scale of number of cycles. Accordingly, using S-N curves based on Wohler curve neutralize the effect of static strength to fatigue strength, because S is the ratio of cyclic stress to static strength: $S=\sigma/f_c$ (Torrenti et al., 2010). Three-point bending tests have been conducted for to produce this graph. The loading frequency was 450 cycles per min. The linear lines in the S-N curve show that there is no minimum value of stress below which the fatigue life of concrete become infinite (ACI Committee 215R-74, 1997).

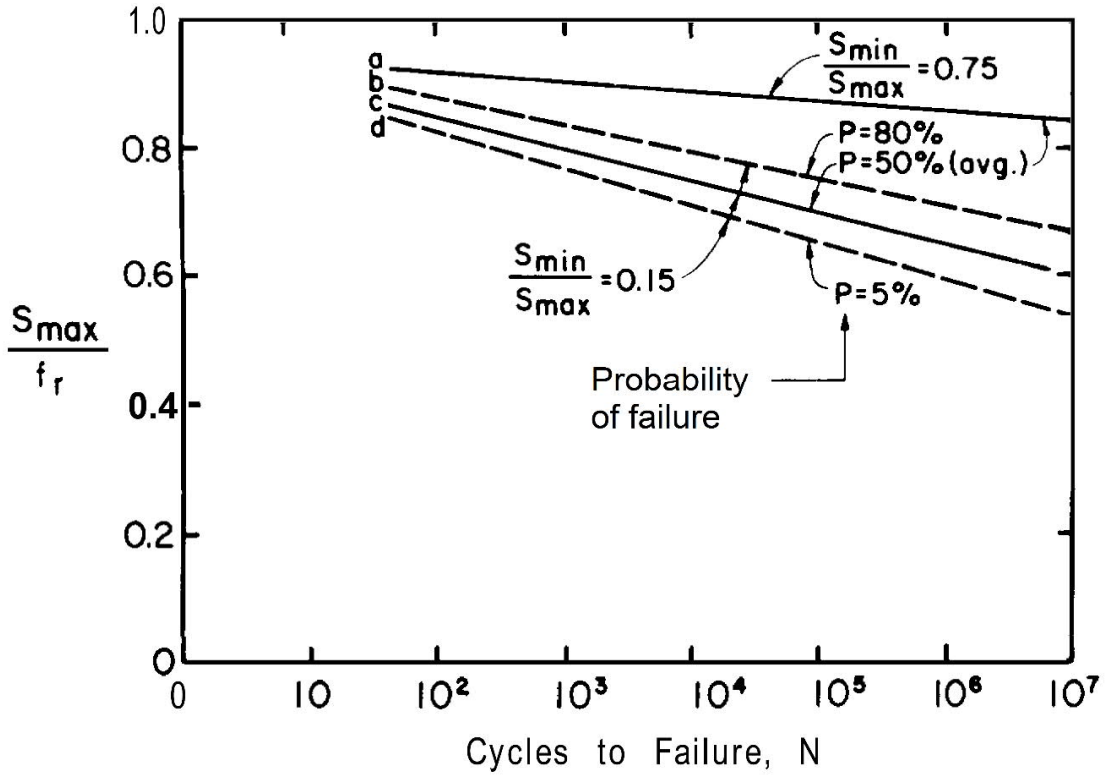

Figure 2.27. Fatigue strength of concrete (ACI Committee 215R-74, 1997)

2.7.2. Fatigue damage accumulation

As discussed in previous sections, the modulus of elasticity decreases during the process of fatigue. It is assumed that modulus of the intact part of the sample is unchanged, and the intact faction is resisting the loading. The ratio of damage can be related to modulus of elasticity with Equation 2.16 where D is the damage ratio, E_0 is the initial modulus and E_D is the actual modulus.

$$D = 1 - \frac{E_D}{E_0}$$

Equation 2.16 (Torrenti et al., 2010)

The nature of fatigue loading in a marine environment is variable, meaning that the cycles have variable levels of loading and amplitude. Palmgren-Miner hypothesis presented in Equation 2.17 is typically used to quantify the level of damage in variable fatigue loading. This hypothesis assumes that loading history consists of several loading cycles, with n_i cycles and σ_i stress level which correspond to conventional S-N curves. When the sum of the series becomes one, failure will occur.

$$\sum_i \delta_i = \sum_i \frac{n_i}{N_{Fi}} = 1$$

Equation 2.17 (Torrenti et al., 2010)

This law is equivalent to the rule of accumulation of damage. This rule assumes that the damage value at the beginning of testing is zero and reaches one at the time of failure. The increase of damage for each sequence of loading is equivalent to the cycle ratio of that sequence. Some experiments have shown that Palmgren-Miner's does not exactly work when the cycle ratio sequences are applied in increasing manner. This means that the sum of cycle ratios to failure will not be one. Accordingly, it can be concluded that the rate of damage evolution can be non-linear. Some modification to Palmgren-Miner law resulted in Equation 2.18, α depends on stress level and decreases by increasing the loading cycle (Torrenti et al., 2010).

$$D = \sum_{i} \left(\frac{n_i}{N_{Fi}}\right)^{\alpha_i} = 1$$

Equation 2.18(Torrenti et al., 2010)

2.7.3. Fatigue design

Offshore codes are the main standards which consider fatigue. Offshore guidelines like DNV-OS-C502 (2010) have some recommendations regarding designing concrete under fatigue loading.

Three following main methods or combination of them are suggested for fatigue design of concrete:

- Fatigue testing
- Linear Cumulative damage analysis in case of variable stress ranges, mean stress and duration.
- Fracture mechanics (strain- energy)

S-N curves and Cumulative linear damage theory ($D=\sum_{i=1}^{k} {n_i}/{N_i} \leq \eta$), as mentioned in previous chapters, are applicable. Table 2-4 mentions η, the limit for cumulative damage limit.

Table 2-4. Limit of cumulative damage ratio DNV-OS-C502 (2010)

No access for inspection and repair	Below or in the splash zone	Above splash zone
0.33	0.5	1.0

S-N curves should consider the various factors like concrete quality, load type (flexure, axial etc.), environmental parameters and combination of loads. Fatigue strength of concrete is expressed by DNV-OS-C502 (2010) :

$$\log_{10} N = C_1 \frac{1 - \frac{\sigma_{max}}{C_5 f_{rd}}}{1 - \frac{\sigma_{min}}{C_5 f_{rd}}}$$

Equation 2.19 DNV-OS-C502 (2010)

C1: Related to the exposure situation (see Table 2-5)

Table 2-5. C1 values according to the exposure condition DNV-OS-C502 (2010)

Exposure condition	C1
Structures in air	12
Structures in water having stress blocks with stress variation in the compression-compression range	10
Structures in water for those stress blocks with stress variation in the compression-tension range	8

C5: This value is 1 for concrete

σ_{max}: Maximum stress during cycles

σ_{min}: Minimum stress during cycles

f_{rd}: Static strength

2.7.4. Summary of factors influencing cyclic loading testing of concrete

The effective factors in fatigue life of concrete can be summarized as follow:

1. ***Number of cycles:*** increasing number of cycles cause reduction of fatigue strength
2. ***Range of stress (R= σ_{min}/ σ_{max})*:** in the range of 15 to 75 %, fatigue strength increases by increasing R, which means a decrease in the difference between maximum and minimum applied load.
3. ***Frequency:*** Frequency range between 70 and 900 cycles per minute is not a sensitive factor for low and moderate loading levels (wave and wind). It can be important when maximum loading is more than 80% of static strength (earthquake or storm). Creep effect becomes important in the case of higher stress levels.
4. ***Load shape:*** rectangular shape of loading leads to fastest fatigue failure and triangle loading shape delays the fatigue failure comparing to sinusoidal cycle shape. The effect of loading shape is more obvious in higher level of loading $S_{max} \geq 0.8$ (Lenschow, 1980)
5. ***Repeated and sustained load:*** if the loading level is very high ($S_{max} \geq 0.8$), sustained loading and rest periods can have a detrimental effect on fatigue strength. Also, there will be an accumulated creep damage which leads to failure in less cycles. However if the sustained load level is low, the fatigue strength tends to increase by having rest periods or sustained loading between cycles (ACI Committee 215R-74, 1997).

6. ***Variable cyclic loading:*** In natural environment, fatigue loading is a combination of random variable level of loading and amplitude. It is not possible to develop S-N curves for cyclic loading with variable parameters based on the spectrum of real loading for each condition. Therefore, Pamgren- Miner law ($\sum(n_i/N_{Fi})=1$) can be used to predict the number of cycles to failure from the S-N curve related to each loading cycle (Torrenti et al., 2010).
7. ***Alternate uniaxial loading:*** there are conflicting ideas in the case of applying compression and tension alternatively in a cyclic manner. The response changes based on the predominant loading.
8. ***Multi axial loading:*** The understanding of fatigue in this case is very limited. Two-dimensional loading can be shear and cyclic normal stress and three dimensional can include transversal confinement like a lateral pressure which typically improve fatigue performance of concrete if there is a cyclic compression loading.
9. ***Torsion (biaxial loading):*** Subramaniam and Shah (2003) conducted a fatigue torsional test on hollow cylinders where a cyclic tension was applied in orthogonal direction and cyclic compression was applied along one principle direction. The test showed that the Uniaxial testing parameters would be enough for considering biaxial fatigue response. It means that torsional stiffness will degrade in the same manner that longitudinal modulus of elasticity degrades in uniaxial testing. Figure 2.28 shows the typical crack growth under torsional loading which follows the same pattern as uniaxial loading.

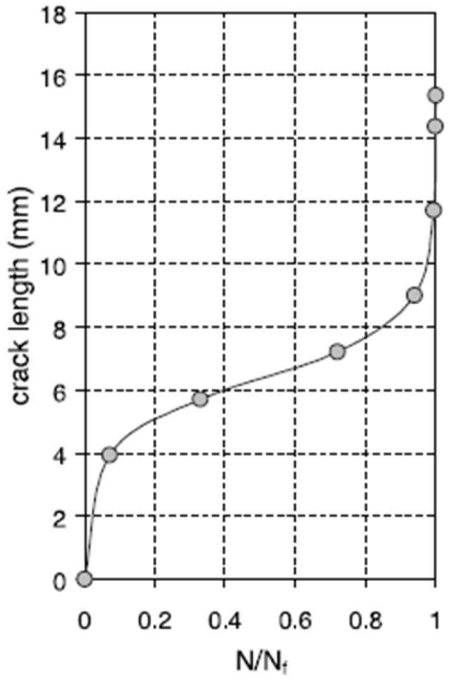

Figure 2.28. Crack growth during torsional fatigue loading (Subramaniam and Shah, 2003)

10. ***Moisture effect:*** Moisture has a negative effect on fatigue performance of concrete due to increasing creep and affecting deformation properties. Drying or saturation phases can have the most harsh effect on concrete under fatigue loading (Waagaard, 1982).
11. ***Temperature effect:*** Fatigue performance of concrete is better in the lower temperatures (Ohlsson et al., 1990).

2.8. PERFORMANCE OF THE JOINTS UNDER CYCLIC LOADING

2.8.1. Plate bonded joints under cyclic loading in the aerospace industry

The main issue in assessing the behaviour of adhesive joints is the numerous factors which affect the crack initiation and propagation. There are two methods for analysing fatigue loading on adhesive joints. The first method is fracture mechanics and the Griffith energy approach. In this method, parameter G is considered as strain energy released rate which is related to crack growth under fatigue loading. The other main method is the study of the classic S-N curves (Stress versus Number of cycles) (De Goeij et al., 1999). There are several experimental and numerical research pieces on fatigue loading with both methods, but they are focused on bonded aluminium or steel in normal and hostile environments.

The UK'S National Physical Laboratory (NPL) conducted a comprehensive program between 1996 and 1999 and published the reports on adhesive joint performance. The institute tested single-lap, scarf and tapered strap joints and determined that linear logarithmic stress ratio versus number of cycles representation can be used for fatigue behaviour of joints. Another comprehensive report was published in 2007 regarding design and testing of bonded and bolted joints. This report is mainly focused on steel, titanium and aluminium. They suggested Equation 2.20 for S-N curves of the adhesive joint and Table 2-6 for K values.

$$\frac{\sigma_{max}}{\sigma_o} = 1 - KlogN_F$$

Equation 2.20 (Broughton, 1999)

Table 2-6. Usual K values for jointed sections (R=0.1, frequency=5 Hz) (Broughton et al., 2007)

Joint configuration	K
Scarf (aluminium adherents with 30° taper)	0.055
Double- Lap (titanium adherents)	0.075
Double-Strap (aluminium adherents)	0.088
Single-Lap (mild steel adherents)	0.093
Double-lap (woven fabric)	0.097
T-joints (direct tension)	0.104
T-peel (mild steel adherents)	0.130

Since bonded plate to plate is not the topic of current research program, the numerous works in this field are not mentioned here. However, the same approaches can be adopted for assessing fatigue behaviour of bonded concrete.

2.8.2. Bonded joints under cyclic loading for civil engineering applications

There are few studies and limited guidance available for fatigue design of bonded concrete segments. CEB-FIP (2012) recommends reduction of 50% of static capacity for fatigue strength if no crack is expected in bonding. In the case of presence of the cracks, 40% reduction for all the mechanisms involved in static resistance is recommended. These suggestions are not developed based on detailed experiments on fatigue performance of bonded concrete and they are expressed for concrete cast at various times. Therefore, they are too simplistic to satisfy the needs of an offshore segmental design.

Randl (2013) reported on ongoing small-scale tests with cracked concrete (see Figure 2.29), but all the tests have reinforcing bar going through the joint, producing more ductile behaviour and the possibility of cracking. The results presented in Figure 2.30 shows that shear strength of cracked concrete interface is lower under cyclic loading.

The main question for fatigue design of bonded concrete is about considering cracking of interface or not. If calculated adhesive resistance is larger than the design shear load, the probability of crack formation at interface is low and behaviour is like that of monolithic concrete.

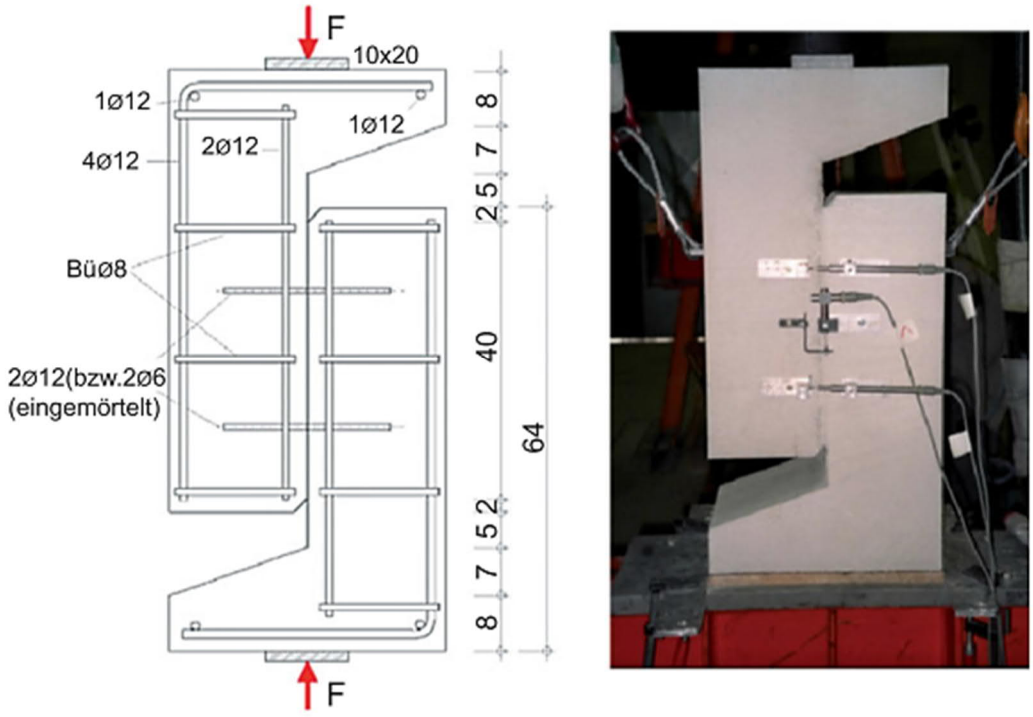

Figure 2.29. Fatigue test set up considering possibility of cracking of the interface (Randl, 2013)

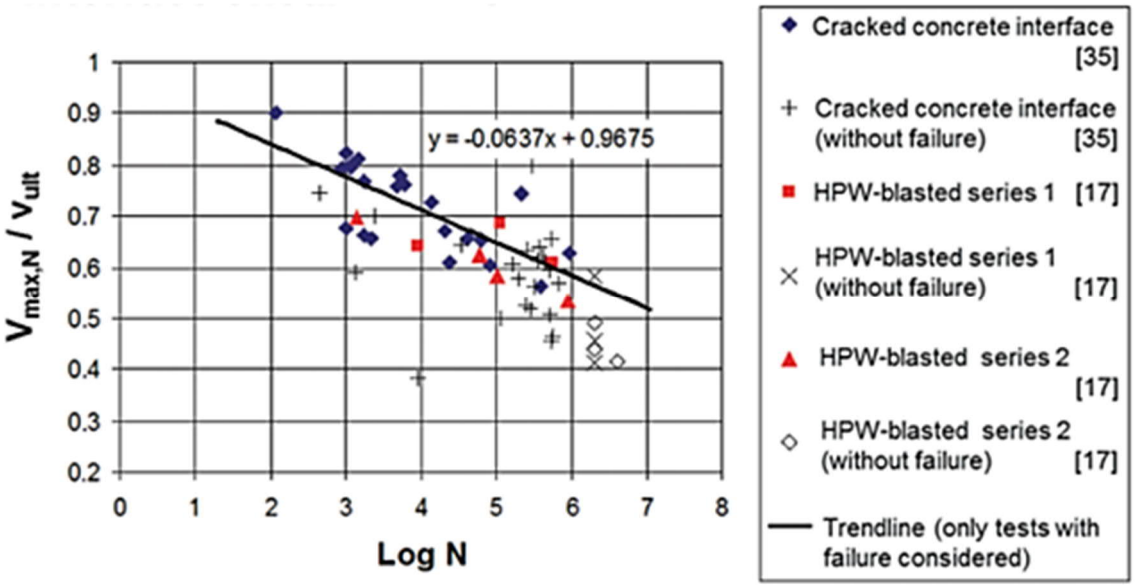

Figure 2.30. Fatigue test results for cracked interface, reinforcement passing through the joint (Randl, 2013), HPW: high pressure water jet for surface roughening

The other sets of related tests are seismic loading experiments which are inherently different from fatigue mainly because of much higher frequency and applied stress. Yet they are mentioned in this section to just review the failure modes. Megally et al. (2002) did a large scale experimental and numerical simulation of post tensioned super structure of bridges. They evaluated seismic performance of bonded precast segmental bridges with and without crossing reinforcements. It should be mentioned that both kind of tests had shear keys. A thin layer of concrete adjacent to the joint failed in epoxy bonded joints and the main flexural crack occurred through shear keys alignment (see Figure 2.31). The cracking pattern is the same for both type of tests under downward loading. Significant opening and closing of the joints happened before failure in both type of joints. However, the permanent deformation and openings are less in the presence of steel reinforcement through the joint. This opening and closing are due to presence of post tensioning in both sets of tests otherwise the epoxy joints without reinforcement passing through are expected to have a brittle failure.

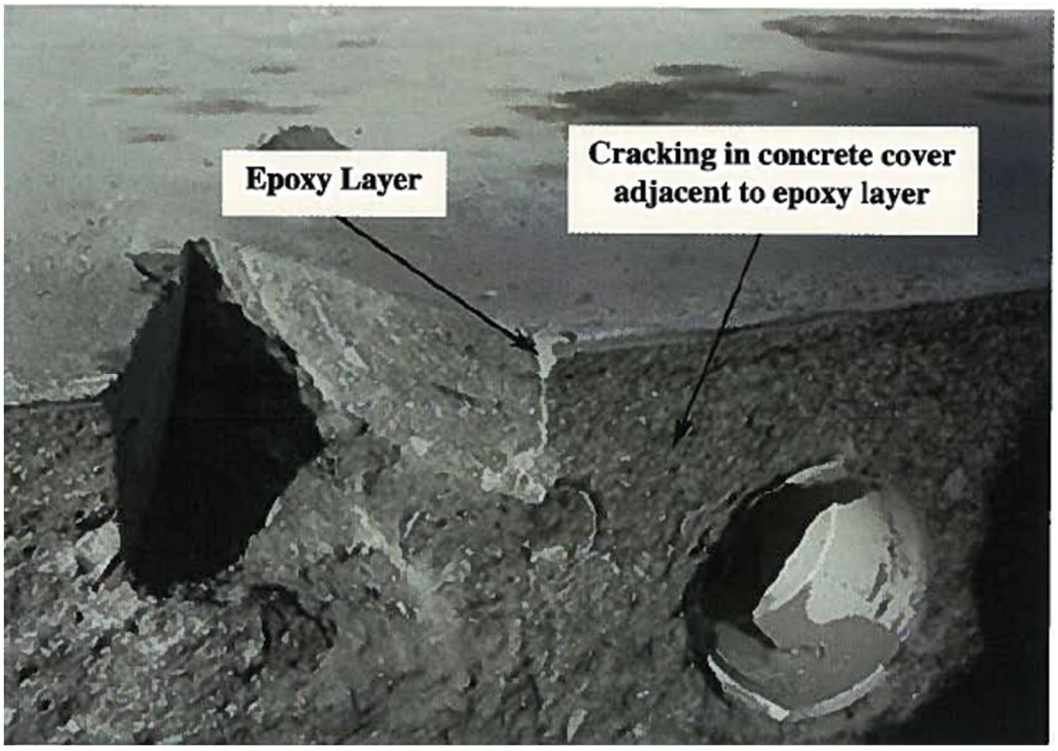

Figure 2.31. Failure of concrete adjacent to the epoxy joint under seismic loading, without any crossing reinforcement (Megally et al., 2002)

Saibabu et al. (2013) also Conducted a scaled experimental program for dry and epoxy joints with shear keys under cyclic and static loading. They applied static load on simply supported post tensioned sections until the first crack occurred, then by displacement control increased the cyclic loading till failure. The results showed better performance of epoxy joint compared to dry joints regarding flexural strength, but both joints behaved monotonically. In both cases, the cyclic loading caused opening and closing of the joints and final crushing of concrete adjacent to the joint. The seismic load failure mode is very similar to static ultimate load failure of the joints but it may not be the same for fatigue.

The Concrete Society (2009) conducted some test on fatigue performance of bonded FRP to concrete. They observed no significant damage for load range between 30% to 60% of the static strength, but major damage occurred at higher load ranges. Therefore, the design should always consider the effect of high stress ratio fatigue.

2.8.3. Meso/micro mechanical behaviour of the joints under cyclic loading

It is generally accepted that quality of concrete, like binder type and water-cement ration, is the most important factor in chloride induced corrosion, but chloride diffusion and corrosion can also be affected considerably by other factors like duration and type of loading (Blagojevic et al., 2012). The first mechanical loading can cause a damage which leads to penetration of ions into the concrete, but this is not representative of the real simultaneous effect of repeated loading and environmental effects. Especially in case of a marine structures, corrosion and cracking under various loading are inter-related phenomena. The importance of wave impact and cyclic loading may also arise by the physical action that can destroy the protective layer of brucite and aragonite on the surface of concrete. Consequently, the chloride ingress pattern may change and corrosion rate may vary.

In the case of the jointed system, there is also the possibility of chloride piping through the joint interface due to opening and closing of that area under cyclic loading or weakening of the bond line. There are different properties of crack like crack width, crack orientation, frequency or density of crack, self-healing, active or dormant crack and crack geometry (shape) that affect the rate of reinforced corrosion with various rates. Coincident cracking and chloride ingress from end of the reinforcing bar can increase severity of corrosion (Arya and Wood, 1995). This situation can happen in jointed systems because chloride may be able to penetrate through interfacial zones and reach the end of reinforcement on the side of the epoxy layer.

The simultaneous damage of cyclic loading and environmental effect is not even well documented in the case of concrete. Consequently, there is no study to consider the chloride movement through the jointed system under cyclic loading. Therefore, the current section can only present the limited data available for healthy and cracked concrete under cyclic loading.

2.8.4. Effect of loading type and crack width on chloride induced corrosion

Jaffer and Hansson (2008) claim that sufficient information is not available regarding initiation and propagation of corrosion by variable loadings which result in opening and closing of cracks. Most of the experiments have been run by three point bending static loading in a salt solution environment while in the real situation of a marine environment, the structures are exposed to variable loads.

Espelid and Nilsen (1998) tested concrete reinforced beams under static and cyclic loading in simulated submerged seawater conditions. They observed that corrosion in crack regions does not have considerable differences compared to other parts of concrete. They attributed these observations to lack of oxygen in seawater and concluded that type of loading makes no difference in corrosion state of concrete.

While chloride penetration and corrosion initiation and propagation for intact concrete just depends on permeability properties of concrete and the corrosion resistance of the bars, cracking can provide a path for penetrating more water, oxygen, or chloride to the bars. Otieno et al. (2010) cited Francois

and Maso (1988) experimental results which indicate that crack width in the range 0.05-0.5 mm directly increase chloride penetration. However, Otieno et al. (2010) conducted an experiment to evaluate corrosion in cracked and un-cracked concrete as well as the effect of reopening of the cracks. The results showed that crack width, effective depth, orientation in respect to steel, frequency, and self-healing properties are effective in corrosion rate. They showed that crack width between 0.4 mm and 0.7 mm does not have significant effect on corrosion rate. Küter et al. (2005) also asserted that frequency and rate of loading are more effective than the crack width, and chloride ingress increase especially at the crack tip in case of cyclic loading. Overall, assigning a crack threshold in the codes without taking in to account the loading type lead to a conservative design (Blagojevic et al., 2012).

Ahn and Reddy (2001) stated that cyclic loading accelerates the process of corrosion in reinforced concrete. They accelerated corrosion in a tidal zone environment and used Galvano-static corrosion techniques for monitoring. They observed that the middle maximum moment region exhibits more corrosion products compared to other parts. The corrosion damage close to the transverse cracks is larger due to the larger negative half-cell potential measured. Yao et al. (2017) also indicate the importance of loading on chloride induced corrosion and provides a test method for measuring the effect of environmental actions and sustained load.

Jaffer and Hansson (2008) also designed an experiment to apply three-point bending loads and exposed them to chloride solution. They used potentiostatic Linear Polarization Resistance (LPR) and potentiodynamic (cyclic) polarization techniques to measure microcell corrosion. Also, electrochemical noise measurement was used to monitor macro cell corrosion. The result of their study showed that concrete type and exposure condition can be more effective than type of loading on chloride induced corrosion.

It can be concluded that many factors like amount of oxygen, loading type, concrete quality, width and direction of the crack can affect chloride induced corrosion. The author could not find any research to cover and assess all these factors together. In the case of the current project, the complexity is even higher due to the presence of joint and lack of any data about the effect of the epoxy layer and cracking in the unreinforced area on chloride ingress rate.

2.9. CONCLUSIONS

Increasing demand for reducing the costs of wave energy production led to the concept of floating offshore structure. Segmental concrete construction can be considered as one of the cheapest and fastest methods. Marine concrete has a long history and durability of concrete segments are secured if they are designed based on standard specifications and using supplementary cementitious materials. The most challenging part of this construction method is the epoxy joints between concrete segments or concrete and steel end plates.

The main proceedings on epoxy joints are related to the aerospace industries with very thin joints of two plates, bridge construction with the presence of pre-stressing or post-tensioning, casting fresh concrete on old concrete, and structural repair or retrofitting with bonded FRP/steel to concrete. Although none of these works exactly match epoxy bonded segmental construction for a marine environment, they are important to make a base for an understanding of behaviour of joint and find the gap of knowledge of epoxy bonded concrete for a floating structure.

Reviewing macro scale behavior of epoxy bonded concrete to concrete in static situation revealed that shear keys are not necessary for transferring shear stress between segments and epoxy joints show stronger and more brittle failure even without shear keys. However, the role of shear keys in special loading cases like torsion is not clear. Moreover, there is not an agreement on the importance of compression on the joints. Since there are many factors like surface roughness, joint thickness and most importantly presence of defects affecting the tests, vast number of shear and tension tests have shown scatter data and different failure modes. Generally, rougher surface leads to higher bond strength but the extent of this effect is not clear in the presence of adhesive. Thicker joints show higher interface stress and lower average stress but it seems stiffness of the substrates is more important because stiffer substrates can provide more constraint and stress concentration in the middle of the adhesive. Design models also have deficiencies because they all rely on reinforcement passing through the joint, and they are devised based on small sample testing. Considering all the tests and no certain quantification for the macro scale bond strength of epoxy bonded concrete, perhaps as Tuakta and Büyüköztürk (2011b) concluded for bonded FRP to concrete, the failure is local and initiates with an existing defect. Therefore, bond strength should be presented with fracture toughness rather than global strength.

Epoxy bonded concrete to steel normally fails in the thin layer of concrete adjacent to the joint. There are many models for bond length and bond strength of bonded FRP to concrete but they may not be applicable for steel mainly due to different stiffness of the plates. Furthermore, bonded FRP has been used for retrofitting with very thin layers of epoxy so adhesive properties are not really considered while it can be important for bonding an end steel plate with a thicker epoxy layer.

Regarding meso/ micro scale mechanical behavior of joints in a static situation, the majority of the literature showed reduction of ultimate bond strength and failure mode change in temperatures higher than 40^0 C, and in a humid environment, but the amount and reason of this reduction is not well defined. Furthermore, the coupled effect of loading and a hostile environment was not addressed by the researchers. 50% -60% of bond strength reduction is suggested for designing epoxy bonds in a humid environment, but this claim is not strongly supported by the research.

The literature covered basic knowledge of concrete under fatigue loading. Bonded epoxy is not sufficiently studied under fatigue. Simplistically, if no crack is expected in good bonding, approximately 50% of static capacity can be considered for fatigue strength. If there is any crack, 40% reduction of all the mechanisms involved in static resistance is recommended. Yet even these recommendations are based on samples with reinforcement going through the joint. Other related studies are some seismic loading experiments for bridge construction. It could be seen that failure of first layer of concrete has happened in all cases even in the presence of shear keys but the failure mechanisms under fatigue loading with lower frequency and lower stress can be different.

The author could not find any published work regarding meso/micro mechanical behaviour of epoxy bonded concrete, especially chloride and water penetration through the joint under cyclic loading conditions. However, researches on chloride diffusion in reinforced concrete have highlighted the complexity of this issue and its dependency on type of concrete, loading condition and crack width. It should be mentioned that the studies in this field are very limited.

Overall, the subject of this study is very broad and the literature tried to cover many aspects from macro mechanical to micro mechanical aspects under different loading conditions. It was clear that there is deficiency of knowledge in all aspects of epoxy bonded concrete in a marine environment especially stress transfer through the joint, effect of special loadings like torsion, environmental effects and simultaneous effects of fatigue and the marine environment. Therefore, this research program looks at performance of epoxy bonded concrete under static and cyclic loading in sweater salt solution to find out if the epoxy bonded segmental construction is a suitable option for a floating structure like Pelamis wave energy converter.

3. EXPERIMENTAL PROGRAM, MATERIALS AND TEST METHODS

3.1. INTRODUCTION

The research approach of the current project is based on physical modelling due to deficiency in thorough understanding of epoxy bonded concrete in the marine environment and subsequent lack of input parameters for numerical modelling of performance characteristics. A range of experiments were designed and conducted for static and cyclic loading situations. Macro to micro mechanical behaviour of epoxy bonded concrete, and simultaneous impact of mechanical loading accompanied with exposure to cycles of wetting and drying in artificial seawater salt solution were assessed.

The project comprised of three main phases. This Chapter presents a summary of the research approach and methodology of each phase following by the details of the test methods.

Figure 3.1 summarizes the main phases of the project and their succeeding parts. Established test methods for some aspects of the study were lacking, so test method designs were an important part of the research.

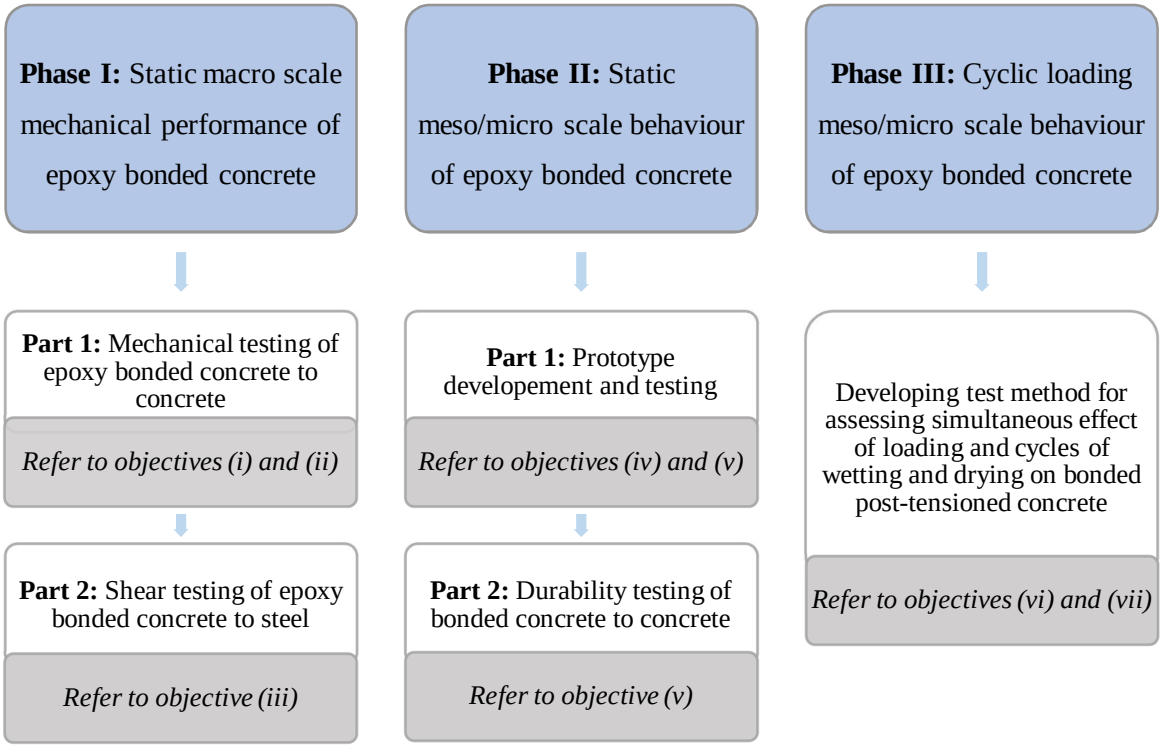

Figure 3.1. The main Phases of the research project

This Chapter is structured by firstly explaining each phase of the research program. The area of this study is very broad and there are many interconnected parameters affecting the performance of the epoxy bonded concrete system. The important influencing parameters are extracted from the

literature and summarized in the flow charts of each research program Phase. Secondly, the material specifications are detailed. Finally, details of each test method for each specific Phase are described.

3.2. PHASE I: STATIC MACRO SCALE MECHANICAL PERFORMANCE OF EPOXY BONDED CONCRETE

Phase I examined macro scale behaviour of joints through conducting shear/compression, tension, and torsion testing in Part 1. Variables such as surface preparation, joint thickness, and epoxy type were tested throughout Part 1. Part 2 evaluated shear capacity of bonded concrete to steel.

3.2.1. Phase I: Part 1: Mechanical testing of epoxy bonded concrete to concrete

The literature review revealed the numerous variables affecting the performance of epoxy bonded concrete. Phase I: Part 1 considered the main variables and their inter-connected effects in order to identify the sensitivity of the joint performance to each parameter and quantify the joint strength accordingly. Figure 3.2 summarizes the main parameters considered in Phase I: Part 1.

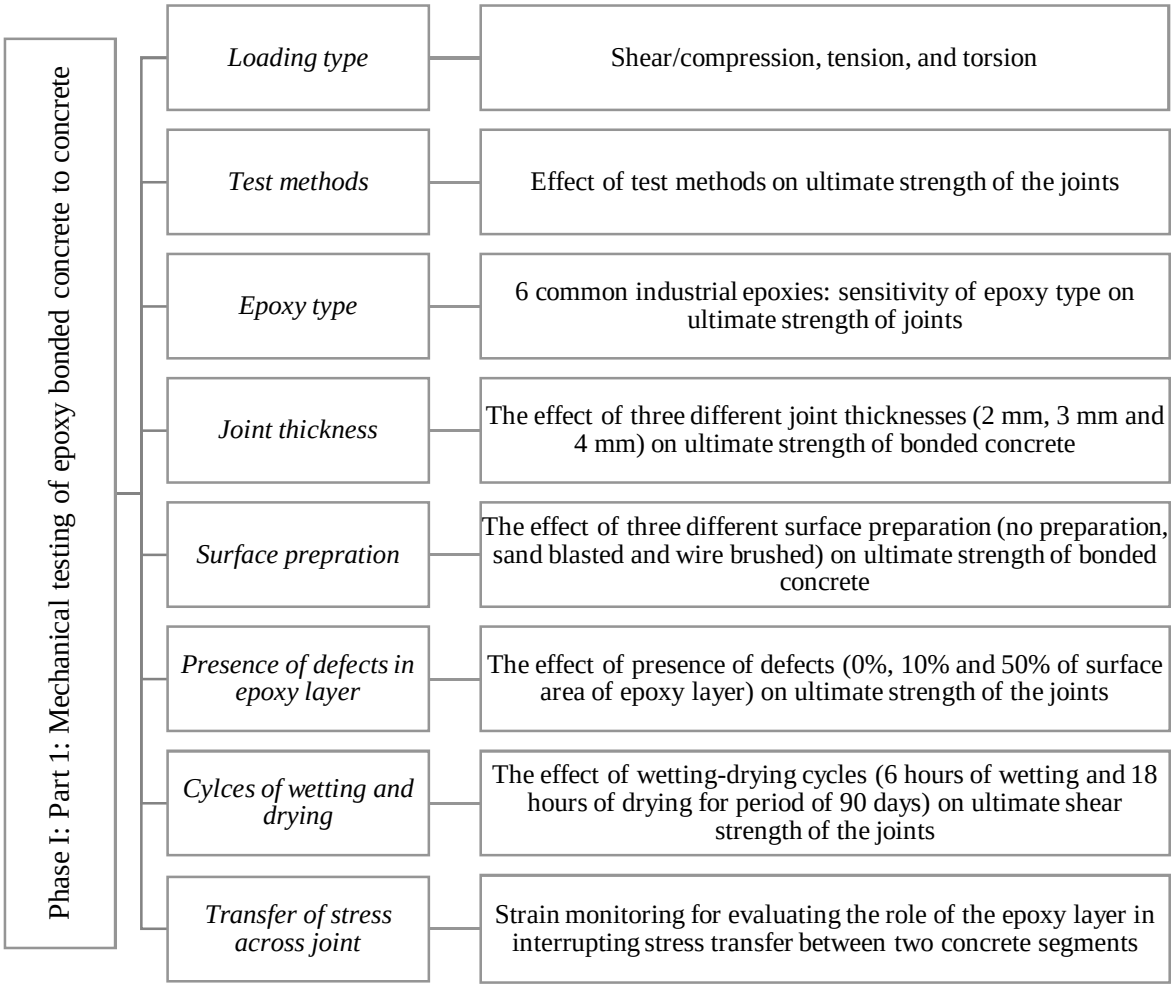

Figure 3.2. Main aspects of the research program in Phase I: Part 1: Mechanical testing of epoxy bonded concrete to concrete

This study used the standard test method for slant shear BS EN 12615 (1999), and a bi-surface shear test devised by Momayez et al. (2005) for assessing bonded joint behaviour. Moreover, the split cylinder test BS EN 12390-6 (2009e) and flexural strength tests BS EN 12390-5 (2009d) were modified for bonded specimens. Two types of shear and tension tests were used in this study because each test examined the shear or tensile performance of the joints in a different loading state. The combined results provided a comprehensive insight into the joint mechanics. In addition, an innovative method was developed for testing the joints under torsion. This method is explained in detail in the test methodology section.

The test programme summarized in Table 3-1 gives detail of joint thickness (2 mm, 3 mm and 4 mm), substrate surface preparation (No Preparation (NP), Sand Blasting (SB) and Wire Brushing (WB)) and the corresponding test methods (slant shear, bi-surface shear, split cylinder, flexure and torsion). Joint thicknesses were based on those typically used in industry (Hewson, 2003).

Table 3-1. Phase I: Part 1: Summary of mechanical testing of epoxy bonded concrete to concrete (concrete Mix 1 in Table 3-9)

Epoxy code[1]	Test method	Nominal Joint Thickness			Cycle of wetting & drying	DIC[8]
		2 mm	3 mm	4 mm		
A	Slant Shear	3NP[2], 3SB[3], 3WB[4]			-[5]	-
	Bi-Surface shear	3NP			-	-
	Bi-Surface shear, Defect[6], UPV[7]	3NP (90% defect), 3NP (50% defect)			-	-
	Split cylinder	6NP, 3SB, 3WB		6NP,2SB, 3WB	-	-
	Flexure	3NP, 3SB, 3WB			-	-
B	Slant Shear	-	1NP,4SB	1NP, 6SB	3 mm 1NP,4SB	3 mm - 1SB
	Bi-Surface shear	-	1NP, 5SB		3 mm 1NP,6SB	
	Split cylinder	-	2SB	-	-	
	Flexure	-	3SB	-	-	
C	Slant Shear	-	3SB		[1] Epoxy codes detailed in Table 3-7 and Table 3-8 [2]NP - No surface Preparation with 3 samples tested [3]SB-Sand Blast surface preparation with 3 samples tested [4]WB-Wire Brush surface preparation with 3 samples tested [5] - not tested [6] Defect (in %) induced by reducing epoxy coverage on joint [7] Ultrasonic Pulse Velocity [8] Digital Image Correlation	
	Bi-Surface shear	-	3SB			
D	Slant Shear	-	3SB	-		
	Bi-Surface shear	-	4SB	-		
E	Slant Shear	-	2SB	-		
	Bi-Surface shear	-	2SB	-		
F	Slant Shear	-	2SB	-		

Table 3-1 also shows the number of specimens tested, for example, 3NP, 3SB, 3WB means that 3 untreated (NP), 3 sand blasted (SB) and 3 wire brushed (WB) specimens were tested. Six specimens of each joint thickness with an induced 90% and 50% surface area defect were also examined using the bi-surface shear test and prior to testing, these specimens were inspected using Ultrasonic Pulse Velocity (UPV) (2004d). Only specimens with 3 mm thick joints were used for cycles of wetting and drying in seawater and for strain monitoring using Digital Image Correlation (DIC). The concrete mix used in this Phase was according to concrete Mix 1 (see Table 3-9),

3.2.1. Phase I: Part 2: Shear testing of epoxy bonded concrete to steel

The concrete bonded to steel or any other plate fails in a thin layer of concrete adjacent to the joint. However, the ultimate failure mode is complicated when anti-corrosion paint is used to protect steel in corrosive environment. Moreover, the effect of applying fresh concrete with epoxy on the steel plate on shear capacity pf the bond is not addressed in the literature. summary of the main variables considered in this Part are presented in Figure 3.3.

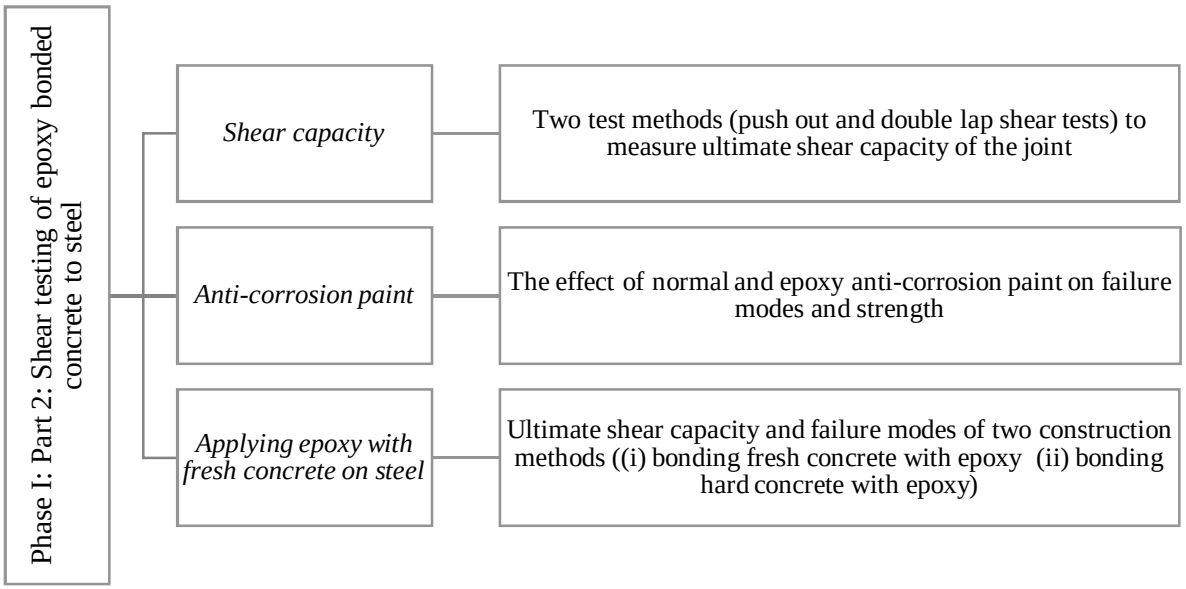

Figure 3.3. Main variables in Phase I: Part 2: Shear testing of epoxy bonded concrete to steel

The main reason of using concrete for WECs has been for reducing the cost; hence, using stainless steel does not support this main intention. GFRP is also more expensive and has just been used as retrofitting and repair of structures, so using it as the main loading bearing structural element in the marine environment also needs more research. Therefore, Phase I: Part 2 tried to test various types of anti-corrosion paint and their effects on failure modes and consequent deformation. A push out test suggested by Si Larbi et al. (2007) was used to assess the effect of paint on failure mode and ultimate strength. This method was adopted because the concrete segments do not have any reinforcement (like critical area of the jointed sections in Figure 1.1). Moreover, Si Larbi et al. (2007) claimed that the chosen geometry conforms to Eurocode 4 (2004c) requirements for connecting steel

plates to concrete slabs. It should be mentioned that this code does not directly address epoxy bonded sections. Perhaps, Si Larbi et al. (2007) meant the same geometrical precautions for avoiding imperfections. Therefore, the chosen geometry by Si Larbi et al. (2007) was adopted in the current project as well.

Although Tuakta and Büyüköztürk (2011b), Benzarti et al. (2011), and Nishizaki and Kato (2011) did extensive research about long term behaviour or epoxy bonded plates (refer to section 2.6.2), the effect of applying fresh concrete on the steel plate on ultimate shear capacity of bonded system and long term consequences of this method is not covered by the researchers. This method have the problem of sensitivity of epoxies to presence of humidity at the time of application, while higher aggregate interlocking may happen when the fresh concrete is applied with epoxy. Therefore, A double lap shear test equipment was designed according to Barnes and Mays (2001) method to examine the difference between shear strength of epoxy bonded fresh concrete to steel and epoxy bonded hard concrete to steel. Barnes and Mays (2001) suggestions for optimum bond length and geometry were taken into account.

Table 3-2 summarizes the experimental programme in Phase I: Part 2. All the surfaces of steel and concrete were sand blasted prior to applying epoxy. The number of samples tested for each condition is mentioned in Table 3-2 . The concrete mix in this Phase is according to Mix 1 (see Table 3-9)

Table 3-2. Summary of experimental programme in Phase I: Part 2: Shear testing of epoxy bonded concrete to steel (concrete Mix 1 in Table 3-9)

Epoxy[(1)] code	Test methods	Joint length (mm)	Anti-corrosion paint			Fresh concrete & epoxy	LVDT[(2)]
			Non	Normal	Epoxy		
B	Push out	100	3SB[(3)]	3SB	3SB	_	3SB
B	Double lap	200	_	_	3SB	1SB	_

(1) Epoxy codes detailed in Table 3-7 and Table 3-8,

(2) Linear Variable Differential Transformer,

(3) Number of samples tested and surface preparation technique of Sand Blasting (SB),

3.3. PHASE II: STATIC MESO/MICRO SCALE BEHAVIOUR OF EPOXY BONDED CONCRETE

Phase II focused on meso/micro scale mechanical behaviour of epoxy bonded concrete after exposure in seawater. Phase II is also categorized into two parts. Part 1 focused on constructing and floating a concrete structure prototype in accordance to Pelamis WEC, and Part 2 assessed chloride and water ingress through the bond line of epoxy and concrete with samples made in the laboratory.

3.3.1. Phase II: Part 1: Prototype development and testing

Phase II focused on durability and floatation of a Pelamis WEC prototype in order to evaluate challenges involved in buoyancy calculations, casting, construction, quality control, and maintenance of a segmented floating concrete structure accompanied with steel end plates. Hence, a scaled (1:11) unreinforced prototype of Pelamis was constructed to investigate durability of flat-face epoxy bonded concrete within a post-tensioned unit in order to assess the degree of damage and chloride ingress in the jointed area after 2 years of exposure in seawater salt solution. Figure 3.4 summarizes the main aspects of research in Phase II: Part 1.

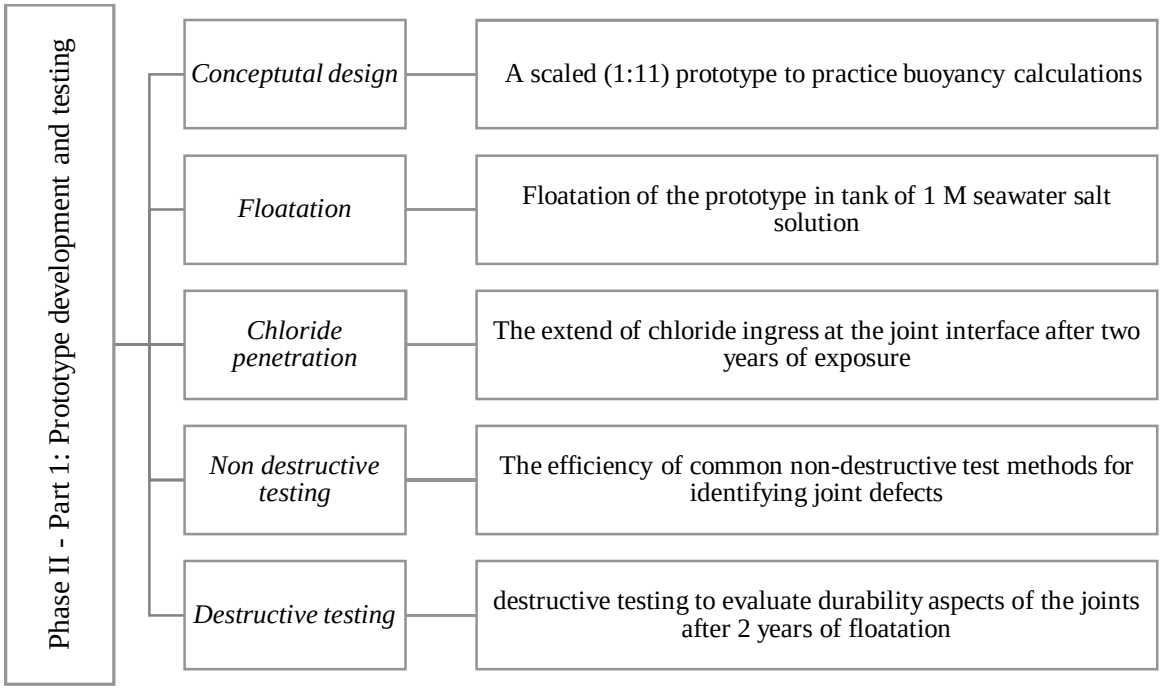

Figure 3.4. Main aspect of research in Phase II: Part 1: Scaled (1:11) WEC prototype development and testing

The prototype segments were cast in a local precast factory and assembled at University of Dundee. The initial base examination was conducted, and the tube floated at 55% buoyancy level in a 1 M seawater salt solution tank for the period of 1 year. After 1 year, the tube was tested again and continued its floatation on the west coast of Scotland. The prototype was back in Dundee for the final

examination After 1 more year of exposure in west coast of Scotland. The summary of tests conducted in these three main stages is mentioned in Table 3-3.

Table 3-3. Dundee prototype, summary of testing procedure in Phase II: Part 1: Scaled (1:11) WEC prototype (concrete Mix 2 in Table 3-9)

[3] Epoxy type	Testing stage	Non-destructive testing				Chloride analysis		
		CT scan	Hydrogen sniffing	UPV	Rebound hammer	XRF	Titration	$AgNO_3$ Spray
A	Stage 1[1]	-	✓	✓	✓	-	-	-
	Stage 2 [2]	-	-	✓	✓	-	-	-
	Stage 3[3]	✓	-	✓	✓	✓	✓	✓

[1]Base line assessment,[2]After 12 months exposure in sweater salt solution tank, [3] At the end of second year i.e. after 12 months exposure in west coast of Scotland,[3] Epoxy codes detailed in Table 3-7 and Table 3-8

3.3.2. Phase II: Part 2: Durability testing of bonded concrete to concrete

Chloride diffusion and water ingress in static state was the focus of Phase II: Part 2. The main concern was the chloride and water penetration through the interface and reaching the reinforcement on the side of the joint. Therefore, several chloride and water penetration tests were conducted considering various variables mentioned in Figure 3.5.

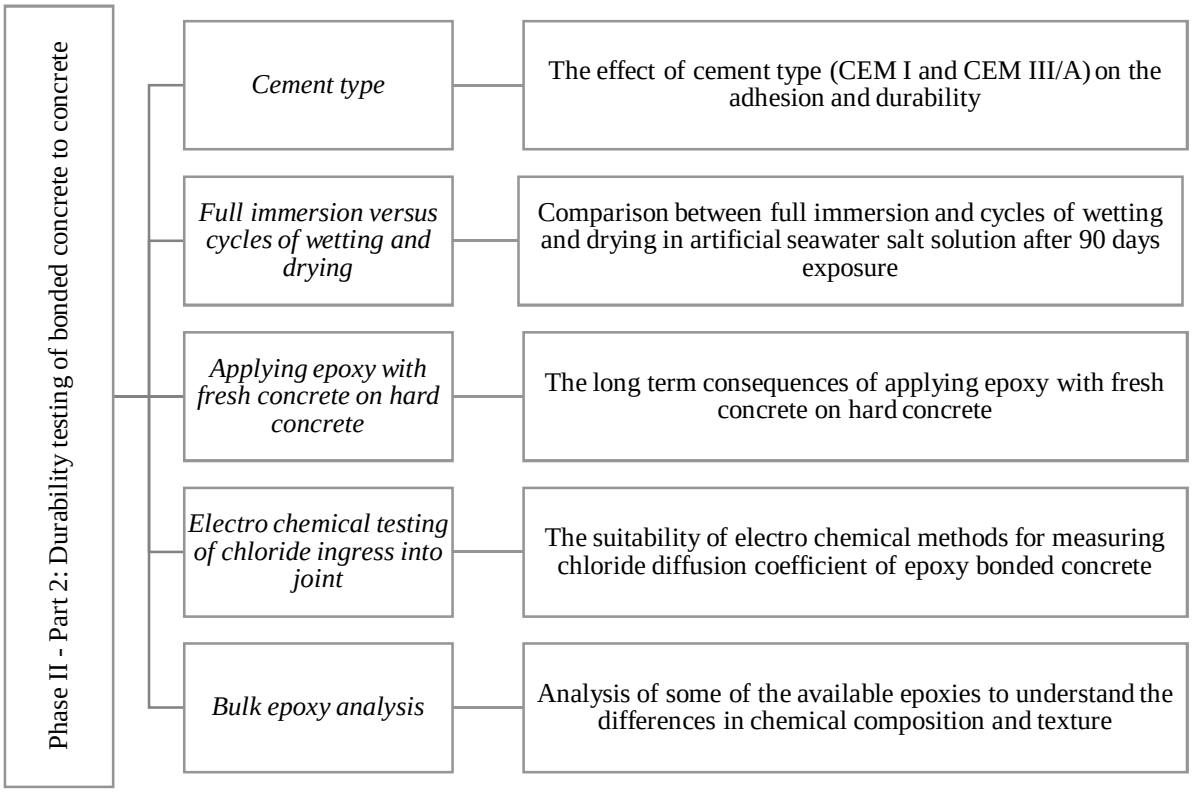

Figure 3.5. Main variables in Phase II: Part 2: Durability testing of bonded concrete to concrete

Table 3-4 summarizes the testing programme in Phase II: Part 2. Firstly, BS EN 12390-8 (2009f) for testing water penetration into concrete was conducted on epoxy bonded samples under two exposure conditions: (i) full immersion for 90 days and (ii) cycles of wetting and drying for 90 days, with two different concrete Mix 1 and Mix 3 (Table 3-9) , and two construction methods (i) applying fresh concrete with epoxy, (ii) epoxy bonding hard concrete. Water penetration tests were conducted for 10 samples of each condition. Secondly, initial Surface Absorption Test (ISAT) BS 1881-208 (1996) was adopted for comparison between the surface absorption of pure concrete and bonded concrete. The testing program continued by natural chloride diffusion according to CEN TS 12390-11(2010) for full immersion and cycles of wetting and drying conditions as well as the two different construction methods mentioned above. This test was also conducted for 10 samples of each case. Moreover, accelerated chloride diffusion electro chemical tests of NT Build 492 (1999) and Multi regime method invented by Castellote et al. (2001) were used. Three samples were tested with these accelerated methods. Finally, the bulk epoxy was analysed by Scanning Electron Microscope (SEM) and Energy-Dispersive X-ray spectroscopy (EDX) for determining the major differences in composition and structure of the epoxies. ASTM D638 Standard (2014) test method for tensile properties of plastics was performed after 3 months of exposure under cycles of wetting and drying.

Table 3-4. Summary of experimental programme of Phase II: Part 2 (all the joints had 3 mm thickness and the surfaces were sand blasted)

Epoxy code[1]	Test method	CEM III/A[2] (50% GGBS)		CEMI[5]	
		Hard/hard[3]	Hard/fresh[4]	Hard/hard[3]	Hard/fresh[4]
B	Water penetration	Full immersion & cycles of wetting and drying	Full immersion & cycles of wetting and drying	Full immersion & cycles of wetting and drying	-[6]
A	ISAT	✓	-	-	-
A, B	Natural chloride diffusion	Full immersion & cycles of wetting and drying	Full immersion & cycles of wetting and drying	Full immersion & cycles of wetting and drying	-
A	NT Build492	✓	-	-	-
A	Multi regime	✓	-	-	-
A, B,C	SEM & EDX	-	-	-	-
B	ASTM D638	-	-	-	-

[1] Epoxy codes detailed in Table 3-7 and Table 3-8, [2] Concrete Mix 1 in Table 3-9, [3]Hard concrete bonded by epoxy , [4]Hard concrete bonded by epoxy to fresh concrete, [5] Concrete Mix 3 Table 3-9, [6]not tested

3.4. PHASE III: CYCLIC LOADING MESO/MICRO SCALE BEHAVIOUR OF EPOXY BONDED CONCRETE

Phase III explored the effect of simultaneous mechanical loading and cycles of wetting and drying on epoxy bonded post-tensioned concrete. The experimental programme was continued in this phase by conducting fatigue testing on jointed sections. Post-tensioned epoxy bonded concrete beams were exposed to cycles of wetting and drying in artificial seawater salt solution. The rate of chloride diffusion and microstructural changes were monitored under various loading states. Figure 3.6 summarizes the key factors considered in Phase III.

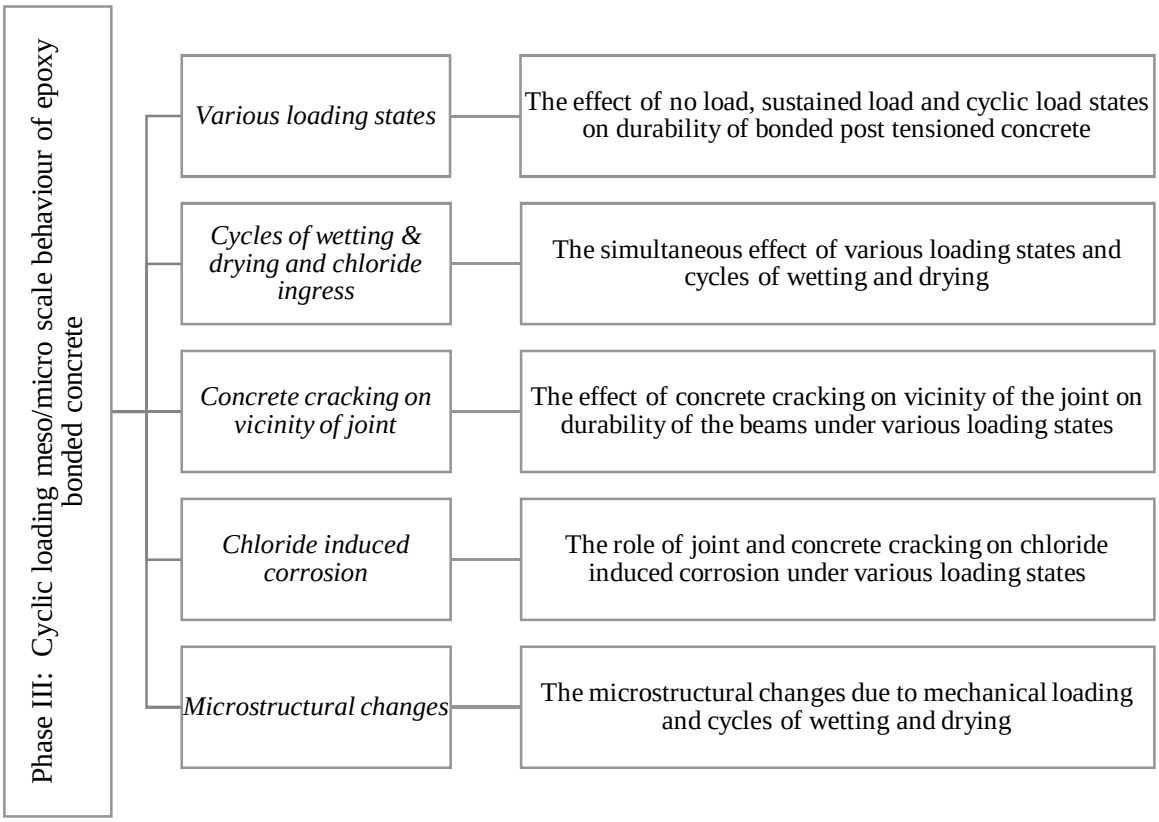

Figure 3.6. The important parameters of Phase III: Cyclic loading meso/micro scale behaviour of epoxy bonded concrete

A test rig was designed for testing the effect of loading on evolution of micro cracking and chloride or water ingress through the joint and concrete. Moreover, the possibility of cracking in body of concrete and its consequent effect on joint performance was evaluated. Four point bending test according BS EN 12390-5 (2009d) has been the base for this test set up. Two samples were tested for each loading condition: (i) no load, (ii) sustained load, and (iii) cyclic loading. All the samples experienced cycles of wetting and drying in artificial sweater salt solution for the period of three months.

The concrete mix was according to Mix 3 in Table 3-9 with using CEM I. All the samples were post-tensioned and an initial saw cut defect was induced in the body of concrete to ascertain the position of the crack. Table 3-5 summarizes the exposure condition and monitoring methods throughout this phase. The details of experimental set up will be explained in the corresponding section of the test methods.

Table 3-5. Summary of the experimental programme in Phase III: Cyclic loading meso/micro scale behaviour of epoxy bonded concrete

Loading condition	Post-tensioning	Pre-loading /cracking	Cycles of wetting and drying	Half cell(1)	UPV(2)	$AgNO_3$ Spray(3)	CT-scan(4)
No Load	✓	✓	✓	✓	✓	✓	✓
Sustained load	✓	✓	✓	✓	✓	✓	✓
Cyclic load	✓	✓	✓	✓	✓	✓	✓

Half-cell potential test ASTM C876 (2015a) ,(2) Ultrasonic Pulse Velocity BS EN 1250-4 (2004d), (3)Chloride analysis (4)Computed Tomography

3.5. MATERIAL PROPERTIES, CONCRETE DESIGN AND SPECIMEN PREPARATION

3.5.1. Cement

CEM I 52.5 N (Portland cement) conforming to BS EN 197-1 (2011) was used in this project. In most of mixes, 50% of CEM I is substituted with Ground Granulated Blast-furnace Slag (GGBS) conforming to BS EN 15167-1 (2006) to be more environmental friendly and provide a denser microstructure. This cement mixture is called CEM III/A conforming to BS 8500-2 (2015b).

3.5.2. Aggregate

Aggregates used in this project are granite quarried in Fife. The fine aggregates were maximum 4 mm and coarse aggregates were 4/10 mm and 10/20 mm. The shape of the aggregate was rounded and smooth-edged gravel. Absorption and particle density of the aggregates were tested based on BS EN 1097-6 (2013c) and the total and free water in the mix were specified according to the water absorption.

3.5.3. Water

Tap water conforming to BS EN 1008 (2002a) was used throughout this project for making concrete mixes.

3.5.4. Admixtures

Glenium Sky 544, conforming to BS EN 934-2 (2009a) was used as high range water reducing admixture due to low water cement ratio of the mixes. The precast factory chose ADVA 576 for casting the prototype segments.

3.5.5. Artificial seawater salt

Table 3-6 shows seawater salt composition. The artificial seawater salt used throughout various phases of the project contains sodium chloride, NaCl, magnesium sulphate, $MgSO_4$, magnesium chloride, MgCl, calcium chloride, $CaCl_2$, potassium chloride, KCl, manufactured specifically by Red Sea Salts®to represent marine salinity. 1 M artificial seawater salt solutions (66 g/L) was used in all the phases. This is a higher molarity compared to the marine environment (around 35 g/L), but it was chosen for accelerating the tests.

Table 3-6. Average composition of seawater salt (Mehta, 2002)

Ion	Concentration, g/L
Na^+	11
K^+	0.4
Mg^{2+}	1.33
Ca^{2+}	0.43
Cl^-	19.80
SO_4^{2-}	2.76

3.5.6. Epoxy adhesive properties

Different companies offer a diverse range of epoxies for structural performance. It can be quite confusing to choose a proper one for a WEC application. Phase I includes various types of epoxies from different companies in order to evaluate sensitivity of the tests to the type of epoxy and finally recommend some main characteristics of epoxy regarding macro scale behaviour of bonded concrete. Table 3-7 and Table 3-8 present general and mechanical characteristics of the epoxies. Due to confidential agreement with the manufacturers the commercial name of these epoxies are not mentioned here.

3.5.7. Anti-corrosion paint

Normal anti-corrosion paint supplied by Blackfriar Ltd. was used for protecting steel plates to prevent corrosion. This paint is one component paint which contains zinc phosphate to inhibit rust.

Epoxy anti-corrosion paint supplied by Sika Ltd. is two components (epoxy resin and hardener). This paint has micaceous iron oxide and can provide durable corrosion protection under various atmospheric conditions.

Table 3-7. Epoxy adhesive general characteristics, based on manufacturer data sheet

Epoxy Code	Application Temperature, °C	Thermal expansion, Coefficient, per °C	Shrinkage, %	TG[2] °C	Density, kg/l	Resin Content, %	Hardener Content, %	Filler Content, %	Mix Ratio[3] (resin: hardener+ filler)
A	+10 to +30	9.3×10^{-5}	0	+49	1.35	nd	nd	nd	1:1
B	+8 to +35	2.5×10^{-5}	0.04	+62	1.65	nd	nd	nd	1:3
C	min 5	nd[1]	nd	41.5	1.02	nd	nd	nd	1:1
D	min 5	nd	nd	nd	1.85	19	4	77	nd
E	+5 to +45	nd	nd	nd	1.60	23	7	70	nd
F	nd	nd	nd	nd	nd	63	37	nd	nd

[1]nd: no data , [2] Glass Transition Temperature, [3] Mix ratio by mass

Table 3-8. Epoxy adhesive mechanical characteristics, based on manufacturer data sheet

Epoxy Code	Strength Characteristics, MPa					Moduli Characteristics, GPa			Tensile elongation (%)
	Compressive	Flexural	Shear	Tensile	Bond[2]	$E_{compresive}$	$E_{tensile}$	G_{shear}	
A	50	nd[1]	20	10 - 15	> 5	nd	nd	nd	nd
B	65 - 75	nd	13 - 16	21 - 24	> 4	9.6	11.2	1.5	nd
C	56.7	60.8	nd	32.7	nd	nd	2.58	nd	3.3
D	80	21	nd	13.2	3.8	nd	nd	nd	nd
E	65	34	nd	14	5.9	nd	nd	nd	nd
F	-	65	nd	41	nd	nd	nd	nd	nd

[1] nd: no data, [2]Based on substrate failure

3.5.8. Concrete mix

The concrete mixes used in these experiments were designed based on standard specifications BS 8500 (2015b) to prevent any degradation of the structural performance in harsh marine environment. Concrete fresh properties as slump and plastic density were tested based on BS EN 12350-2 (2009b) and BS 12350-6 (2009c) respectively.

Three different concrete mixes were used throughout this project named as Mix 1, Mix 2 and Mix 3 detailed in Table 3-9. Table 3-10 shows the concrete mix adopted for the different phases of the research program.

Table 3-9. Test concrete mix proportions and selected properties

Concrete mix No.	Constituent Proportions (kg/m^3)							w/c ratio	Slump (mm)	$f_{c,\ 28\ days}$ (MPa)
	CEM I 52.5 N	GGBS	Water	Aggregate [1]			SP (%)			
				Fine 0/4	Coarse 4/10	Coarse 10/20				
Mix 1: CEM III/A	225	225	170	680	363	727	0.4[2]	0.38	100	60
Mix 2: Precast	383	-	150	766	1149		0.65[3]	0.39	-	80
Mix 3: CEM I	450	-	170	680	1090	-	0.4[2]	0.38	100	60

[1] Coarse aggregate and granite fine aggregate glacial sand (1% water absorption),
[2] Superplasticizer Glenium Sky 544, % of total cementitious material by weight,
[3] Superplasticizer ADVA 576, % of total cementitious material by weight

Table 3-10. Concrete mix assigned for various Phases of the project

Project Phase	Project Part	CEM III/A[1] (50% GGBS) Mix 1	Precast concrete CEMI Mix 2	CEMI Mix3
Phase I	Part 1	✓	-	-
	Part 2	✓	-	-
Phase II	Part 1	-	✓	-
	Part 2	✓	-	✓
Phase III	-	-	-	✓

[1] BS 8500 (2015b) define CEM III/A as a Portland cement with 36% to 65% Ground Granulated Blast furnace Slag (GGBS).

The concrete mix used in the experimental program Phase I and Phase II were a 50% GGBS concrete which is typical of marine coastal structures in Europe. Since there are few studies available on meso/micro scale behaviour of concrete under cyclic loading. A more typical concrete was adopted for Phase III to reduce the number of variables and make the results more comparable with available data. Therefore, the mix design used in some parts of Phase II and all of Phase III did not have any supplementary cementitious materials. The total amount of cementitious materials was still the same but CEMI substituted GBSS. The maximum aggregate size was also different in Mix 3 because the specimens for cyclic loading test were relatively small (75 mm width and height) due to limitations of the testing rig. Therefore, the maximum aggregate size was 10 mm instead of 20 mm in order to be a better representative volume considering the specimen size.

3.5.9. Mixing, curing and preparation

All mixing procedures conformed to BS 1881-125 (2013a). After casting the samples left to cure for 24 hours in the moulds, damp hessian covered them. Then the samples were de-moulded and put in the curing water tank at room temperature. After 28 days, the strength of standard cube samples were tested according BS EN 12390-3 (2002b).

The concrete mix of the prototype was made in a local precast factory (Plean Precast Ltd.) with similar w/c ratio to the concrete used in other phases of the project. The details of this mix were provided by the precast factory. The hollow circular sections were cast by using cardboard as outside and foam as inside mould (see Figure 3.7).

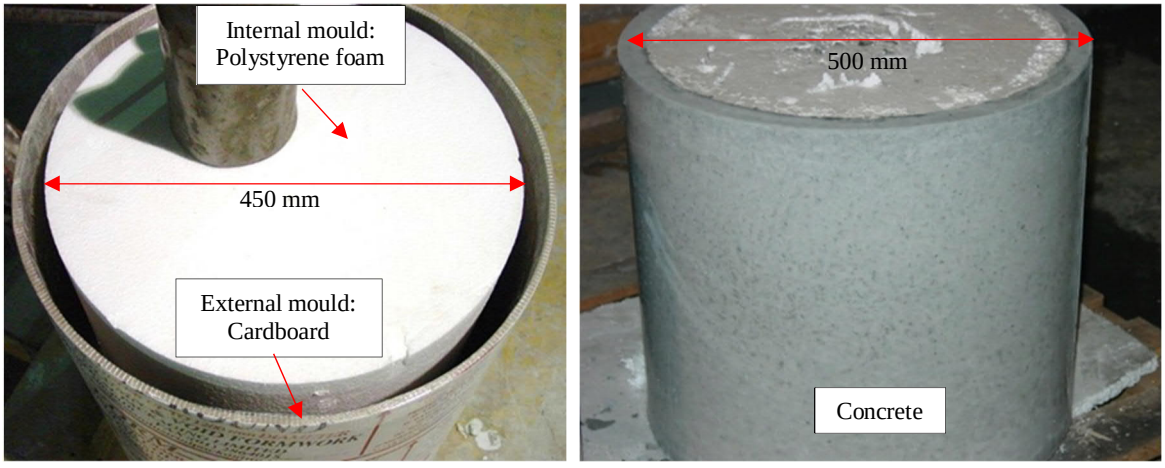

Figure 3.7. Internal and external mould for casting the concrete segments by pre-cast manufacturer

3.6. PHASE I TEST METHODS: STATIC MACRO SCALE MECHANICAL PERFORMANCE OF EPOXY BONDED CONCRETE

The details of testing methods throughout Phase I: Part 1 and Part 2 are explained here. Digital Image Correlation (DIC) for strain monitoring, shear/compression, tension and torsion tests methods are detailed (Part 1). Finally, two testing methods and sample preparations for epoxy bonded concrete to steel are described (Part 2).

3.6.1. Strain monitoring of jointed specimens using Digital Image Correlation (DIC)

The evolution of strain fields on the surface of specimens during shear and tensile testing was monitored using Digital Image Correlation (DIC). DIC is an optical method based on the use of two Photron SA-1 high speed video cameras and software VIC-3D (Correlatedsolutions.com, 2015). The video cameras were able to capture up to 5400 frames per second at 1 mega pixel resolution. In the DIC method, the examined surface was coloured white with a reference grid of black dots. Two cameras were positioned to record the specimen surface from different angles. Reference photographs were taken before testing began and the displacements of the reference dots were recorded during the test by the cameras with a pre-set speed (see Figure 3.8). The surface strain fields were calculated for each photograph, with strain measurements to nearest micro-strain (μm/m). DIC allowed to study the distribution of strain in the jointed system which indicates the transfer of shear, compression, and tension stresses through the joint at different loading levels.

a) Two cameras and light b) Calibration board

Figure 3.8. Digital Image Correlation (DIC) set up for strain monitoring

3.6.2. Jointed sections shear capacity test methods

The slant shear method is a standardised test (BS EN 12615 (1999)) and has been adopted by a number of international codes for determining the shear bond strength of epoxy bonded joints (Momayez et al., 2005).

In this method, a 400 mm ×100 mm × 100 mm concrete prism with an epoxy-bonded joint inclined at 30º to the main axis of the prism is subjected to axial compression, as shown in Figure 3.9. The resulting joint has a 100 mm × 200 mm rectangular area. It is commonly accepted that the slant shear test results in a relatively uniform stress distribution at the joint (Abu-Tair et al. 1996, Júlio et al. 2005, Santos and Júlio 2011).

Additionally, this test is particularly sensitive to a range of parameters such as substrate roughness, joint thickness, epoxy, and concrete material characteristics. BS EN 12615 (1999) recommends calculating the bonding strength of the adhesive layer by dividing the failure load by the area of the bonded surface. However, this method gives only a relative indication of the joint shear strength. The actual state of forces at the joint includes the shear and compression forces (*S* and *C*, respectively) which are the components of the axial compression force (*P*) applied to the concrete prism. *S* and *C* can be found in Equation 3.1 and Equation 3.2.

It is necessary to note that *C* is directly proportional to *S*, i.e., C= S tan (30°) = 0.577 S and the ultimate shear force divided by the joint area was used to enable the direct comparison with bi-surface shear test. In comparison to the other testing techniques, the slant shear test is unique in that both the shear and compressive stresses act on the joint during the test. To enable the comparison of the shear performance of the joint in the slant shear and bi-surface shear tests, the shear strength of the joint has been found in this study as the shear force *S* divided by the area of the joint.

$$S = Pcos(30^o) = 0.87P$$

Equation 3.1

$$C = Psin(30^0) = 0.50P$$

Equation 3.2

S: Shear force

P: Applied load

C: Compression force

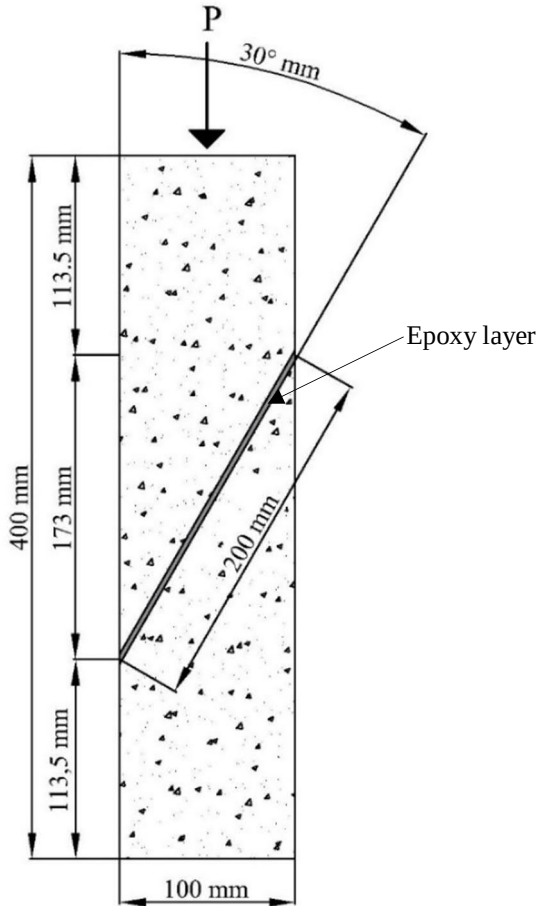

Figure 3.9. Slant shear test set up

The bi-surface shear test is a nonstandard technique for the evaluation of the joint bond strength under shear stress (Momayez et al. (2005). Two variations of the test were used as shown in Figure 3.10. Both versions comprise a 150 mm concrete cube with a flat face joint located at 50 mm from one of cube sides. In Setup 1 shown in Figure 3.10 (a), the cube is resting on two 50 mm wide steel plates on rollers placed along cube edges parallel to the joint, while the load is applied through a third roller placed on a 50 mm wide steel plate at the top face of the larger concrete segment along the joint. In Setup 2 depicted in Figure 3.10 (b), the cube is resting on two 30 mm wide steel plates on rollers, while the load is applied through a half of 50 mm diameter cylinder placed on the top of the larger concrete segment at 30 mm from the joint. In both cases, the joint is only subjected to shear stress. Since the thickness of the joint changes between 2 mm to 4 mm, the shear force in the joint can be slightly different as shown in Table 3-11.

In the experimental programme, Setup 1 was used for specimens bonded by the epoxy A, while Setup 2 for specimens bonded by epoxies B-F (Table 3-7 and Table 3-8). In the bi-surface shear tests, the shear strength of the joint was evaluated as the peak shear force calculated in accordance to Table 3-11 and divided by the area of the bonded surface. The use of Table 3-11 allowed to eliminate the influence of different tests setups used in the bi-surface shear tests.

It is important to note that the stress states of the joint in the slant shear and bi-surface shear tests are different due to the presence of the compressive force in the former test. The comparison between the results of both tests can provide information about the influence of compressive stresses at the joint on its shear response. This information is especially useful for understanding of the shear response of post-tensioned joints used in floating marine concrete structures.

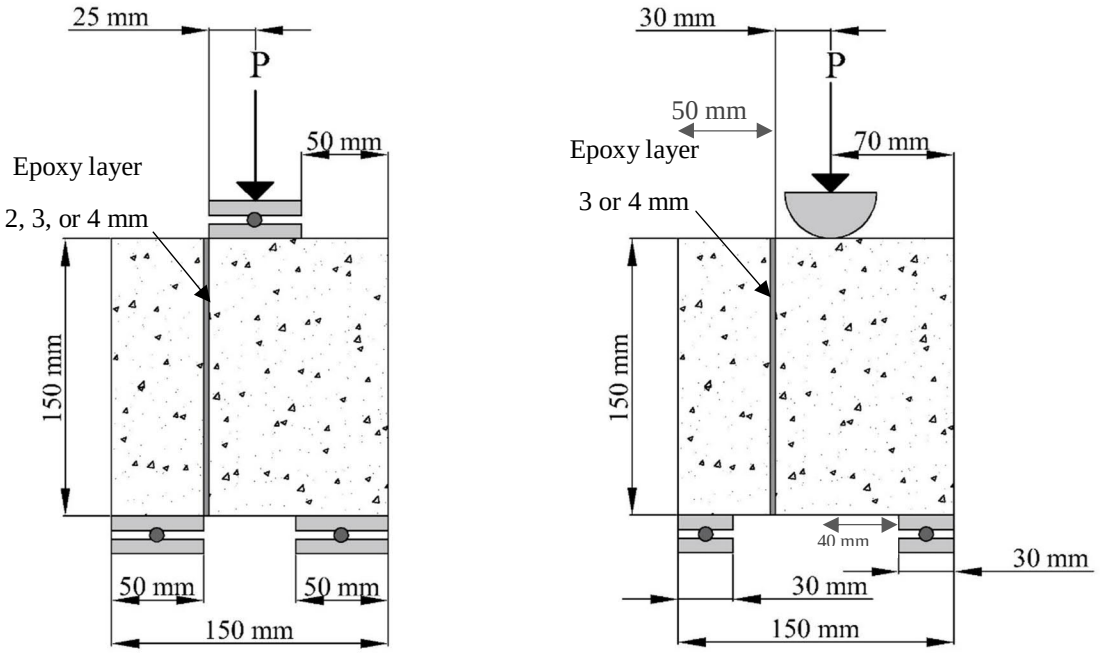

(a) (b)

Figure 3.10. Bi-surface shear test a) set up 1 and b) set up 2. (Shear strain is monitored in this test, and the flexural stress is negligible)

Table 3-11. Shear force in the joint in the bi-surface shear test for two different set up

Joint Thickness	Shear Force in Joint	
	Setup 1	Setup 2
2 mm	0.48P	-
3 mm	0.47P	0.430P
4 mm	0.46P	0.425P

3.6.3. Shear testing of the jointed sections after cyclic wetting and drying

To study the influence of seawater and cycles of wetting and drying on the bonding strength of the epoxy resin, a number of bi-surface shear test specimens were exposed to a wetting and drying cycle in 1 M artificial seawater salt solution for 90 days prior to shear testing. The specimens had 3 mm thick untreated or sandblasted joints bonded by the epoxy B.

3.6.3.1. Cyclic wetting and drying set up

The cycles of wetting and drying were produced as presented in Figure 3.11. The tank was equipped with pumps and fan for circulating air during the drying cycle. The pump was working during the wet cycles to circulate the water between the reservoir and the upper tank drain. The solution was 1 M artificial seawater at ambient laboratory temperature (20 ± 2 °C). The exposure period was divided into 6 hours wetting cycles (specimens are fully submerged) followed by 18 hours drying cycles. A longer period was assigned for drying time because concrete drying is a slower procedure.

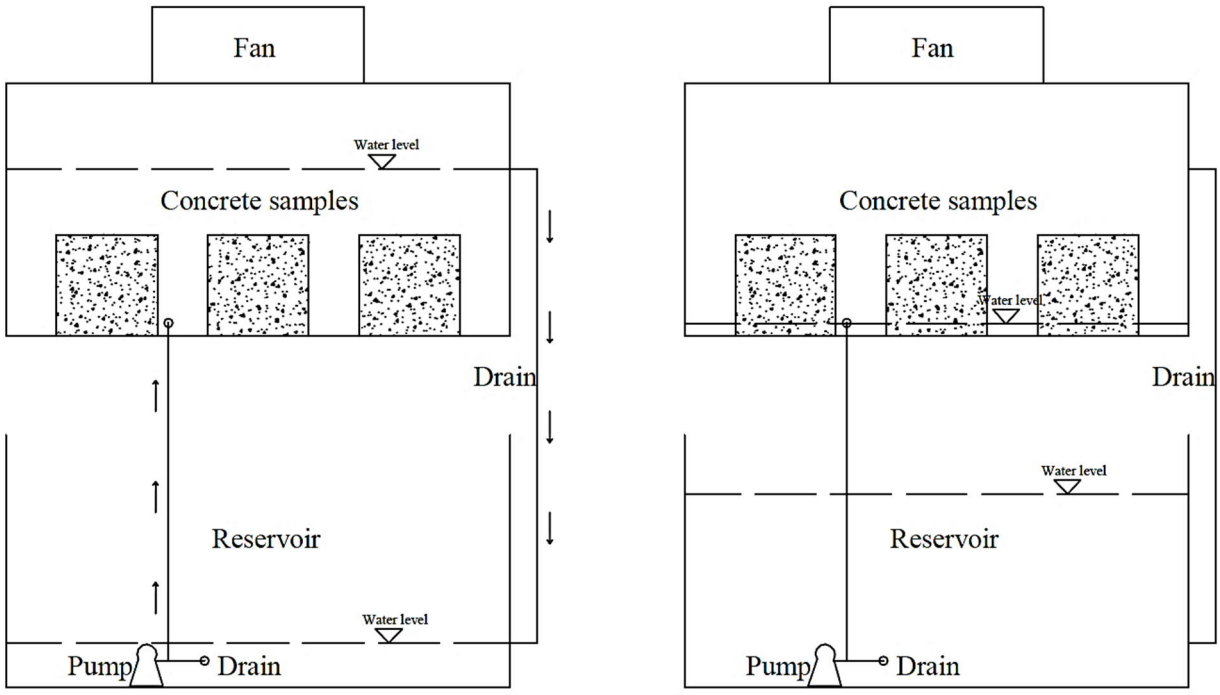

(a) 6 hours wet cycle (b) 18 hours dry cycle

Figure 3.11. Schematic presentation of the tank for producing cyclic wetting and drying

3.6.4. Shear testing of the jointed sections with induced defect

The bi-surface shear test on specimens with no surface preparation joints bonded by the epoxy A was used together with Ultrasonic Pulse Velocity (UPV) method carried out to BS EN 12504-4 (2004d) pick up the induced defects in the epoxy joints. Defects were created by placing a piece of card on the specimen to prevent epoxy coverage measuring the required area on the specimen during preparation. UPV measurements were conducted across and through the joint plain to determine UPV suitability in detecting the defects.

3.6.4.1. Bi-surface shear test accompanied with Ultra Sound Pulse Velocity (UPV)

Ultra sound Pulse Velocity (UPV) was used as a Non Destructive (ND) test method for evaluating the quality of bonded sections according to BS EN 1250-4 (2004d). This test is based on measuring the travel time of a wave pulse, which is passing through concrete longitudinally. The frequency of the wave is between 20 to 150 kHz. An electronic circuit is used to measure travel time between the

initial onset and the surface that receive the pulse. The average velocity of propagation of the wave is calculated by dividing the travel distance of the wave by time of travel.

The test needs an electronic pulse generator, a pair of transducers, an amplifier, and electronic device for measuring the time of travel. It is recommended that high frequency transducers to be used for concrete with short length and the low frequency transducers to be used for longer path. The devices with frequency between 50 kHz to 60 kHz are the most suitable ones (Bungey and Millard, 2010).

A material like grease should be used for coupling. The produced pulse shows different reflections as passes through different material phases of the concrete. A system of waves including longitudinal and shear waves will propagate through concrete. The second transducer converts the first longitudinal wave of the receiving transducer into an electrical signal. Then the transmitting time is measured by the electrical device. The interpretation of the results is qualitative. IAEA (2002) presents a table to explain the values of pulse velocity in term of strength. Table 3-12 shows the interpretation of concrete quality based on pulse velocity.

Table 3-12. General guidelines for concrete quality based on UPV (IAEA, 2002)

Pulse velocity	Concrete quality
>4.0 km/s	Very good to excellent
3.5 – 4.0 km/s	Good to very good, slight porosity may exist
3.0 – 3.5 km/s	Satisfactory but loss of integrity is suspected
<3.0 km/s	Poor and loss of integrity exist.

The aim of combining the bi-surface shear test and the UPV method was to establish a relationship between the defect size and the reduction in the bond strength of the joint and determine whether UPV could be used as a quality control method. The cube specimens were designed as having joints with three different defect sizes namely (i) no defect (100% epoxy coverage of the joint), (ii) 10% defect (90% epoxy coverage) and (iii) 50% defect (50% epoxy coverage). The locations and shapes of the defects are shown in Figure 3.12. UPV measurements were conducted in two main directions, i.e., 5 points were selected as shown in Figure 3.13 for measurements across the joint in the horizontal direction and 3 points for measurements along the joint in the vertical direction. The UPV readings from the two sets of points were averaged.

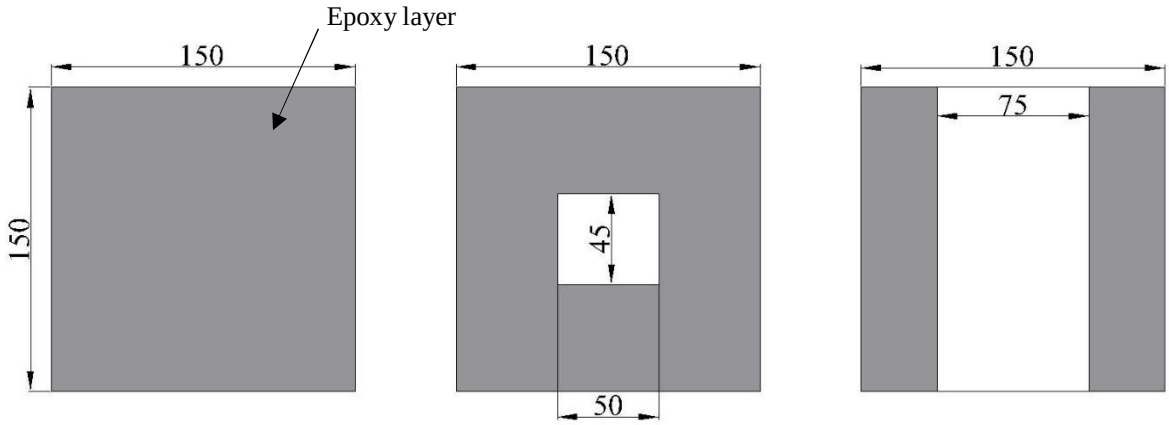

No defect
(100% epoxy coverage)

10% defect
(90% epoxy coverage)

50% defect
(50% epoxy coverage)

Figure 3.12. Location of defects in jointed specimens

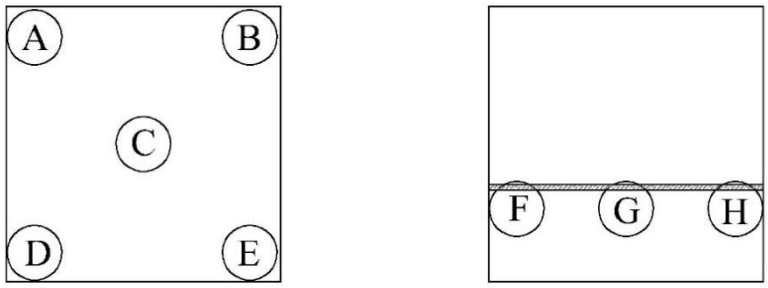

(a) Horizontal measurements – UPV_H (b) Vertical measurements – UPV

Figure 3.13. Location of UPV tests for a) horizontal tests b) vertical tests (along joint testing)

3.6.5. Jointed section tensile capacity test methods

The bond strength of the flat-face joint in tension was examined using two methods: the split cylinder test and the flexural test. The split cylinder test is a standard method BS EN 12390-6 (2009e) shown in Figure 3.14 for measuring the indirect tensile strength of concrete and is based on generating transverse tensile forces in a concrete cylinder by applying a compressive load along its length. In this study, each concrete cylinder (100 mm in diameter and 300 mm in length) was fabricated with an epoxy-bonded joint dividing the cylinder into two equal parts along its length. The compressive line load was applied along the joint from both its sides and as a result, the joint was in the state of compression in its plane and tension out of the plane.

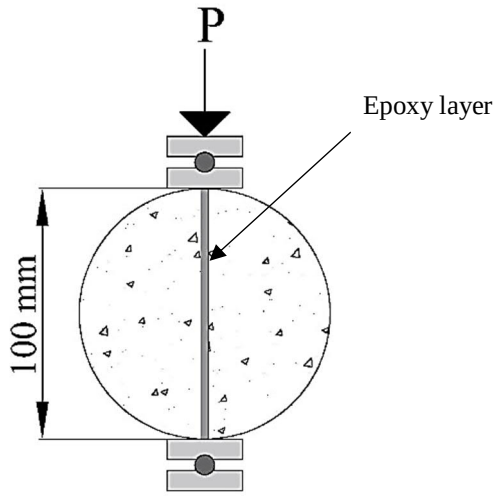

Figure 3.14. Modified split cylinder test set up

The flexural four-point bending test was a modified version of that in BS EN 12390-5 (2009) as shown in Figure 3.15. The supporting and loading conditions of the beam were fully symmetrical and an epoxy-bonded joint was introduced along the line of symmetry of the beam. As a result, the joint was subjected to non-uniform tensile stresses at its bottom half and to non-uniform compressive stresses at its top half.

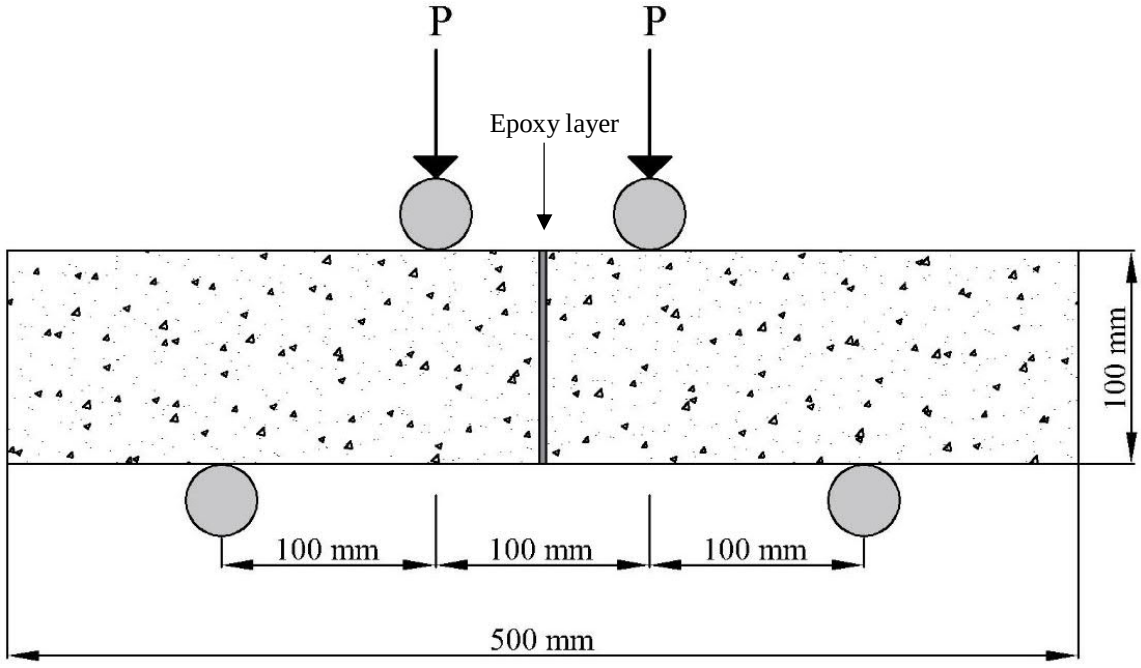

Figure 3.15. Modified flexural test setup

3.6.6. Jointed sections torsion test method

The torsion test method developed by using two hollow 100 mm cube specimens bonded by epoxy resin, as detailed in Figure 3.16. The specimen size was chosen to conform to health and safety handling requirements as well assumptions regarding homogeneity of specimens (Torrenti et al., 2010). Specimens were fabricated with 25 mm thick walls in wooden moulds as can be seen in Figure 3.17.

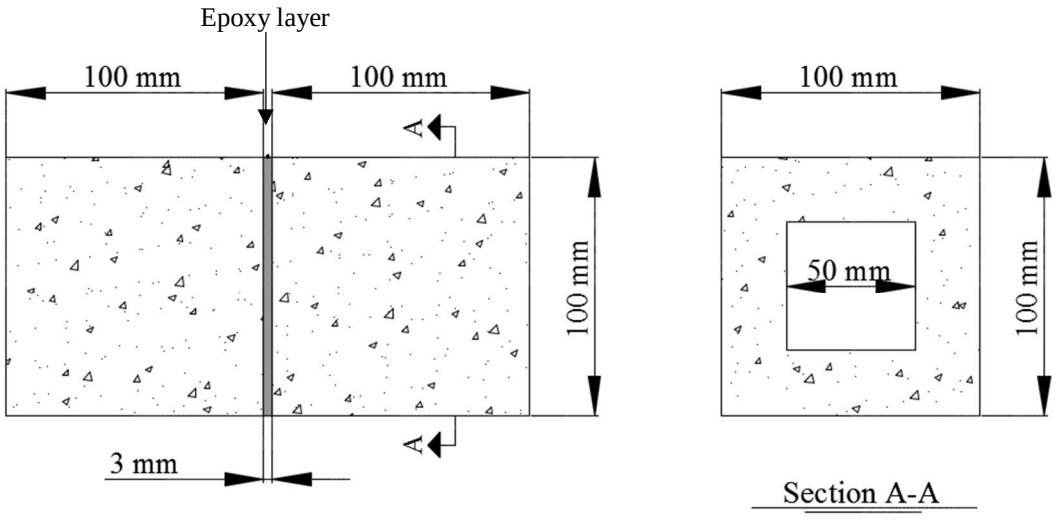

Figure

Figure 3.16. Dimensions of square specimen for torsion test

(a) Wooden mould with the spacers

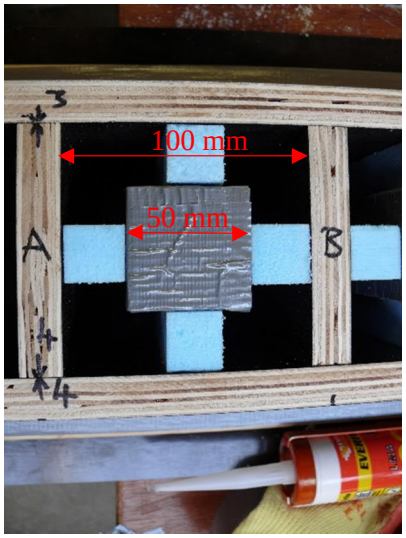

(b) Fixing the middle spacers with silicon and foams

Figure 3.17. Torsion test: mould preparation for rectangular sections

The possibility of testing circular hollow sections with the devised frame was also evaluated. Concrete cylinders were cast and 50 mm diameter cylinder was cored out of centre as can be seen in Figure 3.18.

Figure 3.18. Torsion test: preparation of circular sections

Torsion was applied through two steel frames confining the cubes on both sides of the joint as shown in Figure 3.19. Six bolts were placed in the top plate of each frame to ensure that the specimen was held in position. The frames were connected by a central metal shaft passing through the test specimen. 224 mm long steel lever arm was welded to one frame (the left frame in Figure 3.19), while the other frame was welded to the substructure. This setup enabled application of pure torque to the test specimen through loading of the lever arm by a standard testing machine. The force applied on the lever arm was monitored by a load cell and two Linear Variable Differential Transformers (LVDTs) were used to monitor the horizontal and vertical rotation of the sample. The details of load cell and LVDTs calibration are explained in Appendix A.

The torsional stress, τ, was calculated based on the guidelines of ACI-ASCE Committee 445 (2013) that considered the tested specimens as fully solid prisms, with torsional stresses acting in a continuous manner around the cross-section. τ was calculated using the following formula:

$$\tau = \frac{T}{\alpha \sum x^2 y}$$

Equation 3.3 (ACI-ASCE Committee 445, 2013)

$$\alpha = \left[3 + 1.8\, x/y\right]^{-1}$$

Equation 3.4 (ACI-ASCE Committee 445, 2013)

Where T is the applied torque, x and y are specimen cross-section dimensions, and α is a coefficient dependent on these dimensions. In the considered case, $x = y = 100$ mm and so $\alpha = 0.208$ and $\tau = 4.8 \times 10^{-6} \times T$ MPa. It is necessary to note that rectangular cross-sections under torsion are affected by warping, however, the restrains at the ends of the specimen tried to keep this effect insignificant. In addition, the corresponding rotational deflection was found as the square root of the sum of squares of the readings made by the two LVDTs installed in the vertical and horizontal directions.

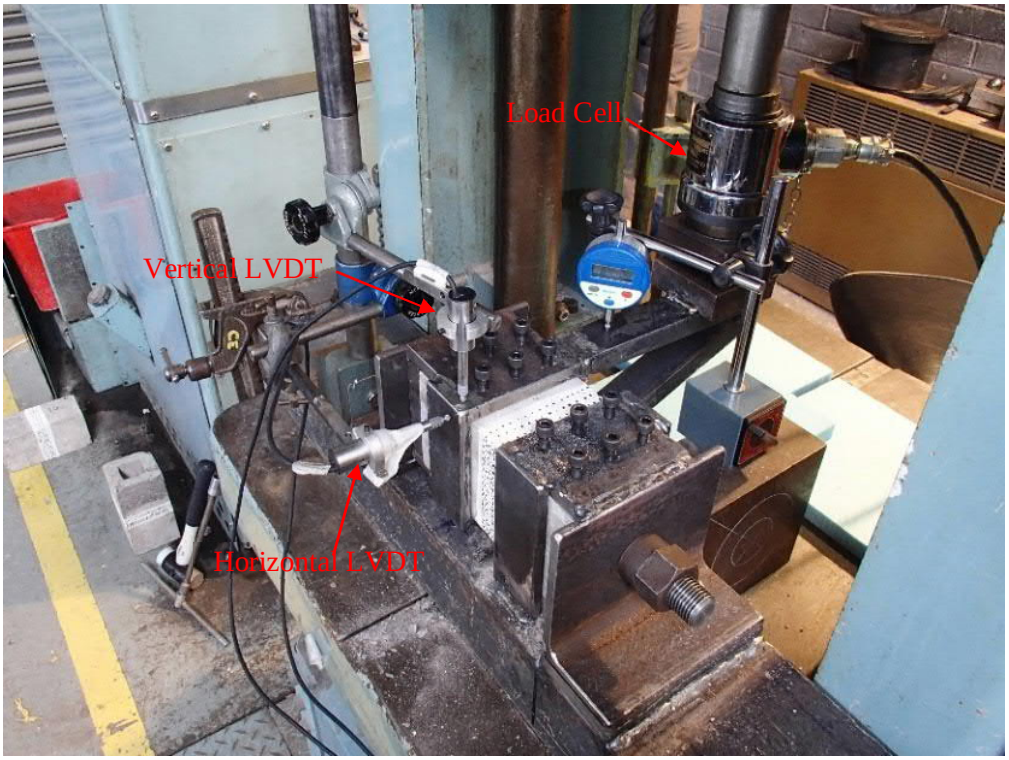

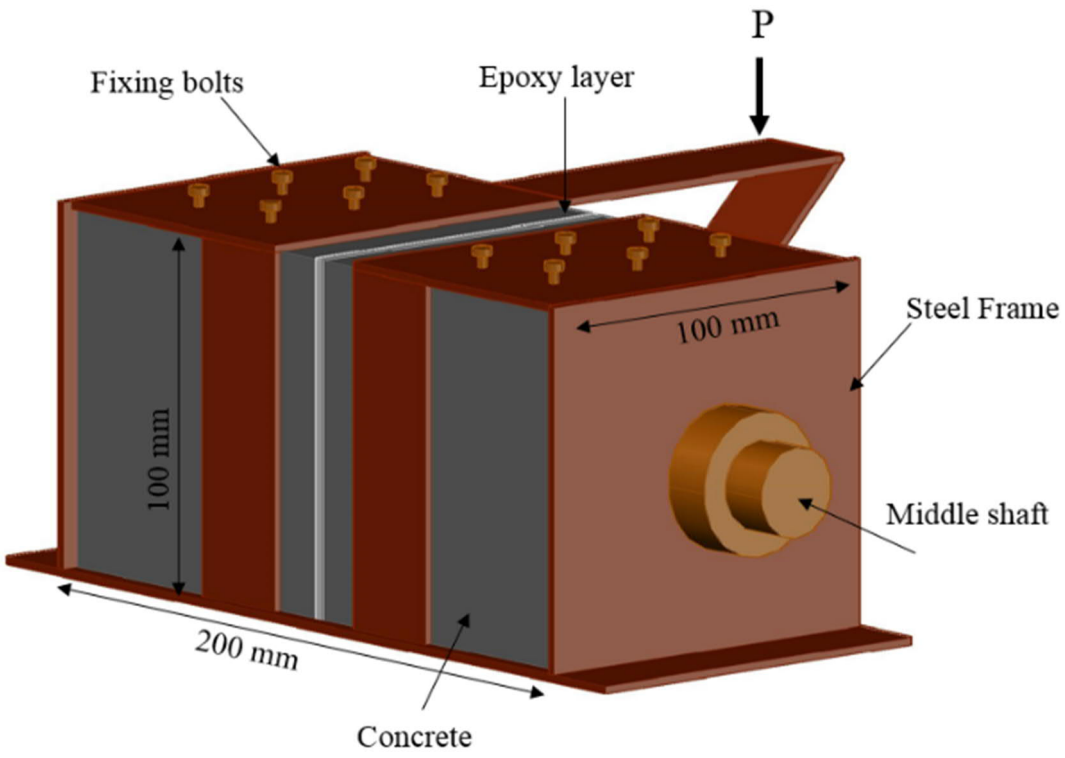

Figure 3.19. Torsion test setup

3.6.7. Shear capacity of bonded concrete to steel: Push out test method

Si Larbi et al. (2007) Suggested a test method for testing bonded concrete to steel. Four LVDTs were installed on each side of the joints and load cell was located on top of the steel beam. Pushing the

beam cause shear stress in the joint and LVDTs record the slipping of the joint until failure (see Figure 3.20).

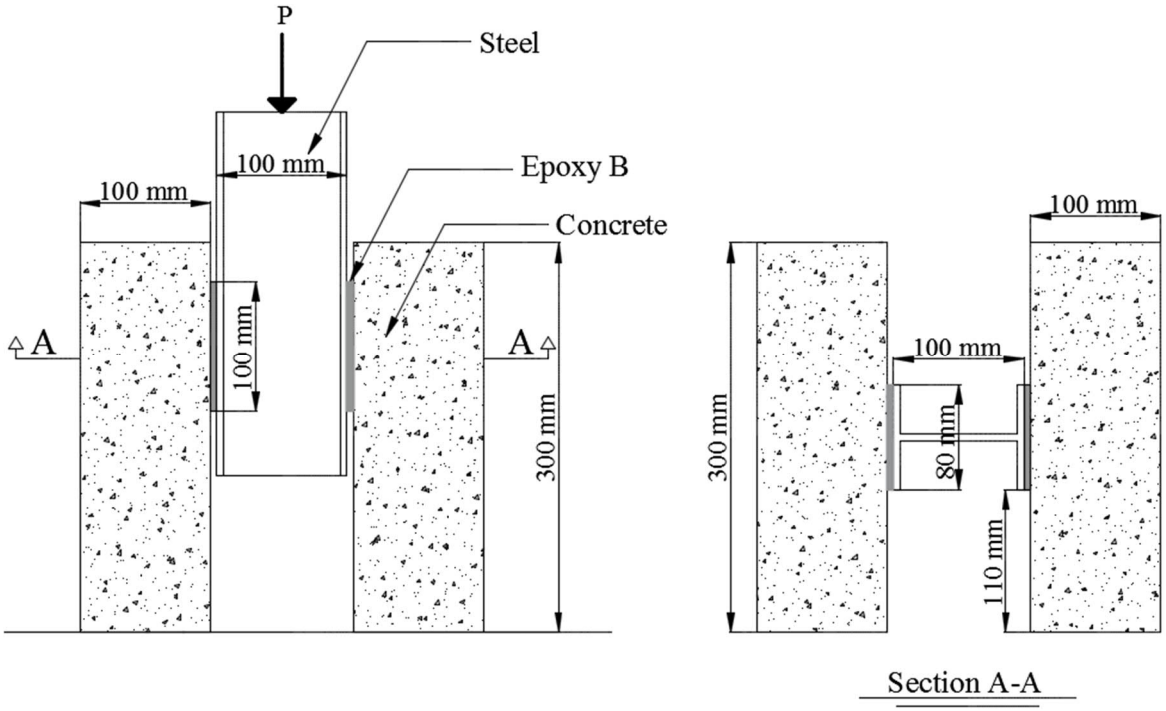

Figure 3.20. Push out test sample size

Four LVDTs were fixed on four sides of the concrete surface by gluing fabricated aluminium rings with Quick set epoxy adhesive. LVDTs were pressed against the external aluminium plates connected to the bottom of the main steel beam. The joint movement was measured by downward movement of the steel beam, which results in releasing the pre-pushing of LVDTs. Figure 3.21 shows the set up for this test.

This test was conducted by using two types of anti-corrosion paint, normal paint and epoxy paint. Surface of steel was sandblasted and cleaned by air pressure and then painted. After 1 day of curing of the paint, one face of the steel was jointed to the sandblasted and cleaned surface of concrete. The precision of applying epoxy on steel and concrete should be very high in order to avoid any eccentricity of load.

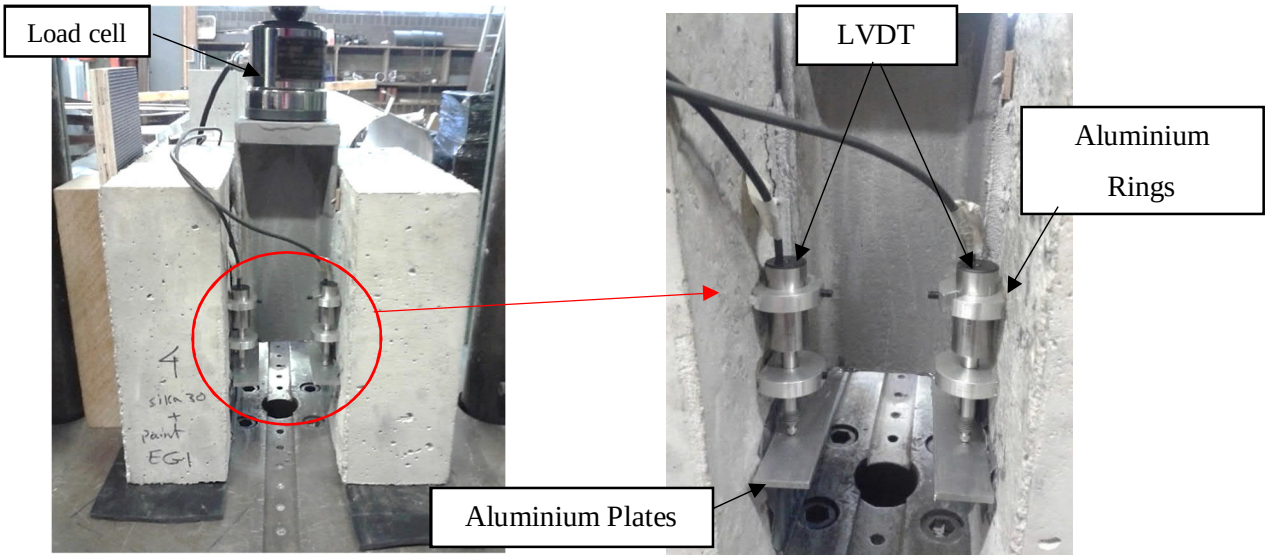

Figure 3.21. Push out test set up

3.6.8. Shear capacity of bonded concrete to steel: Double lap shear test method

Double lap shear test was conducted according to Barnes and Mays (2001) experimental programme and suggestions. However, slight changes were made to suit the testing set up. The bond length was chosen 200 mm because the optimum joint length is supposed to be between 100 and 200 mm. Bond line length less than 100 mm cannot sufficiently provide strength and longer than 200 mm does not contribute in the resistance. The epoxy layer thickness was the typical 3 mm. The double lap test was conducted in two main state: the first one by jointing hard concrete and steel plates and the second one by casting fresh concrete with epoxy on steel.

Figure 3.22 shows mould, steel plates, and concrete dimensions. The wooden mould was fabricated, and some foams were used to adjust the steel plates and concrete in the mould. The steel plates were painted with epoxy paint three days prior to gluing process.

Figure 3.23 shows the process of applying fresh concrete and epoxy on the steel. The precision of gluing fresh concrete to steel plates was very high because the plates were in the right position in the mould so no eccentricity happened but controlling exact epoxy thickness was impossible because both concrete and epoxy were in fresh state and could flow. Concrete vibration could also move both epoxy and concrete. However, the process of bonding hard concrete to steel without causing eccentricity was much more challenging. If there were even small eccentricities in the bonded plates, they could not fit in the fabricated test frame.

An external steel frame with bolts were fabricated as can be seen in Figure 3.24. The test was conducted by placing bonded concrete in the pre-fabricated steel frame. The frame was fixed in one end and the load was applied on the other end pulling the epoxy bonded steel plates. Therefore, the load induced shear stress in the joint.

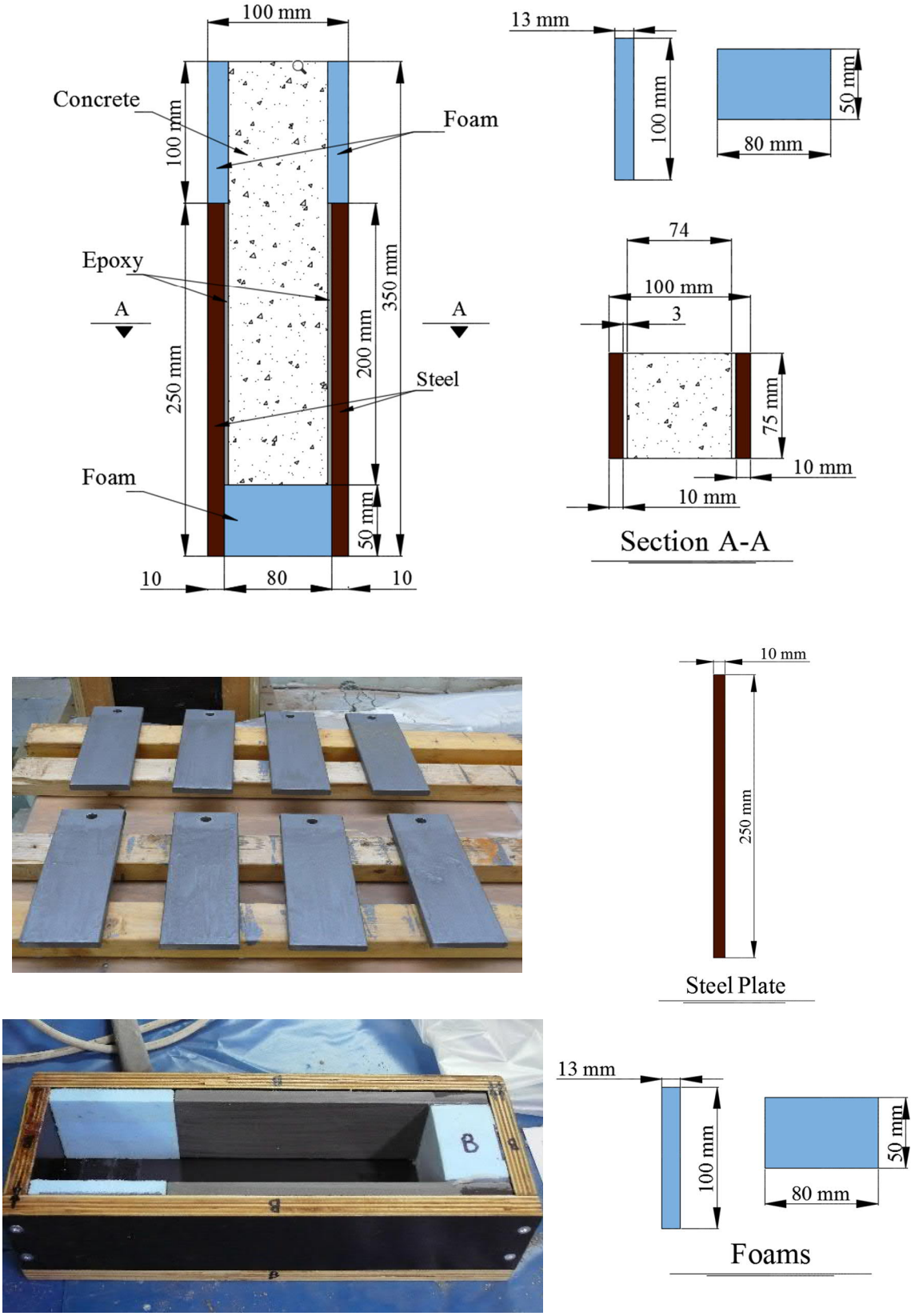

Figure 3.22. Double lap shear test: mould details

Figure 3.23. Fresh concrete casting with epoxy for double lap shear test

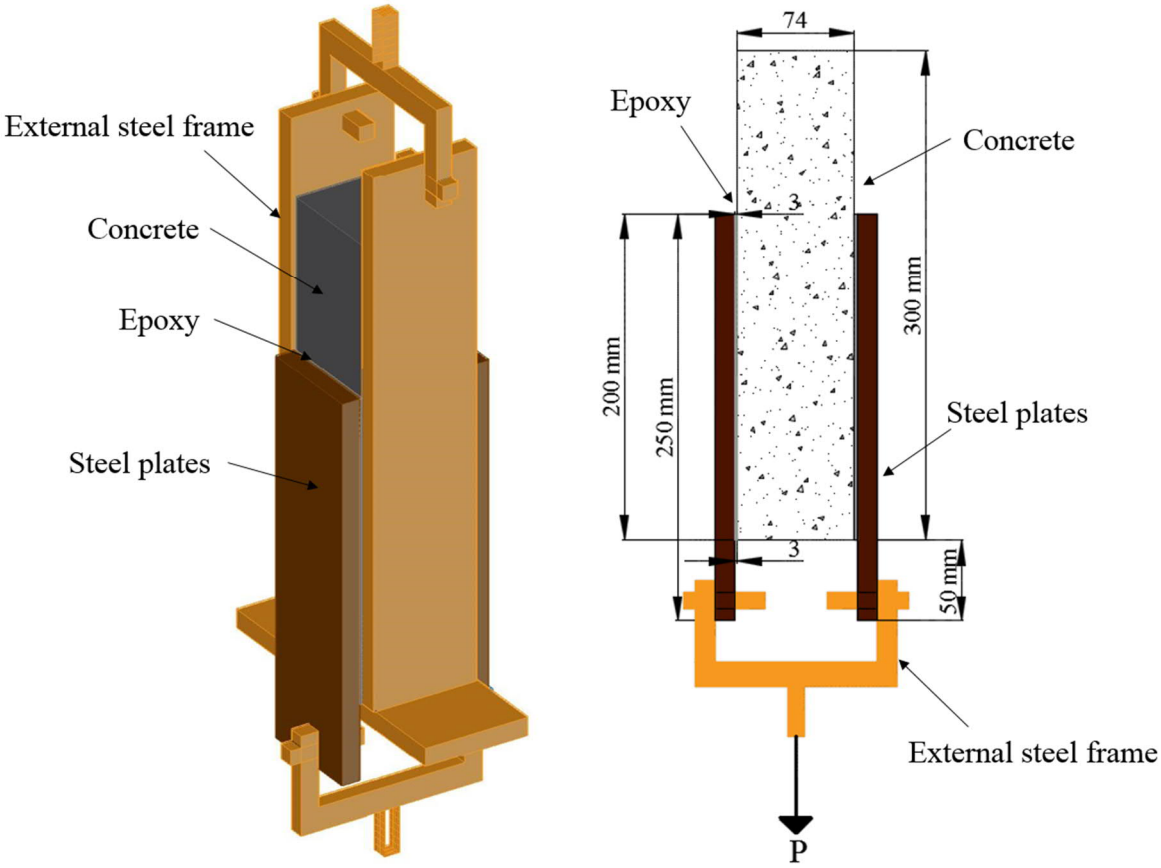

Figure 3.24. Double lap shear test set up

3.7. PHASE II TEST METHODS: STATIC MESO/MICRO SCALE BEHAVIOUR OF EPOXY BONDED CONCRETE

The details of testing methods throughout Phase II: Part 1 and Part 2 are detailed in this section. Design, assembly and testing of the scaled porotype are described (Part 1). Water penetration, ISAT, chloride migration tests, and bulk epoxy tests are explained (Part 2).

3.7.1. Scaled (1:11) prototype development following the Pelamis WEC concept

The prototype consisted of five hollow concrete segments. The outer diameter of the concrete segment was 500 mm with 25 mm wall thickness. The length of each concrete segment was 440 mm (see Figure 3.25 and Table 3-13). The segments were bonded to each other using epoxy A. To evaluate the effect of joint thickness, concrete segments were connected using different joint thicknesses of 1, 2, 3, and 4 mm. Two 550 mm diameter steel plates with 10 mm thickness were used as the end plates. The plates were painted with normal anti-corrosion paint and bonded to the tube by using 3 mm epoxy. Finally, t10 tendons were used to post tension the whole structure. The post-tensioning was not quantified; the nuts were tighten manually using spanner as much as possible.

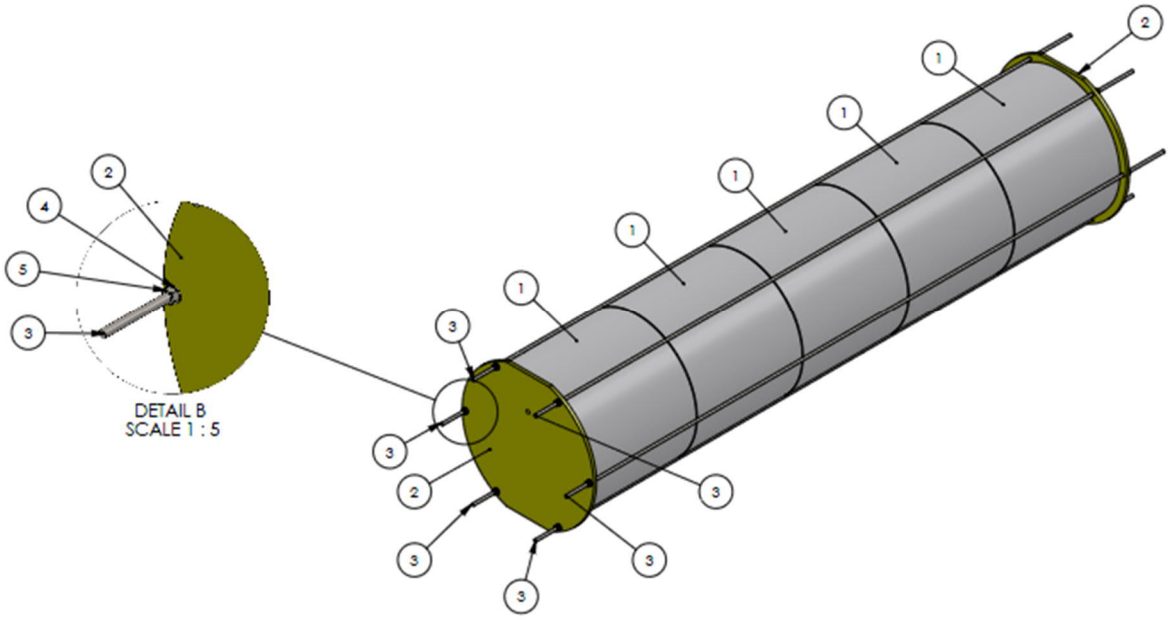

Figure 3.25. Schematic presentation of scaled prototype in accordance with Pelamis WEC

Table 3-13. Parts details of the scaled porotype

Item No.	Part Number	QTY.
1	Concrete sections	5
2	Steel-End-Plate	2
3	M10-A4-70-tendon	6
4	Washer ISO 7089-10	12
5	Hexagon Nut ISO-4034-M10-N	12

3.7.1.1. Design and buoyancy calculations

The buoyancy calculations were conducted based on Archimedes principle and considering 55 % submersion. The calculation stages are as follow:

1. Calculating total mass of structure
   a) Mass calculation for single concrete tube:

      Outer Diameter (OD) = 500 mm

      Inner Diameter (ID) = 450 mm

      Wall thickness (t_w) = 25 mm

      Length (L) = 440 mm

      Assumed Concrete density (ρ_c) = 2500 kg/m^3

      Tube mass (T_m) = π/4 (OD-ID)^2

$$Tube\ Mass = \frac{\pi\ (OD - ID)^2}{4} \times L \times \rho_c = 41\ kg$$

Equation 3.5

   b) Mass calculation for single end plate:

      Plate Diameter (D_p) = 550 mm

      Plate thickness (t_p) = 10 mm

      Steel density (ρ_s) = 7850 kg/m^3

$$End\ Plate\ Mass = \frac{\pi\ (D_p)^2}{4} \times t_p \times \rho_c = 19\ kg$$

Equation 3.6

   c) Mass calculation for each post tensioning tendon:

      Tendon Diameter (D_t) = 10 mm

      Tendon Length (L_t) = 2400 mm

$$Tendon\ Mass = \frac{\pi\ (D_t)^2}{4} \times L_t \times \rho_c = 1.5\ kg$$

Equation 3.7

   d) Total Mass:

$$Total\ Mass = (5 \times Tube\ Mass) + (2 \times End\ Plate\ Mass) + (6 \times Tendon\ Mass)$$
$$= 252\ kg$$

Equation 3.8

2. Calculating volume of water displaced by prototype:

   Water density (ρ_w) = 1025 kg/m^3

$$Volume\ displaced = \left(5 \times \frac{\pi\ (OD)^2}{4} \times L\right) + 2 \times t_p = 0.43\ m^3$$

Equation 3.9

3. Mass of water displaced by prototype

$$Mass\ of\ water\ diplaced = Volume\ displaced\ \times \rho_w = 447\ kg$$

Equation 3.10

4. Buoyancy check confirming that that the mass of water displaced is greater than the mass of prototype
5. Percentage of structure submerged by mass:

$$Submersion\ persentage = \frac{Total\ mass}{Mass\ of\ water\ diplaced} \times 100 = 56\%$$

Equation 3.11

6. Mass of ballast required to achieve target submersion:

$$Mass\ of\ ballast = (Submersion\ target \times Mass\ of\ water\ isplaced) - Total\ mass$$

Equation 3.12

56% submersion is acceptable for the current prototype, so no ballast was added to the prototype

7. Checking that the mass of ballast + mass of structure will achieve desired submersion

3.7.1.2. Casting and assembling

Figure 3.26 shows the assembly procedure. The surface of the sections was wire brushed and air cleaned and jointed by Epoxy A. Finally, the steel plates were attached and the whole tube got post tensioned by hand tightening of the bars.

3.7.1.3. Prototype testing plan

At the end, the prototype was moved to Pelamis Wave Power Ltd. to put in the tank containing seawater salt solution in order to monitor durability. Before putting the tube in the tank, hydrogen sniffing (tube pressurised to 0.1 bar using hydrogen gas, then 'sniffed' using a catalysing probe to sense hydrogen concentration), rebound hammer test (ASTM C805 (2013)) and UPV (BS EN 1250-4 (2004d)) were conducted to find out the weak or leaking point of the prototype.

The testing and monitoring was conducted again after one year and at the final stage (after two years) cores were taken out of prototype to assess the depth of chloride movement through the joint ($AgNO_3$ spraying and chloride profiling). CT-scanner was also used to look at the internal defects of the cored samples.

a) Preparing rail and temporary post tensioning

b) Wire brushing

c) Applying epoxy on the both sides

d) Applying temporary post-tensioning

e) Preparing the steel plate

f) Applying epoxy

g) Applying permanent post tensioning

Figure 3.26. Dundee prototype assembling procedure

3.7.2. Schmidt rebound hammer test

Schmidt rebound hammer test (ASTM C805 (2013)) measures surface hardness of the concrete based on the principle that the hardness of the surface that is in contact with the hammer specifies the rebound of the elastic mass (IAEA, 2002). This hammer can be used both in laboratory and in site. Rebound number is defined as the distance, which is measured on an arbitrary scale from 10 to 100. ASTM C805 (2013) explains the procedure of the test in detail. The position of the hammer can be both horizontally or vertically and it can be set at any intermediate angle. The position of the hammer affects the rebound number. Therefore, the rebound number of a vertical surface is expected to be more than a horizontal surface like a floor.

The calibration curves on the hammer cannot be used in all conditions because the concrete that has been used for calibration can be very different from the concrete that is being tested. However, the concrete with higher rebound number has the higher compressive strength. Finding a right correlation between compressive strength and rebound number needs other parameters (Neville, 2011).

3.7.3. Chloride analysis: $AgNO_3$ spray (colorimetric method)

Spraying $AgNO_3$ is a very fast and simple colorimetric technique to measure the depth of chloride ingress into concrete. This method has been used throughout this project for measuring and comparing chloride penetration depth in concrete and epoxy bond. $AgNO_3$ react with unbound or free chlorides and produce silver chloride. In this procedure, the sample should be split into two pieces and 0.1 M $AgNO_3$ is applied on the cut surfaces one or two times successively. The reaction makes the chloride affected surfaces white or light grey, and the parts without free chloride remain darker (Baroghel-Bouny et al., 2007). Finally, average free chloride penetration depth (x_d) can be calculated based on 10 mm intervals of penetration depth measurements. The measurements are the distance between borderline and chloride-affected depth. The average chloride depth can be used for evaluating non-steady state chloride diffusion.

This method does not give the chloride concentration but Baroghel-Bouny et al. (2007) compared the detected chloride front with chloride profiles achieved by grinding layers of the same samples. This comparison showed that chloride concertation at the detected chloride front by spray test is always lower than the critical chloride threshold (C_{crit}= 0.4% by unit mass of concrete). Therefore, there is no risk of chloride induced corrosion beyond the detected front by spray test. This method has been very useful for the current project because it provided an easy visual comparison between jointed areas and body of concrete.

3.7.4. Computed Tomography (CT) scanning

The Nikon XT H 225 ST CT scanner was used in various phases of this project to look at microstructural changes in the bonded concrete samples. 3D volumetric representation of the samples was reconstructed after capturing sequential 2D X-ray images while the sample was rotating through 360°. Sections were made through 3D object to see the internal situation of eth samples.

X-rays are produced when a filament wire is electrically heated, and the released electrons are accelerated toward a tungsten target in vacuum. The filament wire acts as cathode and the tungsten as anode. The electrons move from the cathode to the anode by a high potential difference (voltage). Bremsstrahlung or characteristic radiation causes X-ray emission by almost 0.2% of these electrons. The rest of the electrons may lose their kinetic energy by interaction with outer shells of tungsten. Higher energy X-ray can be produced by higher peak applied voltage (Powsner et al., 2013).

The Nikon XT H 225 ST instrument has a 2000 × 2000 pixel flat panel detector, measuring 400 mm × 400 mm in size, which is positioned 1130 mm away from the source. Resolution of 3 µm can be

obtained in case of a very small sample closer to the source of X-ray. The biggest object (up to 260 mm in diameter) can lead to about 130 µm resolution. For a typical sample size used in the current project, which was 100 mm in diameter, 100 mm / 2000 = 0.05 mm or 50 µm resolution was obtained, i.e. the smallest distance distinguished between adjacent pixels.

3.7.5. Water penetration test method

The water penetration test was conducted according to BS EN 12390-8 (2009f) by applying a water pressure of 500±50 kPa. The duration of test was 72±2 hours and then the sample was split in to two half and depth of penetration of water was measured to the closest mm. The concrete cube with 150 mm × 150 mm × 150 mm dimensions was cut into halves and jointed together with epoxy again. This jointing technique was called hard-hard bond concrete. Another set of samples were prepared by applying fresh concrete and and epoxy on the hard concrete. This jointing technique was called fresh-hard bond concrete. The test was conducted for these jointed sections with Mix 1 and Mix 3, see Table 3-9, after 3 months of exposure in seawater salt solution.

3.7.6. Initial Surface Absorption Test (ISAT) method

Initial Surface Absorption Test (ISAT) is BS 1881-208 (1996) for measuring the surface absorption of the concrete under a constant 200 mm head of water. The test was conducted for both the pure concrete samples and the jointed sections. ISAT equipment consists of a cap seal, water reservoir and calibrated capillary tube (see Figure 3.27). Oven dried, and cooled samples should be prepared. Before starting the test, the apparatus should be calibrated, and the cap of the test apparatus should be greased so that when it is located on one side surface of the sample, a complete watertight seal is made. Tripod stand was located on top of the cube, and funnel (reservoir) was filled with tap water (20± 2°C). Gradually, the reservoir should be opened and when the water first reaches the concrete surface, a stopwatch measures time. Careful consideration is required to keep the reservoir fill at all time and remove all air bubbles within the apparatus.

The glass tube should be located horizontally against the rule fixed to the tripod. The tap should be closed at 15 seconds before 10 minutes have elapsed and the distance the water surface moves along the capillary tube in 60 seconds should be recorded. After this stage, the tap should be opened, and last two stages should be repeated after 30 and 60 minutes have elapsed from the start of the test. ISAT value is calculated by distance moved by water at time, multiplied by calibration factor of the apparatus. The mean value of ISAT-10, 30, and 60 are reported to the nearest 0.1×10^{-2}. The calculation is as follow:

$$\text{ISAT value (ml/m}^2\text{/s)} = d \times F$$

Equation 3.13

d: Distance moved by water (mm) at time, t (min)

F: Calibration factor for apparatus

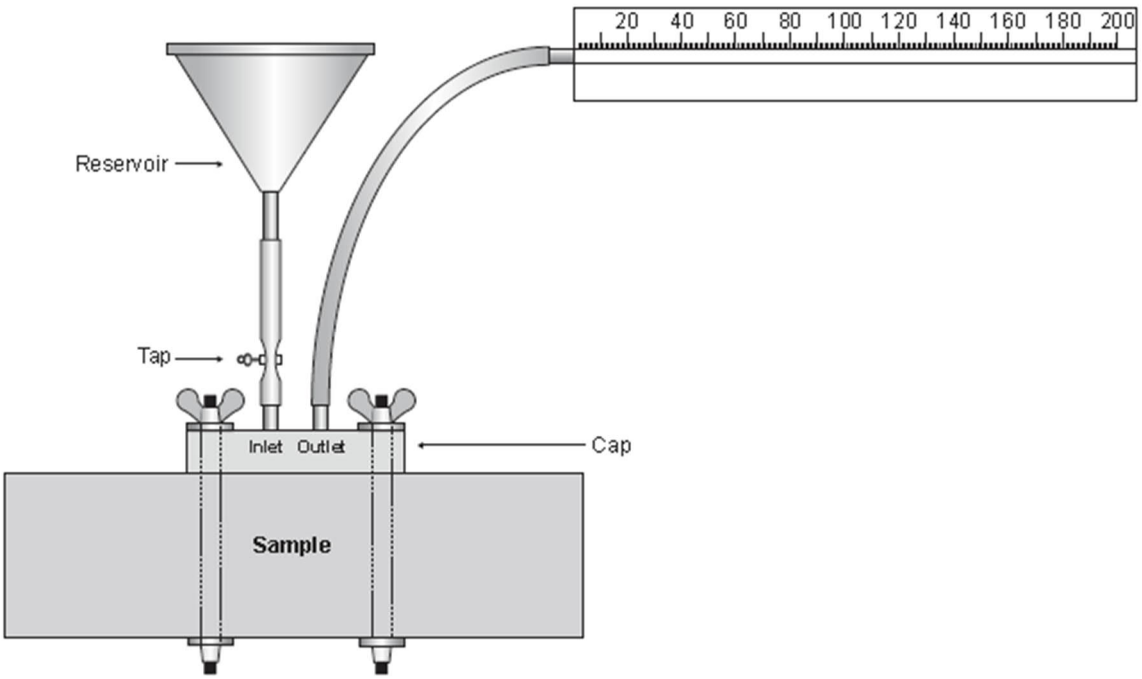

Figure 3.27. ISAT test equipment (Mehta and Monteiro, 2006)

3.7.2. CEN TS 12390-11 test method

CEN TS 12390-11(2010) was used to find the unidirectional non-steady state chloride penetration parameters of hardened concrete. The samples were vacuum saturated prior to the test. For vacuum saturating, the specimens should be washed, brushed surface dried completely. The specimens were placed in the container and the pressure inside the vacuum reduced in the range of 10-50 mbar within a few minutes. The specimens remained in this condition for three hours, as the pump was still working; the container was filled with saturated calcium hydroxide $CaOH_2$ solution. The solution covered the specimens entirely. The air re-entered the container for one extra hour. Finally, the samples remained in the solution for 18±2 hours.

After vacuum saturation, all faces of the sample expect one were coated with wax and exposed in the seawater solution for 90 days. At the end of this period, the samples were grinded, and the chloride profile was achieved by acid soluble chloride titration procedure (this process is explained in detail in Appendix B). Finally, the non-steady state chloride diffusion coefficient was calculated by curve fitting to chloride profile. This test was conducted for samples in two different conditions. First one, the samples were fully immersed in seawater salt solution. Second one, the samples were under cyclic wetting and drying in seawater salt solution with 6 hours of wetting and 18 hours of drying.

3.7.3. Chloride migration test method

Migration tests are based on applying a potential difference to accelerate the movement of chloride ions across a concrete specimen. The tests have been developed to determine the transport properties

in the shortest time possible. The most common tests are the NT Build 492 (1999) and the Multi Regime (MR) (Castellote et al., 2001). Natural diffusion tests like NT Build 443 (1994) and the CEN TS 12390-11 (2010) are often accelerated by providing a higher molar concentration of chlorides than would normally be present in normal environments, however these experiments are still often time consuming, with them regularly lasting up to 90 days.

The migration tests were conducted for pure concrete samples too in order to assess the durability of the mix design and compare with jointed samples. They were conducted by considering plain concrete disks, vertically jointed section and horizontally jointed sections (see Figure 3.28).

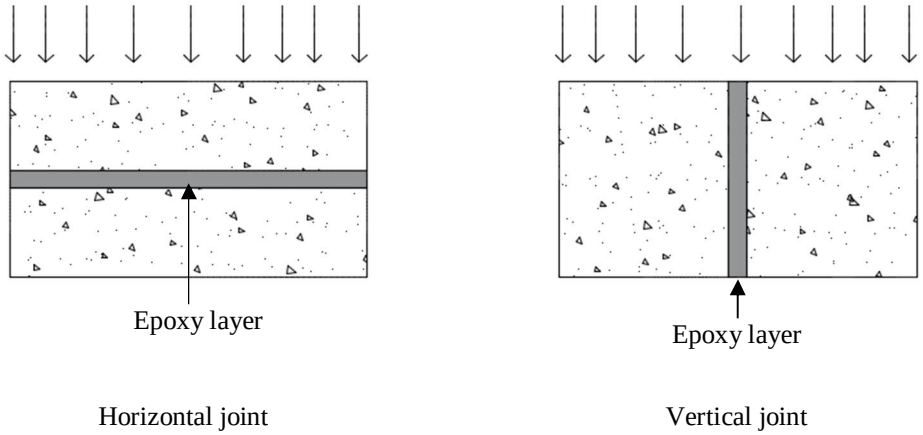

Figure 3.28. Direction of joint in migration test

3.7.4. NT Build 492 test method

NT Build 492 (1999) is a method for measuring the non-steady state migration coefficient of hardened concrete. The cylindrical sample should be drilled to achieve 100 mm diameter cylinder, then the outermost thick layer should be cut off. The final sample is 50±2 mm thick concrete disc cut with water-cooled saw. The samples should be vacuum saturated as explained before.

The schematic test set up can be seen in Figure 3.29. The samples were placed in a rubber sleeve and they were clamped to prevent any leaking. After setting up the equipment, the power was turned on and 30 V voltage was applied, and the initial current was recorded. The voltage and current were adjusted based on the initial current.

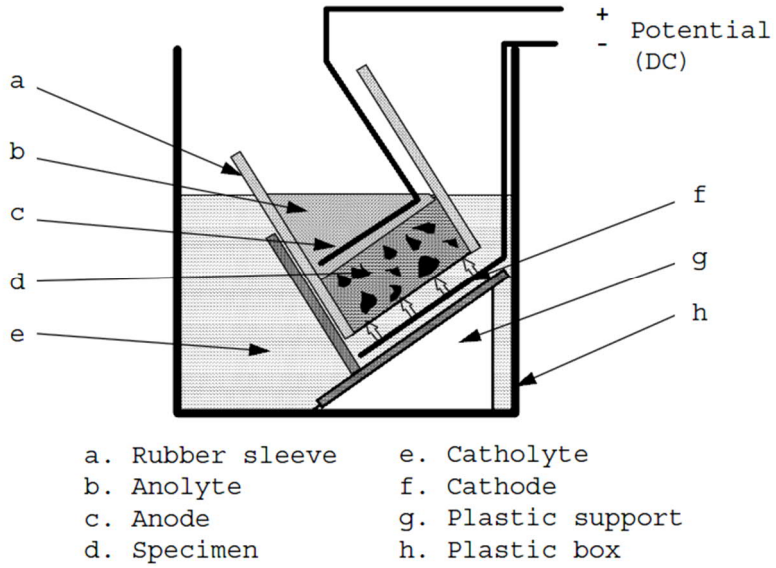

Figure 3.29. NT build 492 set up (NT BUILD 492, 1999)

After specified duration of the test, the temperature and the final current were recorded, then the samples were removed from the rubber sleeved and were split into two equal sections. The 0.1 M silver nitrate ($AgNO_3$) was sprayed on the split surfaces immediately and a Vernier was used to measure the penetration depth. The test result is expressed by calculating non-steady state migration coefficient with Equation 3.14.

$$D_{nssm} = \frac{0.0239(273+T)L}{(U-2)t}\left(x_d - 0.0238\sqrt{\frac{(273+T)Lx_d}{U-2}}\right)$$

Equation 3.14 (NT BUILD 492, 1999)

D_{nssm}: Non-steady-state migration coefficient $\times 10^{-12}$ m^2/s

U: Absolute value of the applied voltage (V)

T: Average value of the initial and final temperature in the anolyte solution (°C)

L: Thickness of the specimen (mm)

x_d: Average value of the penetration depth (mm)

t: Test duration (hour)

Reproducibility and repeatability of the test are 36% and 18% respectively (Castellote and Andrade, 2006).

3.7.5. Multi Regime (MR) test for jointed samples

Multi regime method invented by Castellote et al. (2001) is biased on conductivity measurements to calculate both steady and non-steady state chloride diffusion coefficient. Calculated non-steady diffusion coefficient is reported here. The test consists of two compartments. One of them contains seawater salt solution and the other one contains distilled water. A drop voltage was applied between the compartments. The upstream compartment had the negative electrode, so the chloride ions migrated to downstream compartment with the applied force of external electrical potential. By measuring the conductivity, the amount of chloride migrated to the downstream cell (anolyte) can be measured (Figure 3.30 and Figure 3.31). The empirical correlation between chloride concentration and conductivity was used to measure the concentration of chlorides. The flux of chlorides through the specimen was used for calculating the steady state coefficient and time lag of chloride ions to make a constant flux to calculate the non-steady state diffusion coefficient.

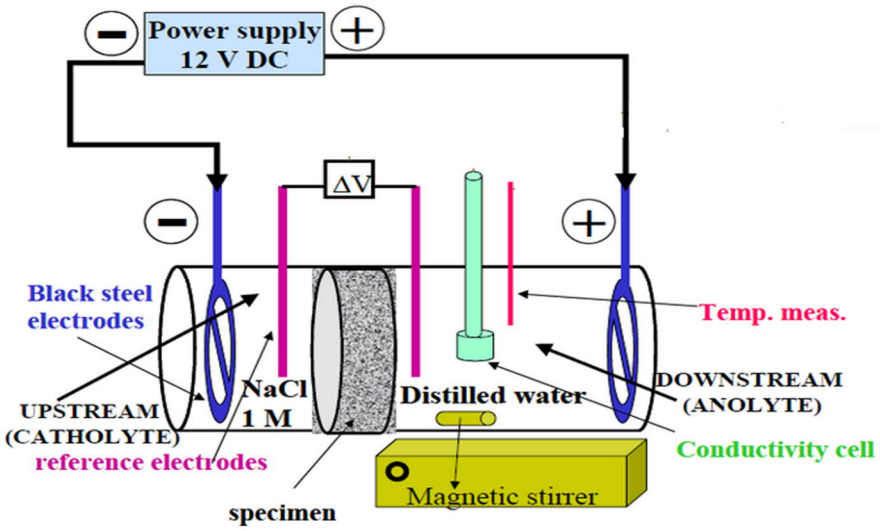

Figure 3.30. Multi Regime (MR) equipment (Castellote et al., 2001)

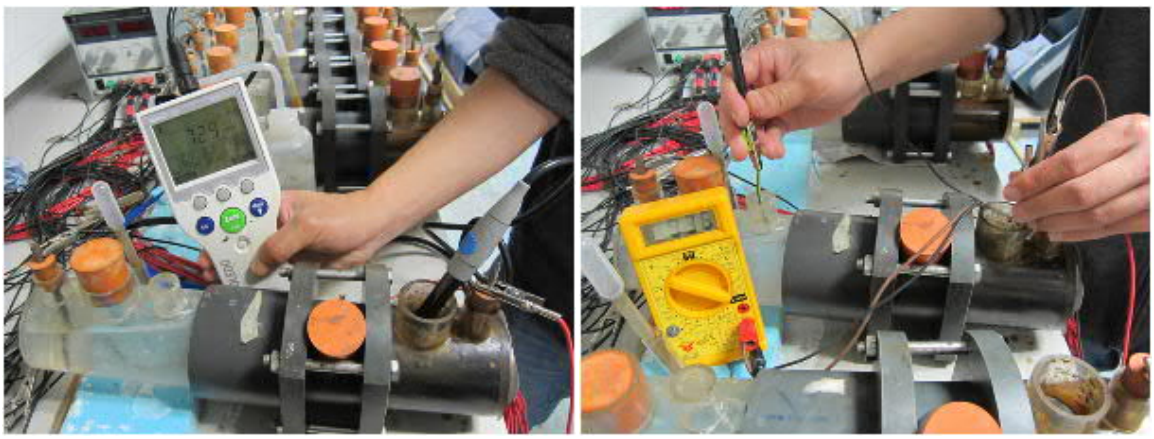

Figure 3.31. Measuring conductivity and voltage in Multi Regime testing

The test result is expressed by calculating non -steady state migration coefficient by Equation 3.15:

$$D_{ns} = \frac{2l^2}{\tau\nu^2}\left(\frac{\nu \coth \nu}{2} - 2\right)$$

Equation 3.15(Castellote et al., 2001)

τ: Time-lag in the migration test (s)

l: Thickness of the specimen (cm)

ν: $ze(\Delta\varphi)_t/kT$, where:

z=1 is ion valence

k= 1.38064852 × 10-23 m^2 kg s^{-2} K^{-1} is Boltzmann´s constant

$(\Delta\varphi)_t$: Averaged effective voltage (V) through the specimen from the beginning of the test until the time lag

T: Average temperature during the test (K)

For the values of voltage drop usually used in the test, can be simplified into Equation 3.16

$$D_{ns} = \frac{2l^2(\nu - 2)}{\tau\nu^2}$$

Equation 3.16 (Castellote et al., 2001)

Reproducibility and repeatability of the test has been reported as 69% and 22% respectively.

3.7.6. Scanning Electron Microscope (SEM)

Philips XL-30 Scanning Electron Microscope (SEM), which is coupled with an Energy-Dispersive X-ray spectroscopy (EDX) analysis, was used to compare different kind of epoxies available in this study. The samples were coated by gold- palladium layer and put on distance of 10 mm, SEM use 20 keV energy to show the samples and analyse the composition using EDX. Epoxy A, epoxy B, and Epoxy C were tested by SEM and EDX in this study.

3.7.7. Tensile testing of bulk epoxy

ASTM D 638 (2014) test method for tensile properties of plastics was used to assess the behaviour of bulk epoxy under tension. One of the epoxy samples were placed in the tank under cycles of wetting and drying in artificial seawater salt solution. The test was conducted on that sample after 90 days of exposure to examine the extent of plasticization of the bulk epoxy.

Dumbbell-shaped specimen is used in this standard with the dimensions shown in Figure 3.32 and Table 3-14. Epoxy B with 11.2 GPa tensile E modulus can be categorized as a rigid plastic. Therefore, the chosen dimensions are related to tensile testing of rigid plastic.

Epoxy B was cast in prefabricated aluminium mould shown in Figure 3.33. Mould release agent with commercial name of Buehler (provided by RS Ltd.) for use with cold mounting materials like epoxies was used to avoid sticking of epoxy to the mould. The epoxy was mixed and placed in the mould and cured in the lab temperature (20 ± 2 °C). After three days, the epoxy specimen was de-moulded and tested using INSTRON 5985 with mounted 50 kg Load cell and LVDTs.

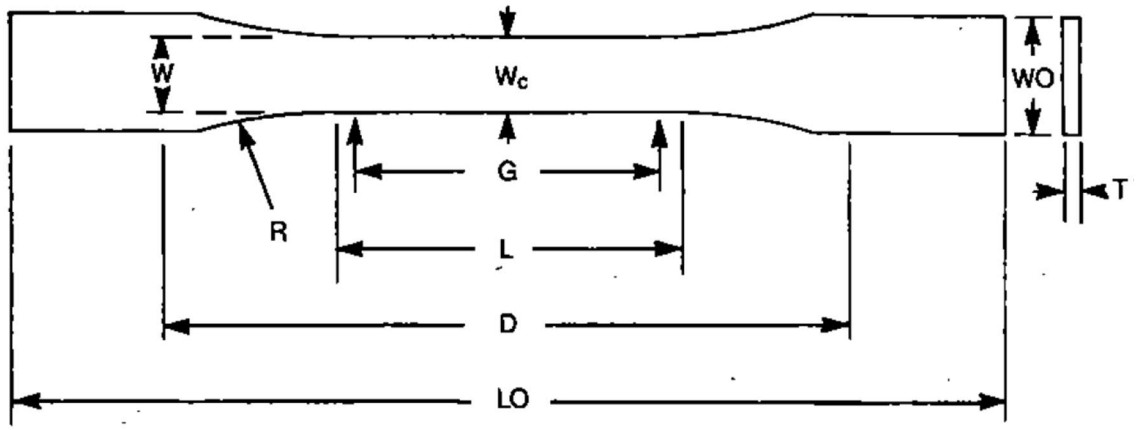

Figure 3.32. ASTM D 638 specimen dimension for Type I (rigid and semi rigid plastic)

Table 3-14. ASTM D 638 specimen dimension Type I (rigid and semi rigid plastic)

Dimension (see Figure 3.32)		Dimension (mm)
T	Thickness	3.2±0.4
W	Width of narrow section	13
L	Length of narrow section	57
WO	Width over all	19
LO	Length over all	165
G	Gage length	50
D	Distance between grips	115
R	Radius of fillet	76

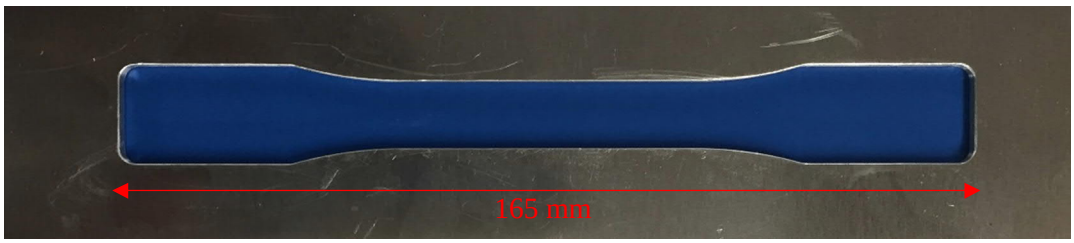

Figure 3.33. Aluminium mould for casting epoxy according to ASTM D 638 (2014)

Figure 3.34 shows the INSTRON 5985 and wedges used in this test. The distance between the grips was adjusted based on the standard recommendation. The surface of epoxy had to be smooth to avoid any local stress concentration in the grip, hence the ends of epoxy specimens were levelled by sand paper. The set up should be accurate enough to avoid any eccentricity in the loading that can lead to shear failure of the specimen instead of tensile.

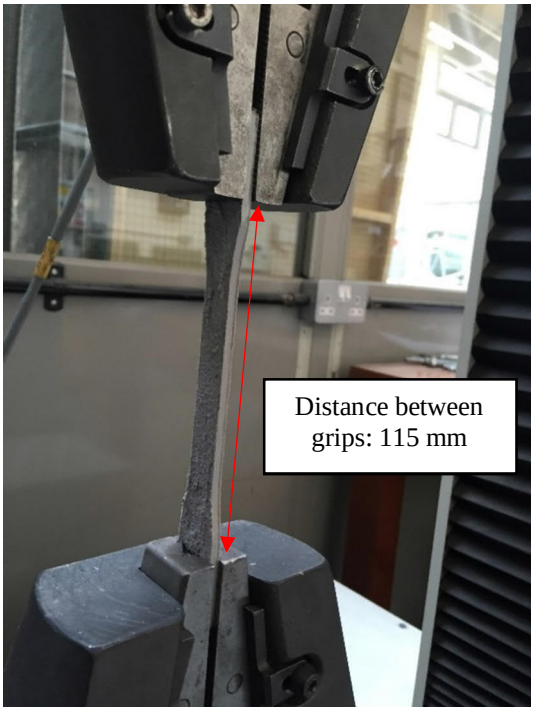

Figure 3.34. Bulk epoxy tensile test

3.8. PHASE III TEST METHODS: CYCLIC LOADING MESO/MICRO SCALE BEHAVIOUR OF EPOXY BONDED CONCRETE

Step by step design and installation of the cyclically loading test is explained in this section. An innovative test rig was set up to evaluate the simultaneous effect of loading and exposure to cycles of wetting and drying in artificial seawater salt solution. Four point bending test based on BS EN 12390-5 (2009d) was adopted as the basis for this set up. This test method was chosen due to inducing constant moment in the critical jointed area. Therefore, the critical area was under pure tension (mode I). Figure 3.35 shows the moment and shear diagram of the beams which conforms to BS EN 12390-5 (2009d). In order to avoid any shear failure in the areas of constant shear, external steel plates were glued on the concrete to provide shear reinforcement.

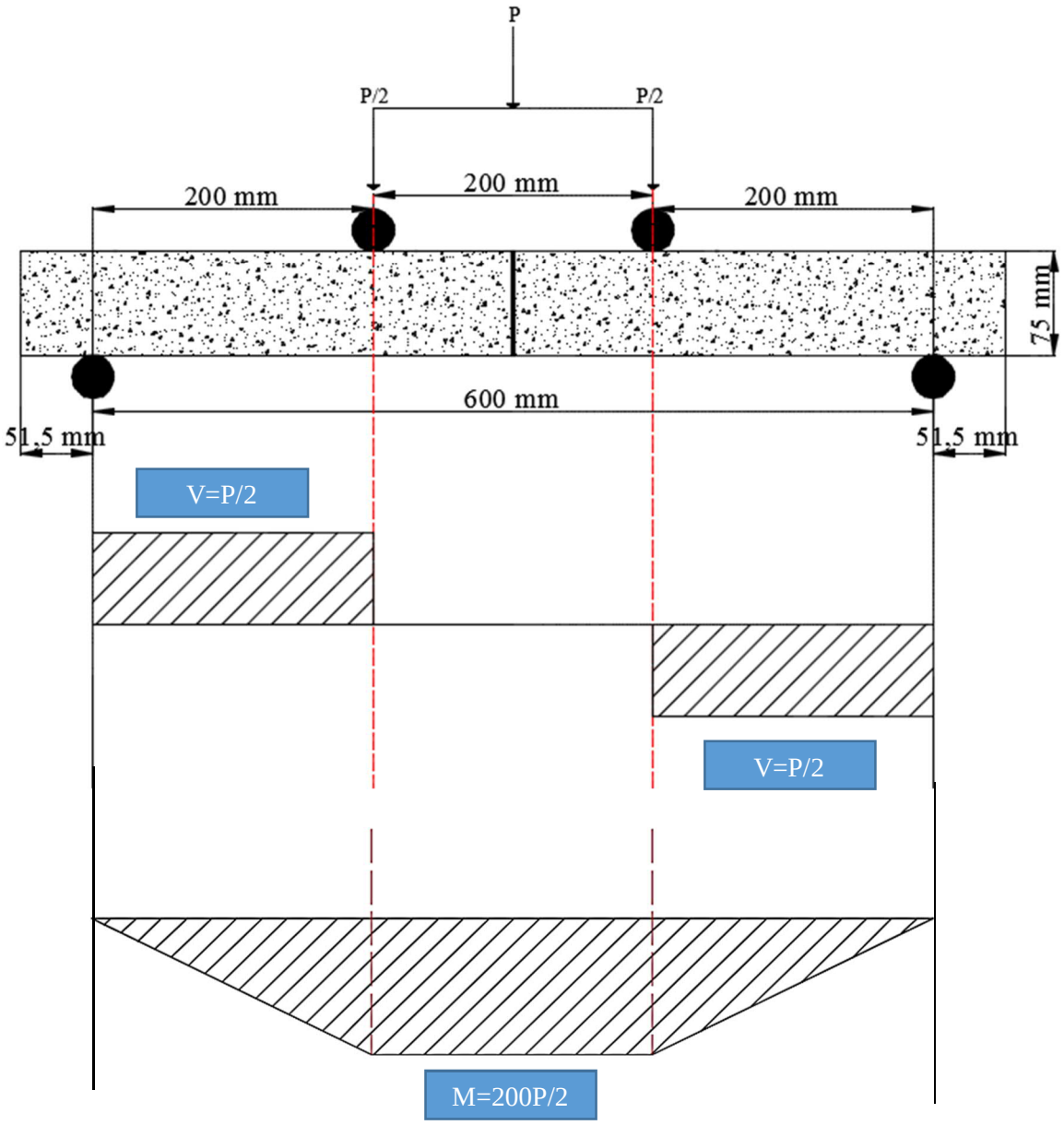

Figure 3.35. Four point bending test according to BS EN 12390-5 (2009d)

The samples were cast and cured as it was described before, but they were oven dried for a period of one months after the 28 days curing. The drying was done for accelerating the chloride and water ingress into the concrete. All the samples were also post-tensioned with 10 mm bars and an initial saw cut defect was induced in the body of concrete. The samples were preloaded to induce the 0.7 mm crack. Although the maximum allowable crack width is 0.3 mm according to Eurocode 2 (2004b), 0.7 mm crack width was chosen to magnify the effect and presents a very harsh environment. Finally, UPV, $AgNO_3$ spraying, CT scan, and Half-cell potential were used as monitoring methods during the testing period.

3.8.1. Samples size and configuration

The sample dimension was chosen to conform to minimum representative sample of concrete by considering the maximum aggregate size in this mix design (10 mm). Ease of handling, tank size and actuator loading capacity are other reasons for the chosen sample size. Figure 3.37 shows the detail of sample size and assembly. Concrete sections with 75 mm × 75 mm × 350 mm width, height, and length respectively were cast with single 6 mm internal rebar. The rebar was not covering the whole length of the concrete sample, it left 50 mm free at the end of the specimen. Therefore, after bonding two pieces of concrete there were total of 100 mm unreinforced area around the joint.

The rebar was also used throughout the testing period for monitoring corrosion. A small hole was drilled at the end of the rebar in order to fit a screw and connect the wire. The wire was attached for measuring Half-cell potential. Finally, the end of bars was coated using Pro black epoxy potting compound (supplied by UK RS Ltd.) for insulation and protecting the free end of the bars from corrosion. Figure 3.36 shows the fabricated wood mould and the bar position with the connected wire.

Figure 3.36. Mould, 6 mm rebar, and connection wire

Although the critical area of interest is under highest bending moment stress, there is a chance of shear failure on the adjacent areas under cyclic loading. Therefore, some steel plates with 15 mm × 75 mm × 1 mm width, height, and thickness respectively were connected by epoxy in the highest shear area to avoid the shear failure during the test. The distance between plates were adjusted to conform to minimum shear reinforcement requirements of EC2 (2004b).

The end steel boxes were used for support of external post tensioning bars. A single thick plate could also be used but the box sections assure occurrence of no bending in the end plates. External 10 mm diameter stainless steel bars were used for external post-tensioning. These bars were externally located in the middle height of the section and passing through the end boxes. Suitable washers and nuts for M10 were used to connect all the external M10 bars and boxes. The post tensioning was applied by the relationship between the strain and stress with in the external bar section. The detail of post tensioning process is mentioned in the following sections.

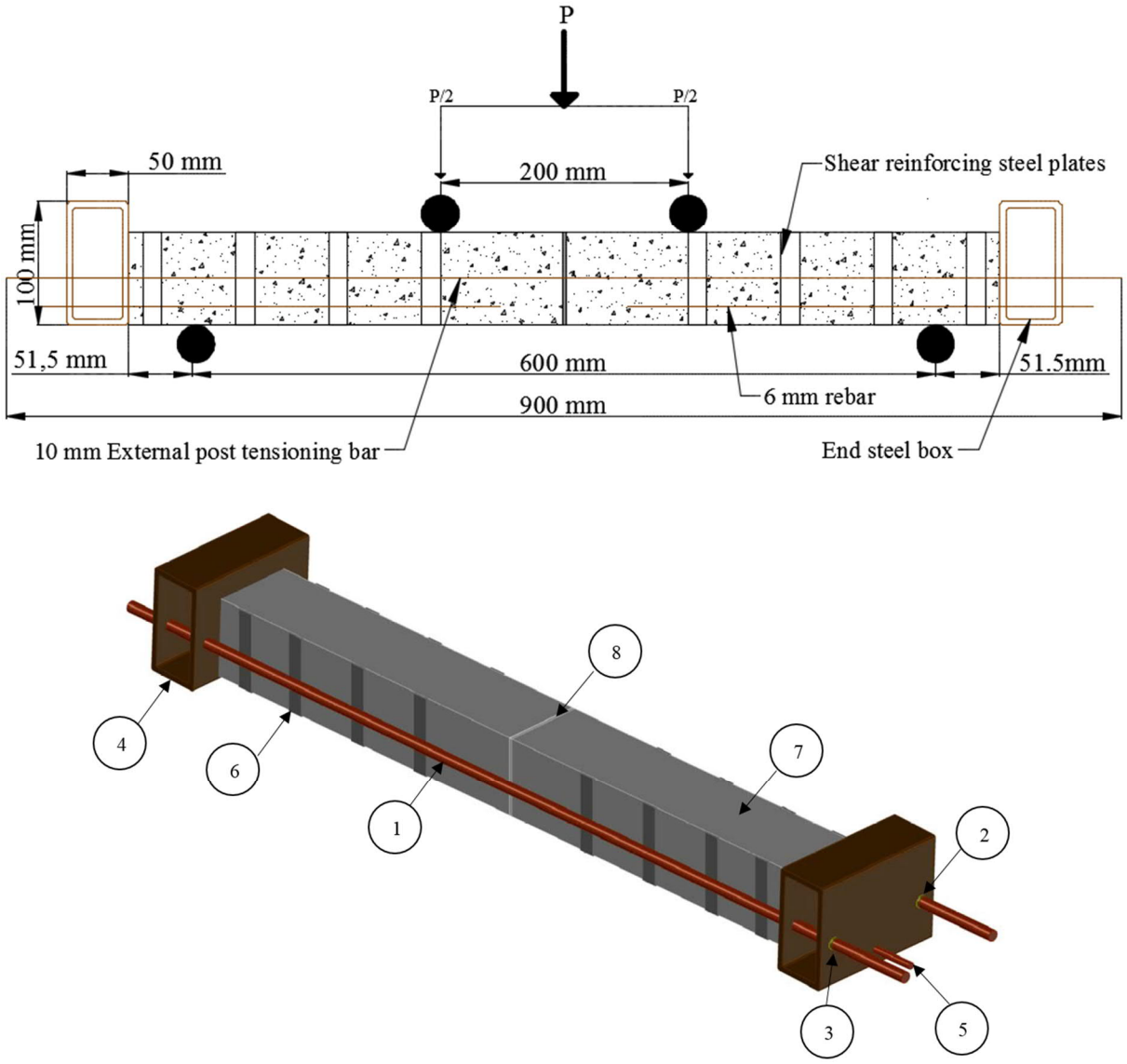

Figure 3.37. Loading position and constituting element of the beams in Phase III

Table 3-15/ Details of the beams in Phase III

Item NO.	Part Number	QTY.
1	M10	2
2	Washer for M10	4
3	Hexagon Nut for M10	4
4	Steel box	2
5	6 mm diameter rebar	2
6	Shear reinforcing steel plates (15 mm × 75 mm)	16
7	Concrete (75 mm × 75 mm × 350 mm)	2
8	Epoxy B	3 mm

3.8.2. Stress analysis

The cyclically loaded samples experienced two different stress conditions of unload and loaded during each cycle. The unload condition includes the post tensioning and self-weight (see Table 3-16 and Figure 3.38 (a)) which is named as σ_{min} situation in Figure 3.38. In this condition, the beam is under compression, but the gradient of compressive load slightly change from top to bottom of the beam due to self-weight. σ_{max} condition shown in Figure 3.38 happens when the load is applied by the actuator. The combination of the applied load, post tensioning and self-weight cause highest tension at the bottom of the beam and gradually change to highest compression at the top of the beam.

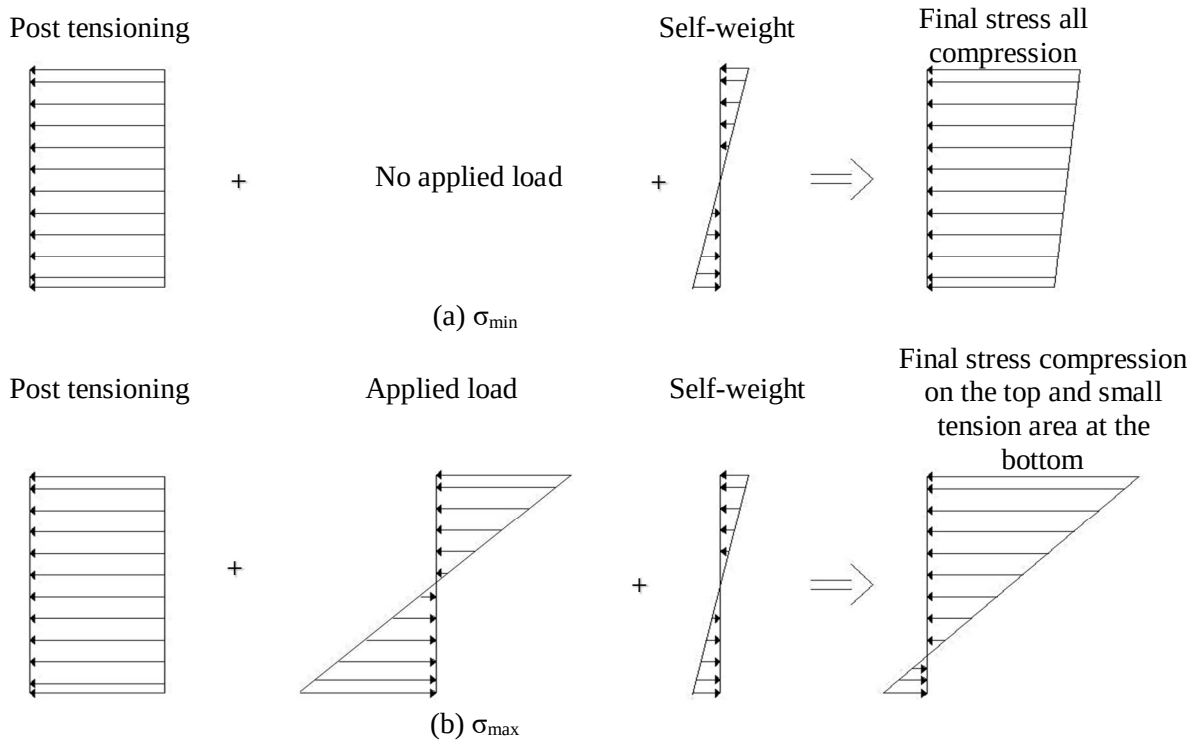

Figure 3.38. Schematic stress diagram of the critical area (assuming un-cracked section) (a) At the beginning of each cycle, (b) At the highest applied cyclic load

Stress in these two different conditions were calculated by considering total 6 kN post tensioning and 4 kN applied cyclic loading. This loading scheme was chosen to induce 80% of tensile strength of section at each cycle which represent wave loading. Higher percentage of stress can be considered as storm or earthquake.

The detail of self-weight calculation is mentioned in Table 3-16. The elastic stress analysis is conducted just for the middle part of the beam that experiences the constant bending moment.

Table 3-16. Approximate self-weight of the sample

Steel density	Assumed concrete density	Steel boxes	Steel bars (PT+Reinforcing)	Jointed concrete beam	Total sample weight
kg/m^3	kg/m^3	kg	kg	kg	kg
7850	2500	1.42	1.54	9.84	12.80

$$\sigma_{PT} = \frac{P_{PT}}{A} = \frac{6000}{75 \times 75} = 1.07\ MPa$$

Equation 3.17

$$M_{CL} = \frac{L_1}{2} P_{CL} = \frac{200}{2} \times 4000 = 400 \times 10^3\ N.mm$$

Equation 3.18

$$\sigma_{CL} = \frac{6M_{CL}}{bd^2} = \frac{6 \times 400 \times 10^3}{75 \times 75^2} = 5.69\ MPa$$

Equation 3.19

$$M_g = \frac{mgL_2^2}{8} = \frac{0.018 \times 9.8 \times 10^3 \times 600^2}{8} = 8.06 \times 10^3\ N.mm$$

Equation 3.20

$$\sigma_g = \frac{6M_g}{bd^2} = \frac{6 \times 8.06 \times 10^3}{75 \times 75^2} = 0.11\ MPa$$

Equation 3.21

L_1: Distance between applied load and support roller (200 mm)

L_2: Distance between support rollers (600 mm)

b: Width of sample (75 mm)

d: Height of sample (75 mm)

A: Section area of un-cracked section (mm^2)

σ_{PT}: Post tensioning compression stress (MPa)

P_{PT}: Post tensioning load (N)

P_{CL}: Maximum cyclic load (N)

M_{CL}: Four point bending moment ,BS EN 12390-5 (2009d) (N·mm)

σ_{CL}: Cyclic loading compression/tension stress at the point farthest from Neutral Axes (N.A) (MPa)

m: Total sample weight assuming constant over the span ($\frac{12.80}{700} = 0.018\ kg/mm$)

g: Gravitational acceleration (9.8 m/s^2)

M_g: Bending moment of self-weight (N·mm)

σ_g: Self weight compression/tension stress at the point farthest from Neutral Axes (N.A) (MPa)

3.8.2.1. Elastic section unloaded situation:

σ_{min}: Final stress of the unloaded section at the point farthest from neutral axes:

a) At the farthest from neutral axes at the top of beam (compression area)

$$\sigma_{min} = \sigma_{PT} + \sigma_g = 1.07 + 0.11 = 1.18\ MPa$$

Equation 3.22

b) At the farthest from neutral axes at the bottom of beam (tension area)

$$\sigma_{min} = \sigma_{PT} - \sigma_g = 1.07 - 0.11 = 0.96\ MPa$$

Equation 3.23

3.8.2.2. Elastic section loaded situation:

$\sigma_{max:}$ Final stress of the loaded section at the point farthest from neutral axes:

a) At the farthest from Neutral Axes at top (compression)

$$\sigma_{max-top} = \sigma_{PT} + \sigma_{CL} + \sigma_g = 1.07 + 5.69 + 0.11 = 6.87\ MPa$$

Equation 3.24

b) At the farthest from Neutral Axes at bottom (tension)

$$\sigma_{max-bottom} = \sigma_{PT} - \sigma_{CL} - \sigma_g = 1.07 - 5.69 - 0.11 = -4.73\ MP$$

Equation 3.25

Overall, the bottom of the critical area (farthest from neutral axes at the bottom of the beam in the middle part of the beam) experienced 0.96 MPa compression stress at the initial stage and -4.73 MPa tensile stress at the time of applied load by the actuator. The maximum tensile capacity of bonded concrete with epoxy was assumed 5 MPa according to the tests conducted in the first phase of the project. The applied post tensioning stress was about 1 MPa which add to the tensile capacity of bonded specimen. Therefore, the tensile capacity of bonded section can be assumed 6 MPa. Hence, the -4.73 MPa tensile stress applied through cyclic loading was around 80% of tensile capacity of the sample.

3.8.3. Post tensioning method

Prior to post tensioning, tensile test was performed on the M10 external bars in order to find a correlation between the applied stress and strain measurements in the bar. This data was used later for assessing the applied post tensioning by tightening the bars.

Digital DEMEC mechanical strain gauge with 200 mm gauge length was used for measuring displacement along the M10 bars. Two aluminium studs with 200 mm distance were glued in the middle part of the bar. Quick set epoxy adhesive supplied by UK RS Ltd. was used for gluing the studs on the bars. The bars were fixed in INSTRON 5985 and DEMEC was externally fixed by the clamps on the studs (see Figure 3.39).

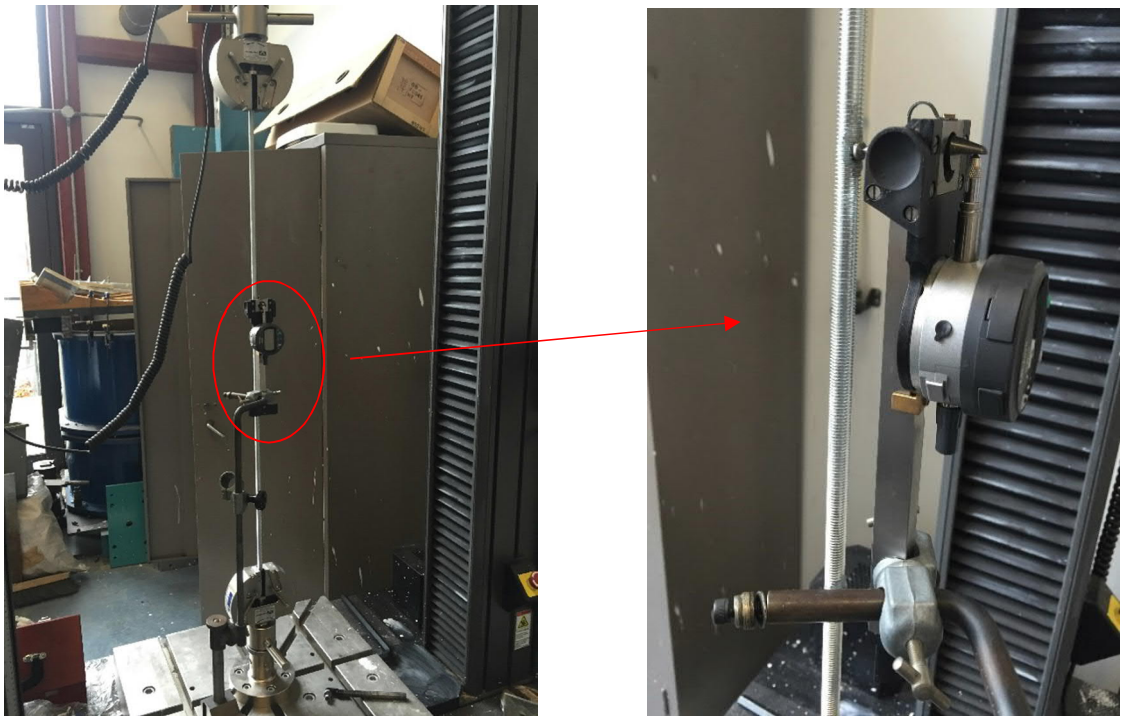

Figure 3.39. Tensile test of M10 and monitoring the strain in the middle 200 mm of the bar using DEMEC

The load was applied with 1 mm/s rate. The LVDTs and load cell were recoding the load and displacement. At every 500 N intervals, the DEMEC readings were also recorded. The recorded DEMEC readings were subtracted from the initial reading and divided by 200 mm (DEMEC gauge length). The gauge factor was not considered in this strain measurements because the correlation between load and DEMEC instant readings were important for this project not the exact strain values of the bars. Figure 3.40 shows the relationship between strain readings and the applied load. A straight line was fitted to the points and the equation used for applying the target posttension on the beams.

For example, for 6000 N post tensioning on the concrete specimens, the bars were fixed in the box end plates. The initial DEMEC reading was recorded. Based on the equation in Figure 3.40,

y=6000 N and the required strain changes will be 1087.90 μm/m. Hence, the strain gauge displacement should be 1087.90 e^{-6}×200, which leads to 0.22 mm gauge displacement. The final expected reading from DEMEC can be calculated by adding the initial reading to 0.22 mm. Finally, the bars were tightened until they reached the final expected DEMEC reading.

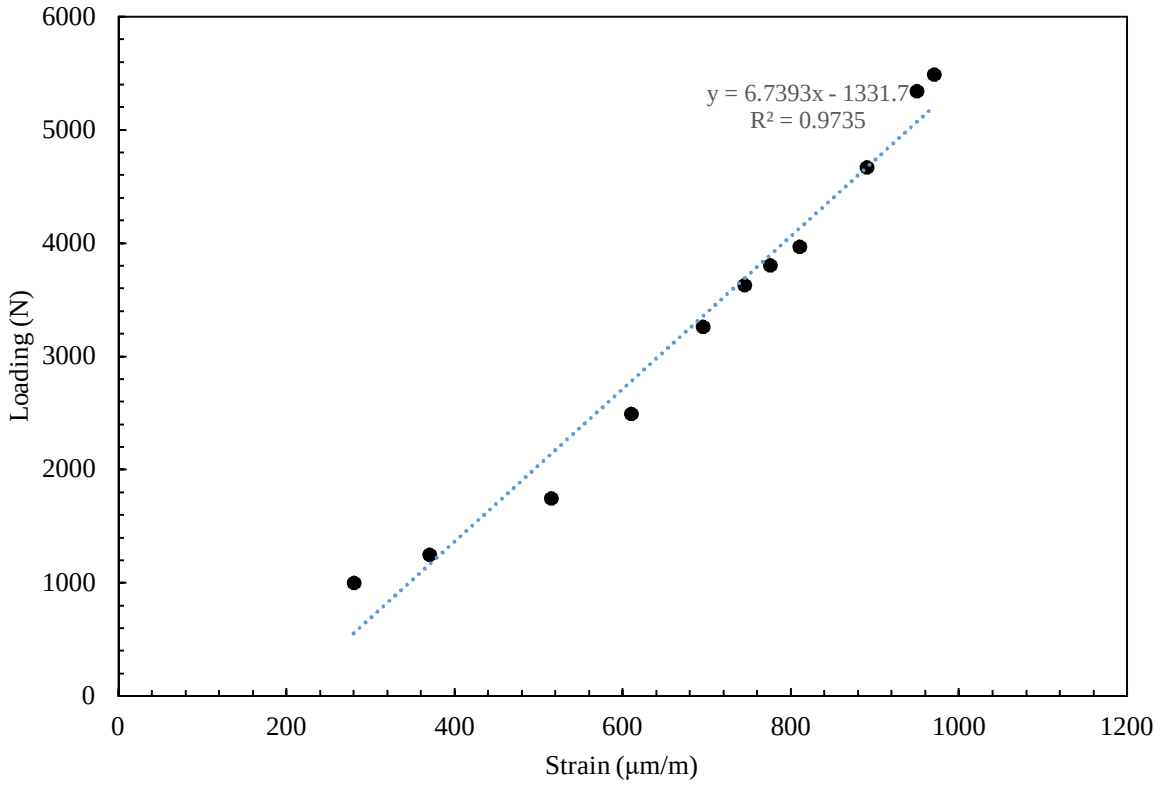

Figure 3.40. Relationship between strain of the bar and loading

3.8.4. Preloading and cracking

All the samples were preloaded and cracked before the exposure in seawater salt solution. To dictate the position of the crack, a saw cut crack was positioned in the bottom of the beam in 50 mm distance from the joint. The induced crack depth was 5 mm and was produced by saw cutting along all the width of the sample at the bottom in the designated location. Then, the sample was located and loaded upside down in the INSTRON 5985 to make the crack opening measurements possible (see Figure 3.41). The first loading was applied with 1 mm/s rate. The load and displacement were automatically recorded.

The crack opening was recorded using crack microscope and crack ruler in every 1000 N interval of the loading. Although the allowable crack width in BS EN 1992-1-1 (2004b) is 0.3 mm, the target crack opening was considered 0.7 mm in order to magnify all the effects.

After occurrence of the first crack with the target 0.7 mm width (the target crack width more than regular 0.3 mm to accelerate the and magnify the effect). The samples went through some limited

4000 N cyclic loading to record the initial hysteresis using the internal LVDTs and Load cell in the INSTRON 5985.

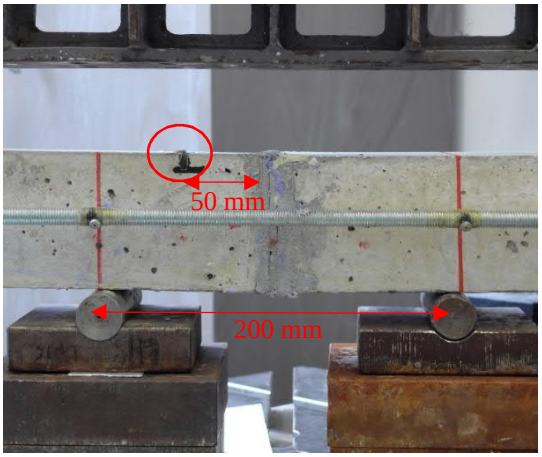

a) Induced saw cut crack position

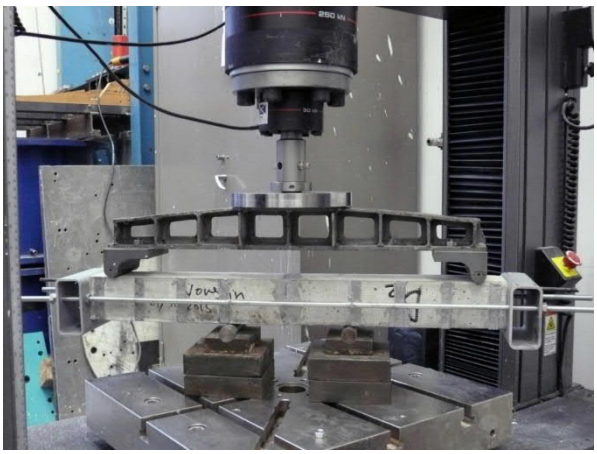

b) First loading for inducing the crack with 0.7 mm width

Figure 3.41. The induced saw cut and first loading to induce the major crack

3.8.5. No load and sustained load application

The beams were placed in the tank under cycles of wetting and drying for the period of 90 days. No load situation was just simple positioning of the beams in the tank.

Sustained loading was applied by pushing the beams down with jacking to the ceiling. The amount of push was adjusted according to the 0.7 mm crack width target i.e. when the crack reached 0.7 mm the push was not increased and kept constant for 90 days. The sustained load samples also experienced 90 days of cyclic wetting and drying in the artificial seawater salt solution.

3.8.6. Actuator setting and cyclic loading pattern

ROBO Cylinder RCP2-RA10C electrical actuator with 2.5 mm lead and 50 mm stroke supplied by LC Automation Ltd. was used for applying cyclic loading. The commercial name of the supplied controller is PCON-CFA-86PWAI-PN-2-0. The controller was mounted in house using the guidance provided by the supplier with 24 V DC power supply rated 4.2 A / max. 6 A and emergency stop switch.

The actuator did not have any load cell so the current limit value ratio (%) was used to estimate the applied load on the sample. Current limit value is the upper limit on the current which protects the circuit from harmful effects and voltage drop. The relationship of the push force and the current-limiting value is only way to assess the push force in small electrical actuators.

Since the actuator is a 2.5 mm lead actuator, the maximum possible current ratio is 70% and the corresponding load is 6000 N (see Figure 3.42 (a)). It means that the current remains constantly 70% or more during load application.

Another important feature to be considered for setting up the actuator was the maximum mounted load in the vertical position because there was a steel fork attached to the actuator and the actuator was installed vertically (see Figure 3.42 (b)).

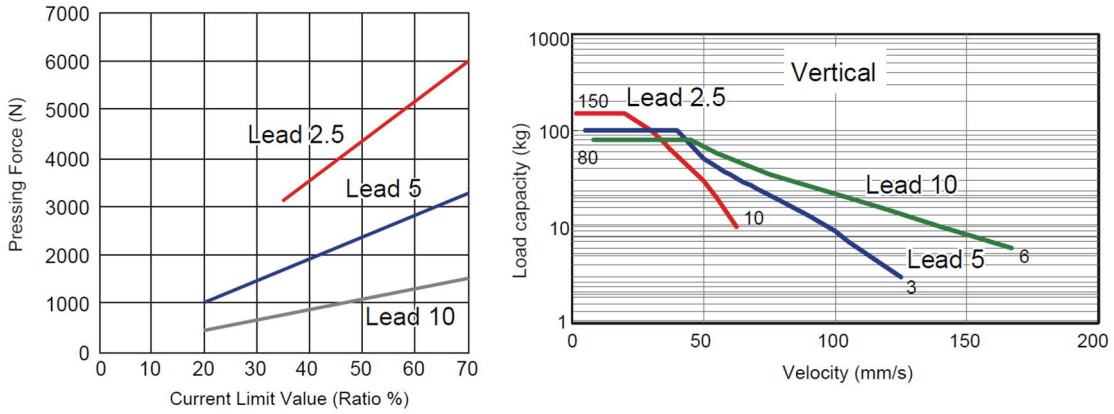

a) The relationship between current limit value and applying load

b) Relationship between velocity and allowable mounting load capacity in vertical position

Figure 3.42. Actuator features for loading (2.5 mm lead) provided by LC automation ltd.

The actuator software has two loading options: positioning band and push band. In positioning option, the force will be applied until it reaches the target position. In pushing mode, the force is applied until it reaches the target force (see Figure 3.43). Push band option was chosen for applying cyclic loading because the target 4000 N cyclic loading could be adjusted with that. Since the beam could lose stiffness over the period of the test, the deflection could increase. In push band, even if the stiffness of the beam decreases and the deflection increase, the stroke moves until it reaches the target force. Therefore, the maximum load will always be applied.

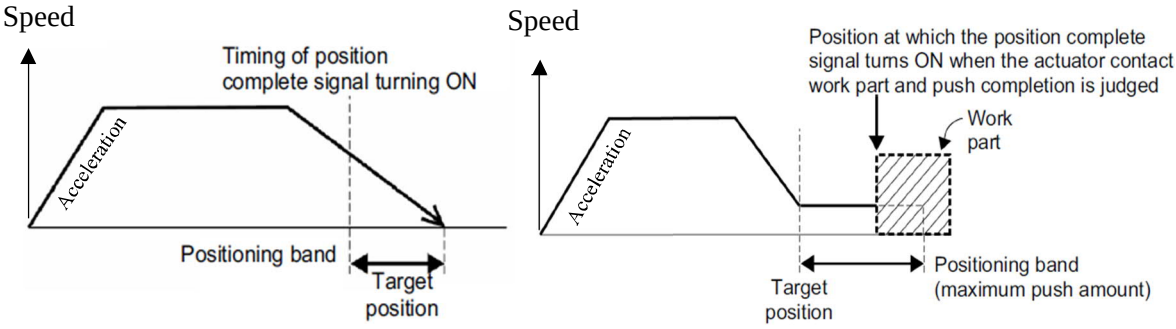

a) Positioning option

b) Push option

Figure 3.43. ROBO Cylinder RCP2-RA10C loading options-showing the position of Lead 2.5 (Load control by using push option was used for the main loading stage)

Considering all these specifications, the loading was adjusted in the following three steps (see Table 3-17 and Figure 3.44):

Step 1:

The actuator started moving from initial position by pose band function (just the displacement matter) with 8 mm/s speed. This speed was the maximum possible speed at this stage to make the least noise and vibration with the current configuration. Acceleration and deceleration were adjusted based on actuator specifications. (Positioning mode)

Step 2:

The distance travelled between the bottom of the rollers of the fork and the surface of the samples was adjusted as 15 mm (minimum allowable travel distance by the actuator specifications). Therefore, the stroke moved 15 mm with 8 mm/s speed until it touched the surface of the sample. (Positioning mode)

Step 3:

Step 3 was the actual loading step which can be considered as load control mode of cyclic loading. The actuator stroke touched the sample and loading mode changed to push mode. According to Figure 3.42, the required push percentage for 4000 N loading is 45% with 2.5 mm lead actuator. However, the rigidity of the frame isn't infinite, so extra 10% push loss was considered due to movements of the frame and the bolts. Therefore, the push was chosen to be 55% (current limit value ratio, see Figure 3.42). At this stage, the actuator moved with 1 mm/s speed until the loading reached 4000 N. Based on the pre-cracking load-deflection results of the specimens, the initial possible deflections were between 1 and 2 mm under 4000 N load. However, this deflection may increase during 3 months of loading due to loss of the post-tensioning and reduction of stiffness. Hence, up to 4 mm increase in deflection was allowed in the initial loading schedule, which led to position 20 mm (see Table 3-17), (Push mode). This could assure the maximum load application even after increased deflection.

The unloading condition included the same 3 steps but backward, going from final position to the initial zero position.

Table 3-17. Loading programme using Robo cylinder actuator

Step No.	Position (mm)	Acceleration (G)	Deceleration (G)	Speed (mm/s)	Push %	Pos.band (mm)
1	0	0.01	0.01	8	-	0.01
2	15	0.01	0.01	8	-	0.01
3	20	0.01	0.01	1	55	-

Considering the above loading pattern, the load frequency was calculated based on the speed and the travelling distance of the stroke. Moving from position 0 to 15 mm took about 1.9 seconds and considering 2 mm of deflection at push position, it took 2 seconds and then back to the position 15 which added another 2 seconds and back to position zero in 1.9 s to finish the cycle. In total, each cycle took about 7.8 seconds. Therefore, there is about 7 cycles per minute, which is the frequency of loading for this test. Figure 3.44 shows the loading cycles schematically. After 3 months of loading, each beam experienced about one million cycles.

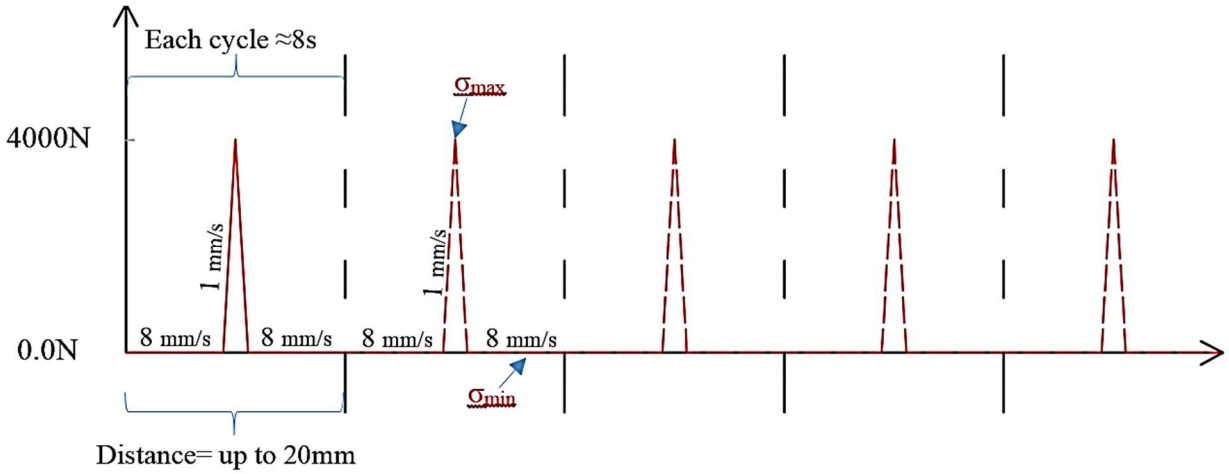

Figure 3.44. Schematic demonstration of the loading cycles –Load control at loading step 3.

In the case of concrete, any frequency lower than 900 cycles per minute is not a sensitive factor in fatigue strength, as long as the maximum loading is less than 80% of static strength because the higher value can be considered as a storm or an earthquake (ACI Committee 215R-74, 1997). The loading regime was almost 80% of static strength and the adjusted frequency was in the range of possible wave frequencies in the North sea (Venugopal and Nemalidinne, 2015).

3.8.7. Installation

The actuator was mounted on the scaffolding frame as can be seen in Figure 3.45. The frame was assumed rigid. All the bolts were tightened as much as possible manually. The actuator was placed vertically in the middle of the frame.

The frame and actuator were placed in the tank under cycles of wetting and drying. 1 M artificial seawater solution was prepared and covered the samples during the wet cycle (see Figure 3.46). There was another reservoir tank under the tank of the actuator. Both tanks had a pump with timers. Every cycle consisted of 6 hours of wetting and 18 hours of drying. The timers of each pump were adjusted accordingly to drain the water from the tank and send it back at the end of each cycle. Finally, the samples were placed on the frame and the fabricated fork was attached to the actuator.

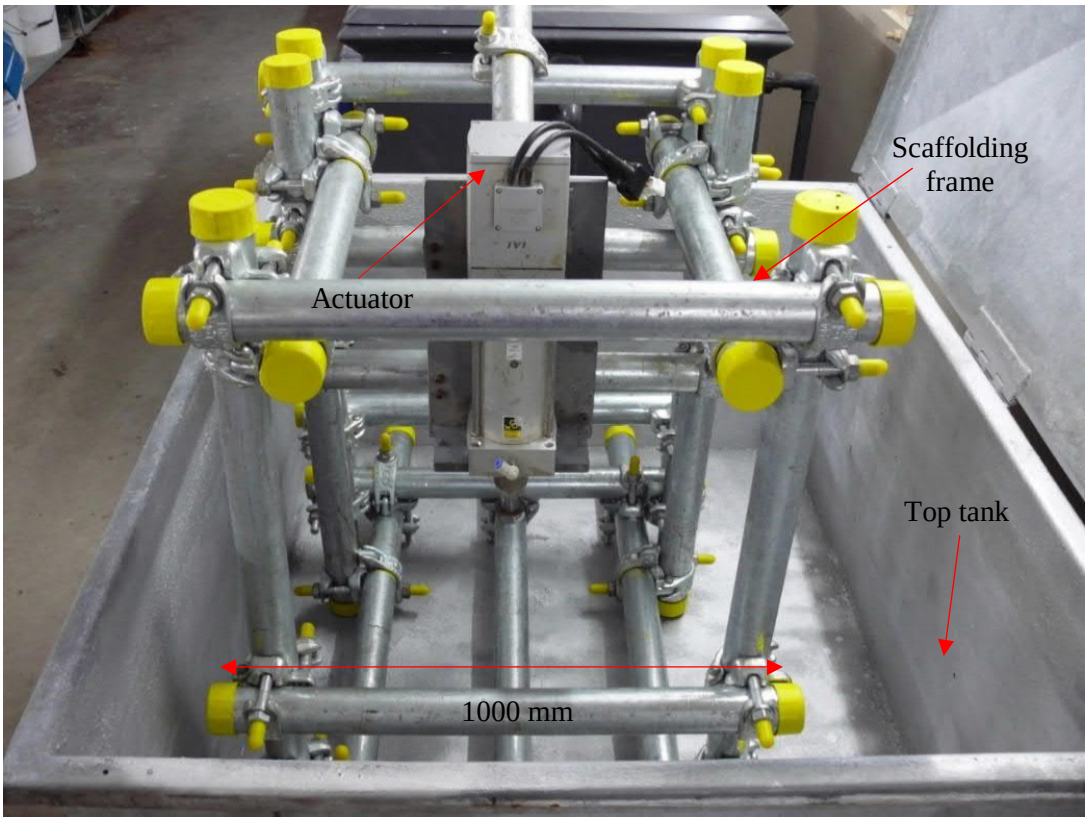

Figure 3.45. The actuator and installation of the frame in the tank

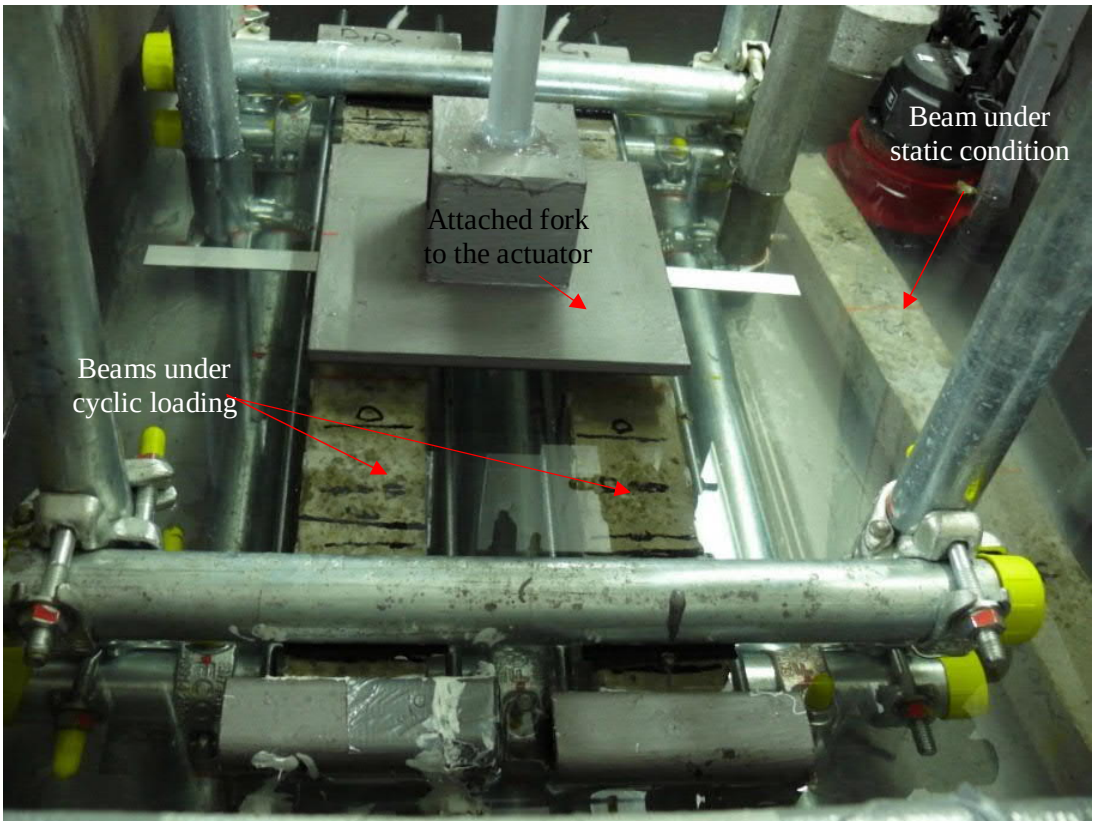

Figure 3.46. The cyclic wetting and drying tank and applying the load with the steel fork attached to the actuator

3.8.8. Monitoring methods

3.8.8.1. CT scan

The CT scanner was used for monitoring the microstructural changes. The scans were taken at the initial and final stage of the tests. Since the samples were large and could not easily fit into the CT scanner's shielded enclosure, a metal frame was constructed to support the beam diagonally (see Figure 3.47). The distance from the X-ray source was adjusted to include the critical area of interest (200 mm middle part of the beam with joint). Therefore, the highest achievable resolution of the scans became 78 µm.

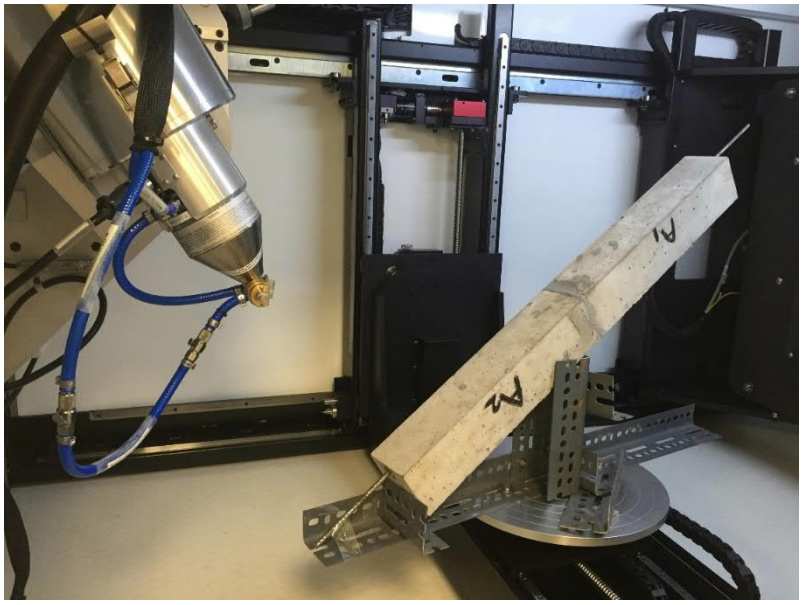

Figure 3.47. CT scanning set up achieving 78 µm resolution

3.8.8.2. Ultra Sound Pulse Velocity (UPV)

UPV was also used to monitor the reduction of stiffness during the test. According to limitation of space in the beam set up, the possible distance between two probes was considered 400 mm. UPV measurements were conducted at least once in a month during the cyclic loading. Three readings were recorded each time.

3.8.8.3. Half-cell potential

ASTM C876 (2015a) describes the half-cell potential method. This method is used for measuring the potential of steel bars relative to a reference half-cell, which is placed on the surface of concrete. The measurements were conducted at least once in a month during the loading cycles in order to monitor the corrosion initiation. The corroding bar is surrounded by an electric potential field, which is the result of migration of ions between anode and cathode. High negative potentials show high likelihood of corrosion.

The equipment consists of a silver-silver chloride half-cell electrode, connecting wires, and a high-impedance voltmeter. The silver-silver chloride electrode was attached to the negative terminal and

the reinforcement was attached by the positive terminal of voltmeter. A porous plug and a moistened sponge were used to make an electrical contact between concrete and the electrode. The measurements were recorded to the nearest 0.01 V. A more negative voltage is a sign for more excess electrons and therefore it means that bar is more corroded (see Table 3-18).

Table 3-18. Interpretation of Half –cell potential measurements (Gu and Beaudoin, 1998)

Half-cell potential (Ag/AgCl)	Likelihood of corrosion
E>-109 mV	<10%
-109>E>-259 mV	Uncertain
E<-259 mV	>90%

3.8.8.4. Chloride analysis by AgNO3 Spray

$AgNO_3$ spraying was used after finishing the loading period. The samples were cut into two halves and the spraying was conducted as it was explained before.

3.8.8.5. Evaluation of stiffness reduction

The loading and unloading hysteresis could not be recorded during the 3 months cyclic loading with the electrical actuator because the actuator does not have the required instruments for measurements like load cell and LVDTS. Therefore, after finishing the cyclic loading regime, a few cycles of loading were applied using INSTRON 5985 testing machine to record the load-deflection graph and compare the initial and final stiffness of the specimens.

3.9. SUMMARY OF ALL TEST METHODS

A summary of all test methods is presented in Table 3-19. This table summarizes the tests conducted in three main phases of the project (Phase I: static macro scale mechanical performance, Phase II: static meso/micro scale behaviour, and Phase III: cyclic loading meso/micro scale behaviour of epoxy bonded concrete). The details of each test were explained in corresponding sections. Since there were not many specific tests methods for epoxy bonded concrete, some of the test methods were devised or modified to suit the purpose.

To extrapolate data to a full-scale structure, the sample size in all tests should be Representative Elementary Volume (REV). Scaling up may not be very straight forward, but in general, the sample should conform to the assumption of homogeneity of concrete and the specimen diameter/dimensions should be at least three times bigger than the maximum aggregate size to be REV (Torrenti et al., 2010).

Table 3-19. Summary of test/monitoring methods in all Phases of the project

Test method	Standard or Reference	Modified	Developed by Author	Used in Phase I	Used in Phase II	Used in Phase III
Slant shear	BS EN 12615 (1999)	-	-	✓	-	-
Bi-surface shear	Momayez et al. (2005)	✓	-	✓	-	-
PV	BS EN 1250-4 (2004d)	-	-	✓	✓	✓
DIC	Correlated solutions Ltd.	✓	-	✓	-	-
Cyclic wetting and drying	-	-	✓	✓	✓	✓
Split cylinder	BS EN 12390-6 (2009b)	✓	-	✓	-	-
Flexure	BS EN 12390-5 (2009d)	✓	-	✓	-	✓
Torsion	-	-	✓	✓	-	-
Push out	Si Larbi et al. (2007)	✓	-	✓	-	-
Double lap shear	Barnes and Mays (2001)	✓	-	✓	-	-
The prototype	-	-	✓	-	✓	-
Rebound hammer	ASTM C805 (2013)	-	-	-	✓	-
CT scan	Nikon XT H 225ST CT	✓	-	-	✓	✓
Chloride analysis $AgNO_3$ Spray	Baroghel-Bouny et al. (2007)	-	-	-	✓	✓
XRF	Zetium XRF spectrometer	-	-	-	✓	-
Water penetration	BS EN 12390-8 (2009f)	✓	-	-	✓	-
ISAT	BS 1881-208 (1996)	✓	-	-	✓	✓
Natural chloride diffusion	CEN TS 12390-11 (2010)	✓	-	-	✓	-
NT BUILD 492	NT BUILD 492 (1999)	✓	-	-	✓	-
Multi regime	Castellote et al. (2001)	✓	-	-	✓	-
SEM & EDX	Philips XL-30	-	-	-	✓	-
ASTM D638	ASTM D638 (2014)	-	-	-	✓	-
Cyclic loading	-	-	✓	-	-	✓
Half-cell potential	ASTM C 876 (2015a)	-	-	-	-	✓

4. MECHANICAL STRENGTH AND DEFORMATION OF EPOXY JOINTS

4.1. INTRODUCTION

This chapter presents the results of an experimental programme in Phase I. The testing program provided the data on failure modes, ultimate strength, and deformation of the epoxy bonded concrete.

Shears, tensile and torsional capacity of flat-face concrete joints were tested. Special attention was given to the effect of substrate surface preparation, joint thickness, properties of epoxy resins, exposure to seawater and presence of defects. The effectiveness of UPV in detecting the defects in the epoxy layer was examined and Digital Image Correlation (DIC) was used to observe the surface strain flow between two concrete segments.

Moreover, shear capacity of bonded concrete to steel was evaluated. The effect of anti-corrosion paint and applying fresh concrete with epoxy on steel plate were considered.

4.2. MODES OF FAILURE

The specimens subjected to mechanical tests exhibited three characteristic modes of failure: adhesive (failure in the epoxy), cohesive (failure in the concrete), and mixed (both adhesive and cohesive) examples of which are shown in Figure 4.1.

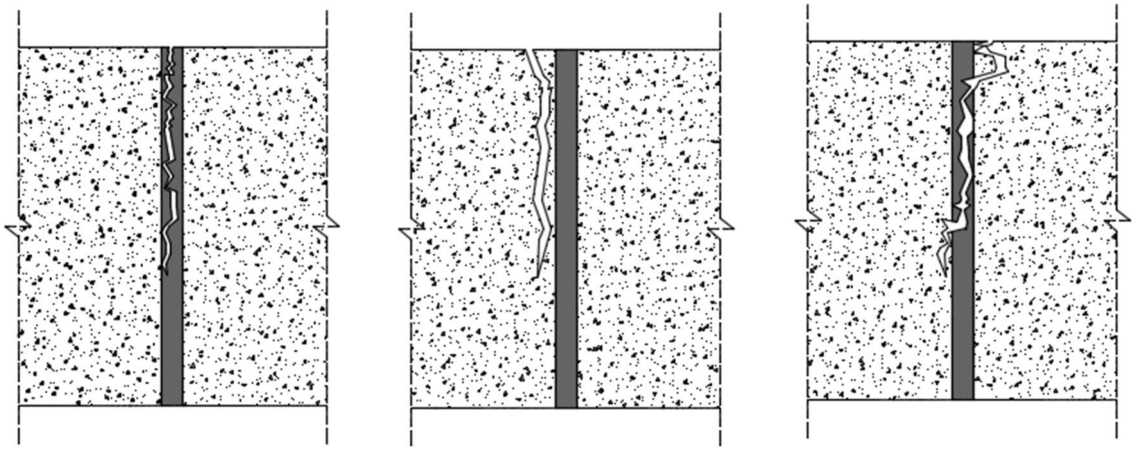

a) Adhesive failure

Failure of epoxy layer

b) Cohesive failure

Failure in body of concrete (one side or both side of the joint depending on the test method)

c) Mixed failure

Combined failure of epoxy layer and concrete

Figure 4.1. Possible modes of failure

The mode of failure depended on the mechanical strengths of the adhesive (epoxy resin) and concrete. The cohesive mode of failure (see Figure 4.1 (a)) was characterised by splitting of the concrete with the failure surface developing in one or both concrete segments. The adhesive mode of failure (see Figure 4.1 (b)) occurred when the epoxy resin was weaker than the concrete. In this case, the failure

of the adhesive layer resulted in de-bonding of the concrete segments. The mixed failure (see Figure 4.1 (c)) was a combination of the adhesive and cohesive modes of failure.

4.3. SHEAR CAPACITY OF JOINTED CONCRETE SECTIONS

4.3.2. Failure modes in shear tests

Figure 4.2 shows the failure modes in slant shear and bi-surface shear tests. Figure 4.3 shows percentage occurrence of each mode of failure observed in the shear performance tests. Cohesive failure was the dominant failure mode occurring in 51% of all shear tests with adhesive failure occurring in 28% of tests and the remainder being mixed mode failure. The majority of specimens with epoxy A failed by adhesive failure in the slant shear test, and cohesive failure in the bi-surface shear test. This aligns with the low compressive strength and high shear strength of the epoxy A. The dominance of the cohesive mode of failure in specimens with epoxies B, C, D and E tested with the slant shear method can be attributed to the higher compressive strength of these epoxies. All slant shear test specimens bonded by epoxy F failed with the adhesive mode. This indicates that the shear strength of epoxy F is lower than that of the concrete used in the tests.

Exposure of specimens under cyclic wetting and drying (extended curing period for 90 days) resulted in a change in dominance of failure mode to cohesive failure in the bi-surface shear test.

The results of tests with the epoxies A and B presented in Figure 4.3 show that the thickness of the joint influenced the failure mode in the slant shear test, while its effect on the bi-surface shear test specimens was not conclusive. In the slant shear tests, the increase in the joint thickness resulted in the increase of the percentile occurrence of the adhesive failure with the rate of about 11% increase per 1 mm joint thickness for the epoxy A and about 13% per 1 mm for the epoxy B. The influence of the joint thickness on the failure mode of the specimens bonded by the epoxy C was not clear from the tests. Finally, it is necessary to note that the analysis of the test data did not indicate any dependency of the failure mode on the method of surface preparation.

(a) (c) (e)

(b) (d) (f)

Adhesive mode: failure surface is wholly in the epoxy joint

Cohesive mode: failure surface occurs near the joint but remains in the concrete.

Mixed mode: failure surface occurs in both the epoxy joint and the near-joint concrete.

Figure 4.2. Failure modes observed in slant and bi-surface shear tests

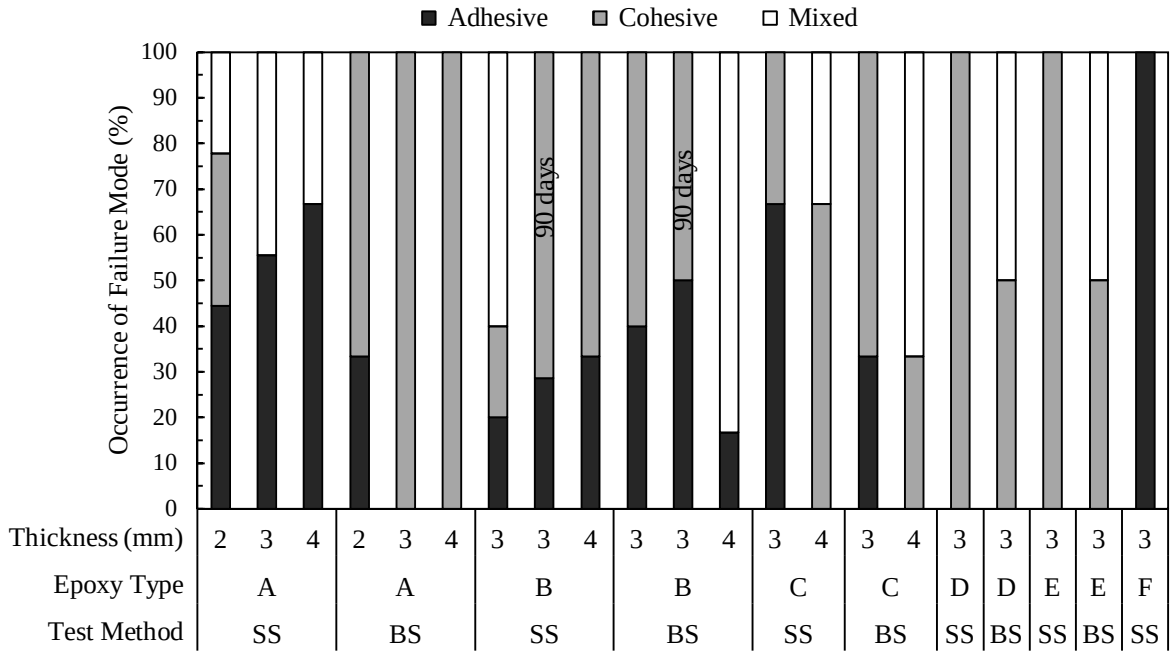

Figure 4.3. Percentile occurrence of different failure modes in slant shear (SS) and bi-surface shear (BS) tests

4.3.3. Calculated shear strength of the jointed sections

Figure 4.4 shows the variation of the calculated shear strength of the joint depending on the joint thickness, epoxy type, and testing method. The graph is presenting mean value and corresponding standard error of each data set. Standard error was calculated by dividing standard deviation by the square root of number of samples. The standard error gives an understanding on how the mean is representing the population. Smaller value of standard error shows that the mean is standing for the population more precisely.

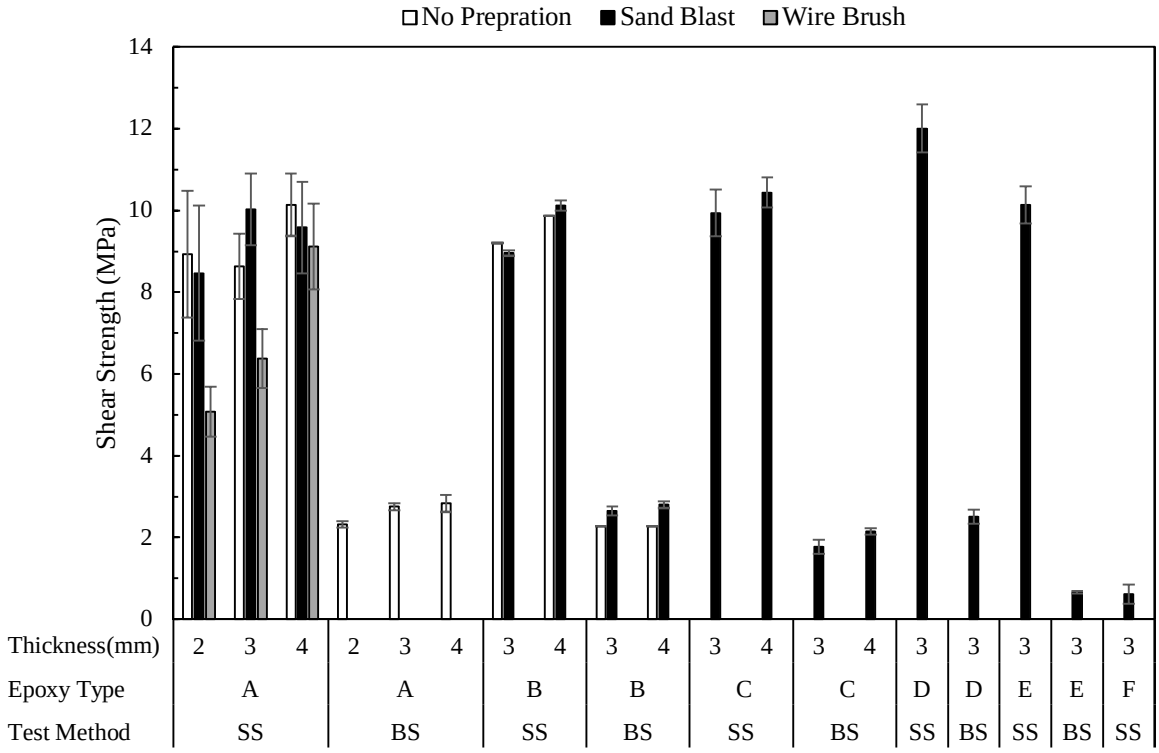

Figure 4.4. Shear strength obtained from the slant (SS) and bi-surface (BiS) shear tests

The slant shear test yielded higher joint shear strengths than the bi-surface shear test regardless of surface preparation, type of epoxy resin and thickness of joint and this difference highlighted the influence of compressive stresses at the joint. It can be inferred from Figure 4.4 that the compressive stresses comprising about 58% of the shear stresses increased the shear strength of the joint by 3-4 times, (refer to Equation 3.1 and Equation 3.2). All joints had shear strengths which were higher than the manufacturer bond strength data (Table 3-7 and Table 3-8), however, specimens that failed in adhesive mode had shear strengths smaller than that of the bulk epoxy (refer to Table 3-8 shear strength of epoxies which is, for example, more than 13 MPa for epoxy B). Epoxy F showed the lowest joint shear strength and failed in the adhesive mode. Therefore, this epoxy was deemed unsuitable for the segmental construction of floating marine concrete structures and was excluded in the rest of the experimental programme. The other epoxies performed much better in the shear tests. The influence of substrate preparation was less clear with control specimens (no substrate

preparation) exhibiting marginally higher strengths in 2 mm and 4 mm joints. In most slant shear tests, the surface preparation had limited influence on the shear strength, however, in all cases, wire brushing preparation showed lower shear strengths and was thus considered unsuitable as a surface preparation method. Sandblasting was chosen as the comparative method for the influence of epoxy type as it is common practice in industry.

4.3.4. Effect of cyclic wetting and drying on shear capacity of the joints

Table 4-1 compares the shear strength of specimens before and after 90 days exposure to artificial seawater (extended curing period). Control specimens (no substrate preparation) showed a small reduction in shear strength with both slant shear (12%) and bi-surface shear (3%). However, specimens with sandblasted substrate preparation showed an increase in shear strength indicating that in the longer term, surface preparation may be an important factor. An examination of failure modes also showed a shift from cohesive to adhesive failure, however, this may have been influenced by the extended curing period of the concrete due to the length of the test method.

Table 4-1. Effect of simulated seawater exposure on shear strength

Type of exposure	Shear strength (MPa)			
	Slant shear test		Bi-surface shear test	
	NP(1)	SB(2)	NP[1]	SB[2]
No exposure	10.58	10.30	2.29	2.65
90 days of cyclic wetting and drying exposure	9.35	14.48	2.21	3.15

[1)] no surface preparation, [2)] sand blast surface preparation

4.3.5. Surface shear strain of the epoxy bonded sections

Figure 4.5 depicts the distributions of the surface shear strain (γ_{xy}) close to the end of the slant and bi-surface shear tests. Both tests showed cohesive failure of the specimens. The approximate positions of the joints are shown on in the Figure 4.5 by the dashed line. As can be seen in Figure 4.5 (a), the presence of the inclined joint affected the shear strain field in the specimen. The distribution of shear strain along the joint was not uniform. Two zones of high shear strain (reaching γ_{xy} = -0.0063) developed at both ends of the joint at early stages of the slant shear test and remained there throughout the test until failure. This possibly occurred due to localised variations of stiffness introduced by the joint. Strain concentrations at the top and bottom ends of the specimen developed due to the influence of the boundary conditions, so it can be disregarded. The shear strain in the areas between the high strain zones gradually decreased to zero. At the stage of the tests shown in Figure 4.5(a), the field of the shear strain across the joint was uninterrupted by any discontinuities and the specimen still behaved monotonically. In the bi-surface shear test, two high shear stain zones developed at the internal end of the loading plate supporting the smaller concrete segment and at the

top roller. These strain concentrations grew with the increase in the load until they merged as shown in Figure 4.5 (b) creating a high shear strain band passing along and across the joint. At the stage of the tests shown in the figure, the shear stain around the joint was continuous with the maximum reaching γ_{xy} = 0.0038 and the specimen behaved monolithically. The distribution of shear strain in the joint was close to uniform by the end of the test. As a result, the bi-surface shear test can be a very efficient method for evaluation of the shear strength of joints. It should however be emphasized that Figure 4.5 shows the field of the surface shear strain and may be not indicative of the strain distribution in depth of the joint.

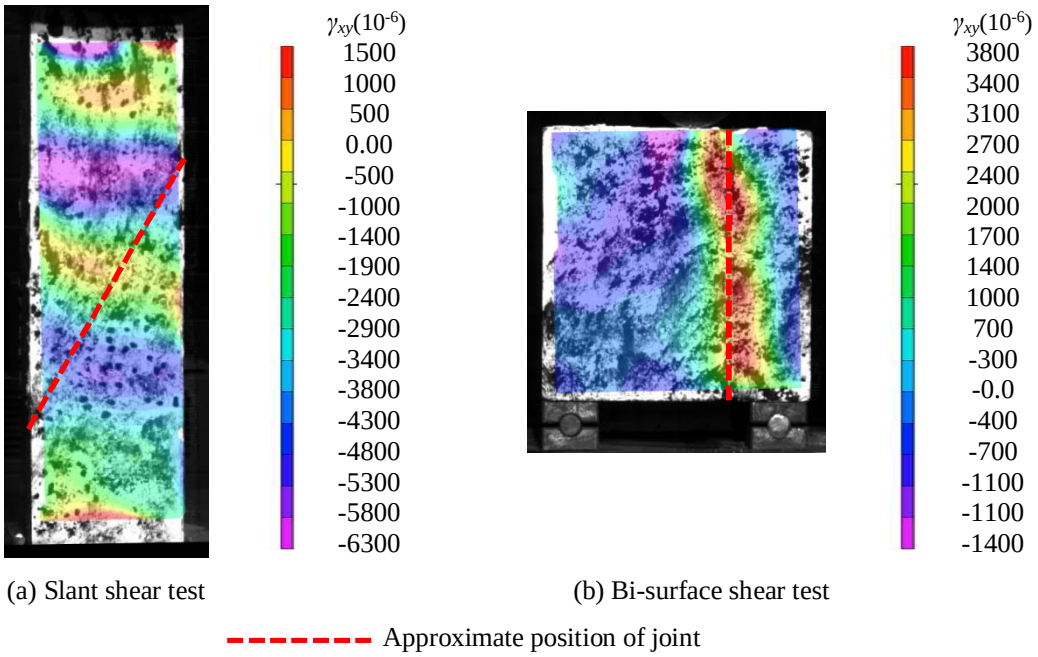

Figure 4.5. Surface shear strain γ_{xy} distribution for (a) the slant and (b) bi-surface shear tests

4.3.6. Effect of induced defect on shear capacity of the joints

The influence of induced defects on shear strength and the average UPV value through and across the joint is shown in Table 4-2. With the same joint thickness, the induced defects led to a loss of shear strength however the influence was reduced with thicker joints with 10% defect indicating that thicker joints may be suitable for offsetting likely workmanship issues resulting in relatively small defects (especially for 10% defect). UPV method was sensitive to the presence of defects, there was a reasonable correlation between the presence of the defect, and the UPV readings for 10% defect case.

Table 4-2. Effect of induced defect on horizontal and vertical UPV

	No defect			10% defect			50% defect		
Joint thickness (mm)	2	3	4	2	3	4	2	3	4
Shear strength (MPa)	2.32	2.81	2.83	1.91	2.52	2.92	1.10	1.81	1.12
Loss of shear strength (%)	-	-	-	17.6	10.3	-3.1	47.4	35.6	60.4
Mean UPV_H (km/s)	4.77	4.75	4.70	4.68	4.63	4.56	4.07	4.17	3.97
Mean UPV_V (km/s)	4.72	4.58	4.68	4.63	4.54	4.58	4.37	4.39	4.42

4.4. TENSILE CAPACITY OF JOINTED CONCRETE SECTIONS

Examples of the failure modes observed in the tensile performance tests are shown in Figure 4.6, primarily being adhesive, cohesive, and mixed as previously discussed. Flexure test failure modes occurs by one big crack through adhesive (see Figure 4.6 (a)), concrete segment (Figure 4.6 (b)) or both adhesive and concrete segment (Figure 4.6 (c)). Split cylinder failures happened by transverse cracking of one concrete segment and concrete adjacent to the joint (Figure 4.6 (c)) or transverse cracking of both concrete segments as well as adhesive de-bonding (Figure 4.6 (f)). A number of split cylinder test specimens also failed by splitting into two parts with the failure surface transverse to the plane of the joint (Figure 4.6 (d)). This failure mode was called as non-standard and was disregarded in mean strength calculation. The non-standard failure mode was the result of difficulties in conducting the split cylinder test on jointed specimens, for example ensuring that the bonded halves of a concrete cylinder are perfectly aligned or applying the load accurately in the plane of the joint.

Flexure test failure modes

(a) Adhesive mode

(b) Cohesive mode

(c) Mixed mode

Split cylinder failure modes

(d) Non- standard mode

(e) Cohesive mode with splitting of one segment

(f) Mixed mode with splitting of both segments

Figure 4.6. Failure modes observed (a), (b) and (c) modified flexural test, (c), (d), and (f) split cylinder test

Figure 4.7 depicts the percentage occurrence of the four modes of failure in the split cylinder and flexural test specimens. The cohesive mode of failure was the most common whilst adhesive mode was only observed in the flexural test. All specimens bonded by epoxy B failed in the cohesive mode

regardless of the test method while in the split cylinder test for epoxy A 17%, 50% and 18% of joints with 2, 3 and 4 mm thickness, respectively, failed in the mixed mode and there was no case of adhesive failure. Regarding flexure test with epoxy A, 22% and 33% of mixed failure for 2 mm and 4 mm joints, and 22%, 11% and 22% of adhesive failure for 2 mm, 3 mm and 4 mm joints correspondingly was observed.

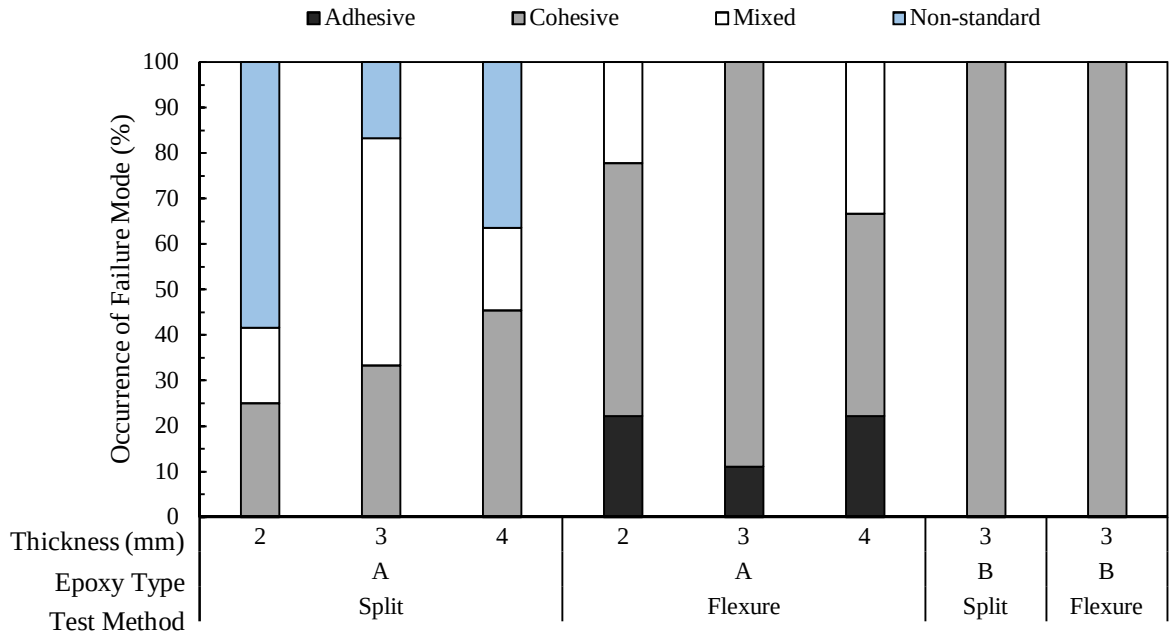

Figure 4.7. Percentile occurrence of different failure modes in the split cylinder and modified flexural tests

4.4.2. Tensile strength of the jointed sections

Figure 4.8 shows the average tensile strength of jointed specimens along with the strength of control non-jointed specimens obtained using the split cylinder and flexural tests. In all but one case with epoxy A, the jointed specimens had a lower strength compared to the control, with an average reduction of around 26% for the split cylinder test and 6% for the flexural strength. The flexural test on jointed specimens yielded an average tensile strength of around twice that obtained with the split cylinder test using epoxy A however specimens bonded by epoxy B exhibited the opposite behaviour with the flexural test giving a lower tensile strength.

CEB-FIP (2012) states the mean value of the characteristic tensile strength of a 60 MPa concrete is f_{ctm} = 4.4 MPa, with lower and upper bound values, (5% and 95% fractiles) equal to 3.1 MPa ($f_{ctk,min}$) and 5.7 MPa ($f_{ctk,max}$), respectively. Only the split cylinder test specimens bonded by epoxy A showed the tensile strengths that were lower than the Model Code values.

Figure 4.8 shows that flexural tests lead to larger values of tensile strength than the split cylinder tests. This phenomenon is the result of inherent differences in the testing techniques. According to Jackson and Dhir (1997) the ratio between the tensile strengths obtained in the flexural and direct

tensile tests is expected to be around 1.56. Given that the tensile strength obtained from the direct tensile test should be about 5-12% less than that from the split cylinder test (Neville, 2011), the ratio between the tensile strengths obtained from the flexural and split cylinder tests should be in the range of 1.39-1.48. The tests on the control non-jointed specimens yield the ratio equals 1.46 (see Figure 4.8) which is within the calculated range.

The control specimens showed higher strength than the jointed specimens except in the split cylinder test with the epoxy B and in the flexural test with the 3 mm sandblasted joint and the 4 mm wire brushed joint both bonded by the epoxy A. This phenomenon and the fact that most of the specimens failed with the cohesive mode can be the result of the stress concentrations in the concrete introduced by the presence of the joint.

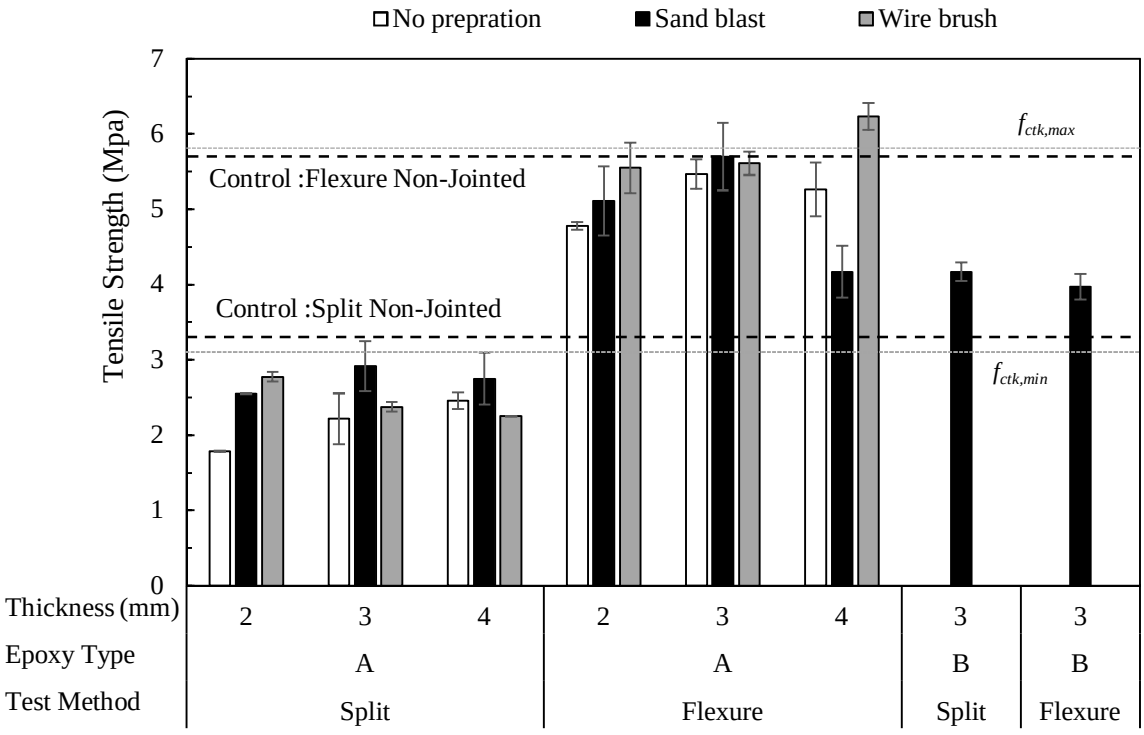

Figure 4.8. Ultimate tensile stress considering various epoxies, surface preparation and joint thickness

The specimens bonded by epoxy B showed higher tensile strength in the split cylinder tests compared to the epoxy A as expected since epoxy B has higher tensile strength (see Table 3-7 and Table 3-8). However, the flexural tests resulted in a sufficiently smaller tensile strength for epoxy B.

The experimental data in Figure 4.9 shows that specimens with no substrate preparation were more sensitive to joint thickness with a joint increase from 2 mm to 4 mm leading to a 40% increase in strength in the split cylinder test. The effect of the increase in thickness on the sandblasted joints was much smaller, while wire brushing exhibited negative influence. In the flexural test, the increase in

the joint thickness generally led to the increase in its tensile strength except for the 4 mm thick sandblasted joint. In most cases, the increase in the surface roughness by sandblasting or wire brushing was beneficial for the tensile strength of the joint. Surface preparation had bigger effect on thinner joints especially in the split cylinder test.

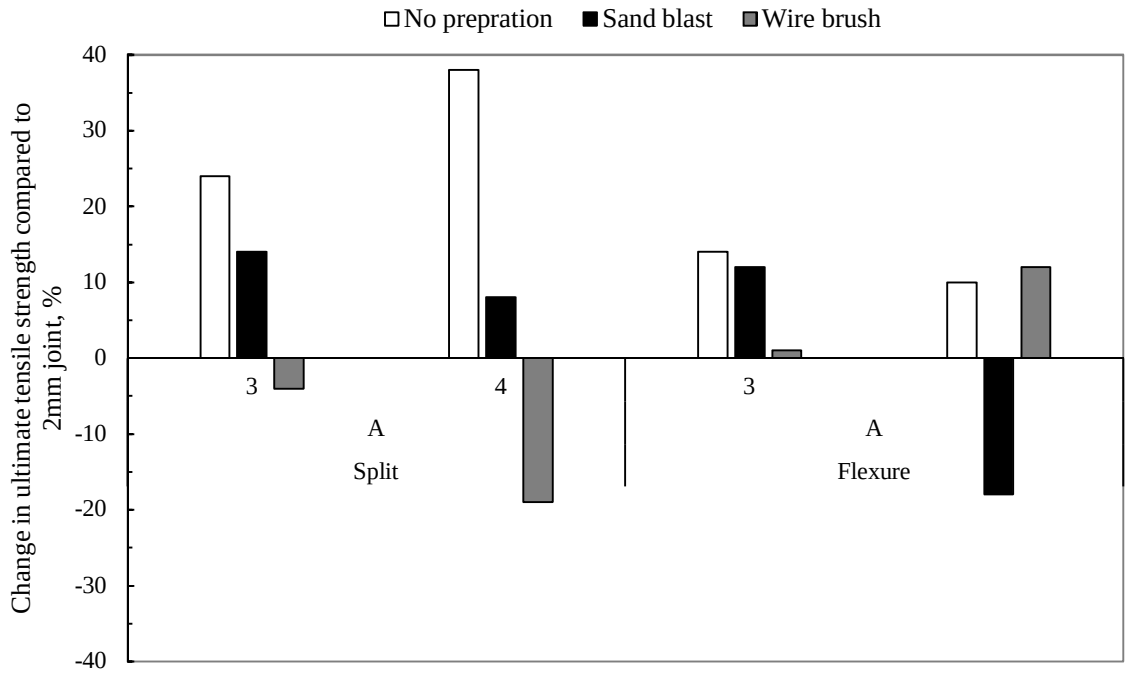

Figure 4.9. Effect of the joint thickness on joint tensile strength, compared to joint with 2 mm thickness

4.4.3. Surface tensile strain of the epoxy bonded sections

Figure 4.10 shows the distribution of the surface horizontal strain (ε_{xx}) obtained using the DIC method in the split cylinder and modified flexural tests close to specimen failure. ε_{xx} was analysed as it provided direct information about the flow of the tensile strain across at the joint. The position of the joint is emphasised in Figure 4.10 by the dashed line.

During the split cylinder test, a band of high tensile strain developed in the middle of the cylinder. This strain band, visible in Figure 4.10 (a), started at the cylinder top from the left of the joint and at the bottom from its right and then connected at the middle. The band was wider in the left half of the cylinder. The presence of the joint did not appear to interrupt the strain field during the test, although there was a zone of high strain concentration (reaching ε_{xx} = 0.00054 in Figure 4.10 (a)) to the right of the joint. The strain concentrations at the top and bottom of the cylinder were introduced by the boundary conditions and can be disregarded. The cylinder failed in the cohesive mode by splitting from the left of the joint. The crack originated at the strain concentration at the cylinder top and progressed downwards parallel to the joint. Full cylinder split followed by the joint deboning due to dynamic redistribution of stresses in the cylinder.

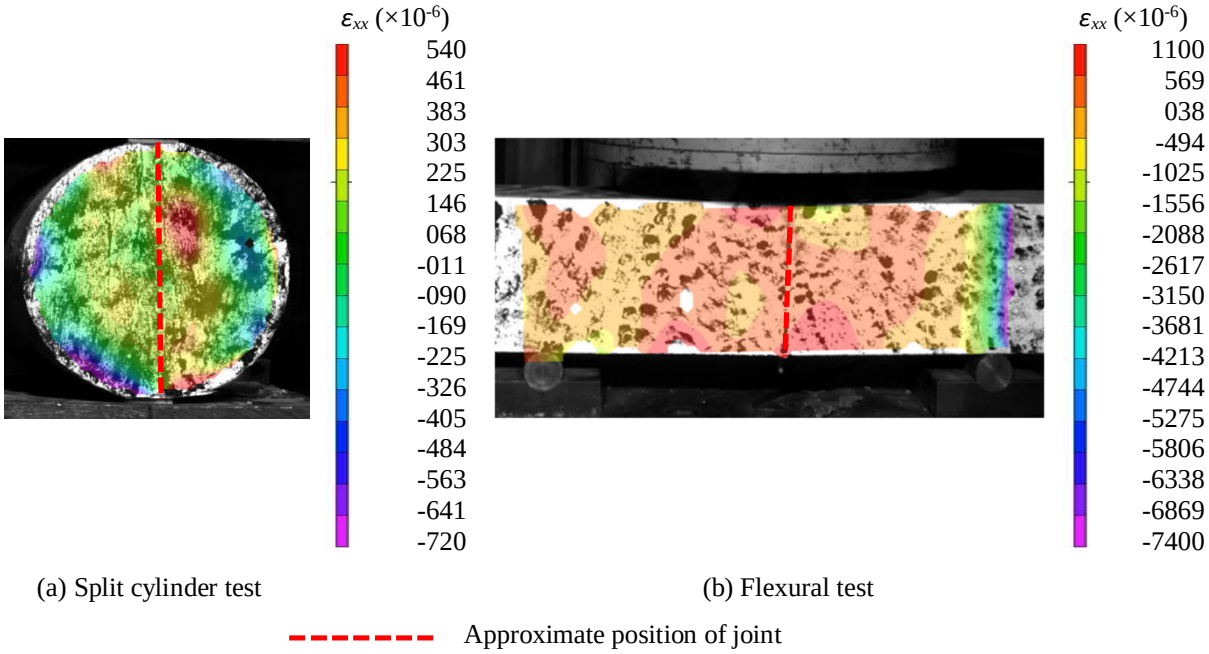

Figure 4.10. Surface strain ε_{xx} distribution for (a) the split cylinder and (b) flexural tests, both tests with 3 mm sandblasted epoxy B joint

In the flexural test, a zone of high tensile strain (reaching ε_{xx} = 0.000569 in Figure 4.10 (b)) developed to the right from the joint close to the bottom surfaces of the beam. The band of high strain values developed on the right of the beam should be ignored as it was most likely introduced by the influence of the support. The joint did not interrupt the flow of strain during testing and the specimen behaved as monolithic. The beam failed in the cohesive mode. The crack originated in the tensile zone of the beam at the strain concentration on the right of the joint and progressed upwards throughout the beam depth from its bottom surface.

The cohesive failure observed in both tests can be explained by the fact that epoxy B was much stronger in tension (f_{tu} = 21-24 MPa see Table 3-8) than the concrete ($f_{ctk,max}$ = 5.7 MPa according to CEB-FIP Model Code 2010).

4.5. TORSIONAL CAPACITY OF JOINTED SECTIONS

The torsion test specimens exhibited two characteristic modes of failure, i.e., cohesive and mixed. Typical examples of these failure modes are shown in Figure 4.11. The cohesive mode of failure was the dominant one that occurred in the specimens T1, T2, T4, T6, T8 and T9 (see Table 4-3) comprising 67% of the tests. This mode was characterised by a serious of cracks developing on different sides of tested specimens. The cracks were either inclined to the axis of rotation or perpendicular to it. Most of the crack inclination angles were in the range between 30º to 60º. Each crack was either confined to one side of a specimen or could continue from one side to another with changing the inclination angle. However, cracks rarely developed on the top sides of concrete cubes that were tightened by bolts possibly due to higher level of confinement. Cracking of the concrete

cubes far from the joint could be the result of insufficient confinement provided by the supporting frames. At least one inclined crack always passed through the joint signifying the fully monolithic behaviour of the specimen. The observed response is typical (Jeng et al., 2013) since the cracking is caused by the torsional shear forces. Unfortunately, in this case, the cohesive mode of failure only indicated that the torsional strength of the epoxy joint was higher that the torsional strength of the hollow concrete cubes.

Mixed failure mode occurred in specimens T3, T5 and T7 (see Table 4-3) comprising 33% of the tests. This mode was characterised by the development of a crack in the concrete adjacent to the joint at least on one side of the specimen. The specimens T3 and T5 developed the joint crack only on one side, while the specimen T7 on all four sides. The adhesive layer stayed intact during the test, although the joint crack crossed the adhesive layer in the specimen T7. The mixed failure was accompanied by cracking of one concrete cube. Most of the cracks in the cube connected with the joint crack continuing over two or three sides. These cracks were inclined to the axis of rotation at angles ranging between 45º to 90º (see Figure 4.14 (b)). The fact that only one concrete cube cracked during the tests was possibly the result of its lower level of confinement. The cracking of the cube could therefore be reduced or entirely eliminated through improving the confining action of the frames in the torsional test setup. After separation of the cubes at the end of the tests, a thin layer of concrete was still attached to the epoxy. It is important to note that this thin layer was not the external layer of concrete which was exposed during casting. The specimens were manufactured as whole (i.e., 200 mm long) then cut in half and bonded by epoxy before testing. The adhesive mode of failure was not observed in the tested set of specimens.

(a) Cohesive failure in specimen T2 (b) Mixed failure in specimen T5

Figure 4.11. Failure modes observed in the torsion tests

4.5.2. Torsional strength

Figure 4.12 presents the evolution of the torsional stress in specimens with rotational deflection and the Table 4-3 the torsional stress and rotational deflection at specimen failure. The corresponding rotational deflection was found as the square root of the sum of squares of the readings made by the two LVDTs installed in the vertical and horizontal directions. As can be seen in Figure 4.12, slip of the specimens T2-T4 and T7-T9 in the confining frames occurred at the beginning of tests leading to the low initial inclination of the curves. The average torsional strength of the specimens with the

mixed failure was equal to 4.1 MPa, while the corresponding average rotational deflection at failure equal to 0.28 mm (see Table 4-3). The specimens with the cohesive failure showed a slightly higher average torsional strength of 4.4 MPa and a higher rotational deflection of 0.42 mm. As a result, the mixed failure was on average weaker and less ductile but stiffer than the cohesive failure. These observations, however, provided only an indication of the torsional performance of the flat faced concrete joints due to the limited number and small scale of specimens tested. Further investigation is required to get better understanding of the joint response to torsion and to derive appropriate scaling laws.

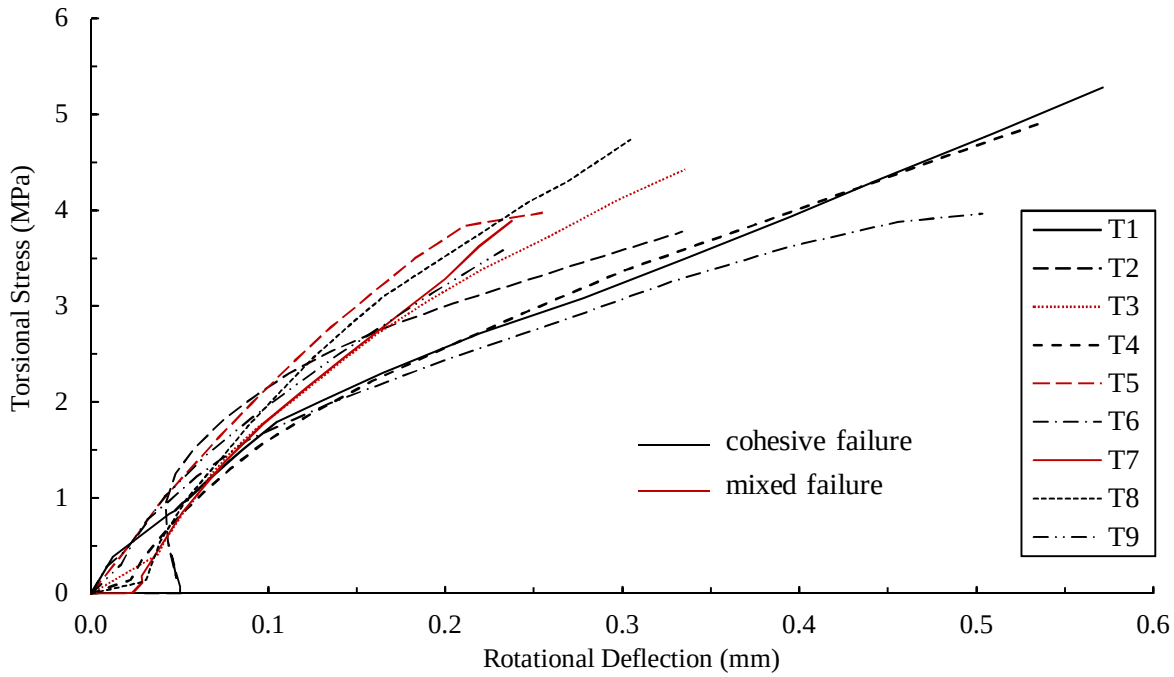

Figure 4.12. Torsional stress vs. rotational deflection

Table 4-3. Torsional test results

Specimen	Failure mode	Failure stress (MPa)	Rotational deflection at failure (mm)	Mean failure stress (MPa)
T1	Cohesive	5.28	0.57	4.37
T2	Cohesive	3.77	0.33	
T4	Cohesive	4.92	0.54	
T6	Cohesive	3.96	0.50	
T8	Cohesive	4.73	0.30	
T9	Cohesive	3.58	0.23	
T3	Mixed	4.42	0.34	4.10
T5	Mixed	3.97	0.25	
T7	Mixed	3.90	0.24	

4.5.3. Surface shear strain of the epoxy bonded sections under torsion

Figure 4.13 and Figure 4.14 present the distributions of the surface shear strain (γ_{xy}) across the joint obtained for the specimens T6 and T7 using the DIC method. The two specimens were selected since T6 failed with the cohesive mode, while T7 with the mixed mode. Both figures show the shear stain distributions before and after failure with cracks emphasised by dashed ovals.

Figure 4.13 depicts four stages of the specimen T6 response to torsion including the pre-cracking strain stage, the stage at the initiation of the first inclined crack, as well as the pre- and post-failure stages. As can be seen in Figure 4.13 (a), a zone of high shear strain (reaching γ_{xy} = -0.00072 in the figure) developed in the lower half of the joint. This zone was part of a high shear strain band passing through the joint and inclined at about 60º to the axis of rotation. The development of this band led to the initiation of the first inclined crack at the bottom side of the specimen as shown in Figure 4.13(b), when the strain in the joint reached γ_{xy} = -0.00164. The cracking process was gradual and continued with growing and branching of the first crack along the high shear strain band towards the joint. Figure 4.13(c) depicts the pre-failure stage (with γ_{xy} = -0.00450 in the joint) just before the growing crack reached the joint. Failure of the specimen corresponded with the crack passing through the joint. Figure 4.13(d) shows the shear strain distribution after specimen failure when the shear strain in the joint reached γ_{xy} = -0.01730. In general, the presence of the joint did not compromise the monolithic behaviour of the specimen under torsion. The development of inclined high shear strain bands and inclined cracks in the specimen was typical in the considered loading conditions.

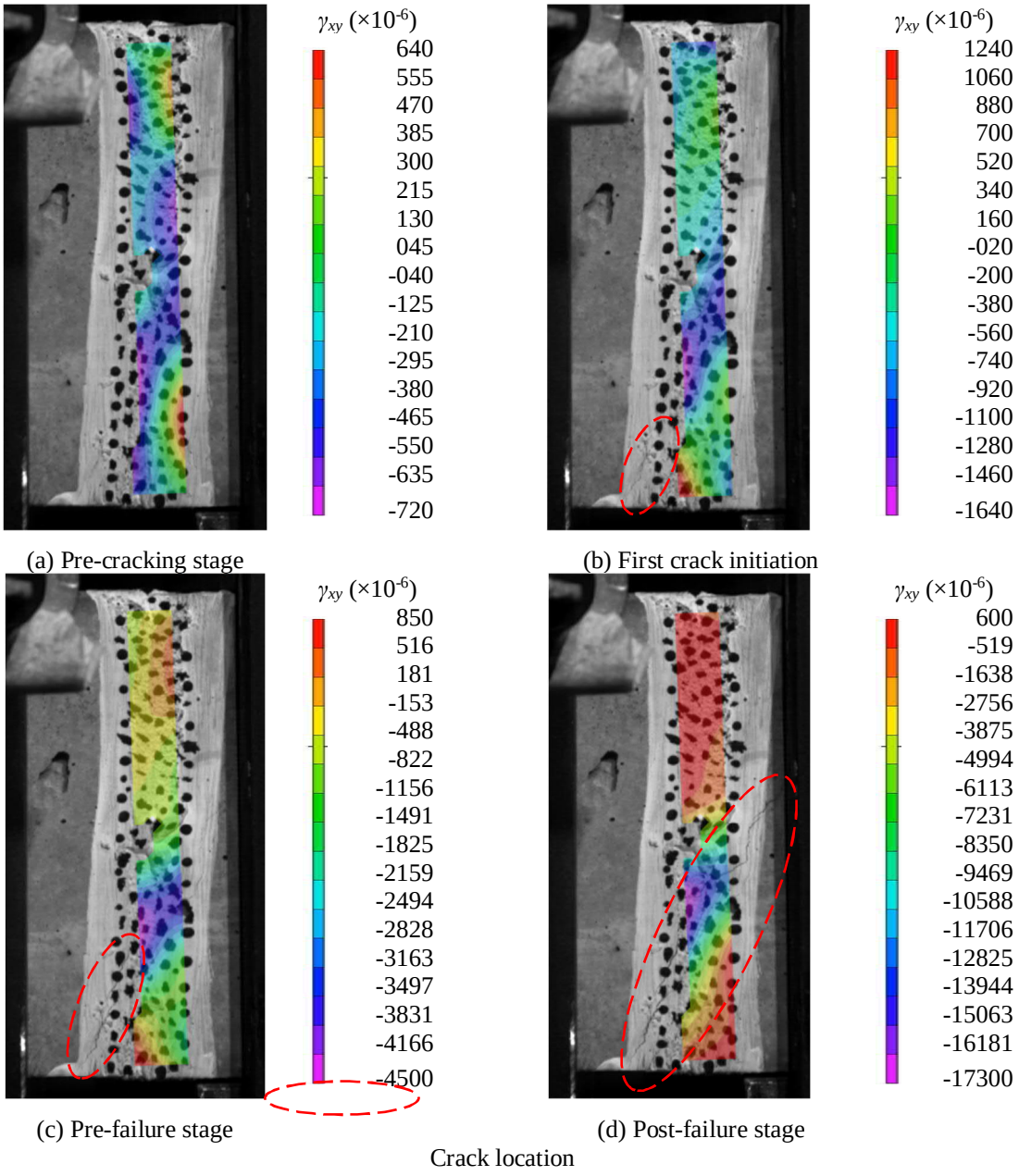

Figure 4.13. Surface shear strain γ_{xy} distribution during cohesive failure of specimen T6 in torsion

Figure 4.14 depicts the shear strain distribution along the joint in the pre- and post-failure stages. Two zones of high shear strain (reaching γ_{xy} = -0.00173) at the top and bottom of the joint can be seen in Figure 4.14a in the pre-failure stage. These zones also were parts of inclined high shear strain bands. The failure of the specimen T7 was immediate with the main crack developing along the joint from the top and three inclined cracks developing along the joint from its bottom right. The cracks were inclined at about 45º to the axis of rotation. The shear strain reaching γ_{xy} = -0.0655 at the top of the joint. The presence of the joint did not introduce any localised strain concentrations in the shear strain distribution and the specimen behaved monolithically during the test.

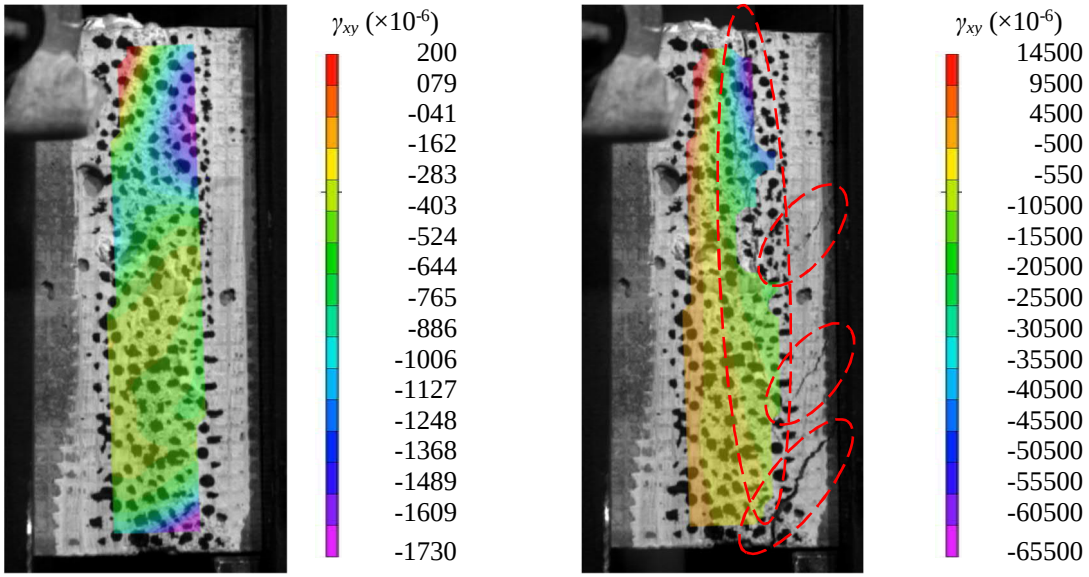

Figure 4.14. Surface shear strain γ_{xy} distribution during joint failure of specimen T7 in torsion

It is important to note that the gradual cohesive failure and immediate mixed failure support the conclusion made above based on the analysis of Figure 4.12 that the mixed failure is stiffer and less ductile than the cohesive failure.

4.5.4. Failure of circular sections in torsion

The same frame was used to apply torsion on the hollow circular sections. Unfortunately, the circular sections were slipping in the frame. The failure was happening under high rotational deflection and very low stress. To fix the samples in the place, the bolts were highly tightened. This high pressure of the bolts also caused damages on the body of concrete and they could not prevent slipping. The failure mode of the circular sections was mixed and no certain pattern of cracking was identified at the time of failure

4.6. SHEAR CAPACITY OF BONDED CONCRETE TO STEEL: EFFECT OF ANTI-CORROSION PAINT

The push out test was conducted according to the method suggested by Si Larbi et al. (2007). The effect of anti-corrosion paint was examined in this test. Samples with No paint on steel, normal anti-corrosion paint, and epoxy anti-corrosion paint were tested. Figure 4.15 shows the average ultimate stress of three samples for each condition.

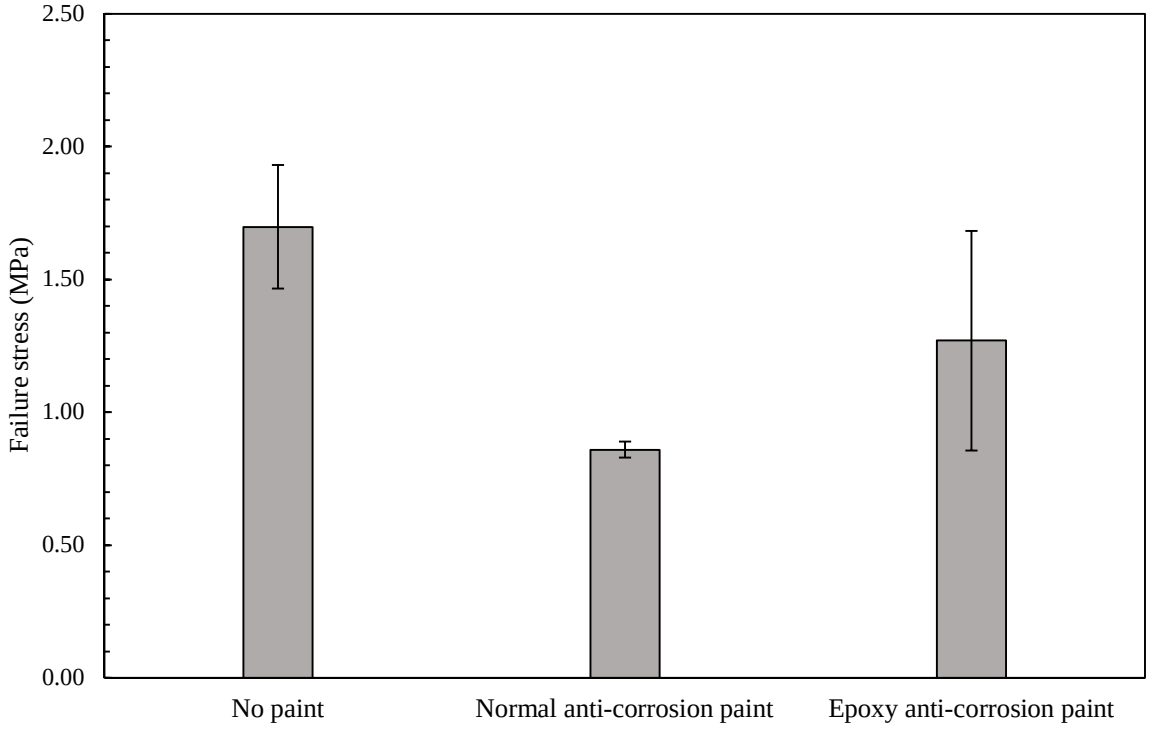

Figure 4.15. Ultimate shear stress in push out test with different steel protection methods

Figure 4.16 shows the steel plates without any protection paint which failed in a thin layer of concrete. It means that the ultimate strength depended on the shear capacity of concrete since concrete was the weakest point. Normal anti-corrosion paint was inappropriate because the paint failed in the shear test (see Figure 4.17). Epoxy anti-corrosion paint worked significantly better than normal anti-corrosion paint since it failed in the first layer of concrete again. The failure of epoxy anti corrosion paint was like the steel plate without any paint. The difference in the average failure stress in these two cases can be due to variation in the concrete mixes and strength of first layer of concrete.

In summary, two failure modes were observed in push out test depending on the steel preparation. First failure mode is the failure of concrete in Figure 4.16 and Figure 4.18 when the steel is not painted or painted with epoxy anti corrosion paint. The second failure mode is failure of the paint in Figure 4.17 when the steel is painted with normal anti corrosion paint.

Figure 4.16. Failure mode in push out test without any paint on the steel

Figure 4.17. Failure mode in push out test with the normal anti-corrosion paint on the steel

Figure 4.18. Failure mode in push out test with the epoxy anti-corrosion paint on steel

The slip before failure was measured for plates without any protection paint using LVDTs connected to four sides of the steel beam. The average movements of four LVDTs are presented for each sample in Figure 4.19. There are very large differences between these three samples because the failures are in the first layer of concrete. The first layer of concrete is most variable part due to the settlements at

the time of curing and presence of thin layer of cement paste without any aggregate. Although the samples show various stiffening behaviour, the slip before failure is small (less than 0.25 mm)

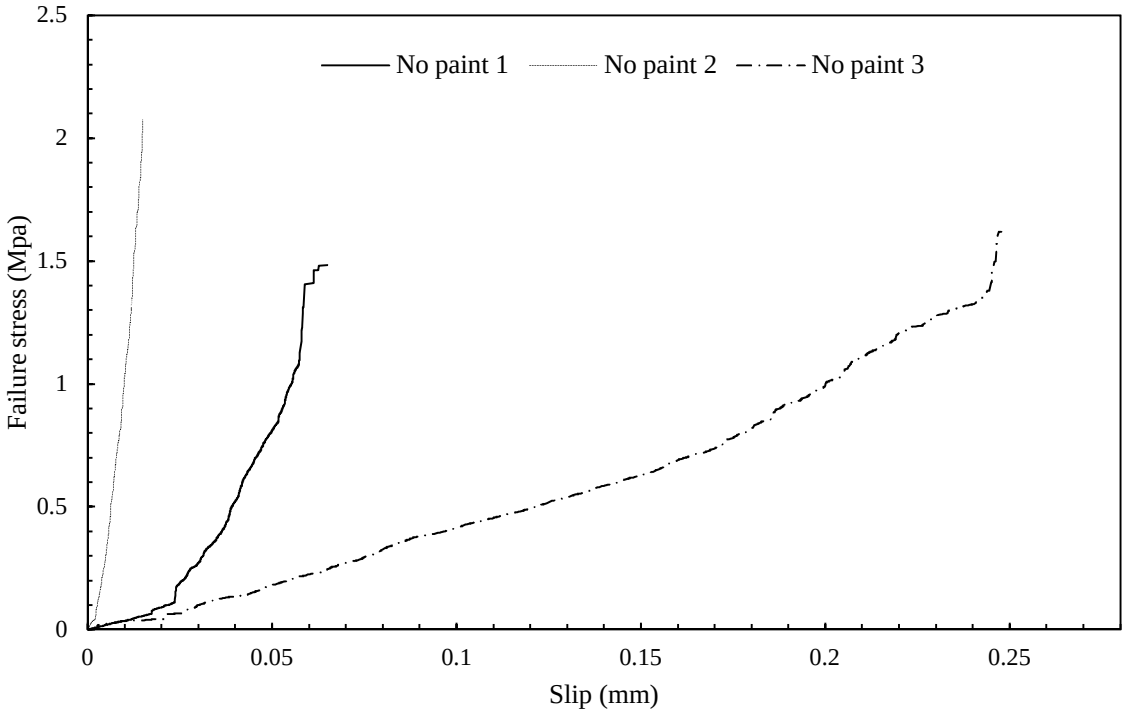

Figure 4.19. Stress-slip graphs for "No paint "specimens in the push out test

4.7. SHEAR CAPACITY OF BONDED CONCRETE TO STEEL: EFFECT OF FRESH CONCRETE BOND

The effect of two jointing techniques was evaluated by double lap shear test. All the steel plates were painted using epoxy anti-corrosion paint. First set of plates were jointed to concrete by applying epoxy on hard concrete (after 28 days of curing). For the second set, the fresh concrete and epoxy were applied on the steel plates. The fresh-hard samples were kept in a plastic bag for 28 days of curing.

The failure mode of hard bond concrete was different from fresh bond concrete. Figure 4.20 and Figure 4.21 show the failure modes of these two methods of construction. Bonded hard concrete failed with a transvers cracking of concrete and failure of the first layer of concrete adjacent to the joint. Bonded fresh concrete failed in deeper layers of concrete. Some paint failure was also observed in the case of fresh bonding. The strength was almost doubled in bonded fresh concrete (see Figure 4.22).

Just one sample was tested for hard bond concrete with double lap shear test. Since the results of bonded hard concrete in this test are very close to the result of push out test and the failure modes are the same, there is no need for further test in this state.

Figure 4.20. Failure mode of bonded hard concrete to steel

Figure 4.21. Failure mode of bonded fresh concrete to steel

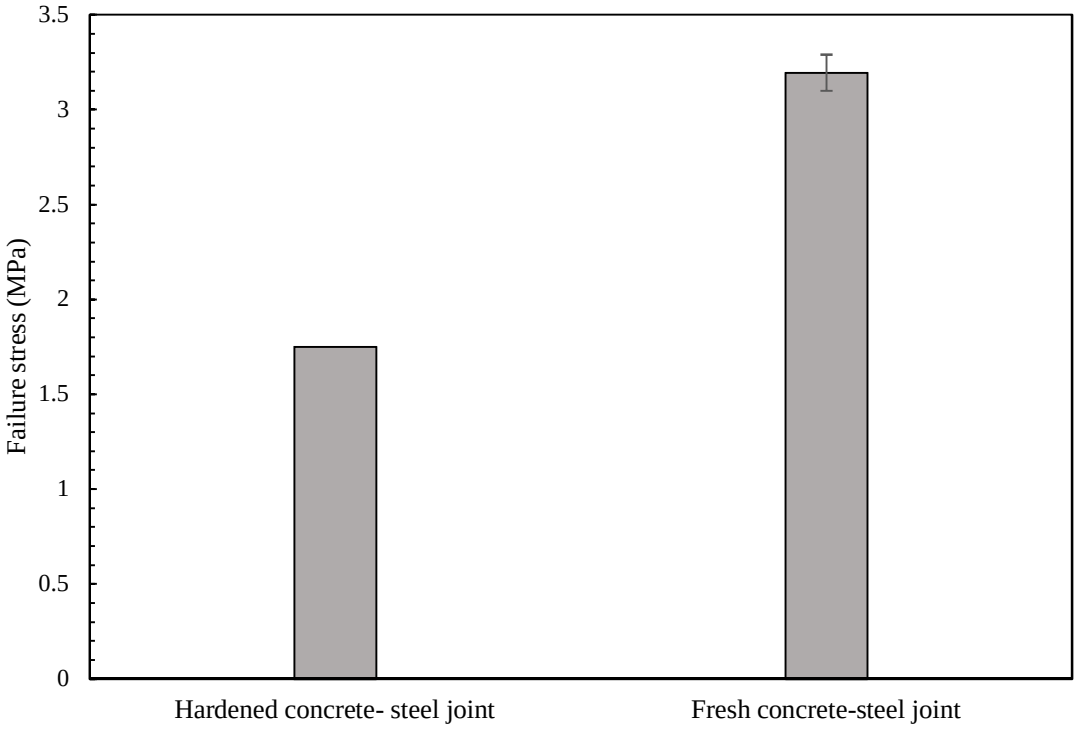

Figure 4.22. Ultimate shear stress in double lap test with different jointing techniques

The increase of strength in the case of bonded fresh concrete was due to higher bond line and aggregate interlock. A standard concrete cube was constructed using this method and was CT-scanned. Figure 4.23 shows that the bond line is longer due to higher aggregate interlocking. The thickness of the epoxy layer is also much higher in some areas. It is impossible to have a constant thickness using the fresh bonding technique.

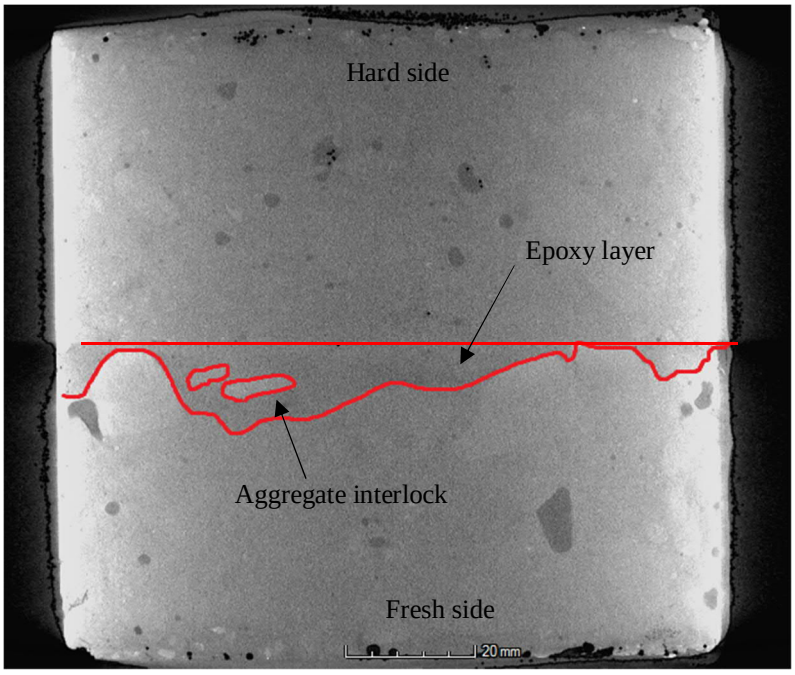

Figure 4.23. CT scan of a standard cube, fresh concrete-epoxy bond

4.8. CONCLUSIONS

This chapter presented the results of extensive experimental programme investigating mechanical performance of flat-face epoxy bonded concrete under shear, tension and torsion. The response of joints to shear was investigated using the slant shear and the bi-surface shear tests, while to tension using the split cylinder and flexural tests. A new testing technique was developed for studying the behaviour of joints under torsion. Moreover, strength and effective factor on epoxy concrete bonded to steel were evaluated using push out and double lap shear test.

Three standard modes of failure including the cohesive, adhesive, and mixed failure were observed in the tests. However, the adhesive failure did not occur in the torsion tests. The cohesive failure was the most common mode in all tests. The failure mode and the joint strength were found to be highly sensitive to the experimental setup, the thickness of the joint and the mechanical properties of the epoxy and concrete and the exposure to seawater. All jointed specimens behaved monolithically until failure. Joints bonded by epoxies with higher density and higher percentage of filler exhibited better mechanical performance. The DIC analysis showed that the presence of joints did not interrupt the flow of strain in specimens. Cracks always initiated inside the zones of strain concentration and propagated along the bands of high strain.

The increase in the thickness of the joint nearly always led to an increase in its strength. However, combined with wire brushing it often resulted in the strength loss. The effect of sandblasting on the joint shear strength depended on test setup. It was negative in the slant shear tests and positive in the bi-surface shear tests. Wire brushing was found inefficient for increasing shear strength of joints. At the same time, sandblasting improved the shear strength of joints exposed to seawater in both types of tests. Since the sandblasted samples under cyclic wetting and drying were older by 90 days than the specimens unexposed to seawater, the augmented shear strength can be an indication that sandblasting can improve the long term mechanical behaviour of joints. Both sandblasting and wire brushing also had a positive effect on the tensile strength of joints.

The presence of the compressive stresses in the slant shear tests significantly augmented the joint shear strength. In the tests, the compressive stresses comprising about 58% of the shear stresses led to the increase of the shear strength of the joint by 3-4 times. Therefore, high shear strength of the flat face concrete joints can be expected in the post-tensioned segmental construction. The increase of the joint thickness and the exposure to seawater in under cyclic wetting and drying led to an increase in the occurrence of the adhesive failure. The DIC observations showed that the presence of the inclined joint in the slant shear test had a strong effect on the shear strain field resulting in a non-uniform strain distribution along the joint with high strain zones at both its ends. This phenomenon can be an indication that the joint locally affected the stiffness of the specimen. In the bi-surface shear test, a band of high shear strain developed along the joint by the end of the test leading to a

relatively uniform distribution of strain in the joint. This indicates that the bi-surface shear test is a very efficient method for evaluation of the shear strength of joints. The bi-surface shear test was also used for studying the influence of defects on joint shear performance. It was found that the defects generally led to the loss of the shear strength. However, the thicker joints were less affected. The applicability of the Ultrasonic Pulse Velocity (UPV) method for defect detection was additionally investigated. The UPV method was able to detect even small defects in thick joints. The UPV readings were sensitive to the size of the defect. Therefore, this method can be efficiently used for quality control of epoxy bonded concrete joints.

In the tensile tests, multiple splitting of concrete segments occurred in some flexural test specimens. Technical difficulties in conducting the split cylinder tests resulted in a high percentage of a non-standard failure where the cylinder split perpendicularly to the plane of the joint. The jointed specimens were weaker than the non-jointed control specimens especially in the split cylinder tests. This can be (i) an additional indication of the influence of the joint on the distribution of strain (and so stiffness and stresses) inside the cylinder which was observed by the DIC method and/or (ii) the result of technical difficulties related to the preparation and testing of jointed specimens. Asymmetry in the strain field at the top of the beam between the loading rollers was also detected using the DIC method in the flexural test despite the symmetrical test setup. It was attributed to imperfections in the testing procedure.

In the torsion test, the failure of specimens was characterised by development of a net of cracks perpendicular or inclined to the axis of rotation. Most of the crack inclination angles were in the range between 30º to 60º. The cracks usually extended over 2 or 3 sides of the specimen. At least one inclined crack always passed through the joint in the cohesive failure. In the mixed failure, the inclined cracks were usually concentrated in one of the two bonded hollow cubes and were connected to the main joint crack. The specimens with the mixed failure were weaker in torsion and exhibited a less ductile and stiffer response. Bands of high shear strain crossing the joint at angles between 45º to 60º were detected using the DIC method. The cracking process was gradual in the cohesive failure and immediate in the mixed failure. The excessive cracking observed in the tests can be the result of insufficient confinement of the specimens in the restraining frames. Thus, further improvement of the torsion test setup is required.

Regarding bonded concrete to steel, using the normal anti-corrosion paint seemed unsuitable since it led to strength reduction by 50% and failed in the paint layer. The plates without any protection paint and epoxy anti-corrosion paint behave similar and failure happened in the concrete layer. Therefore, the expensive option of epoxy anti-corrosion paint is suggested for the marine environment.

Double lap shear test evaluated the construction method of applying fresh concrete with epoxy on the steel plates. This method increased the shear strength by 50% due to increase in the bond line and

aggregate interlocking with the epoxy. However, the suppliers do not recommend wet surfaces at the time of epoxy application. Although this method led to higher shear strength, it may have some negative consequences in long term regarding durability of the joints.

Finally, it is important to note that the conclusions drawn in this section provide only an initial insight into the mechanics of flat faced concrete joints bonded by epoxy resins. Further investigation is required for gaining deeper understanding of this complex structural problem. The results indicate that the epoxy joints behave monolithically and remain undamaged under different types of static loading before the ultimate failure. The joints do not significantly interrupt the flow of strain but can locally affect the distribution of strain (and thus stiffness and stresses) in a structure. An increase in joint thickness and in the density of the epoxy (and the filler content) leads to the increase in the joint strength and thicker joints are less affected by small defects in the bonding layer. The dominant mode of failure in majority of tests was cracking of concrete rather than by de-bonding of the joint. This indicates monolithic behaviour of jointed system. In the case of perfect joint without any defects and the right thickness, it is expected that all shear, tension, and torsion loading lead to concrete cracking as if there is no joint in the section.

5. PROTOTYPE DEVELOPMENT AND DURABILITY BEHAVIOUR OF JOINTS

5.1. INTRODUCTION

Experimental results from Phase II: Part 1 and Part 2 are presented in this chapter to understand the behaviour of chloride and water penetration in epoxy bonded concrete system exposed to seawater salt solutions. A scaled (1:11) prototype of the Pelamis concept was built to assess the challenges involved in design, construction, and durability of a floating segmental WEC.

Water penetration and chloride migration tests (accelerated and natural) were conducted under static condition. Most tests were conducted under combination of both fully submerged, wetting, and drying cycles in seawater salt solution. Moreover, the effect of two construction methods on chloride and water penetration were evaluated, namely (i) connecting two pieces of hard concrete (called hard-hard) and (ii) casting fresh concrete onto epoxy on hard end concrete (called hard-fresh).

The results of three assessment phases during two years of floatation of the prototype are presented and discussed in this chapter. The results of porotype evaluations accompanied by the results of static durability testing provide a basic understanding of the performance of bonded systems and highlight the main areas of concern.

5.2. PROTOTYPE FLOATATION AND ASSESSMENT

The design process of the prototype with 55% target submersion was explained in Chapter 3. The prototype consisted of five hollow concrete segments, which were jointed together by epoxy A. The concrete segments had dimensions of 500 mm outer diameter, 25 mm wall thickness, and 440 mm length.

The surfaces were wire brushed and concrete segments were jointed with varying joint thickness of 1, 2, 3, and 4 mm. The steel plates (painted with normal anti-corrosion paint) were attached to the end sections. The dimensions of steel plates were 550 mm diameter and 10 mm thickness. All the segments were post-tensioned by hand tightening of M10 bars.

Figure 5.1 shows the milestones for development and testing of the prototype. The concrete segments were casted in Plean Precast ltd. and assembled at the University of Dundee. Total exposure time of the prototype was 24 months. The prototype was assessed in three various stages of its life, (i) prior to first floatation, (ii) after 12 months exposure in the salt water tank, and (iii) after 12 months floating in the west coast of Scotland (at Loch Kishorn and Glenmore Bay). The final assessment included both non-destructive and destructive testing.

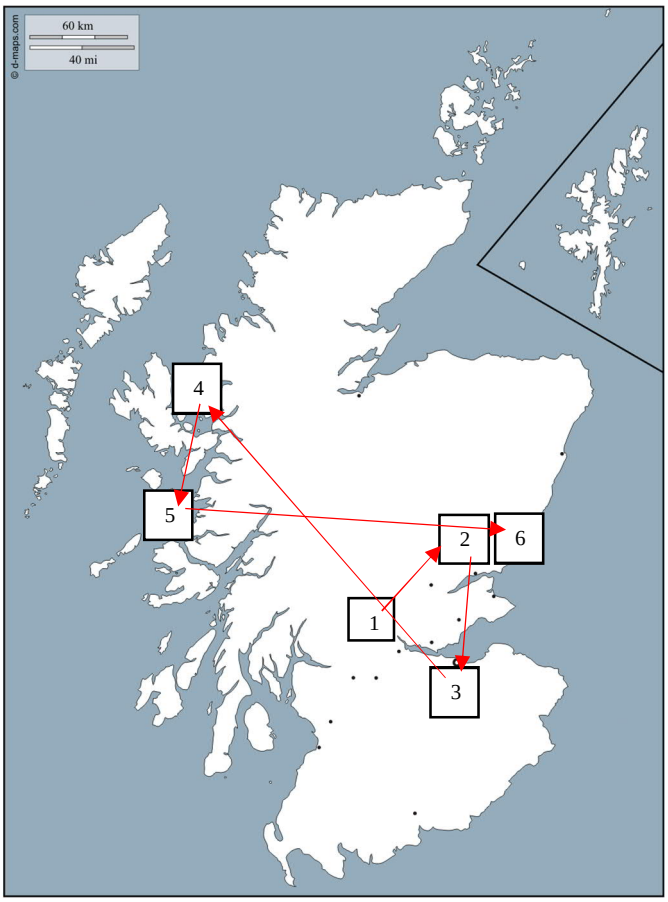

1	Casting the concrete segments Plean Precast Ltd. Stirling
2	Assembling University of Dundee
3	Stage 1: Baseline assessment and floating in the artificial seawater salt solution tank Pelamis Ltd. Edinburgh, 20±2 °C
4	Stage 2: First year assessment and relocation (after 12 months) Relocation to Loch Kishorn (Annual wave height 1.01-1.25 m, and annual temperature range 2.0-12.1 °C)
5	Relocation after 6 months Floating at Glenmore Bay (Annual wave height 1.01-1.25 m and annual temperature range 2.1-13.9 °C))
6	Stage 3: Final assessment University of Dundee

Figure 5.1. Geographic milestones of the prototype development and testing (the wave data were extracted from atlas of UK marine renewable energy resources cited by Venugopal and Nemalidinne (2015))

5.2.1. Base line assessment and commissioning of the prototype in the tank

Prior to floating the prototype, tests were conducted to identify defects and provide a baseline to compare the condition of the tube after floatation. The baseline assessments were conducted on October 2014.

Hydrogen sniffing equipment was used initially and two main areas of leaking were detected. One leak was found at a concrete-steel end plate connection where the epoxy joint was not complete (a small visible hole). This leak was covered using Sikaflex sealant (high strength sealant). The other leaks were through small discoloured patches on the concrete itself. These patches were visible as darker grey regions located at one end of a couple of the tube sections. The end of the tube sections was top of the mould at the time of casting. Therefore, a region of lighter density concrete has formed at the top of the mould due to settlement of aggregates to the lower layers. However, just because hydrogen can escape from these weaker regions, it does not mean that water can get in.

Rebound hammer and UPV tests (ASTM C805 (2013) and BS EN 1250-4 (2004d)) were conducted on the tube on three main areas which were identified visually as good quality concrete, poor quality concrete, and epoxy joints. The results from this baseline assessment are presented in Table 5-1.

Table 5-1. Results of baseline assessment of the prototype

Location	Rebound hammer number (45° inclination)	UPV range (km/s)
Visually good quality of concrete	39	4-5
Visually poor concrete quality	30	3-4
Epoxy joints	29	3-4

After the baseline assessment and required repairing, the porotype floated in 1 M artificial seawater salt solution tank. It successfully floated at 55% submersion as it was designed (see Figure 5.2). The tank was placed in an industrial shed owned by Pelamis ltd. located in Leith. The ambient temperature was 20±2 °C.

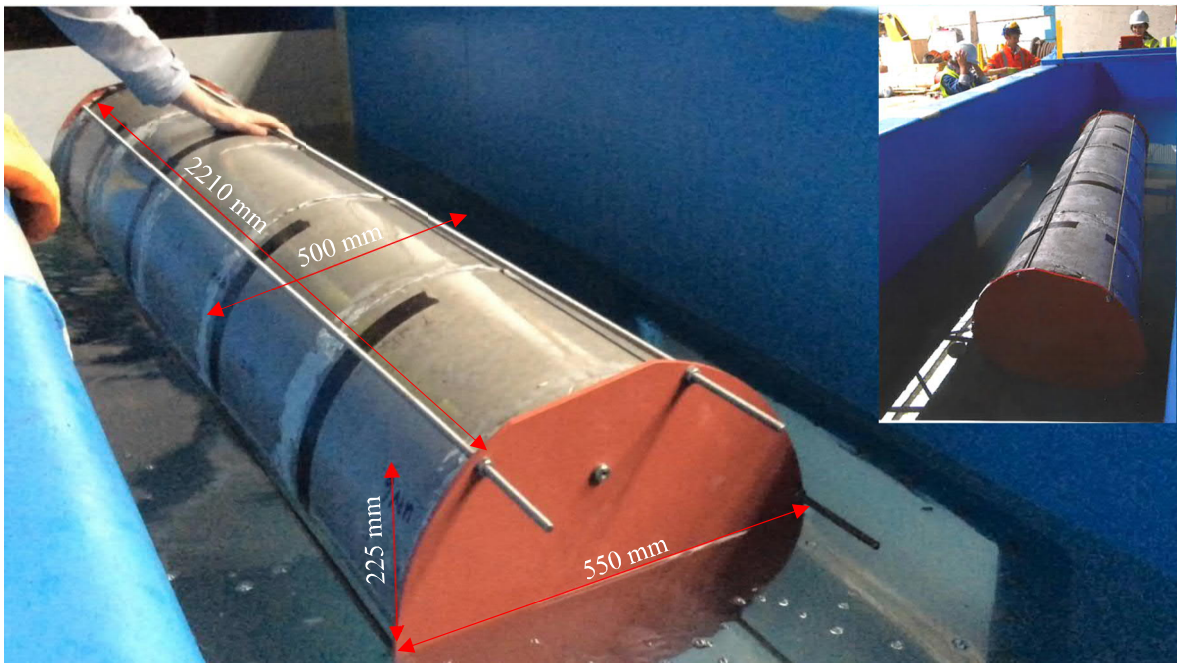

Figure 5.2. Successful floatation of the scaled prototype (1:11), submerged to 55% in 1 M artificial seawater salt solution tank at Pelamis ltd.

5.2.2. Assessment of the prototype after 12 months floating in seawater salt solution tank

The second assessment of the tube was conducted after 12 months. The tube was floating in the artificial seawater salt solution tank. The prototype was removed from the tank and left for 7 days out of the tank to dry in ambient environment. UPV and rebound hammer tests were conducted again on the dried prototype. The results of rebound hammer and UPV were similar to the initial condition. There was no visible damage on the concrete segments, joints, and steel end plates.

5.2.3. Final evaluation after of the prototype after floating in the west coast of Scotland

The third assessment of the tube was conducted after 12 months exposure in the west coast of Scotland. Unfortunately, the prototype had sunk due to failure of one of the bars connected to the mooring rope. There was no information about the certain period that it had been under the water.

Water had entered the tube via the steel plate separation. There was no epoxy bond left at the steel end plates. The plates were kept in place just by post tensioning bars. Figure 5.3 shows the open plan of the prototype. The location of the joints and the major damages can be seen in this plan.

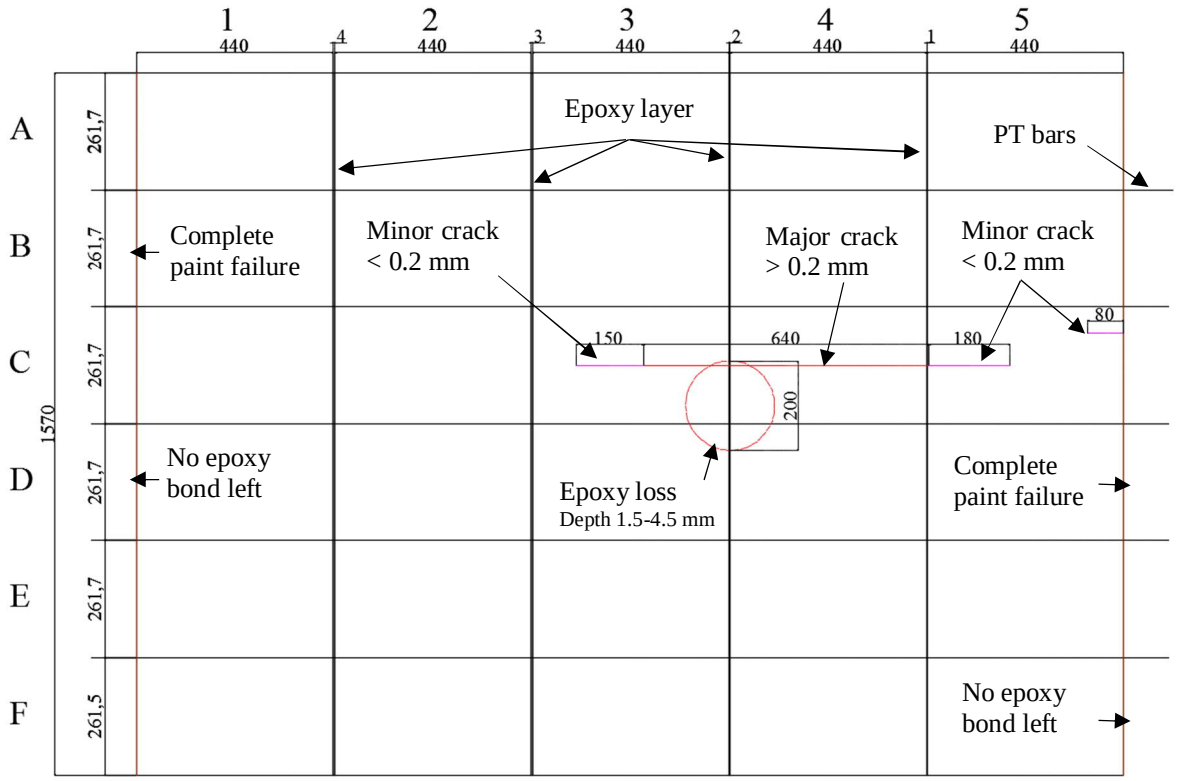

Figure 5.3. Open plan of the prototype and major damages according to visual inspection (unit mm)

Figure 5.4 shows the main damaged parts of the prototype. Wave and wind loading likely led to cracking of the body of concrete. The width of the major crack was 0.2 mm and the width of the continuous minor crack was less than 0.2 mm (Figure 5.4 (a)). The crack width was measured using a crack microscope. The epoxy loss was observed in the layer with 2 mm thickness, but the opening was shallow and had not reached the inner side of the tube (see Figure 5.4 (b)). The depth of the opening was measured using a Vernier scale. Failure of the post tensioning bar and separation of the end plate was the main reason for inundation (Figure 5.4 (c)). The epoxy connection between the steel plates and the concrete was the weakest part of this assembly, with no sign of adhesion left between the steel and concrete.

Initially, the tube was kept intact by the post tensioning bars. It is difficult to say whether the crack in the body of concrete was there before the failure of the post tensioning bars or not. It can be speculated that the failure of the post tensioning led to the crack in the body of concrete, joint opening, and separation of the plate.

The final evaluation was conducted in two different ways. The First one was non-destructive testing with UPV and rebound hammer and the second one was destructive testing by taking some cores

from the tube and conducting CT scanning, $AgNO_3$ spraying, chloride profiling, and XRF on the cored sample.

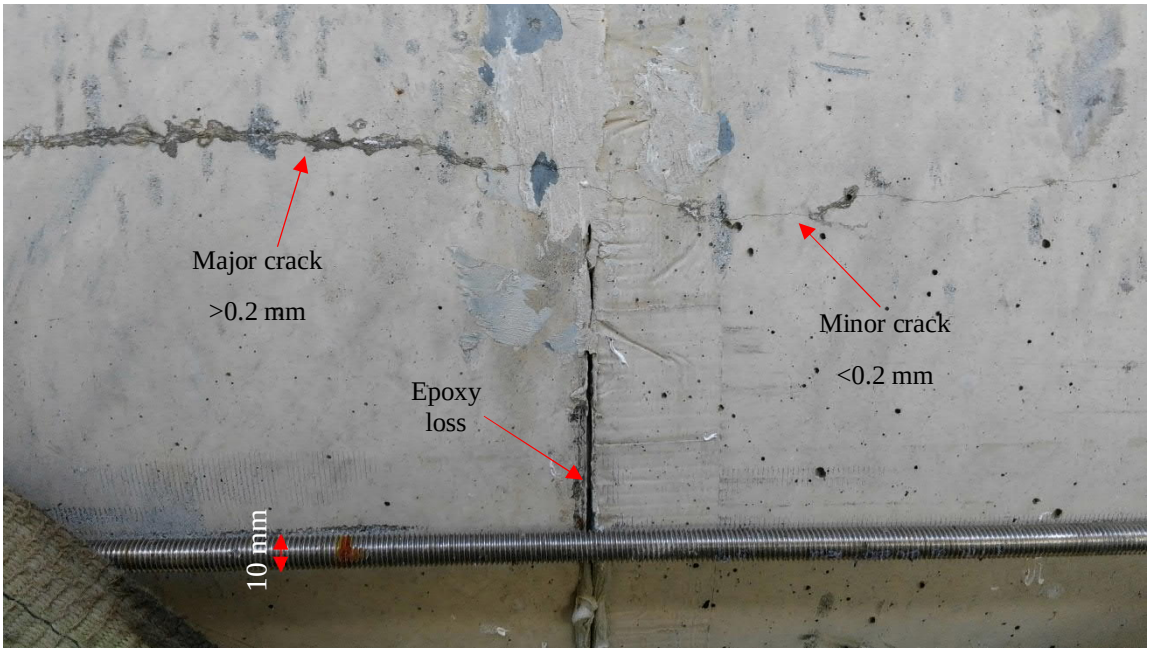

a) Major and minor crack

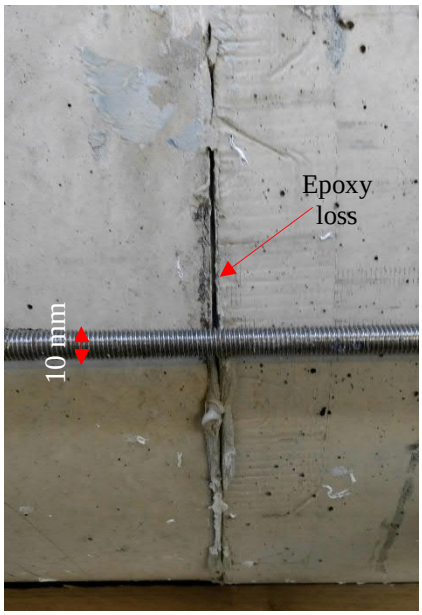

b) Loss of epoxy

c) Plate separation

Figure 5.4. Damaged parts of the prototype (Visual inspection)

5.2.4. UPV survey

Indirect UPV according to BS EN 12504-4 (2004d) was conducted horizontally and vertically. The open plan of the prototype is divided into the concrete parts and the jointed areas and the average of three UPV measurements for each part are presented with the scale colour.

In horizontal measurements, the transducers were placed with 200 mm distance from each other. Figure 5.5 shows the open plan of the prototype with average pulse velocity value of horizontal measurements in each partition. According toTable 3-12, pulse velocity more than 3.5 km/ is an indication of good quality concrete. Pulse velocity between 3.0 to 3.5 km/s represents a satisfactory quality of concrete. Any pulse measurements lower than 3.0 km/s is a sign of poor quality of concrete and loss of integrity. The majority of horizontal UPV measurements in Figure 5.5 represent good or satisfactory quality of the concrete. The lowest pulse velocity of the horizontal measurements was in the range of 2.0-2.5 km/s around the jointed areas. The epoxy layer had lower modulus of elasticity, so it was expected to have lower pulse velocity.

The damaged parts of the tube like the area between parts C1 to C4 (see Figure 5.3) was successfully identified by UPV. However, the horizontal UPV measurements did not identify the difference between the joint and the body of concrete. With 200 mm distance of measurements, the epoxy thickness is so small that does not significantly affect the speed of pulse.

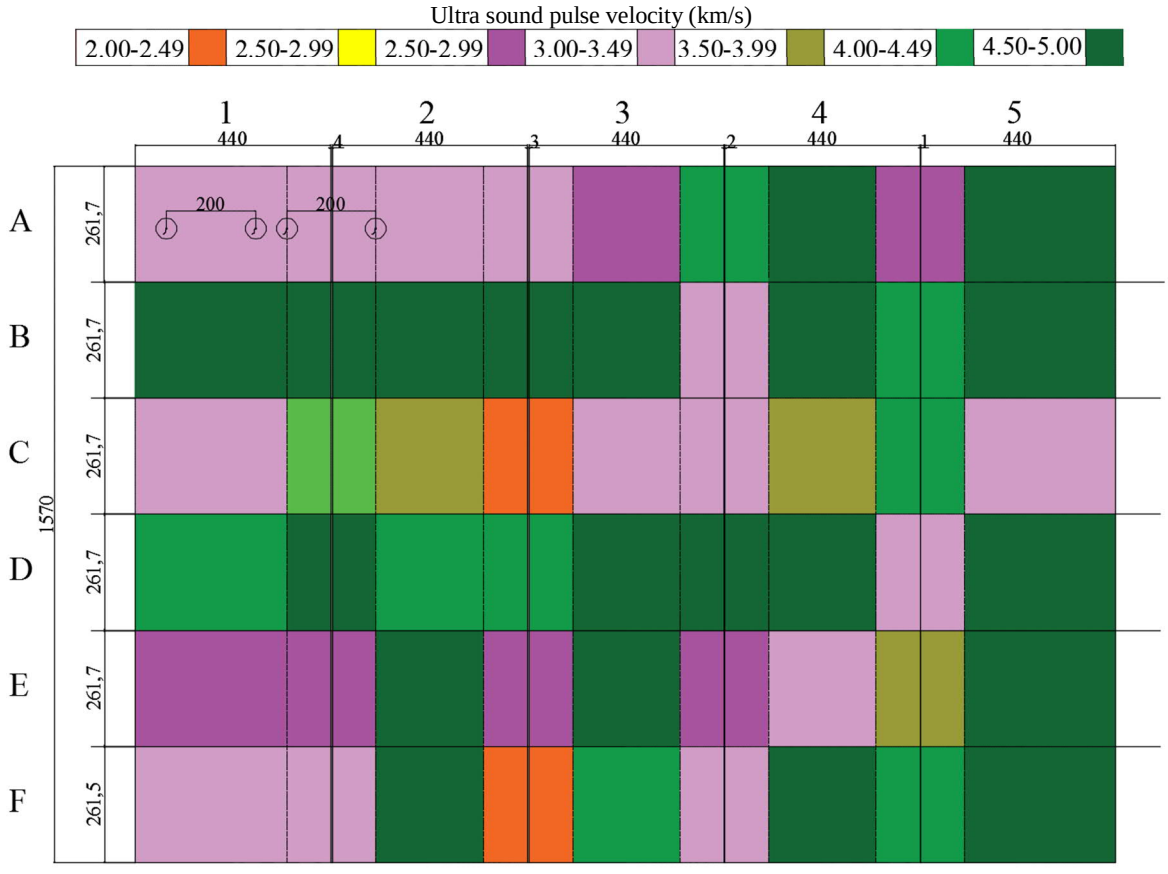

Figure 5.5. UPV horizontal evaluation with 200 mm distance between transducers

Figure 5.6 shows the same colour scale for vertical UPV measurements. Three measurements were also conducted for each part and the averages of these three readings are presented for each part. The vertical readings with 100 mm distance identified the difference between the joint and the body of concrete successfully because the pulse path goes through epoxy layer with less intervention of the concrete.

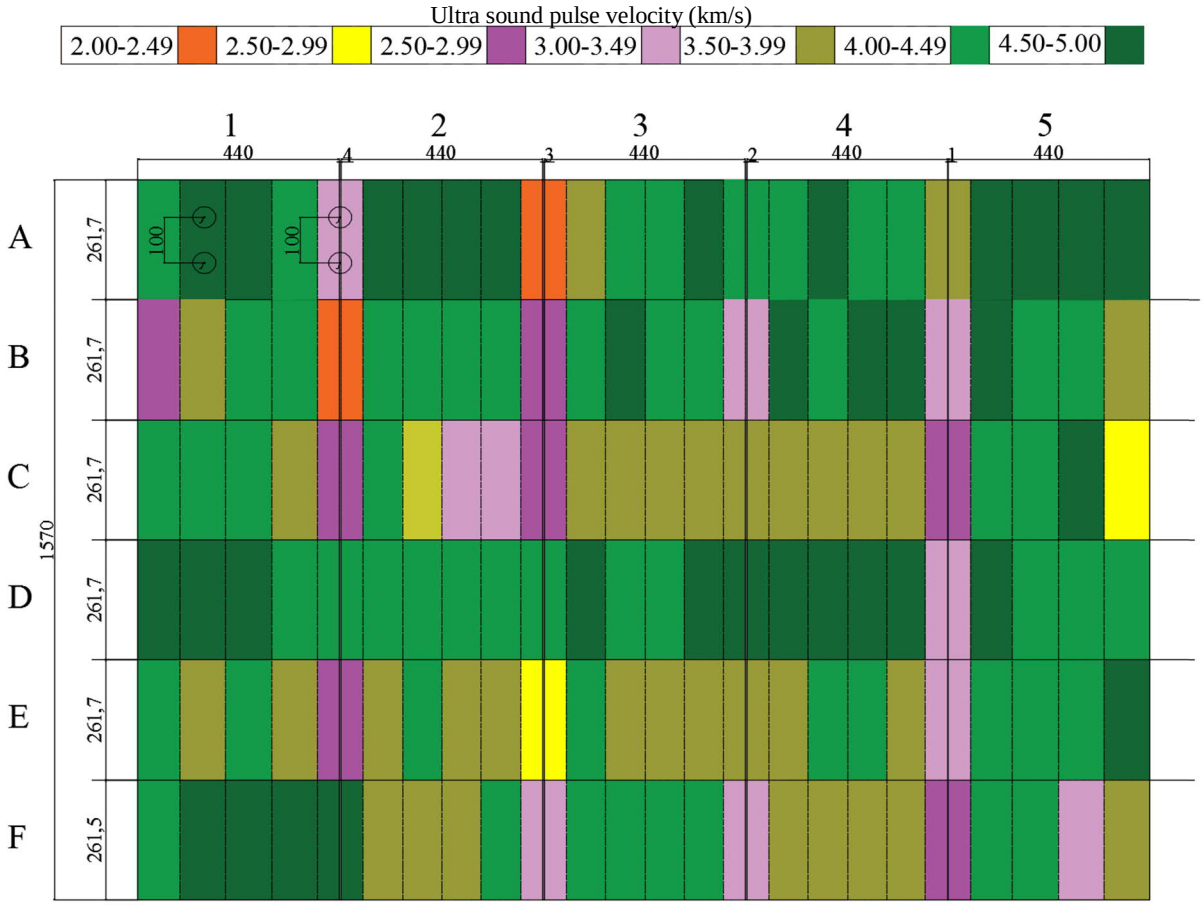

Figure 5.6. UPV vertical evaluation with 100 mm distance between transducers

Minimum recommended path for UPV measurements by BS EN 12504-4 (2004d) is 100 mm for 20 mm aggregate size, but the path length does not play an important role in UPV measurements in most cases (Bungey and Millard, 2010). However, using UPV for identifying the defected parts in the bonded epoxy system depends on the distance of the transducers and direction of the readings. If the pulse passes mainly through the concrete, the concrete will be more dominant (horizontal readings). It means that the pulse velocity is the representative of the concrete quality and the defects within the epoxy layer cannot be found. While the vertical readings which is more concentrated on the epoxy layer identifies the week points of the epoxy successfully.

Overall, the reliability of these measurements can be questioned due to several reasons:

1. The transducers need to be completely in touch with the surface while the prototype surfaces were curved and total contact between transducers and surface were not guaranteed.

2. Indirect measurements (such as the current project) are less reliable and have potential for errors (Bungey and Millard, 2010).
3. The sample should be thick enough to be considered as infinite medium, i.e. the lateral path length should be higher than the wavelength. Equation 5.1 and Table 5-2 show the minimum lateral path according to transducer frequency. The transducers used in this test were 54 kHz (typical transducers) and the thickness of the concrete tube was 25 mm. Based on Table 5-2 the minimum lateral path for 54 kHz frequency should be at least 70 mm. Ideally the higher frequency transducers should be used in this case, but UPV equipment used in this project had an option for testing samples with less than 50 mm thickness. It overcame this problem by adjusting pulsar voltage to lower voltage.

$$Wave\ length = \frac{Pulse\ velocity}{Frequency}$$

Equation 5.1(Bungey and Millard, 2010)

Table 5-2. Minimum lateral path for UPV (Bungey and Millard, 2010)

Transducer frequency(kHz)	Minimum lateral path (mm)	
	V_c=3.8 km/s	V_c=4.6 km/s
54	70	85
82	46	56
150	25	30

4. As a general accepted experience, the voids smaller than the diameter of the transducers cannot be detected. This is confirmed in the supplier manual as well (James Instruments Inc.). The diameter of transducers was 50 mm. Therefore, void less than 50 mm may not be detected.

5.2.5. Rebound hammer survey

Figure 5.7 shows the open plan of prototype and corresponding rebound hammer number with 45^0 inclination measurements. The scale colour shows the average of three measurements at three points in each part. The week areas were successfully identified using this method and they match to the visually detected damaged areas in Figure 5.3.

In conclusion, identifying defects with UPV as the main tool for finding the defect is not enough, but combination of UPV and rebound hammer can give an indication of the location of defects. Both UPV and rebound hammer values were revealing presence of damage in the body of concrete and joints, but they were not able to estimate the extent of damage exactly.

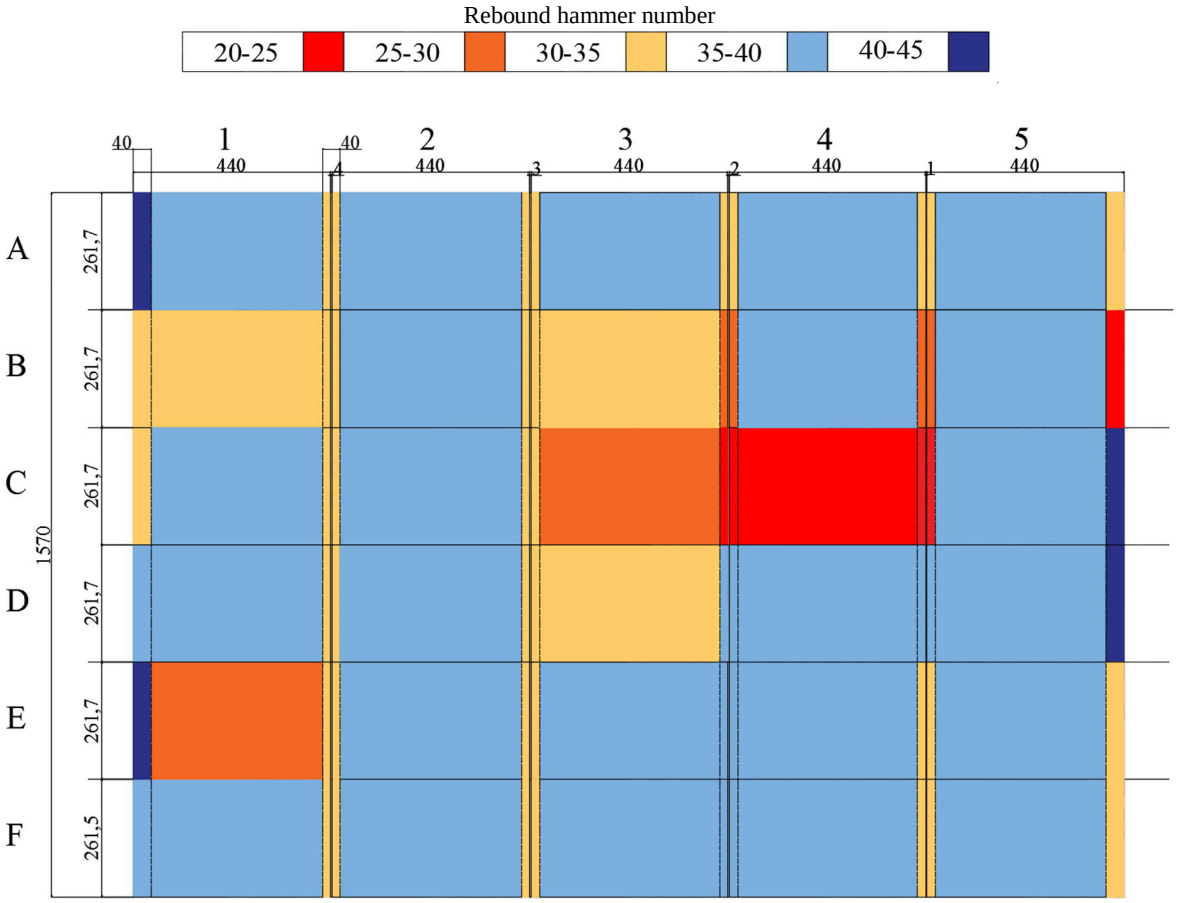

Figure 5.7. Rebound hammer number (for 45^0 measurements)

5.2.6. Coring and destructive testing

The coring and testing plan is shown in Figure 5.8. The samples for these tests were chosen to represent both healthy and damaged parts based on UPV and rebound hammer. The cores were taken by the saw cutting the marked square areas in Figure 5.9. The numbers in the squares are the sampling numbers and the colours show the testing method used for each sample. The saw cutting was performed with as little water as possible to prohibit any chloride to be washed away with the water.

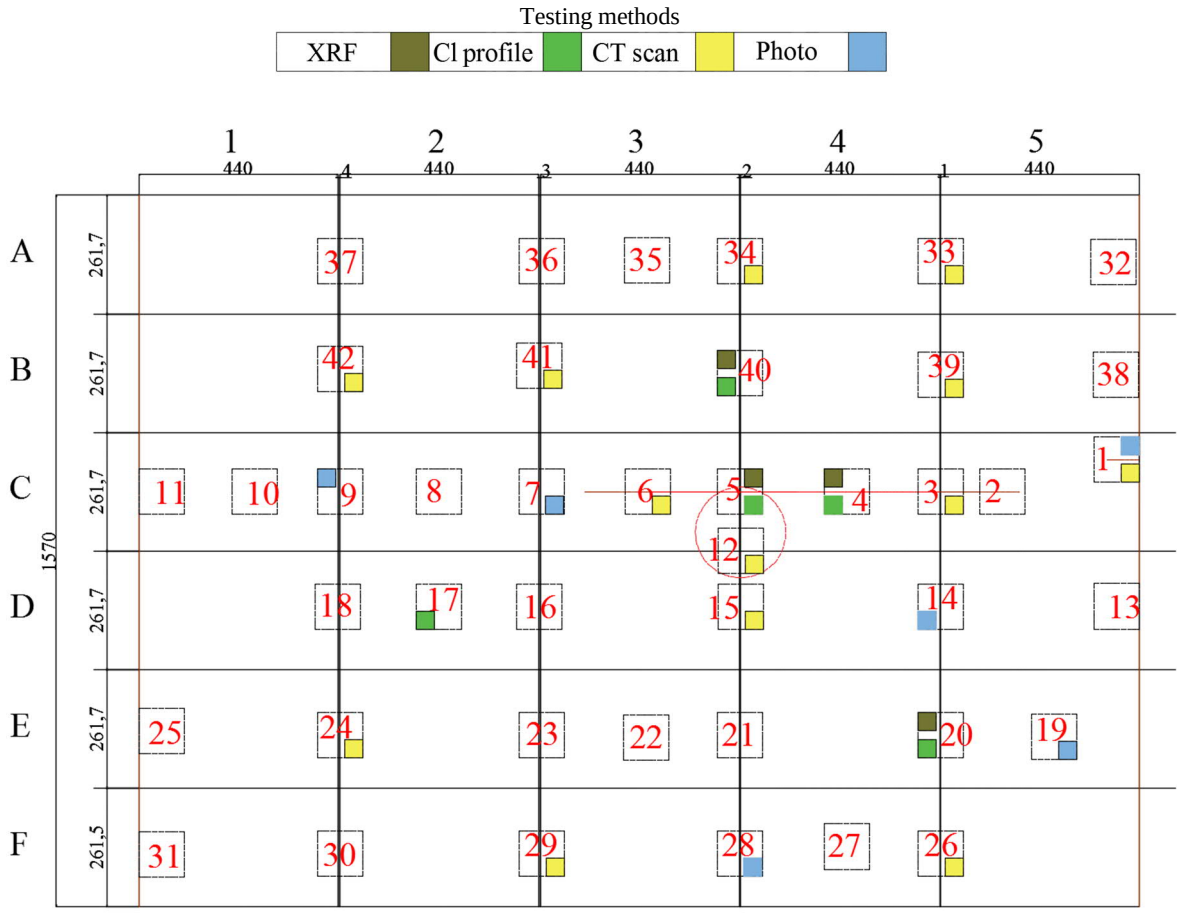

Figure 5.8. Prototype coring and testing plan including the sample numbers

Figure 5.9. Coring of the prototype using the saw

5.2.7. CT-scan analysis of the joints after 24 months exposure

Samples No. 1, 3, 6, 12, 15, 24, 26, 33, 34, 39, 41, 42 in Figure 5.8 were placed in CT scanner. The majority of scanned samples did not have significant defects except some small voids (less than 1 mm) in the joints. The CT scan analysis was found to match the visual inspection.

The epoxy loss from both internal and external side of the prototype can be seen in Figure 5.10 (a). The depth of the major crack was equal to the wall thickness (see Figure 5.10 (b)) but the post tensioning had saved the integrity of the structure. Finally, Figure 5.10 (c) shows an example of flawless joint and concrete. Sample No. 24 showed lower pulse velocity in both vertical and horizontal measurements while there was no problem within the joint and the concrete. These findings arise doubts on reliability of UPV measurements.

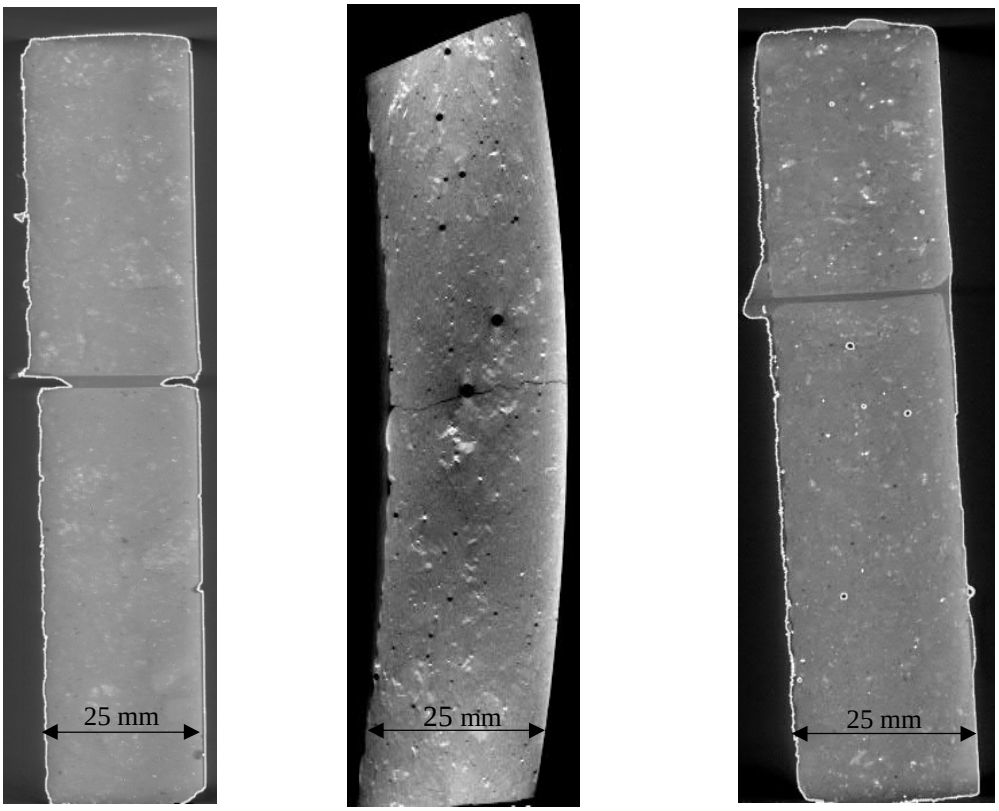

a) Epoxy loss: Sample No. 15

b) Crack through: Sample No. 6

c) Healthy joint: Sample No. 24

Figure 5.10. CT scan analysis of the cores from the prototype

Sample No. 42 was observed to have a large defect in the middle of the epoxy layer. The visual inspection, horizontal UPV and rebound hammer measurements did not reveal any problems in that area. However, CT scan, presented in Figure 5.11, revealed the presence of a large internal defect in the middle part of the joint. Vertical UPV measurements also suggested the presence of a defect with lower pulse velocity value (2-2.5 km/s).

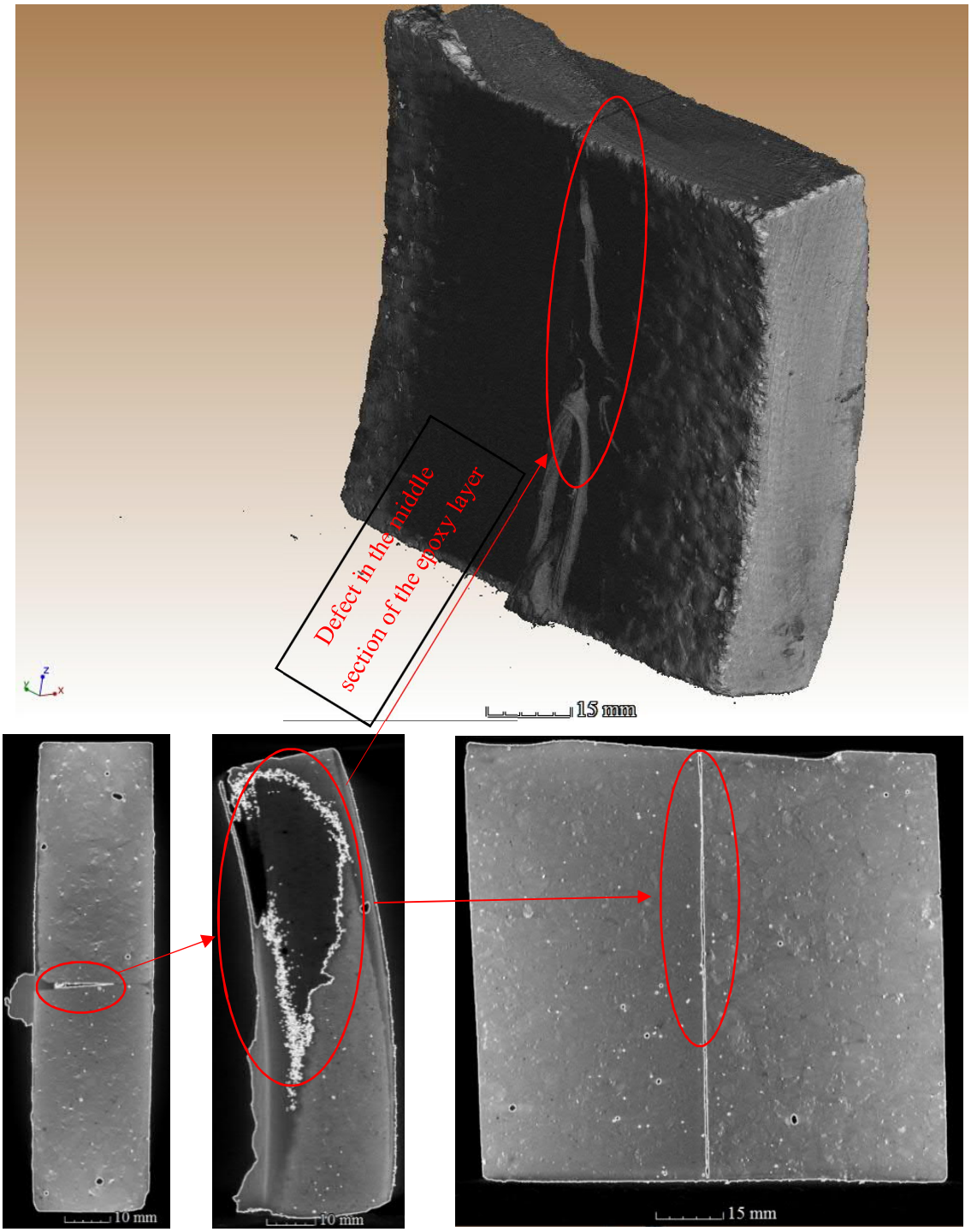

y-x plane z-x plane z-y plane

Figure 5.11. Large internal defect in the joint, sample No. 42

5.2.8. Chloride analysis of the cored samples using $AgNO_3$ spray

12 samples were cored and broken into halves. $AgNO_3$ spraying on these sections showed full depth of chloride ingress in all sections. There was no difference between the body of concrete and jointed areas. Therefore, the chloride penetration depth can be considered as at least 25 mm which is equal to the wall thickness of the tube.

5.2.9. Chloride analysis of the cored samples using X-Ray Fluorescence (XRF)

The X-ray Fluorescence (XRF) was used for qualitative and quantitative analysis of the components of the cored samples. The samples were chosen to represent the defected joints, the cracked concrete, and the healthy parts. The chosen samples were cut in three layers using the diamond saw. Each layer was ball grinded to form a fine powder. XRF was conducted for the powder of each layer. Table 5-4 shows the result of analysis and major components of the three layers of the chosen samples.

Main aspect to consider in Table 5-4 is the amount of chloride in each layer of the samples. The amount of chloride concentration the jointed sections is 0.198-0.292 while the range of chloride in concrete sections is 0.101-0.87. The higher chloride concentration in epoxy layer can be attributed to the presence of chloride in epoxy composition or higher penetration of chloride in epoxy layer.

It should be mentioned that the tube became full of water after sinking so the chloride penetration has occurred from both inside and outside of the tube. Therefore, the concentration of chloride was found to be the lowest in the middle layers compared to the external and the third layers which were inside the tube.

The concrete segments were made according to Mix 2 (see Table 3-9). CEM I was the only type of cement used in this mix. The typical bulk oxides of Portland cement are mentioned in Table 5-3, comparing the bulk oxides with Table 5-4 shows normal composition of the concrete, Moreover, MgO is less than 5% and SO_3 is less than 3.5% which is acceptable for normal concrete (Neville, 2011) .

Table 5-3. Typical bulk oxide of Portland cement (Hewlett, 2001)

Oxide	Composition % by mass
CaO	58.1-68.00
SiO_2	18.4-24.50
Al_2O_3	3.10-7.56
Fe_2O_3	0.16-5.78
MgO	0.02-7.10
Na_2O+K_2O	0.04-1.66
TiO_2	0.1-0.4
P_2O_5	0.1-0.2
SO_3	1.0-3.0

Table 5-4. XRF analysis of the cored samples

Sample location	Sample No. and layer	MgO	Al_2O_3	SiO_2	$P2O_5$	SO_3	K_2O	TiO_2	Cr	Na_2O	Fe_2O_3	Pb	Zn	MnO	CaO	Cl
		(%)	(%)	(%)	(%)	(%)	(%)	(%)	(ppm)	(%)	(%)	(ppm)	(ppm)	(ppm)	(%)	(%)
Joint with epoxy loss (mix of concrete and epoxy)	Sample 5-1[(1)]	1.812	11.104	50.927	0.199	0.849	2.174	0.343	46.3	2.729	2.489	26.5	113.5	503.6	15.552	0.187
	Sample 5-2	1.699	11.76	52.028	0.193	0.781	2.367	0.332	44.7	2.769	2.301	25.1	98.4	468.6	13.876	0.101
	Sample 5-3	2.039	10.522	47.295	0.192	0.91	2.172	0.336	28.5	2.317	2.415	26.8	117.8	477	17.292	0.104
Cracked concrete	Sample 4-1	1.75	11.986	53.808	0.212	0.759	2.359	0.308	42.8	2.972	2.267	29.9	94.9	408.3	12.961	0.166
	Sample 4-2	1.877	12.391	53.416	0.19	0.711	2.435	0.368	57.6	2.817	2.467	24.3	89.1	458.2	12.603	0.136
	Sample 4-3	1.848	10.766	48.535	0.196	0.849	2.229	0.333	44.9	2.41	2.449	31.2	118.4	464.8	16.211	0.112
Joint (mix of concrete and epoxy)	Sample 40-1	1.812	9.765	44.858	0.18	1.102	1.85	0.346	57.2	2.307	2.368	34.5	166.4	440.3	20.599	0.271
	Sample 40-2	1.876	9.872	43.822	0.204	1.139	1.87	0.358	54.9	2.181	2.462	32.7	170.4	512.5	21.132	0.292
	Sample 40-3	2.046	9.132	40.1	0.192	1.269	1.804	0.384	59.2	1.864	2.637	24.4	150	544.5	23.531	0.212
Healthy Joint (mix of concrete and epoxy)	Sample 20-1	2.245	8.905	39.212	0.204	1.436	1.74	0.382	73	1.71	2.995	47.4	160.3	625.7	25.203	0.244
	Sample 20-2	2.238	8.964	39.31	0.201	1.43	1.673	0.413	85.1	1.742	2.78	35.4	161.4	589.9	25.052	0.203
	Sample 20-3	2.214	8.939	39.192	0.196	1.4	1.694	0.418	80.8	1.784	2.796	37	151.1	545.8	25.197	0.198

[(1)] Sample number according to Figure 5.8 and layer number (layer 1 is the outer layer, layer 2 is the middle layer and layer 3 is the inner layer of the tube)

5.2.10. Chloride analysis of the cored samples using acid soluble titration and chloride profiling

The cores taken from the prototype were sliced in three layers using a diamond saw. Each layer was ball milled and acid soluble titration was used to find the chloride concentration of each layer. The calculated diffusion coefficient based on curve fitting was not possible for most of the cases due to having just a few layers.

Table 5-5. Chloride analysis using acid soluble titration and comparison with XRF

sample location	sample No. and layer	% by mass of powder from titration	Diffusion coefficient from titration	% by mass of powder from XRF	Diffusion coefficient from XRF
Joint with epoxy loss (mix of concrete and epoxy)	Sample 5-1[(1)]	0.110		0.187	
	Sample 5-2	0.059	7.38×10^{-12}	0.101	5.59×10^{-12}
	Sample 5-3	0.068		0.104	
Cracked concrete	Sample 4-1	0.110		0.166	
	Sample 4-	0.063	8.49×10^{-12}	0.136	-
	Sample 4-3	0.070		0.112	
Joint (mix of concrete and epoxy)	Sample 40-1	0.110		0.271	
	Sample 40-2	0.059	15.77×10^{-12}	0.292	20.56×10^{-12}
	Sample 40-3	0.068		0.212	
Healthy Joint (mix of concrete and epoxy)	Sample 20-1	0.194		0.244	
	Sample 20-2	0.139	10.53×10^{-12}	0.203	11.09×10^{-12}
	Sample 20-3	0.125		0.198	
Body of concrete	Sample 17-1	0.089		-	
	Sample 17-2	0.079	-	-	-
	Sample 17-3	0.101		-	

[(1)] Sample number according to Figure 5.8 and layer number (layer 1 is the outer layer, layer 2 is the middle layer and layer 3 is the inner layer of the tube)

The percentage of chloride content identified by XRF and acid soluble titration methods are very different. However, both show the same trend of higher chloride content in the outer and inner layer of the tube. The middle layer still had the lowest chloride content.

As it was mentioned the number of layers were very limited for chloride profiling, so the calculated diffusion coefficients were larger than what it was expected for this type of concrete.

5.3. DURABILITY PERFORMANCE OF EPOXY BONDED CONCRETE TO CONCRETE

The current section presents the results of water penetration and chloride diffusion testing of epoxy bonded concrete in artificial seawater salt solution. The effect of concrete mix type and the difference between two states of hard-hard concrete and hard-fresh concrete bonding are analysed. Furthermore, the suitability of accelerated chloride migration tests for this configuration will be discussed. SEM and EDX of three types of epoxies are also analysed and presented to give an insight to the differences between properties and behaviour of epoxies. Finally, the effect of exposure to cyclic wetting and drying on mechanical performance of the bulk epoxy is presented.

5.3.1. Water penetration depth in epoxy bonded concrete

BS EN 12390-8 (2009f) test was conducted on samples made with Mix 1(see Table 3-9 , with 50% substitution of CEMI with GGBS). The samples were cast in two different condition of hard-hard and hard-fresh. Moreover, some hard-hard samples of Mix 3 (see Table 3-9, CEMI) were also cast to compare the influence of mix design on the bond performance. The average maximum depth of water penetration of 10 samples for each condition is presented in Figure 5.12. The standard errors were calculated by dividing standard deviation by the square root of number of samples.

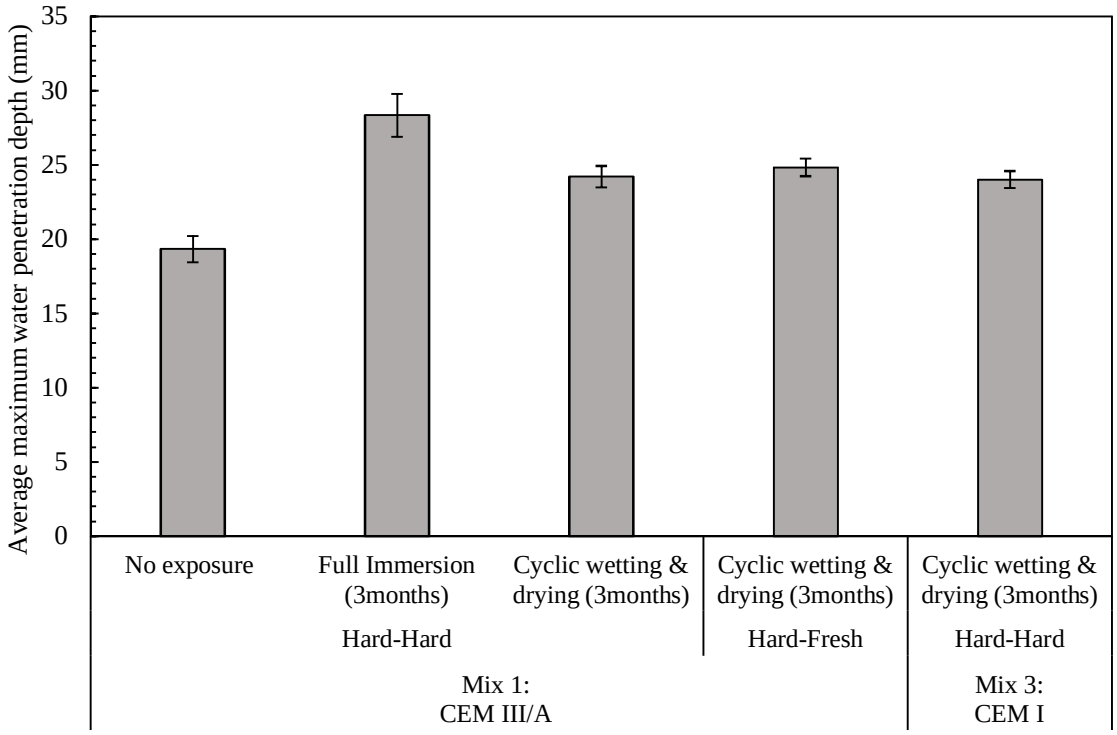

Figure 5.12. Average water penetration depth (mm) of the jointed concrete samples with two different concrete mixes, construction methods and exposure conditions.

According to Figure 5.12, the exposure time affected hard-hard bond concrete. Especially full immersion condition led to 47% higher water penetration depth compared to No exposure condition.

This means that epoxy bond may be affected by water as Büyüköztürk et al. (2011) explained in Figure 2.24. The H_2O molecules can destroy and weaken the bond between the concrete and the epoxy. However, the effect of cyclic wetting and drying was less severe on the epoxy layer (25% increase of water penetration depth compared to No exposure condition). Cement type and differences between these two concrete mixes had limited influence on the water penetration depth. It should be considered that both concrete mixes were high quality and high strength concrete. This effect may be different in case of lower strength concrete.

Figure 5.13 and Figure 5.14 show examples of water ingress for hard-hard bonded concrete. Red lines mark the water penetration depth. The presence of joint was found to affect the water penetration depth. All the images showed that the maximum water penetration depth is right beside the epoxy layer. The water penetration depth is the same on both sides of the epoxy layer for the majority of samples. However, there are samples like Figure 5.14 where the penetration depth differs on each side of the layer.

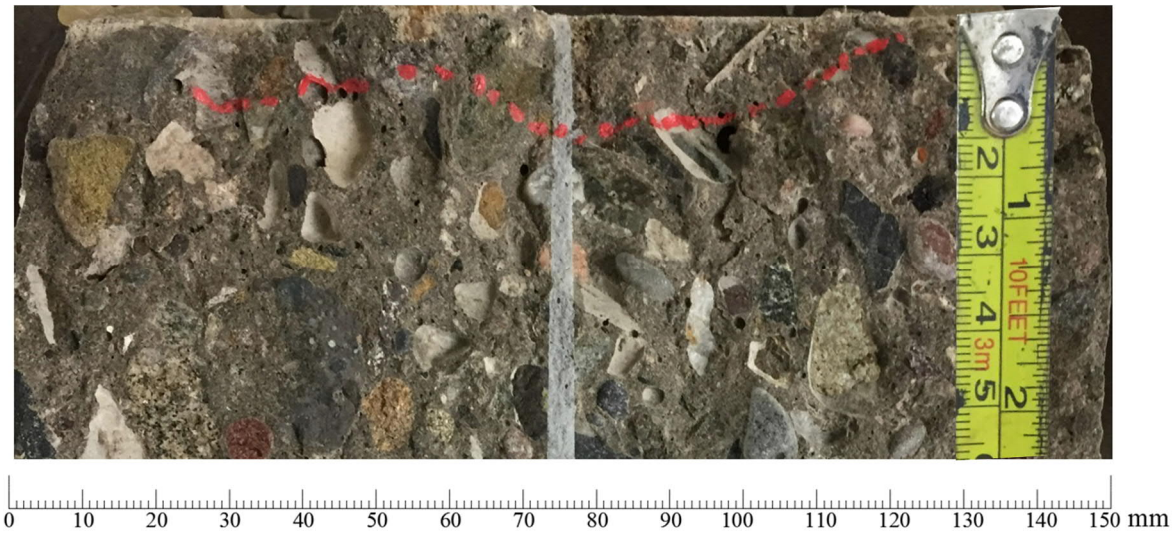

Figure 5.13. Typical shape of water ingress through hard-hard concrete bond

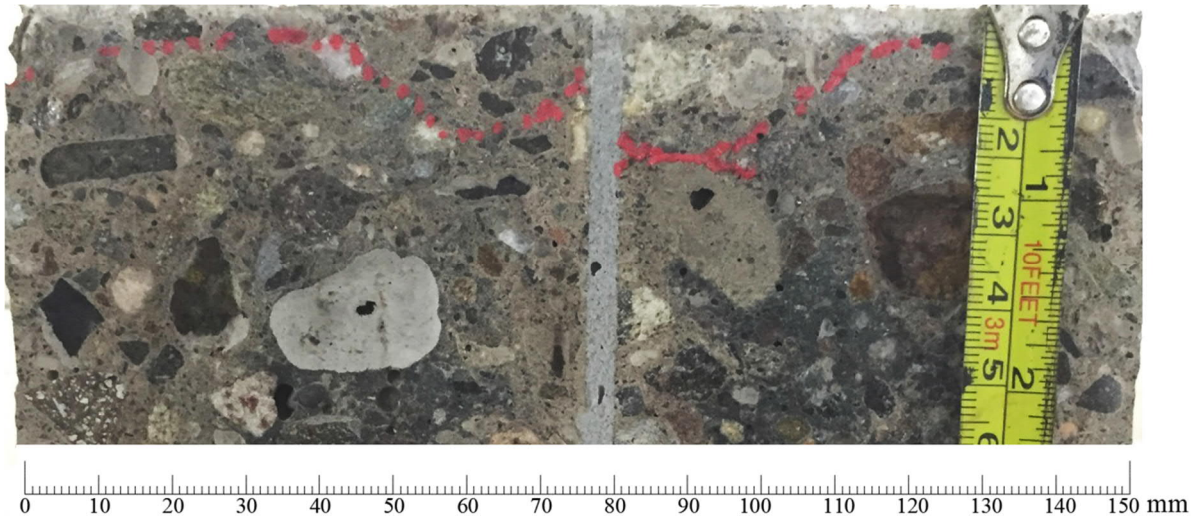

Figure 5.14. Rare case of water ingress through hard-hard concrete bond

The behaviour of hard-fresh concrete bond was not like hard-hard concrete bond. Figure 5.15 shows the typical water penetration depth of hard-fresh concrete bond. The water penetrated in the hard part and it moved through the bond line in hard side. The fresh side was toughened with epoxy and no sign of water penetration was obvious. Considering the average water penetration depth, the water penetrated 0.02% higher in hard-fresh bond compared to similar case of hard-hard concrete bond.

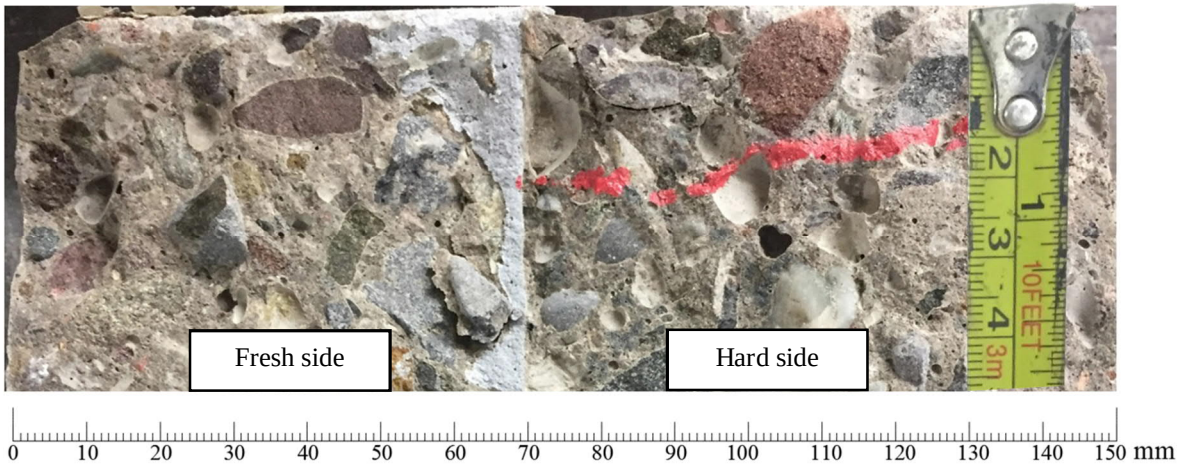

Figure 5.15. Shape of water ingress through hard-fresh concrete bond

5.3.2. Initial surface absorption of epoxy bonded concrete

Table 5-6 shows the results for Initial Surface Absorption Test (ISAT) based on BS 1881-208 (1996). Two pure concrete and one hard-hard bonded concrete (Mix 1 and epoxy A) were tested. The penetration depth was very low for both cases and bonded concrete showed even lower results from the rest of specimens. It means that water absorption was not influenced by the presence of the joint.

Table 5-6. ISAT 1881-208 results

Sample type	10 minute ISAT (ml/m^2/s)	30 minute ISAT (ml/m^2/s)	60 minute ISAT (ml/m^2/s)
Pure concrete	0.21	0.14	0.10
Pure concrete	0.22	0.15	0.10
Bonded concrete	0.10	0.06	0.05

5.3.3. Natural chloride diffusion in epoxy bonded concrete

5.3.3.1. Acid soluble titration and chloride profiling after three months exposure

Figure 5.16 shows average non-steady state chloride diffusion coefficient (D_{nss}) after 3 months exposure in artificial seawater salt solution. The non-steady state chloride diffusion codefined was obtained from acid soluble titration and chloride profiling of bonded concrete samples according to CEN TS 12390-11(2010) , (concrete Mix 1 and epoxy A). Overall, the diffusion coefficient values

were very small. Unlike the water penetration, cycles of wetting and drying had significant effect on chloride diffusion, especially, the bonded concrete seems to be sensitive to cyclic wetting and drying.

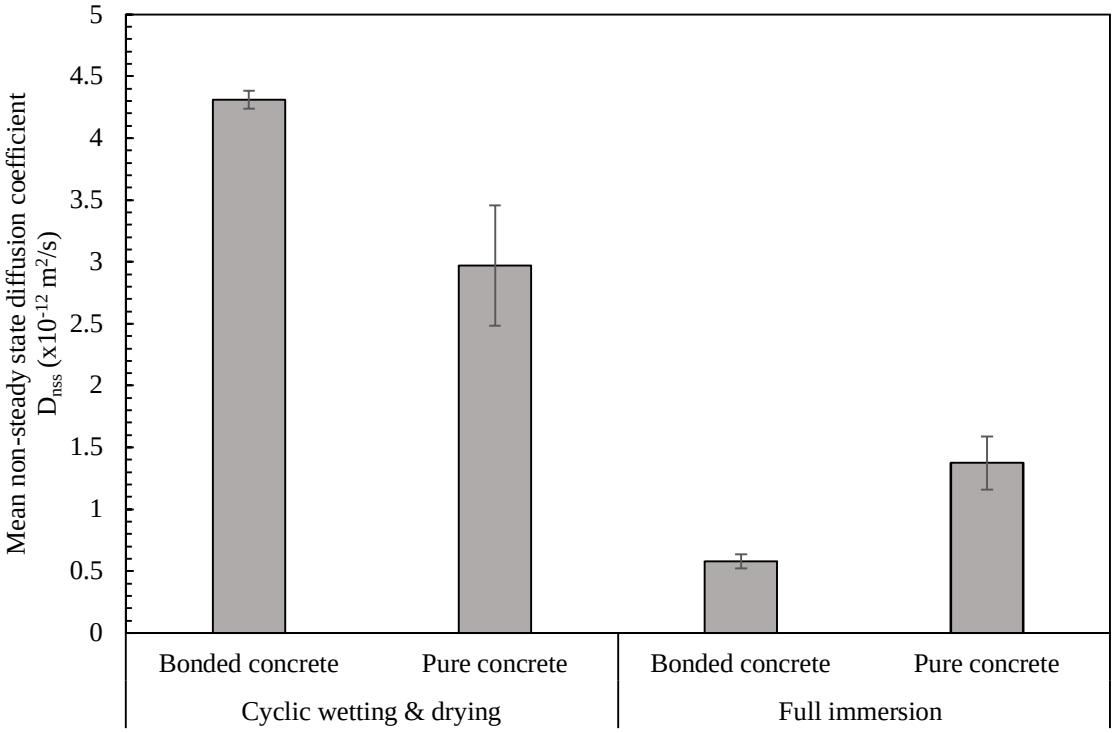

Figure 5.16. Average diffusion coefficient according to CEN TS 12390-11(2010) method

5.3.3.2. Chloride analysis using $AgNO_3$ spraying after three months exposure

Epoxy B was used for bonding concrete samples with Mix 1 and Mix 2 (see Table 3-9). The samples were made in two different condition of hard-hard and hard-fresh. The exposure conditions were full immersion and cyclic wetting and drying for 3 months. Figure 5.17 presents the free ion penetration depth of bonded concrete using 0.1 M silver nitrate spray after 3 months of exposure. The error bars show the standard error. The results are obtained from average of 10 samples for each condition. However, there were some faulty samples like Figure 5.18 which were excluded from the results because the poor construction affected chloride penetration along the bond line.

According to Figure 5.17, samples of Mix 3 showed the highest chloride penetration depth. Analysing the shape of chloride ingress depth of all the samples showed that there was no significant difference between the chloride ingress around epoxy layer and body of concrete (for example see Figure 5.19). Therefore, this higher depth of chloride penetration for Mix 3 can be attributed to the type of cement. The presence of GGBS in the samples with Mix 1 improved binding capacity of the concrete and reduced chloride ingress about 10%.

Again, ion penetration was considerably affected by the cycles of wetting and drying. In case of hard-hard concrete bond with 50% GGBS, the cyclic wetting and drying caused 45% higher chloride penetration after 3 months of exposure compared to full immersion. In case of fresh-hard concrete

bond, the cyclic wetting and drying led to 25% higher free ion penetration compared to full immersion.

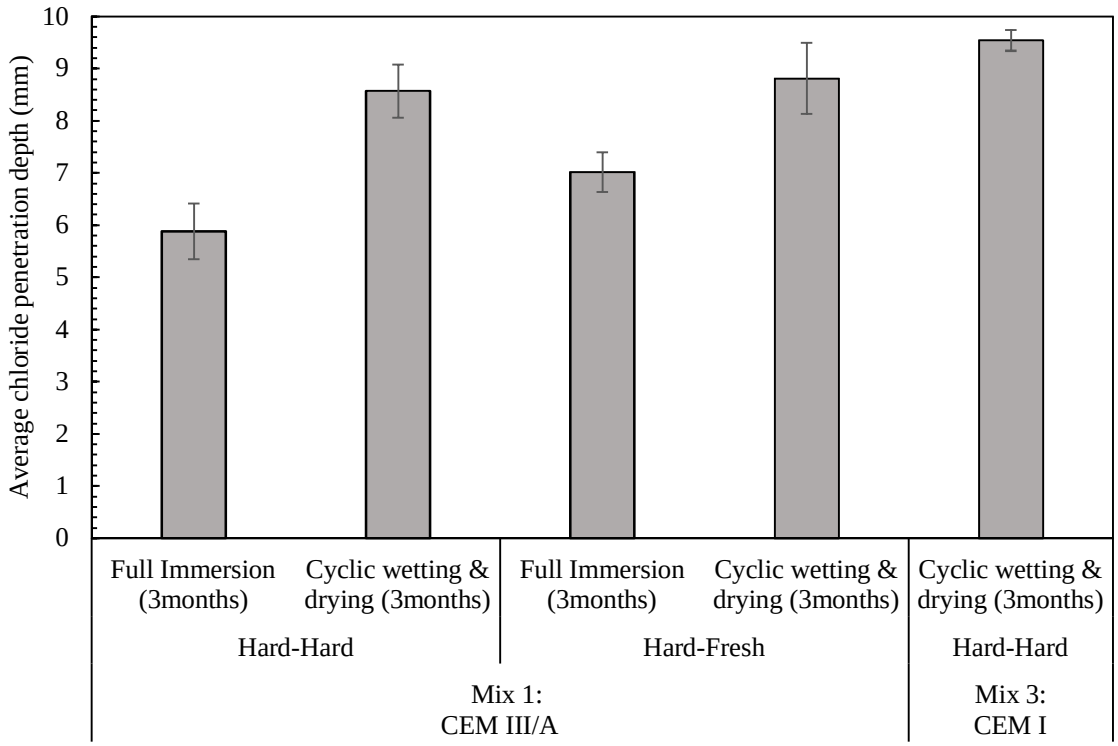

Figure 5.17. Chloride ingress depth through bonded concrete by spraying 0.1 M of $AgNO_3$ after 3 months of exposure

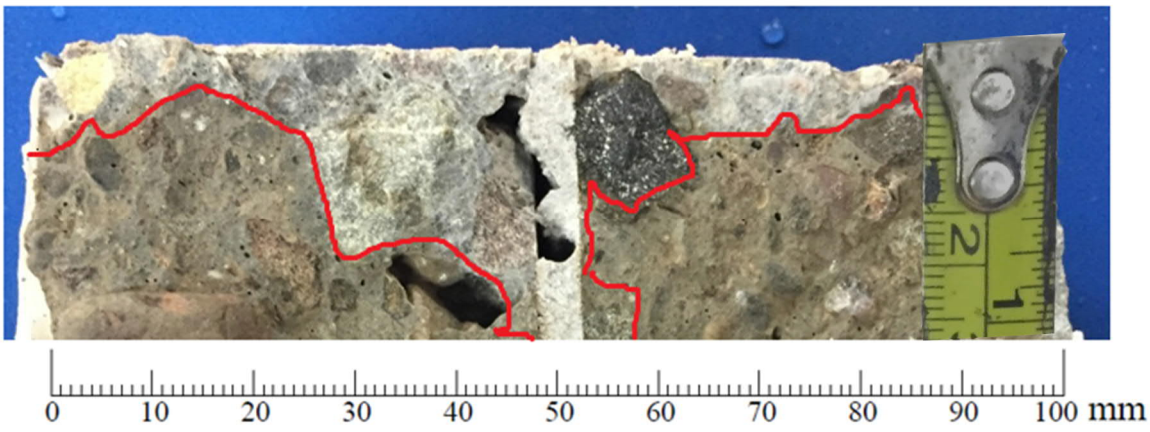

Figure 5.18. Poor jointing technique and high chloride ingress around the epoxy layer

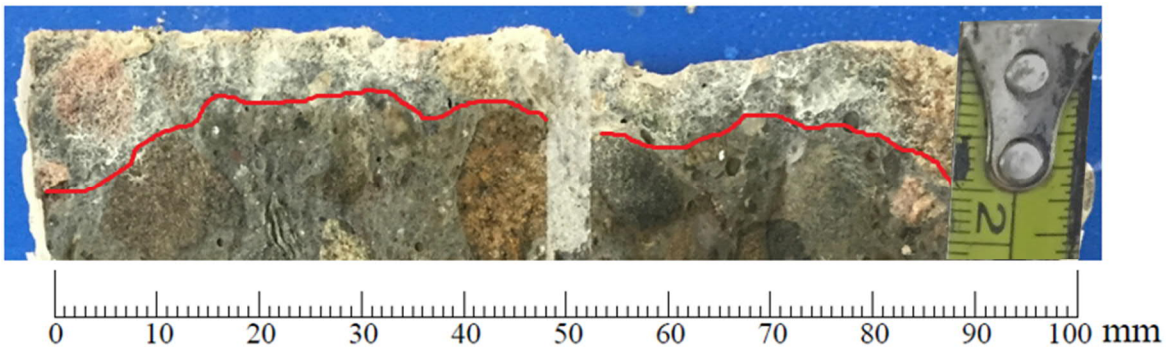

Figure 5.19. Typical shape of chloride ingress through hard-hard concrete bond

The construction method has also affected the ion penetration. Comparison between Figure 5.19 and Figure 5.20 shows the higher chloride penetration depth for hard-fresh concrete bond. In the case of full immersion, 19% increase of chloride penetration was observed and cyclic wetting and drying caused 2% increase in chloride penetration for fresh-hard concrete bond. This increase in ion penetration of fresh-hard concrete bond has two reasons. First reason is the differences between concrete curing regimes. The fresh-hard concrete samples were not cured for 28 days in the water because the epoxy is sensitive to water, while hard-hard concrete samples were cured for 28 days prior to applying epoxy. Second reason is the sensitivity of epoxies against presence of moisture at the time of application. During the process of bonding fresh concrete to hard concrete with epoxy, the surfaces and epoxy become moist and it might have affected the integrity of the bond and lead to higher chloride ingress. Although there was no water penetrating (see Figure 5.15) chloride penetrated in this type of construction.

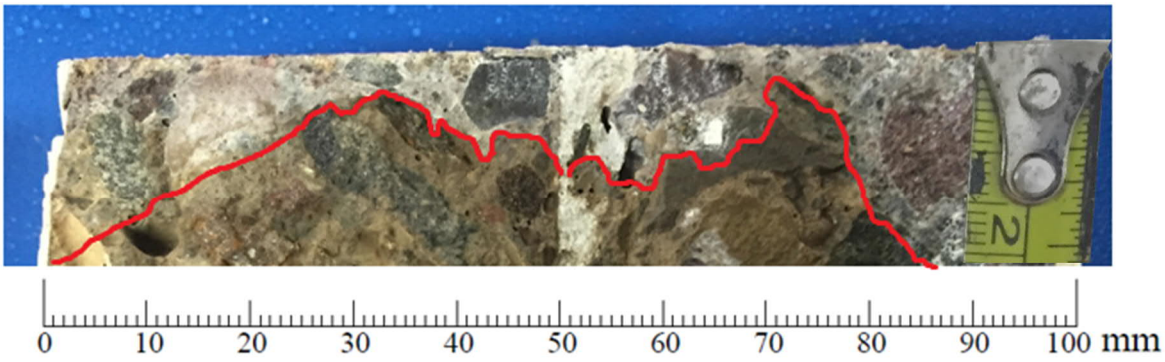

Figure 5.20. Typical shape of chloride ingress through fresh-hard concrete bond

5.3.4. Accelerated chloride diffusion in epoxy bonded concrete

The results of NT Build 492 (1999) and Multi regime are presented in Figure 5.21. Overall, the diffusion coefficients were less than 2×10^{-12}. The horizontally jointed samples showed a significant difference because epoxy is a dielectric material and it causes repelling of negatively charged chloride ions. Epoxy acts as an insulator in an electrical field. Therefore, the horizontally jointed samples showed a much lower non-steady state diffusion coefficient. It can be concluded that

electrically accelerated methods are not proper methods for jointed sections and these results may be questioned.

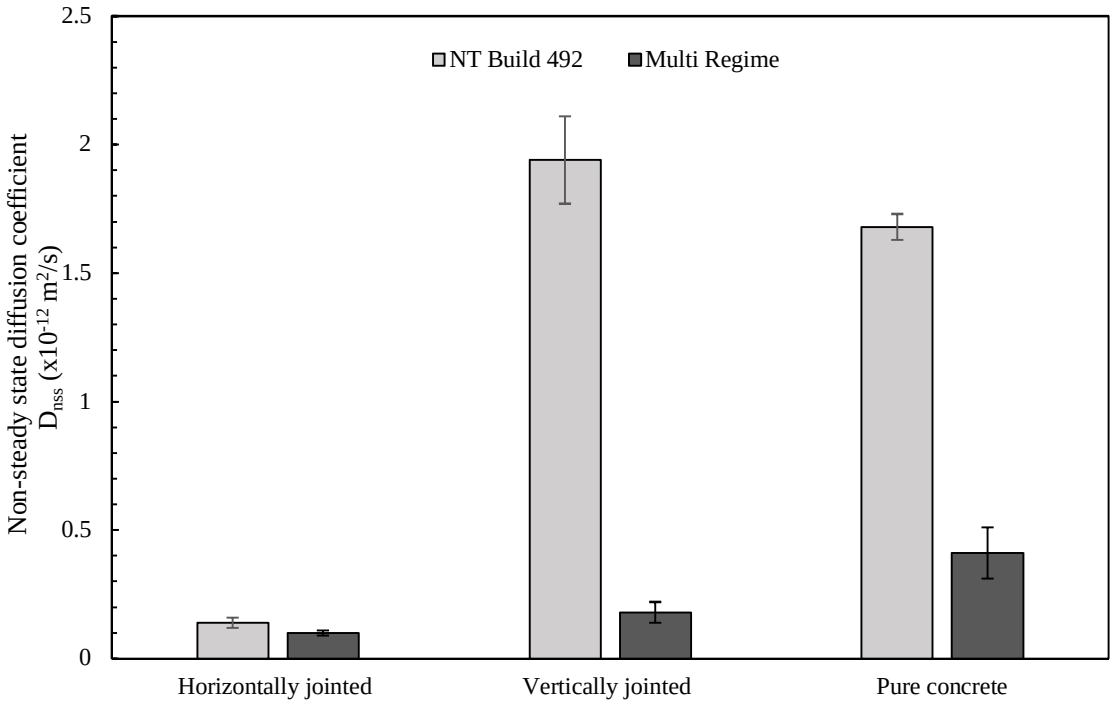

Figure 5.21. Accelerated chloride migration tests (epoxy A)

5.4. BULK EPOXY ANALYSIS

5.4.1. SEM and EDX of the bulk epoxy

EDX analysis of bulk epoxy A, B, and C show that the main components of the epoxies are carbon and oxygen (see Figure 5.22 (a), (c), and (e)). The difference in all other constituent components of the epoxies can be attributed to the filler type. The filler type may also affect the texture of epoxy as shown in Figure 5.22 (b), (d), and (f).

Epoxy B has the highest mechanical properties according to Table 3-8 and it also shows the roughest surface texture. The effect of filler type and percentage on mechanical performance and texture of the epoxies will be discussed in chapter 6 after reviewing the results of the cyclically loaded samples.

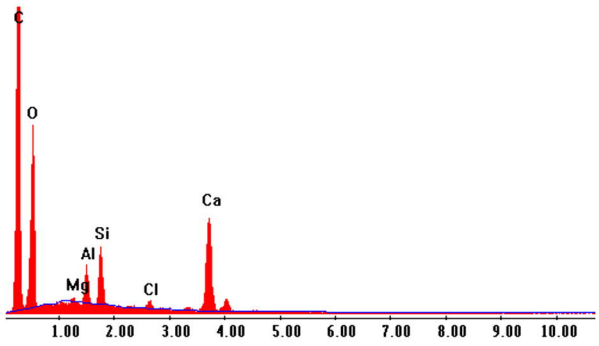

a) EDX of epoxy A

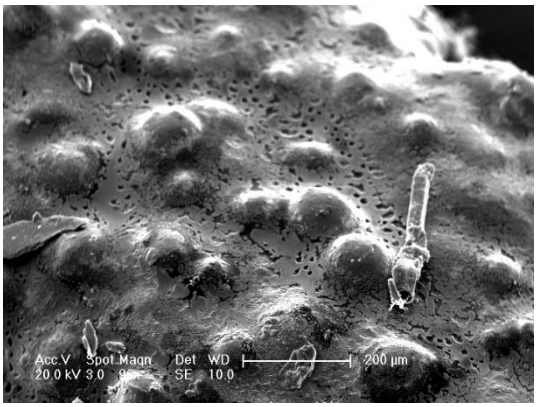

b) SEM of Epoxy A

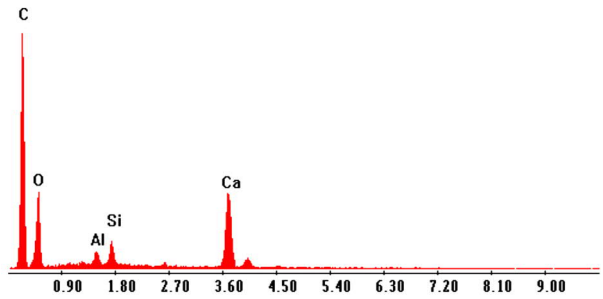

c) EDX of epoxy B

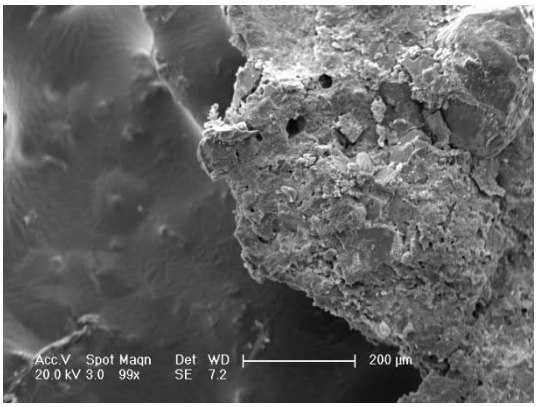

d) SEM of Epoxy B

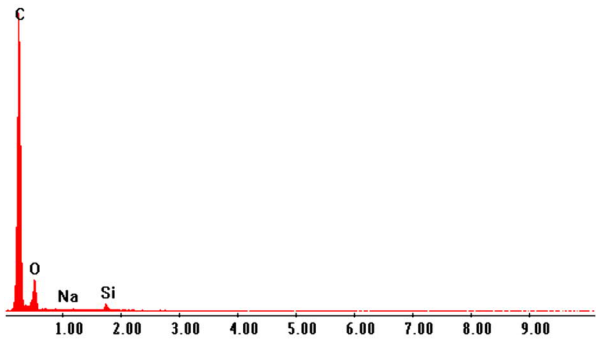

e) EDX of epoxy C

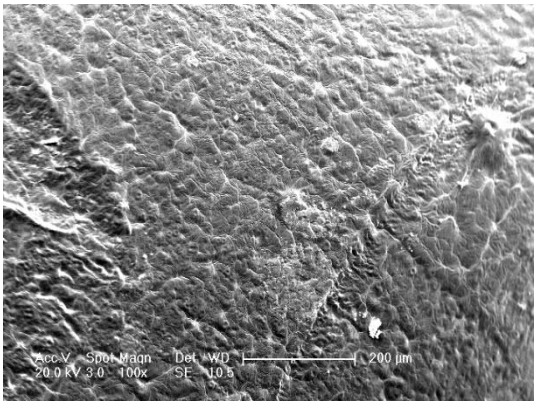

f) SEM of Epoxy C

Figure 5.22. EDX and SEM analysis of bulk epoxy A, B and C

5.4.2. Effect of moisture on tensile capacity of the bulk epoxy

ASTM D638 Standard (2014) test method for tensile properties of plastics was conducted on bulk epoxy B at the initial stage (after 3 days of curing) and after 3 months of exposure under cyclic wetting and drying in seawater salt solution. Figure 5.23 shows stiffness reduction of the bulk epoxy after the exposure time. There was also around 5% reduction of strength after 3 months of exposure. The overall displacement of the epoxy sample before failure has been less than 0.03 mm for both cases.

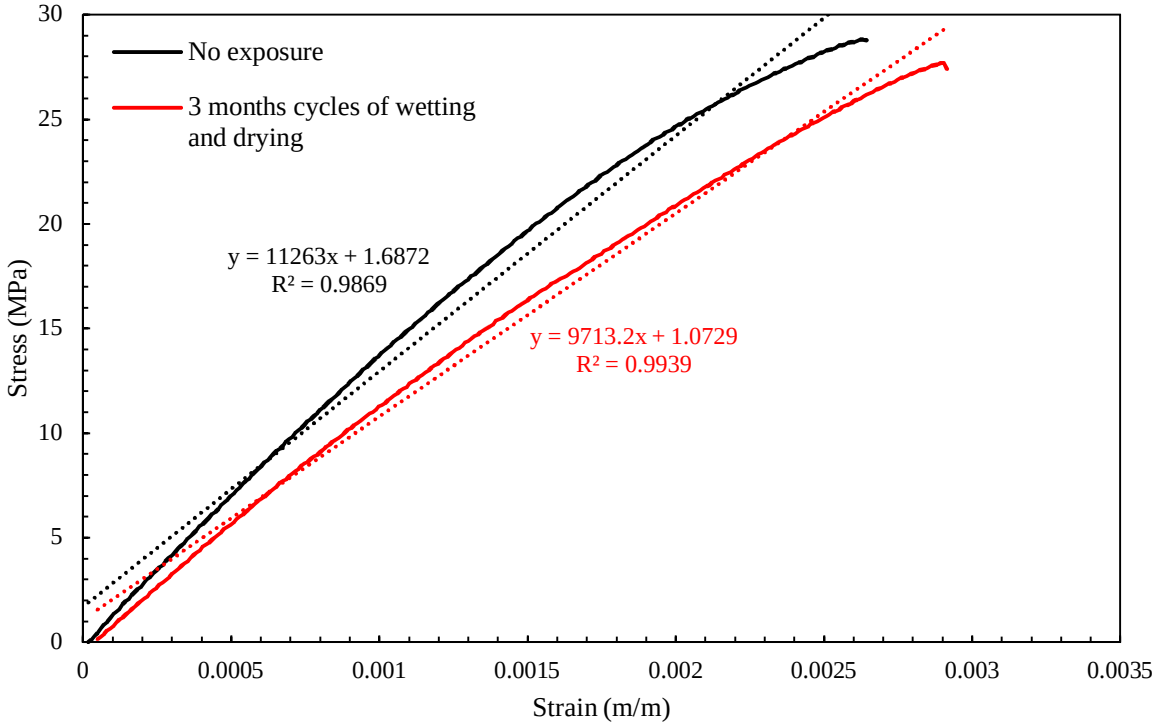

Figure 5.23. Tensile test of epoxy B according to ASTM D638 (2014)

5.5. CONCLUSIONS

The chapter focused on durability aspects of epoxy bonded concrete. A prototype in accordance with the Pelamis concept was constructed and floated for two years in seawater. Assessment of the prototype in various stages highlighted the challenges of non-destructive testing of the joints. It suggested that the combination of UPV and rebound hammer can identify the main weak areas but the exact extend of the defects cannot be assessed with these methods. Regarding UPV, the shorter distance between the transducers (100 mm) which is more focused on the joint has been more effective in finding internal defects within the joints. The main problem within the porotype was the total failure of the epoxy layer of the end steel plates. The concrete bonded to steel can be considered as the weakest part of the system and water had detrimental effect on this bond.

The destructive testing of the prototype showed that the chloride and water penetration through the joint was not the main concern of this system. CT scanning of the samples revealed the presence of some large defects within the epoxy layer, but they did not cause any major problem in the performance of the system. The performance of the assembly seemed to be dependent on the post tensioning because joint cleavage and failure of the end plate bond happened due to the failure of one of the post tensioning bars.

The water penetration and ion diffusion testing of the laboratory samples assessed the effect of exposure condition, cement type, and construction method of hard concrete bonded to fresh concrete.

Full immersion of bonded samples caused up to 47% increase of the water penetration depth in the case of hard-hard concrete bond while this effect became 25% under cyclic wetting and drying. In contrast, the effect of cyclic wetting and drying has been more significant for ion penetration with 45% higher free chloride ingress compared to full immersion after 3 months of exposure of hard-hard bond concrete.

The sensitivity of the epoxy bonded concrete to cement type has been insignificant in terms of water penetration. Regarding chloride diffusion, the 11% increase of free chloride ingress can be attributed to the cement type rather than the problem with the bond line.

Bonding hard concrete to fresh concrete led to normal water penetration depth in hard part of concrete and very low water penetration in the fresh side which was toughened with epoxy. However, the chloride ingress in such samples has been 19% higher compared to hard-hard concrete bonded after 3 months full immersion exposure.

Overall, the worst-case scenario water penetration depth was around 30 mm. The presence of the epoxy layer affected the water penetration depth and it can be considered as one of the main concerns for using epoxy bonded concrete in the marine environment. This effect became more noticeable after 3 months of full immersion because the epoxy layer was weakened and let more water to penetrate at the interface. In contrast, the chloride ingress was not affected by the presence of the joints. The highest chloride diffusion coefficient was recorded as 4.2×10^{-12} and the highest depth of free chloride ingress was 10 mm which indicates a good quality system according to The Concrete Society (2008).

6. CHLORIDE INGRESS IN BONDED CONCRETE UNDER COMBINED ENVIRONMENTAL ACTIONS AND MECHANICAL LOADS

6.1. INTRODUCTION

According to the literature review (e.g. Büyüköztürk et al. (2012)), there is a significant gap of knowledge in understanding the performance of epoxy bonded concrete systems under simultaneous environmental and mechanical stresses. This coupled effect is not adequately analysed even for conventional cracked or un-cracked concrete. Degradation of the epoxy bond under these concurrent effects adds complexity to analysis of this system because chloride or water ingress through the bond-line increases the risk of reinforcement corrosion on the side of joint.

The study comprised several samples with varying loading conditions under cyclic wetting and drying with artificial seawater solution. Table 6-1 shows the name of samples used throughout this phase with the major analysis. Each sample is presented and analysed individually in this chapter. Half-cell potential (ASTM C 876 (2015a)), UPV (BS EN 12504-4 (2004d)) and chloride ingress analysis with $AgNO_3$ spraying were also conducted for all the samples. The CT scanner played an important role for making the key observations in the current phase of the project. The slices of samples presented in this chapter are approximately from the middle section of the samples. The scans at different stages are intended to be from the same layer, however there may be some micron changes of the slice position in different scans. Void analysis was conducted on these images using VG Studio MAX 2.2 software to quantify and compare the extent of damage at various stages. These monitoring methods and measurements provided basic understanding of the challenges involved in designing epoxy bonded concrete under these simultaneous effects

Table 6-1. Post tensioned beams testing schedule

Sample name	Initial CT-scan	After first cracking CT-scan	Loading Status	Final CT-scan	Void analysis
A	✓	✓	No Load	✓	✓
B	✓	-	No Load	✓	-
C	✓	-	Sustained Load	✓	-
D	✓	-	Sustained Load	✓	✓
E	✓	-	Cyclic Load	✓	✓
F	✓	-	Cyclic Load	✓	-

6.2. PRE-CRACKING AND FRACTURE ENERGY OF THE COMPOSITE

The experimental set up of this phase simulated three different areas of stress distributions in the critical zone which was under pure tension.

Figure 6.1 shows the position of these three main areas schematically. There was a constant moment in the joint area and the elastic concrete part, however the stiffness of these two areas are different due to the presence of the epoxy layer. The damaged area experienced a complex stress field concentrated at the tip of the crack. The stresses distribute diagonally from the tip of crack. Therefore, the area around the crack and joint at the bottom of the beam is the least stressed area.

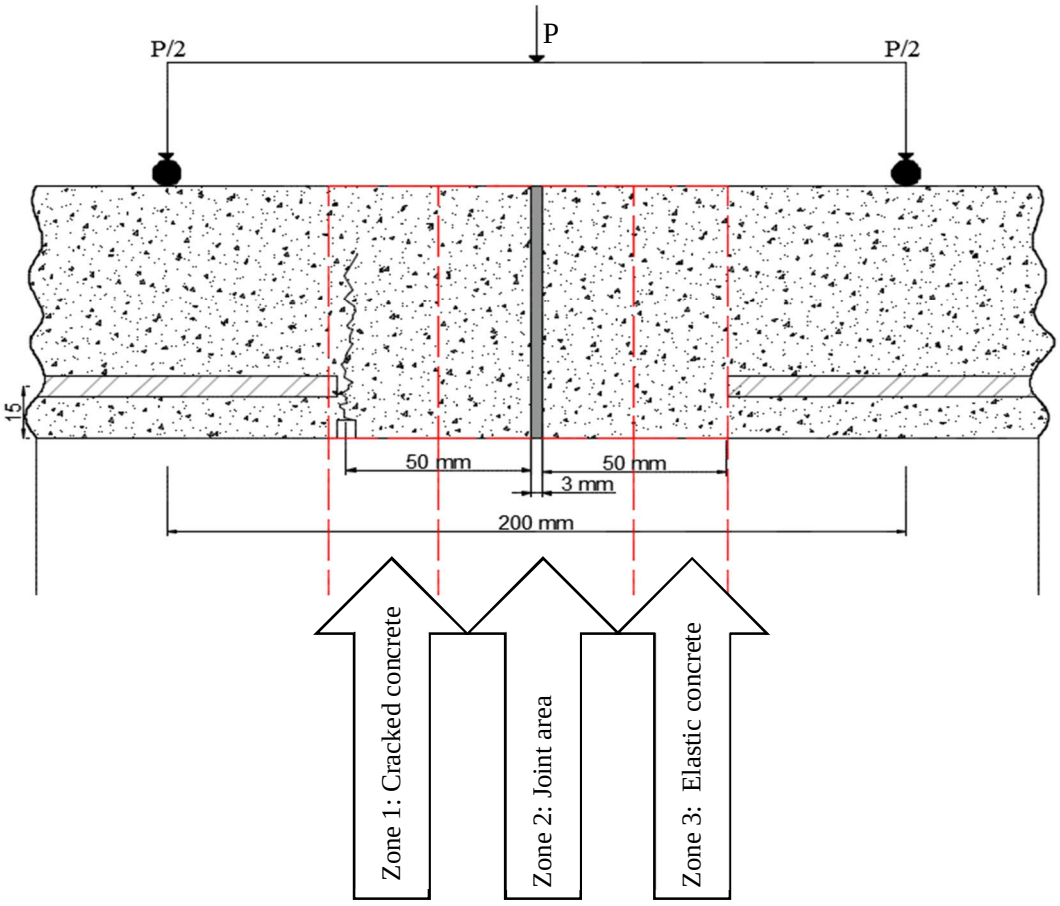

Figure 6.1. Schematic moment distribution along the beam after cracking

The macro scale assessment of the bonded concrete under four-point bending test in Phase I showed that the dominant mode of failure is a major crack in the body of concrete. Accordingly, the notch was placed in the body of concrete 50 mm from the joint. The fracture energy of this assembly was calculated to aid any numerical modelling based on fracture criteria for such a composite.

First, a trial sample with 11 kN post tensioning and without any notch was tested to observe the overall behaviour of this assembly. The major crack happened in the body of concrete approximately 50 mm from the joint where the bar stops. Therefore, the 5 mm notch was placed in 50 mm distance from the joint. Figure 6.2 shows the load displacement behaviour of these samples after applying the first mechanical load for inducing the major crack. The highest post-tensioning led to the highest

fracture toughness with a smooth post cracking behaviour. The post-tensioning option for cyclically loaded samples was considered as 6 kN since it showed relatively smooth post cracking behaviour.

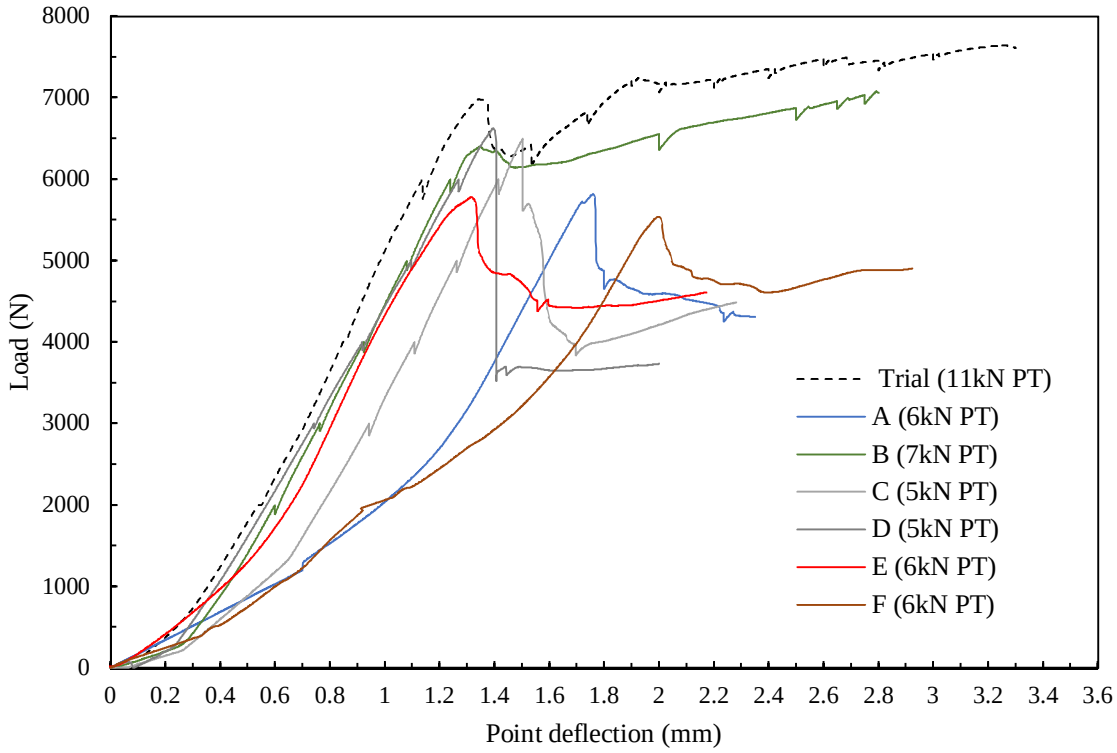

Figure 6.2. Pre-cracking of the samples with various post-tensioning level

Tada et al. (1973) recommendations were used to calculate Mode I (pure tension) fracture toughness and energy release rate. Equation 6.1 and Equation 6.2 were used to calculate the applied stress and stress intensity factor (fracture toughness).

$$\sigma = \frac{6M}{db^2}$$

Equation 6.1

$$k_1 = \sigma\sqrt{\pi a}F(\frac{a}{b})$$

Equation 6.2 (Tada et al., 1973)

d: Section thickness

σ: Tensile stress

k_1: Stress intensity factor

M: Applied moment

a: Crack length

b: Height of specimen

d: Width of specimen

f(a/b): configuration correction factor depending on the ratio of a/b (geometry dependent parameter). It can be calculated with Equation 6.3:

$$F\left(\frac{a}{b}\right) = \frac{1}{\sqrt{\pi}} \cdot \frac{1.99 - \frac{a}{b}(1-\frac{a}{b})(2.15 - 3.93\frac{a}{b} + 2.7\left(\frac{a}{b}\right)^2)}{(1+2\frac{a}{b})(1-\frac{a}{b})^{\frac{3}{2}}} = 1.03$$

Equation 6.3 (Tada et al., 1973)

Fracture energy release rate (G) can also be calculated using Equation 6.4 with stress intensity factor and Young's modulus of the concrete substrate under plain strain condition.

$$G = \frac{K_1^2}{E_1}$$

Equation 6.4 (Tada et al., 1973)

Since $f_{ck,cube}$ of the current concrete mix was 60 MPa, the Young's modulus can be considered 37 GPa based on Euro Code 2 (2004b). E_1 modulus under plain strain can be calculated with Equation 6.5 by considering a Poisson ratio ν=0.2 again according to Euro Code 2 (2004b) for un-cracked concrete.

$$E_1 = \frac{E}{(1-\nu^2)} = 38.54\ GPa$$

Equation 6.5, Euro Code 2 (2004b)

Table 6-2. Mode I fracture toughness and energy release rate for the post-tensioned epoxy bonded concrete samples

Sample name	Applied load (P)	Applied moment (M)	Developed tensile stress (σ)	Fracture toughness (K_1)	Maximum energy release rate (G)
	N	kN.mm	MPa	MPa.m$^{1/2}$	J/m^2
Trial sample	7637.34	763.73	10.86	1.41	51.35
A	5813.89	581.39	8.27	1.07	29.76
B	7078.31	707.83	10.07	1.30	44.11
C	6500.02	650.00	9.24	1.20	37.20
D	6623.39	662.34	9.42	1.22	38.62
E	5777.88	577.79	8.22	1.06	29.39
F	5535.58	553.56	7.87	1.02	26.98

6.3. NO LOAD CONDITION: DEFORMATION AND MESO/MICRO STRUCTURAL CHANGES

The first scenario includes samples A and B. These samples were post tensioned and were under cycles of wetting and drying for 3 months, but no external load was applied on them. Sample A was left in the tank for the longest period (6 months) and scanned in four various stages. Sample B was under cycles of wetting and drying for 3 months and it was scanned at the initial and the final stage. Figure 6.3 (a) shows presence of initial defects within the epoxy layer of sample A. Development of defects during the process of applying epoxy and curing of epoxy seemed inevitable. The applied 6 kN post-tensioning and 6 kN load for inducing the first large crack (9.71 MPa compression at the top and -7.57 MPa tension at the bottom of beams) caused significant deterioration within the bulk of epoxy of sample A (see Figure 6.3 (b)) and created voids/cracks which were concentrated in the middle part of epoxy. Perhaps, the stress flows from tip of the crack and passes through middle part of epoxy and cause high stress area in the middle of epoxy instead of the bottom. Apart from the large crack at the specified position, the body of concrete did not show any significant difference after first cracking compared to the initial scan.

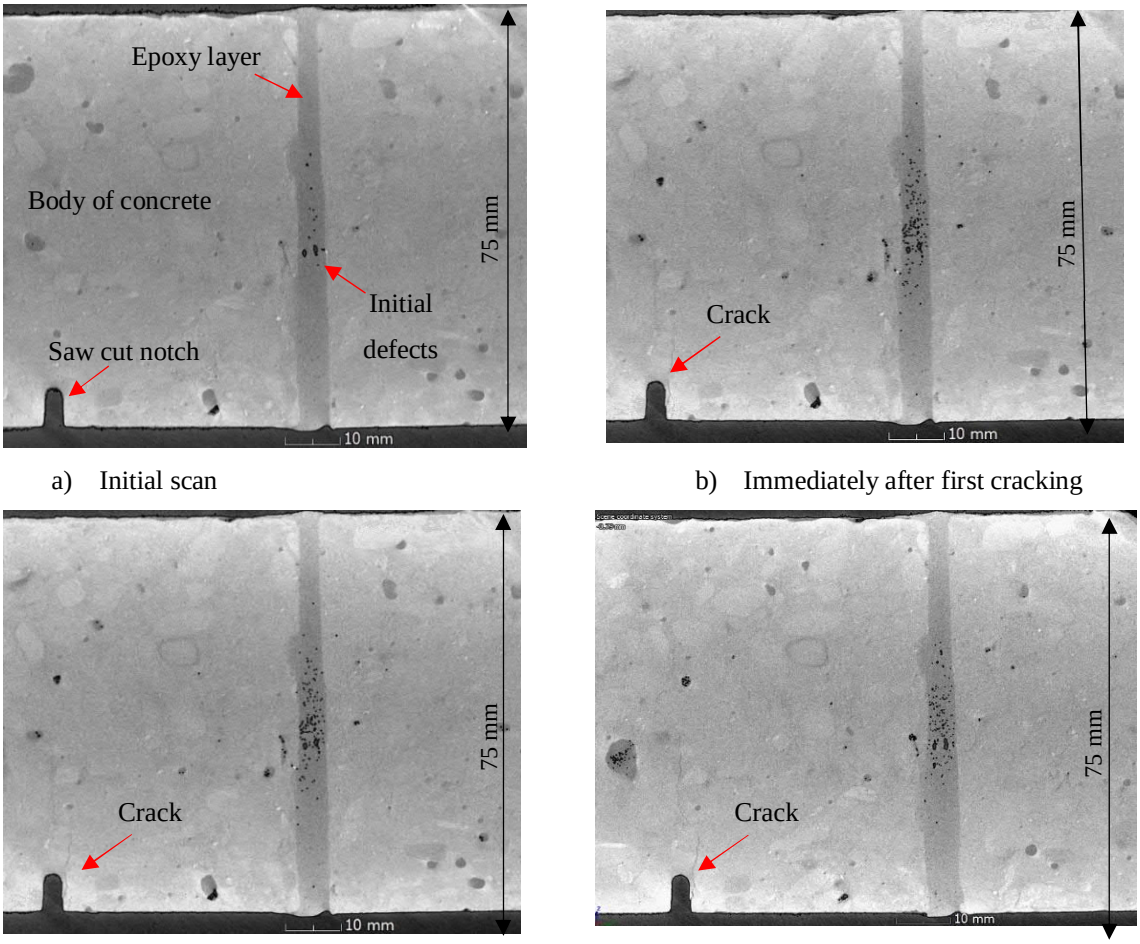

a) Initial scan

b) Immediately after first cracking

c) After 3 months exposure under cycles of wetting and drying

d) After 6 months exposure under cycles of wetting and drying

Figure 6.3. CT-scan images from middle section of sample A (No load condition)

After 3 and 6 months exposure (Figure 6.3 (c) and (d)), there was not significant void increase in the epoxy layer and body of concrete. The cycles of wetting and drying did not cause any visible change in the body of concrete and epoxy layer in the time scale of this test, which was short for a concrete structure. The most considerable damage occurred due to the first mechanical loading which induced the major crack.

The final loading of the sample A after 6 months (see Figure 6.4) showed stiffness reduction of the assembly. This stiffness reduction could be due to loss of post-tensioning or plasticization of bond or epoxy in seawater salt solution. It was not possible to identify which effect was dominant because the glued studs on the bars got detached from the bars during the test due to presence of water. Therefore, post-tensioning losses were not measured.

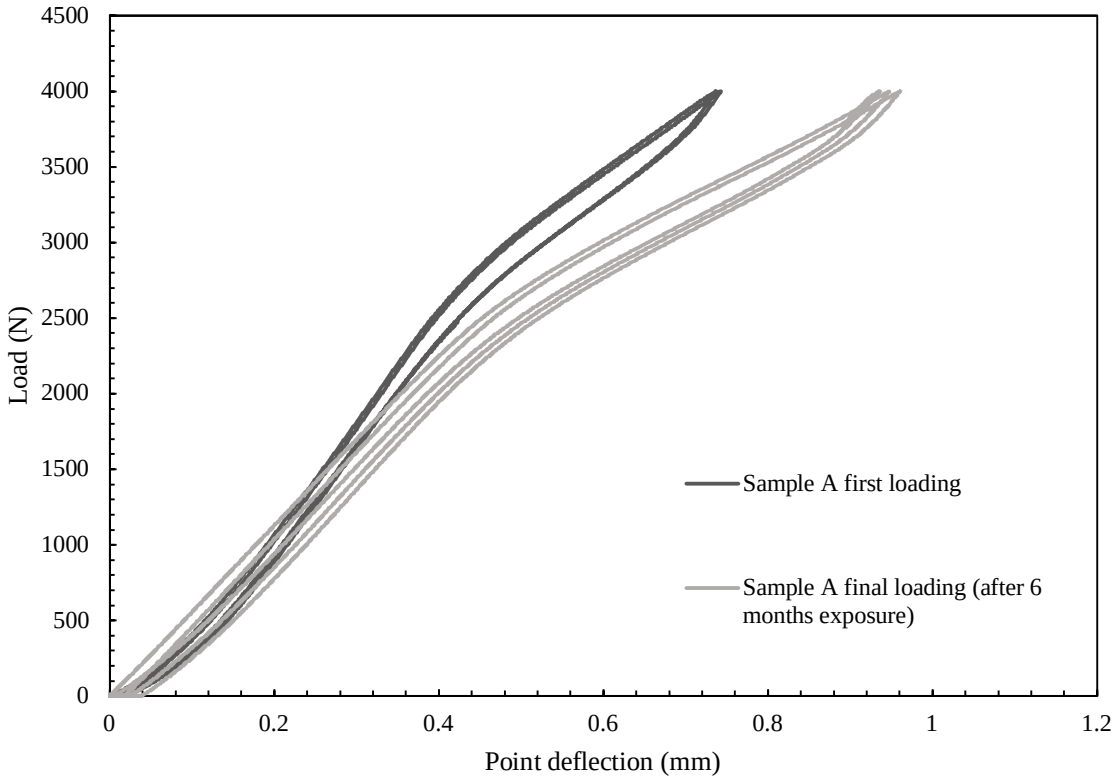

Figure 6.4. Initial and final loading of sample A (No load condition)

Figure 6.5 shows the result of CT-scan from the middle section of sample B. The presence of initial defects was also obvious in Figure 6.5 (a). After three months of exposure, the most damaged part of the beam was middle part of epoxy again (see Figure 6.5 (b)). It is difficult to tell if the void increase is due to a mechanical or environmental effect. However, considering sample A and observing the same pattern of void increase in the middle section of the epoxy layer, the void increase is more likely to be due to mechanical effects.

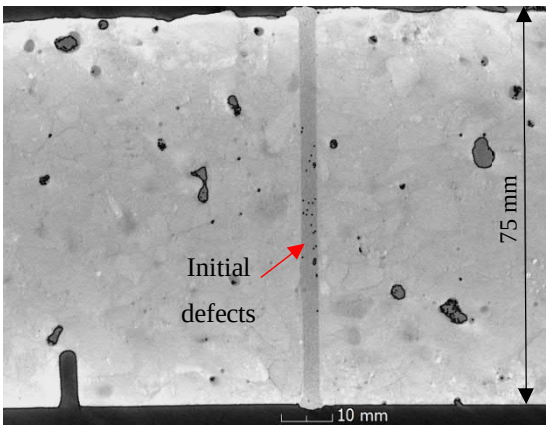

a) Initial scan

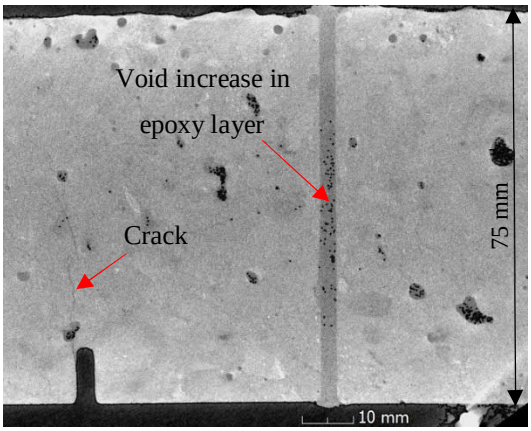

b) After 3 months exposure under cycles of wetting and drying

Figure 6.5. CT scan images from middle section of sample B (No load condition)

6.4. SUSTAINED LOAD CONDITION: DEFORMATION AND MESO/MICRO STRUCTURAL CHANGES

The second scenario was two sustained loaded samples under cyclic wetting and drying for three months. The sustained load was applied by fixing a shaft on the sample until the crack opening reached the target 0.7 mm. Then the tightened shaft was left there for 3 months. The exact applied stress during the sustained load was not measured, but according to pre-cracking graphs, the required load for 0.7 mm of crack opening was 6000 N, which is equivalent to 9.71 MPa compression at the top and -7.57 MPa tension at the bottom (tension and compression side are different due to presence of post tensioning.)

Figure 6.6 (a) shows the typical initial defects within the epoxy layer. Sample C was loaded to failure after 3 months and the jointed area was scanned. The effect of sustained load was not significant since the increase of voids in the middle part of epoxy was due to the first loading for pre-cracking (see Figure 6.6 (b))

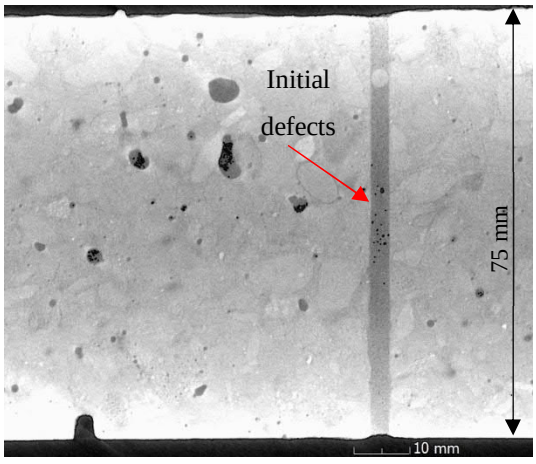

a) Initial scan

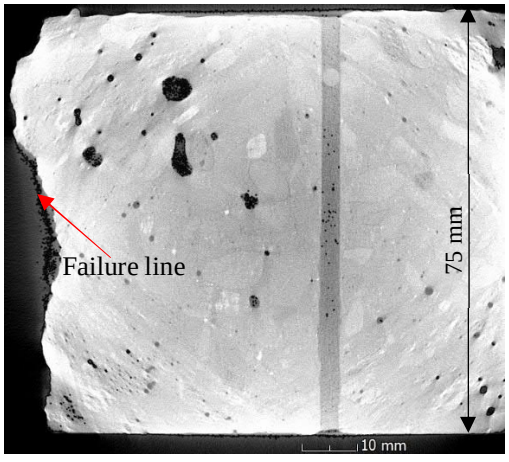

b) After 3 months of sustained

Figure 6.6. CT-scan images from middle section of sample C (Sustained load condition)

The CT scanner also offered 3D reconstruction of the layers. There are many initial defects in both concrete and epoxy layers in Figure 6.7 (a). The 3D reconstruction of sample D in Figure 6.7 (b) shows the considerable increase of voids in the epoxy layer.

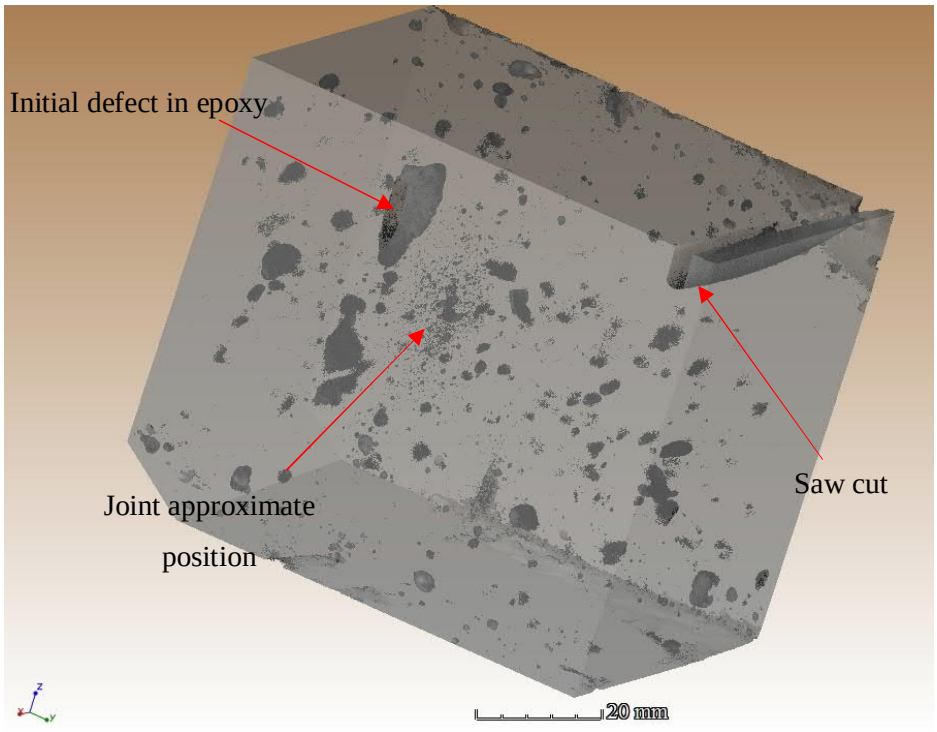

a) Initial scan

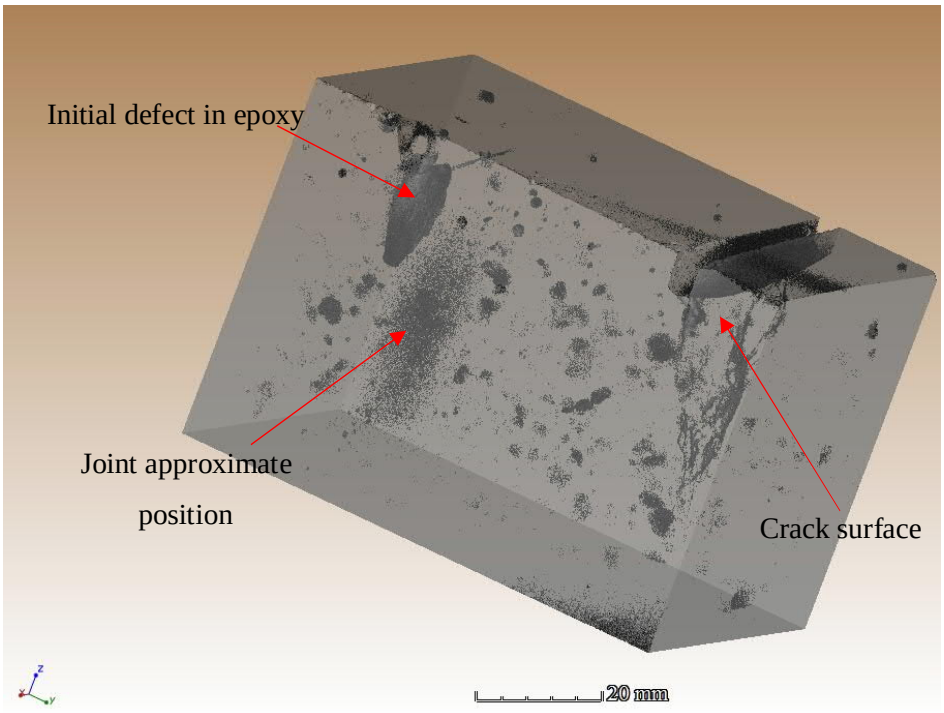

b) Scan after 3 months of sustained load

Figure 6.7. 3D reconstruction from CT-scan images of sample D (Sustained load condition)

6.5. CYCLIC LOAD CONDITION: DEFORMATION AND MESO/MICRO STRUCTURAL CHANGES

The third scenario includes sample E and F under cyclic loading and cyclic wetting and drying for period of 3 months. Each sample experienced about one million cycles with 6.87 MPa compression stress at the top and 4.73 MPa tension stress at the bottom at farthest from the neutral axes (as calculated in section 3.8.2).

Sample E went to a large deformation close to the end of loading period. Figure 6.8 compares the load deflection behaviour of sample E at the first and final loading. At the final stage, the sample showed plastic behaviour and it could not resist high stresses without going through high deformation.

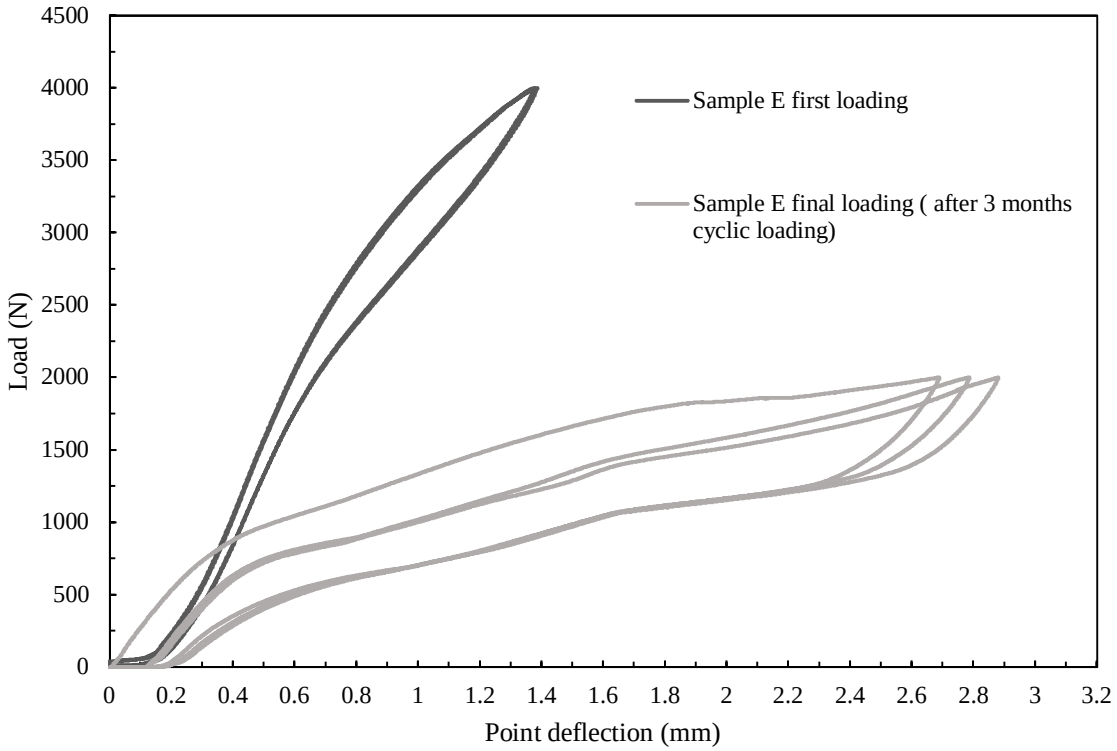

Figure 6.8. Initial and final loading of sample E (Cyclic load condition)

After opening the post tensioning, it was observed that the sample was not integrated any more. It was broken into two parts with a separate cone at the top of the major crack. The two separate parts were scanned and reconstructed (see Figure 6.9). The failure mode can be categorized as compression failure at the top of the crack which made a cone to separate from the top. This failure can be due to losses of post tensioning over the loading period or movement of neutral axes to a higher position until it could not resist the applied compression stress at the top. The high stress intensity at the crack tip and consequent crack propagation under the cyclic loading could cause this phenomenon.

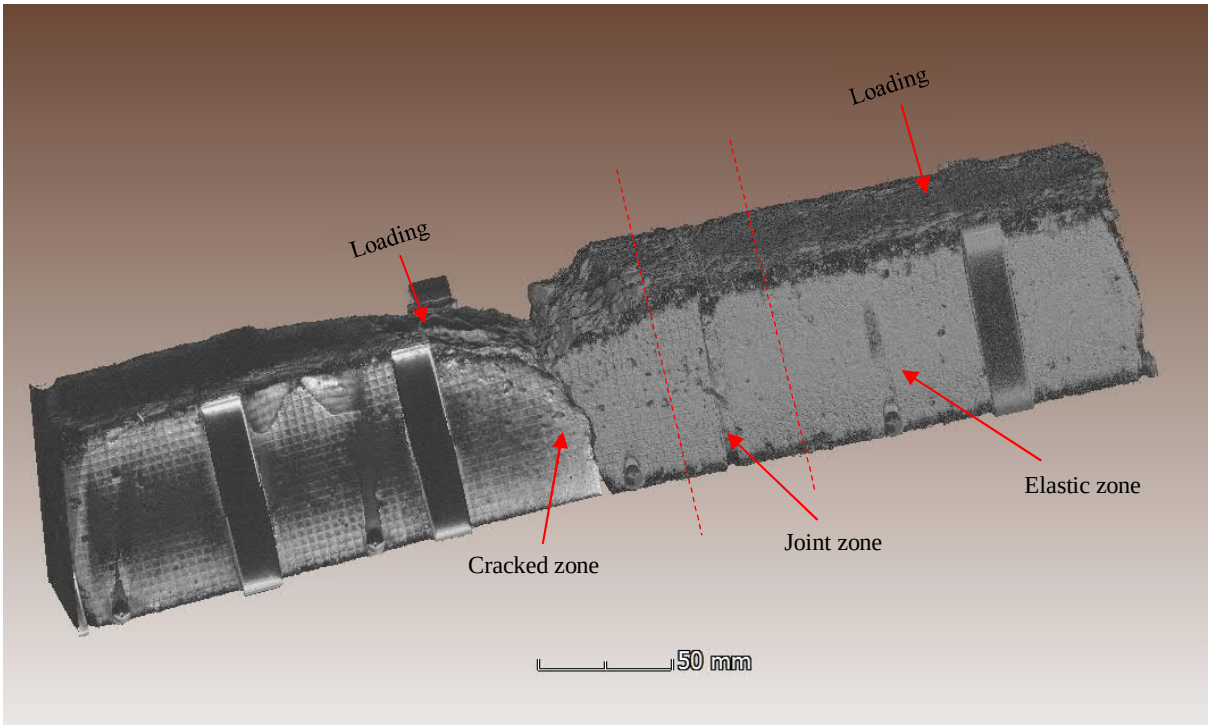

Figure 6.9. 3D reconstruction from CT-scan images of two separate parts of sample E (Cyclic loaded condition), Note: this is not the full beam

Cyclic loading had a detrimental effect on both the concrete and the epoxy. Figure 6.10 (a) shows the initial defects in the epoxy layer, like previous cases. There was a considerable difference in the damage propagation in epoxy layer in Figure 6.10 (b) compared to the previous cases. After three months of cyclic loading, cracks propagated at the bond line as well as the bulk of epoxy. Some voids also appeared within the body of concrete.

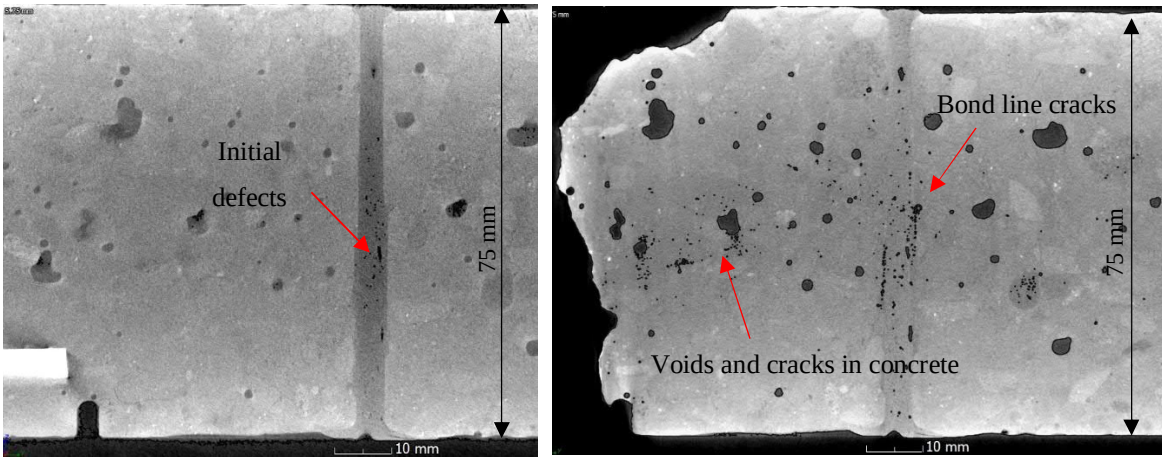

a) Initial scan b) After 3 months of cyclic loading

Figure 6.10. CT-scan images from middle section of sample E (Cyclic load condition)

Cyclic loading mainly influenced the highest moment area. Figure 6.11 shows the side of sample E which experienced higher shear than moment. The cyclic loading and applied higher shear stress on this part of the sample did not cause considerable changes in the body of concrete.

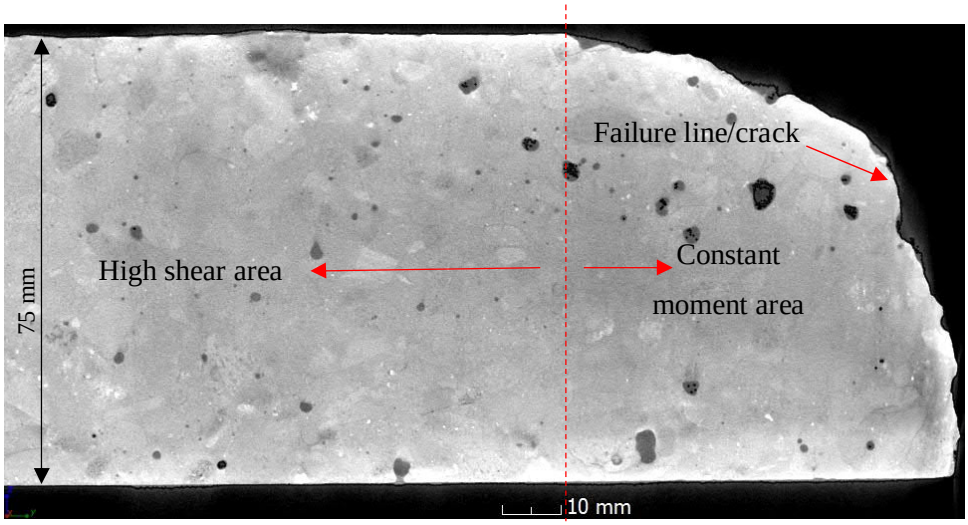

Figure 6.11. CT-scan image of separated part of sample E (the area with lower applied moment and higher shear stress). Note: it is not the full half beam

The second cyclic loading test was conducted on sample F, but this sample did not fail after one million cycles of loading. The load-deflection behaviour of sample F at the initial and final stage is presented in Figure 6.12. The stiffness reduction of sample F was very similar to that of the No loaded sample A after 6 months (see Figure 6.4). Perhaps, the main damage happened at the time of first loading, and it stayed insignificant before the last 10% of number of cycles. It is expected that most detrimental damage occurs at the last stages of loading, right before failure (see Figure 2.25). It seems that one million cycles of loading did not reach last 10% of number of cycles for sample F. Therefore, the damage did not look as significant as sample E which failed under cyclic loading.

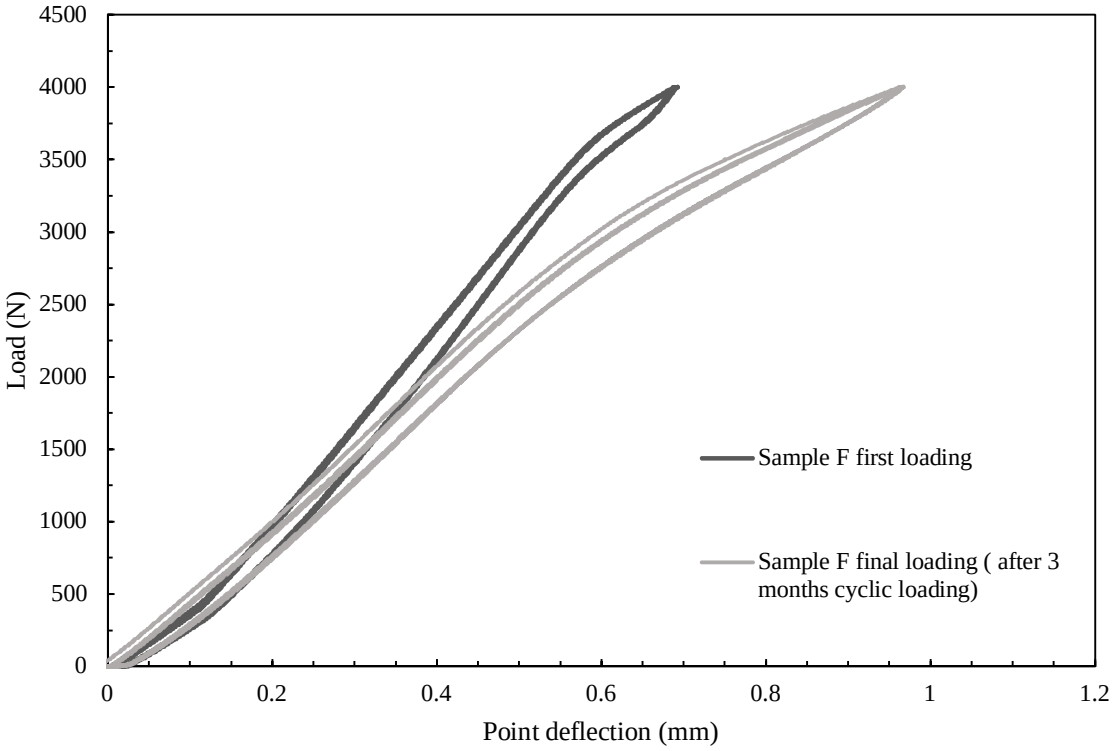

Figure 6.12. Initial and final loading of sample F (Cyclic load condition)

Cyclic loading showed greater influence on the epoxy layer compared to the body of concrete. The damage evolved faster in epoxy compared to concrete under cyclic loading condition. Figure 6.13 shows the void increase in the middle part of the epoxy layer. The void propagation is so extensive that it is difficult to differentiate the bond line and the bulk of epoxy. This damage evolution was certainly larger than that of No load and Sustained load cases, but less than that of the failed cyclic loaded sample E.

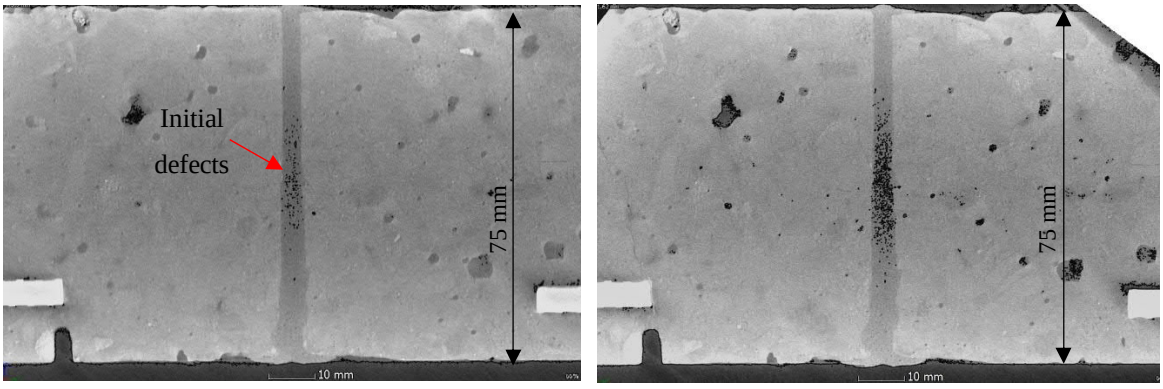

a) Initial scan b) After 3 months of cyclic loading

Figure 6.13. CT-scan images from middle section of sample F (Cyclic loaded condition)

6.6. GROWTH OF THE MAJOR CRACK UNDER VARIOUS LOADING CONDITIONS

The samples under No load condition showed no obvious sign of sealing of the major crack. The depth and width of the crack remained the same (see Figure 6.3). In the case of sustained load, the crack depth did not change, but the permanent width of the crack was bigger (see Figure 6.14 (a)). In the case of cyclically loaded samples, the crack depth and width increased. Sample E failed with an upward move of neutral axes and compression failure at the tip of the crack. Although sample F did not fail, the sign of the same crack growth and movement of neutral axes can be seen in Figure 6.14 (b).

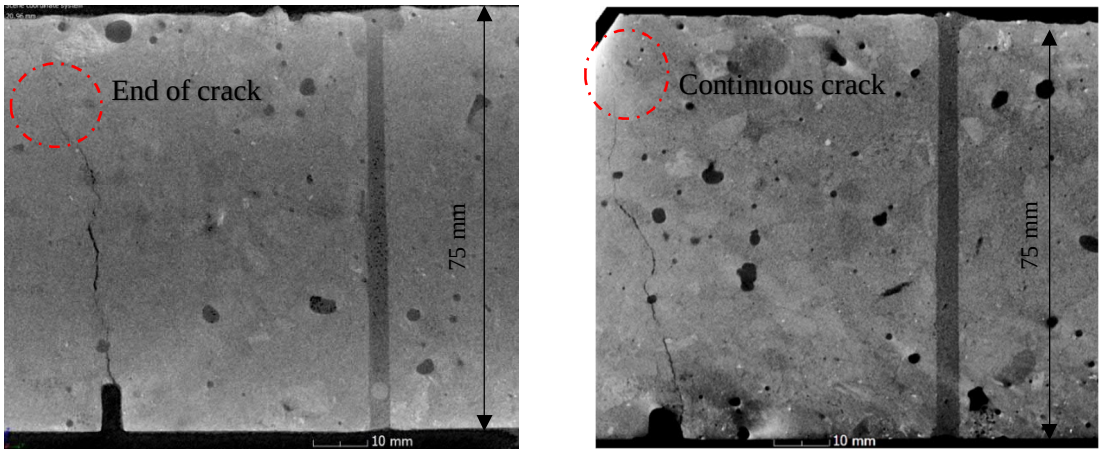

a) Final crack position of sample D (Sustained load condition)

b) Final crack position of sample F (Cyclic load condition)

Figure 6.14. Final condition of the major crack under Sustained and Cyclic load

6.7. VOID ANALYSIS OF THREE STRESS ZONES

The defect analysis tool available with the VG Studio MAX 2.2 software for the analysis and visualization of industrial CT data was used to conduct quantitative void analyses on one sample of each loading condition. The defect analysis tool works with voxel (a point in three-dimensional space which is used as the graphic unit information) and uses the surface determination data (distinguishes the difference between background and the material) to detect voids or inclusions. The default algorithm with maximum defect volume of 10 mm^3 was used for the analysis in this project. The results included volume, position, probability, and size of the voids. It also showed a colour scale of the voids in each chosen slice.

The analysis can be very time-consuming depending on the volume, size, and inter-connectivity of the voids in the material. Therefore, 3 mm radius sphere (about 114 mm^3 volume) was chosen as the representative volume. Figure 6.15 shows the plan for analysis of each sample. The main areas of interest were chosen as tension, middle, and compression parts of the joint, the cracked side, and the body of concrete in un-cracked side. The representative sphere was placed at these areas in the middle section of the samples.

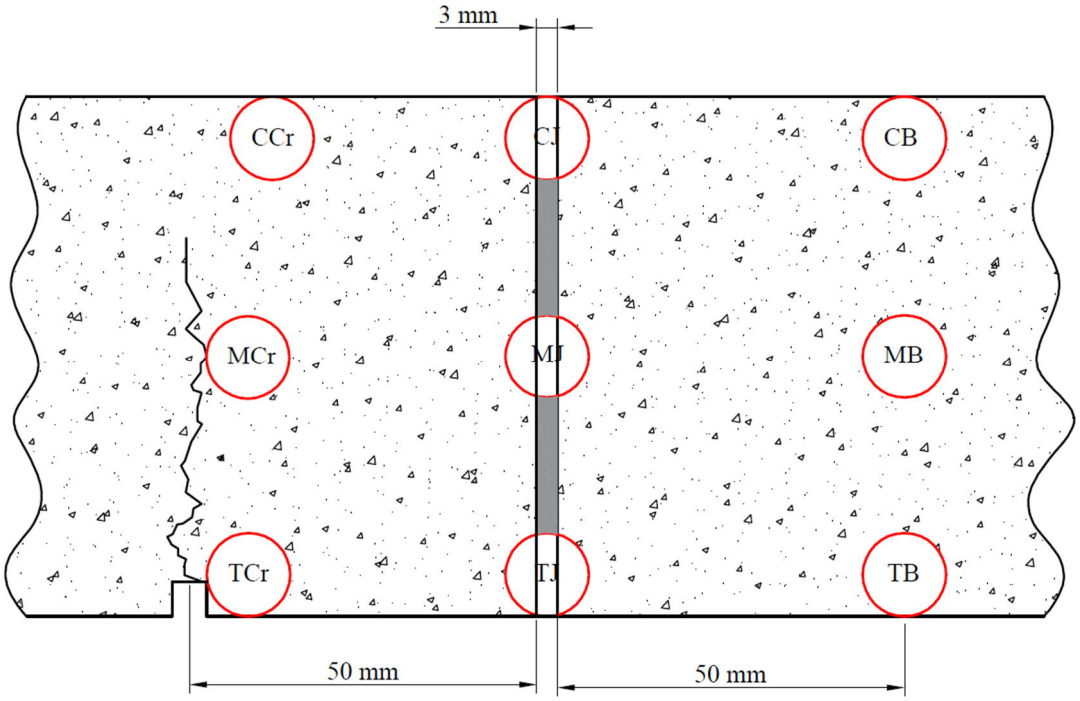

Cracked side	Joint	Body of Concrete
CCr: Compression Crack	**CJ:** Compression Joint	**CB:** Compression Body
MCr: Middle Crack	**MJ:** Middle Joint	**MB:** Middle Body
TCr: Tension Crack	**TJ:** Tension Joint	**TB:** Tension Body

Figure 6.15. Plan for void analysis using VG studio max 2.2 software

Figure 6.16, Figure 6.17, and Figure 6.18 show the analysis of middle parts of the joint at the initial stage and after three months of exposure under cycles of wetting and drying and mechanical loading conditions. The Middle Joint (MJ) area was chosen as an example because the main changes happened at the middle part of the joint. The colour scale shows the volume of each void considering the inter-connectivity of adjacent voids. A significant increase in the volume of voids and their inter-connectivity was obvious in all the cases. The maximum volume of voids was higher than the 10 mm^3 threshold after the mechanical load and cyclic wetting and drying. All the samples showed the void increase mainly in bulk of epoxy except sample E that showed cracking of the bond line.

The compactness analysis (ratio between the surface of void and its volume) and sphericity analysis (ratio between the surface of a sphere with the same volume as the void and the void surface) of the representative areas showed that the voids were not very close to sphere and were not very compacted with dominantly 0.2 and 0.5 compactness and sphericity ratio, respectively.

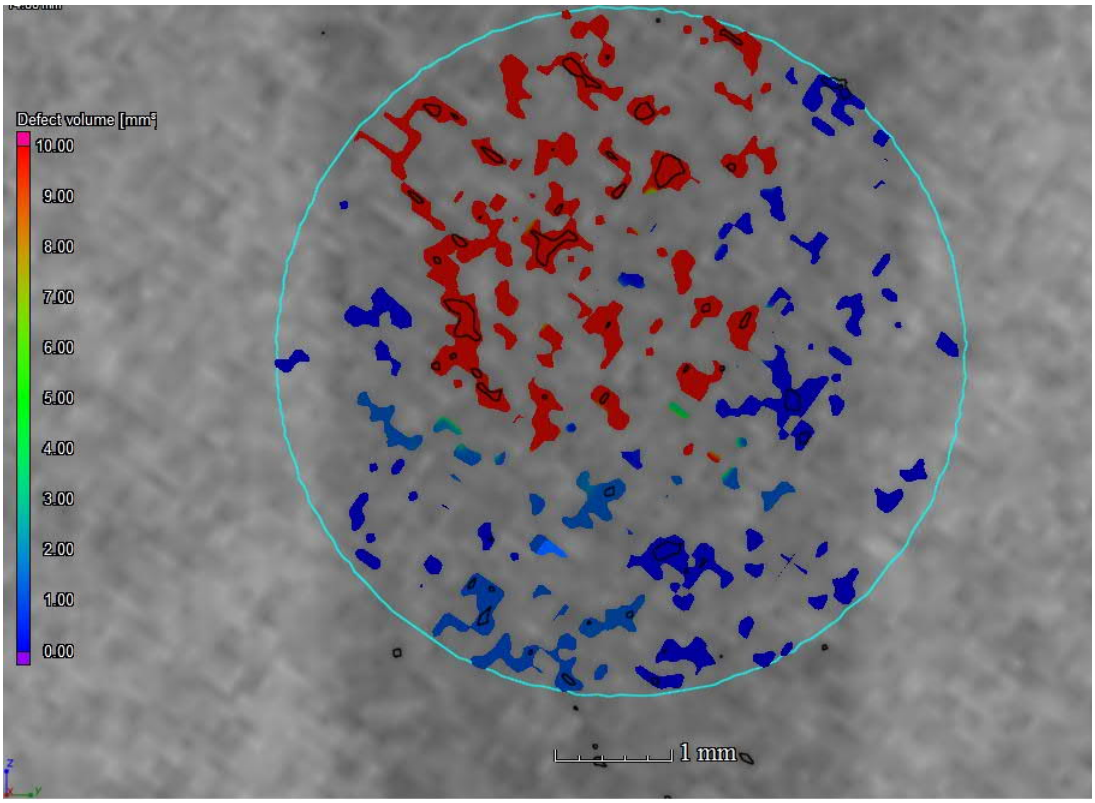

a) Initial scan, Middle Joint (MJ)

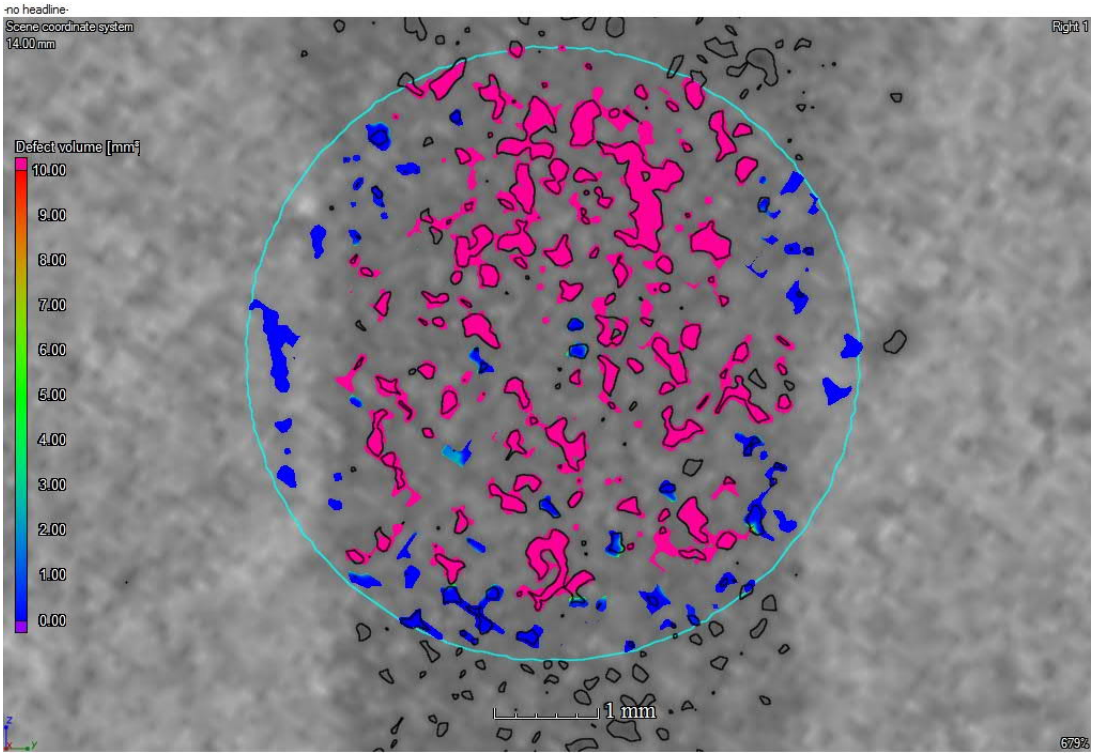

b) Scan after 3 months exposure, Middle Joint (MJ)

Figure 6.16. Example of void analysis of sample A (No load condition)

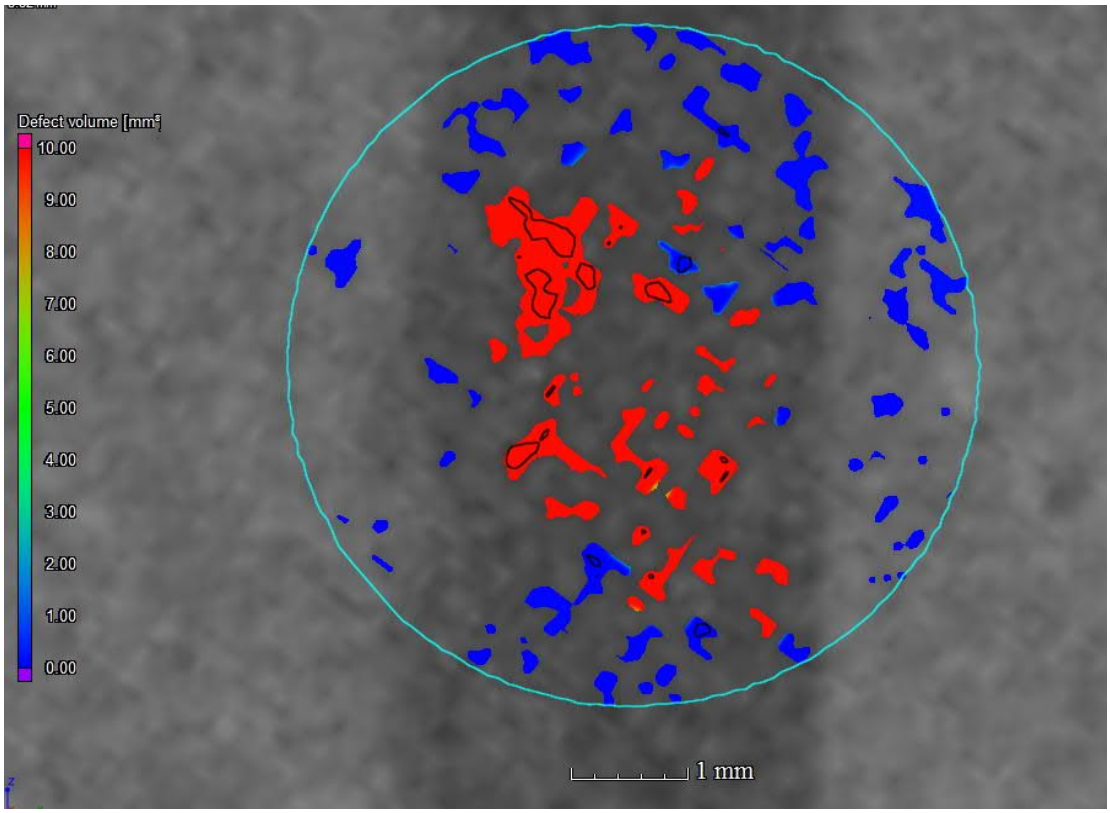

a) Initial scan, Middle Joint (MJ)

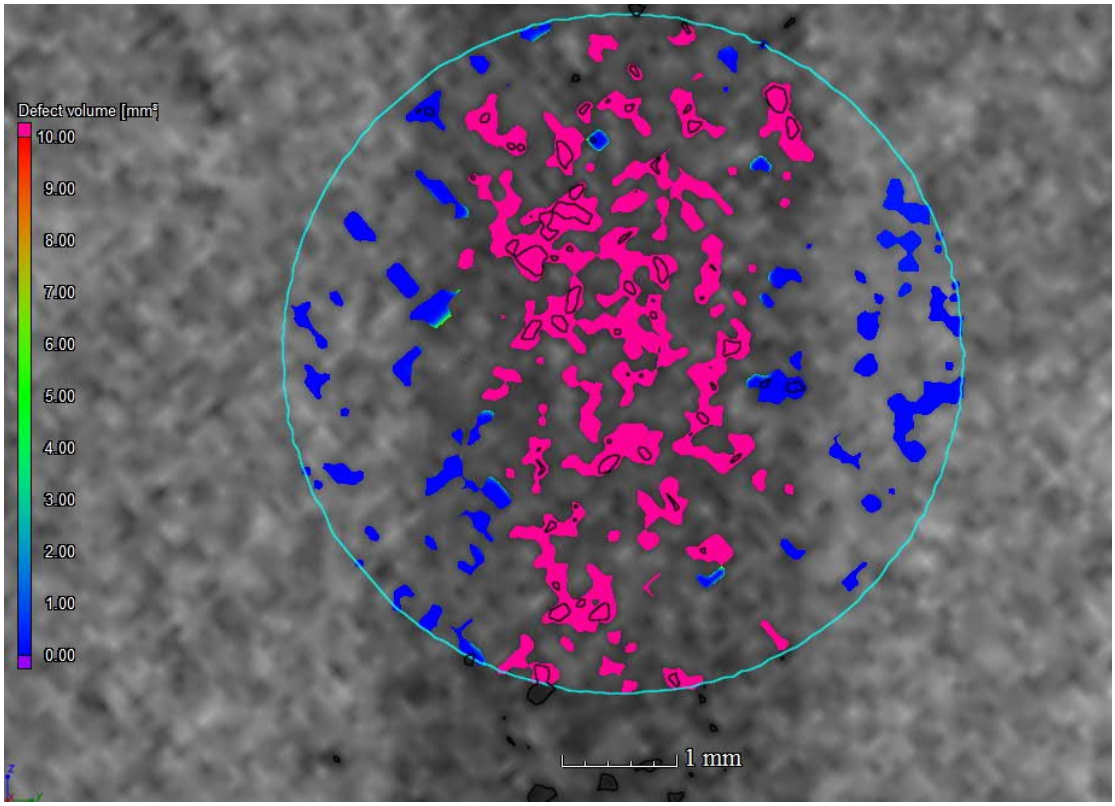

b) Scan after 3 months exposure, Middle Joint (MJ)

Figure 6.17. Example of void analysis of sample D (Sustained load condition)

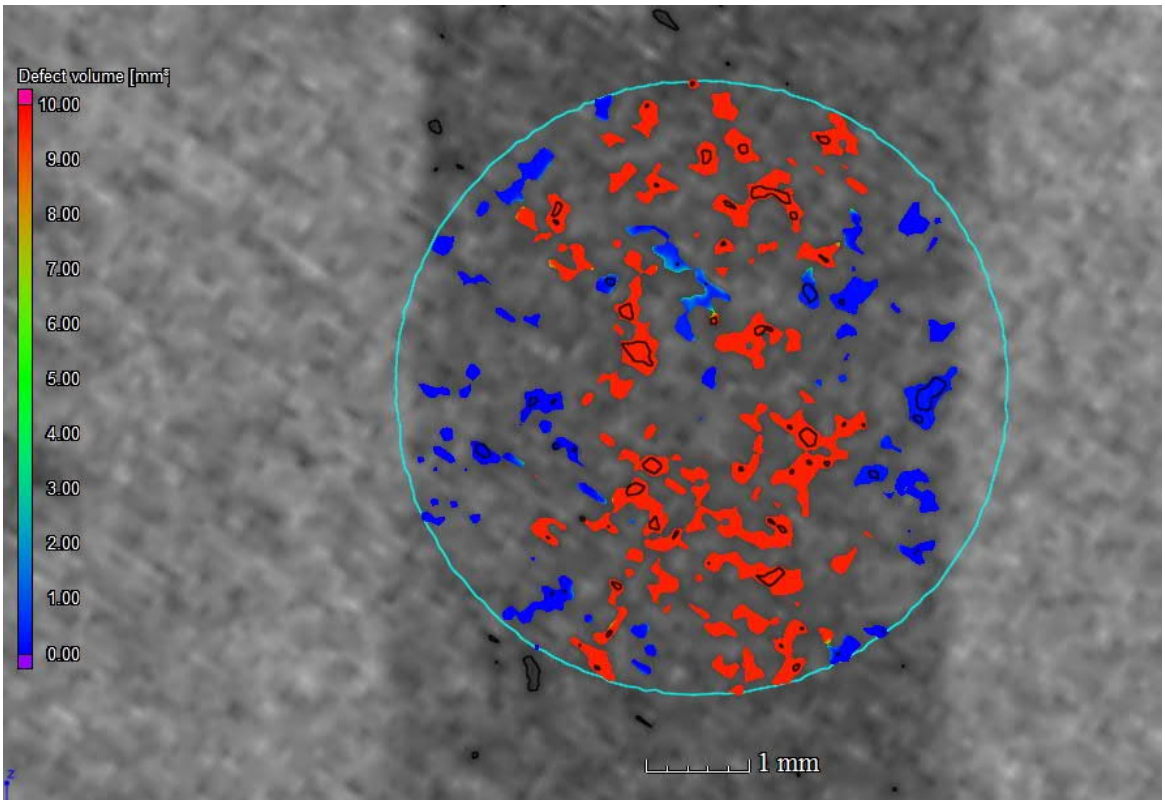

a) Initial scan, Middle Joint (MJ)

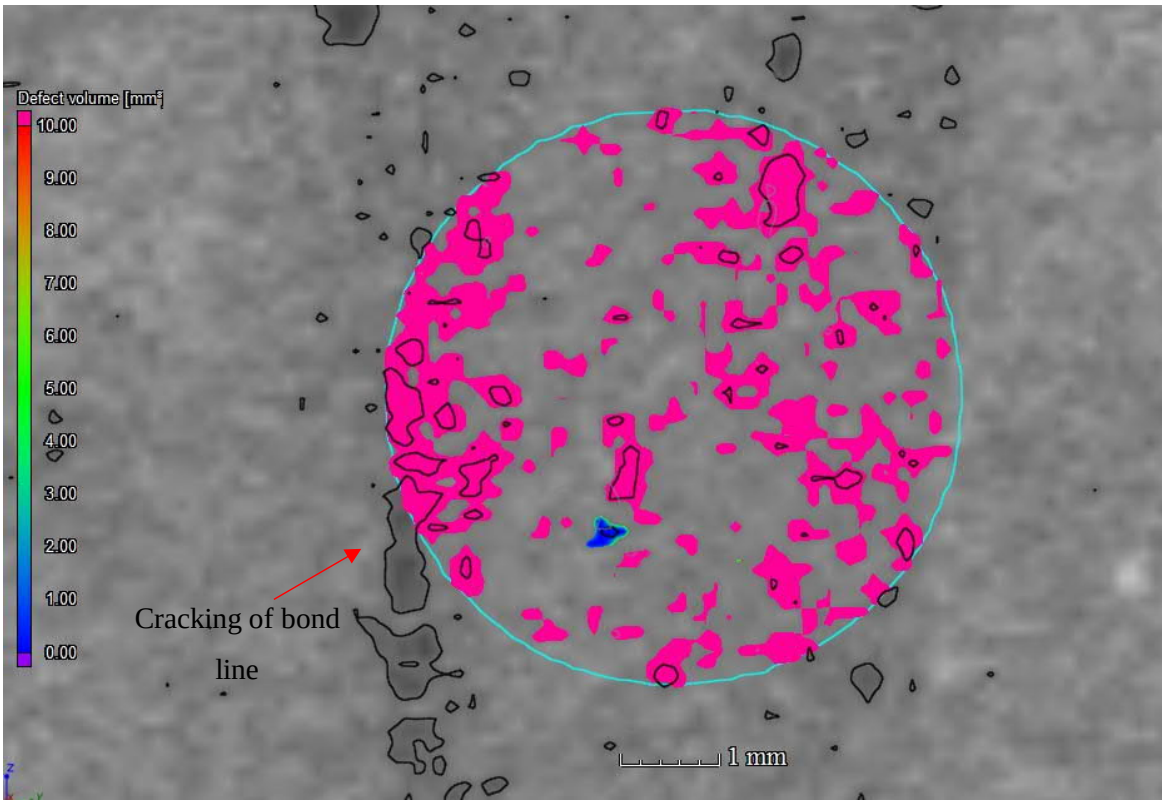

b) Scan after 3 months exposure, Middle Joint (MJ)

Figure 6.18. Example of void analysis of sample E (Cyclic load condition)

The void analysis of sample A immediately after cracking and after 3 months of exposure supported the statement that the major damage in the epoxy and the body of concrete happened mainly with the first mechanical loading for inducing the major crack (see Figure 6.19). The percentage of void increase was almost the same in both body of the concrete and the epoxy after the first mechanical effect and after three months exposure. The middle part of the joint experienced the highest damage with about 3% void increase. Some areas like the Middle Crack (MC) were not affected by the loading or exposure. It can be concluded that the major crack was the sacrificial area, where all the stresses were confined, so the adjacent area was intact.

Figure 6.20 shows analysis and comparison of percentage of void increase at the final stage compared to the initial stage for all of the samples. The void increase is middle of joint in all cases.

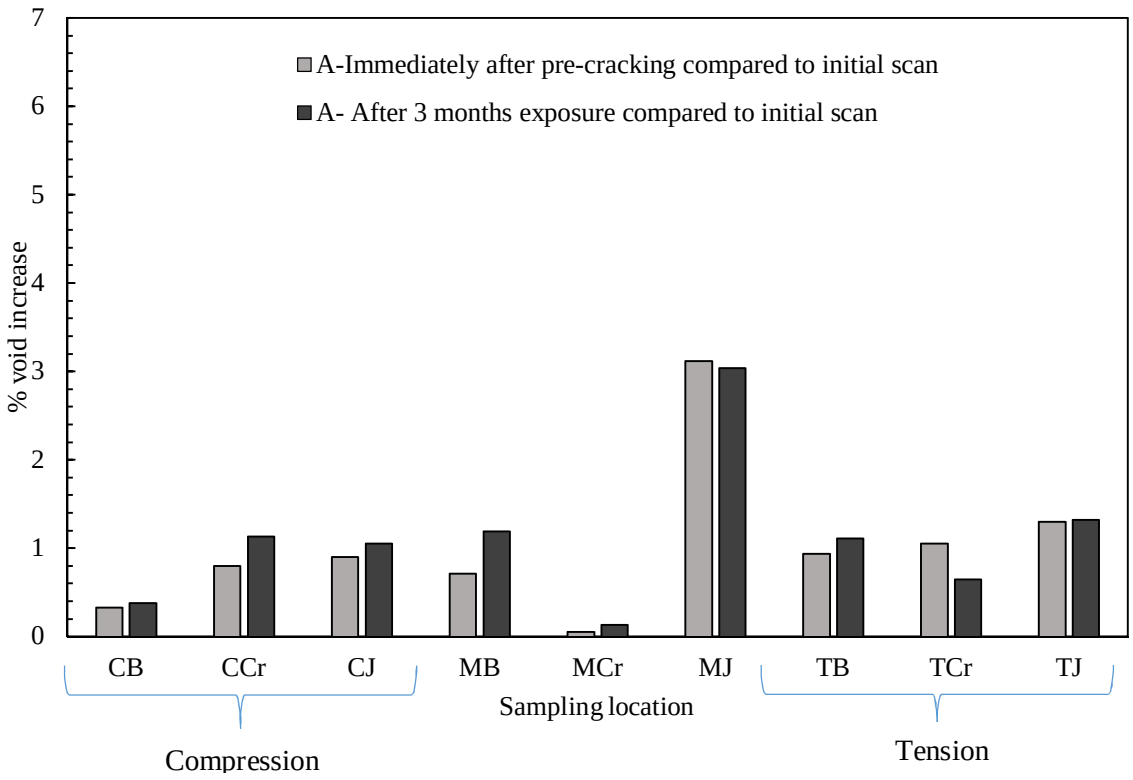

CB: Compression Body MB: Middle Body TB: Tension Body

CCr: Compression Crack MCr: Middle Crack TCr: Tension Crack

CJ: Compression Joint MJ: Middle Joint TJ: Tension Joint

Figure 6.19. Percentage of void increase immediately after pre-cracking and after 3 months exposure compared to the initial scan

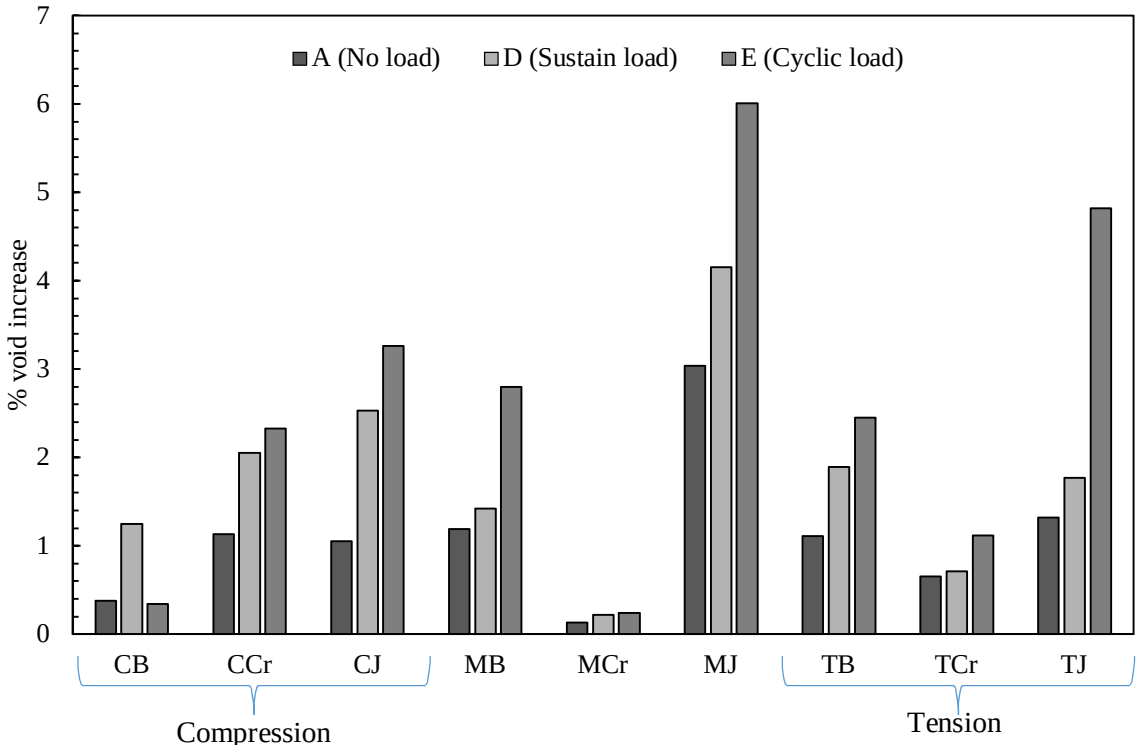

CB: Compression Body MB: Middle Body TB: Tension Body

CCr: Compression Crack MCr: Middle Crack TCr: Tension Crack

CJ: Compression Joint MJ: Middle Joint TJ: Tension Joint

Figure 6.20. Percentage of void increase after 3 months exposure compared to the initial scan

6.8. CHLORIDE INGRESS UNDER VARIOUS LOADING CONDITIONS

Free chloride ingress depth was measured with $AgNO_3$ spray at the final stage after breaking the samples in two halves. Figure 6.21 shows that the loading condition did not have any considerable effect on the chloride ingress depth. The ion diffusion depth was approximately the same for all of the cases. The small variations are negligible since the method is based on the average chloride ingress depth along the sample. Cyclic loading did not provide a network of cracks starting from outer surface of the beam. This network of cracks could accelerate the chloride and water penetration within the body of concrete. Therefore, the ion ingress occurred just because of the gradient of ion concentration. The voids which were observed within the CT-scan images were not well inter-connected and they did not initiate and propagate from the surface of the sample.

Comparison of sample A and B shows that the three months longer exposure period without any load did not affect the depth of chloride ingress. This can be due to the continuous hydration process within the concrete and the reduction of the diffusion coefficient of the concrete over time.

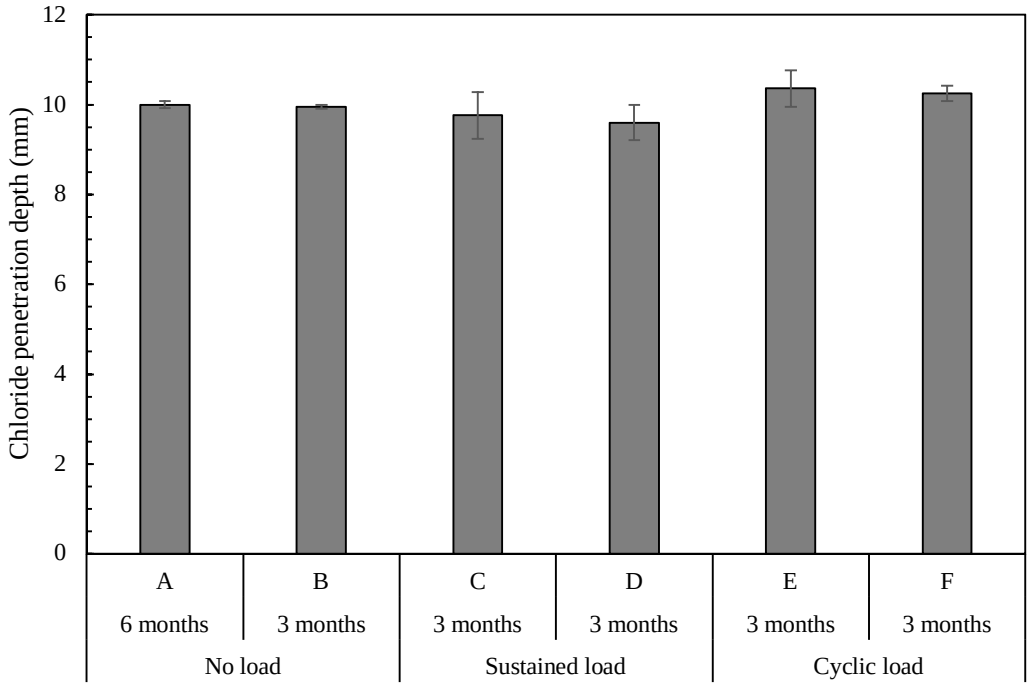

Figure 6.21. Comparison of chloride penetration depth in various loading conditions

The major concern with epoxy bonded concrete was the penetration of chloride or water through the interface zone of the joint. However, the chloride analysis did not show any significant difference in chloride ingress within the body of concrete and the bond line (see Figure 6.23). Colorimetry of chloride gives an indication of water penetration as well. It means that if the ions have not penetrated through the interface, the water have not been able to do so.

Chloride did not ingress to the surface of the major crack of sample A (No load condition). There was no sign of sealing materials on the surface of the crack and the crack width has been around 0.1 mm, but it still did not provide a path for water and chloride to penetrate on the cracked surface and reach the reinforcement (Figure 6.22 (a)).

In the case of the sustained load sample C (Figure 6.22 b), the crack was open with 0.7 mm width and depth of chloride ingress to the cracked surface was like the body of concrete.

Figure 6.23 shows that chloride ingress to the cracked surface was harsher than in the body of concrete under cyclic loading condition. Opening and closing of the crack caused suction and more water or chloride were penetrated in the cracked surface. It can also be due to the presence of more cracks because of the cyclic loading.

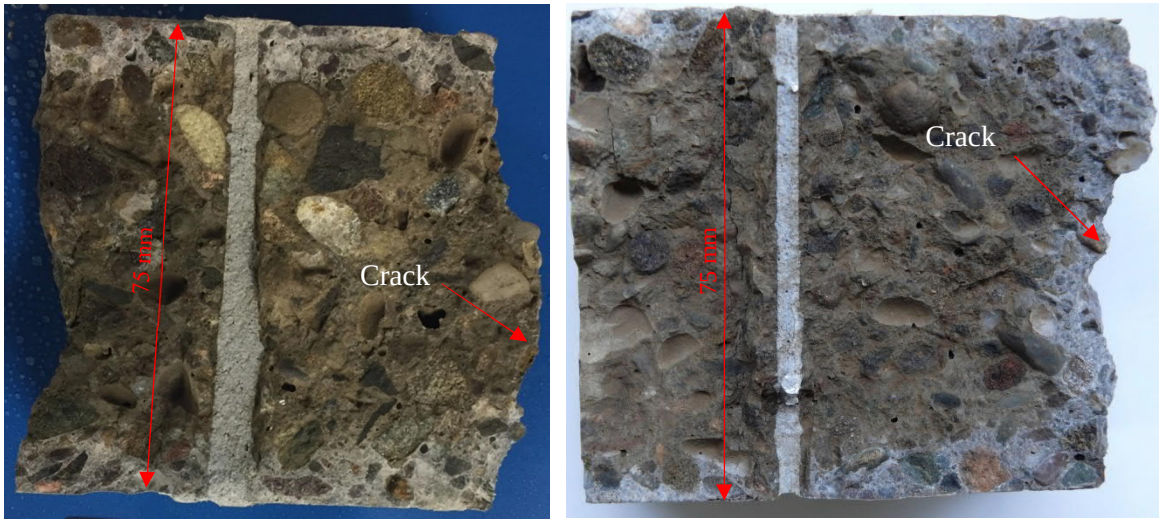

a) No load sample A (six months) b) Sustained load sample C (three months)

Figure 6.22. $AgNO_3$ spraying for determining chloride penetration depth for No load and sustained load condition

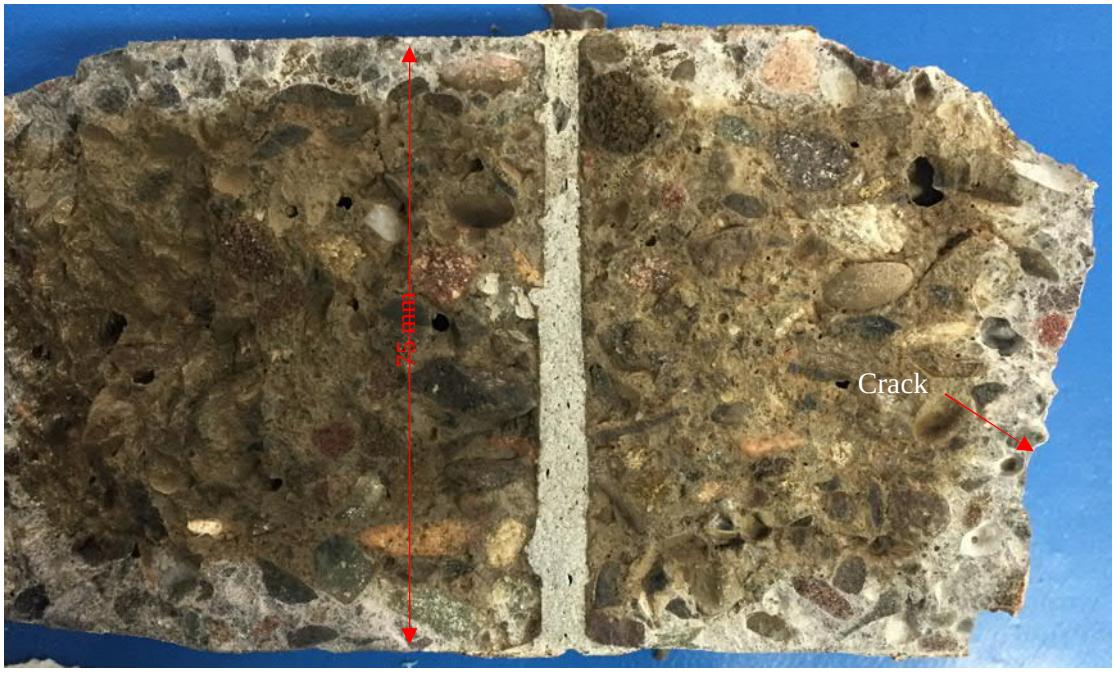

Figure 6.23. $AgNO_3$ spraying for determining chloride ingress depth for sample E (Cyclic load condition)

6.9. CHLORIDE INDUCED CORROSION UNDER VARIOUS LOADING CONDITIONS

As it was expected, corrosion progressed rapidly on the crack surface and tunnelled through the bar under cyclic loading condition. Figure 6.24 shows the difference between corrosion of the bar in two sides of the cyclically loaded sample. This phenomenon was not considerable in any other loading conditions.

Half- cell potential measurements were also conducted on three points on each side of the beam once a week. The potential values at the beginning were positive, but after 1 month of exposure all samples reached over -259 mV criterion of high possibility of corrosion (see Table 3-18). The average final potential measurements for all of the samples except the cracked side of the cyclically loaded sample were around -450 mV. The cracked side of the cyclically loaded sample had the potential of -610 mV. It should be noted that the free side of the bars, where it was connected to the box, were more susceptible to corrosion and the early sign of corrosion initiation can be due to the corrosion of the free end of bar rather than the middle part. Therefore, a half-cell potential test for this configuration was not reliable. Nevertheless, the extraction of the bar at the final stage showed the severe corrosion in the cracked side of the cyclically loaded samples and no serious sign of corrosion in any other cases.

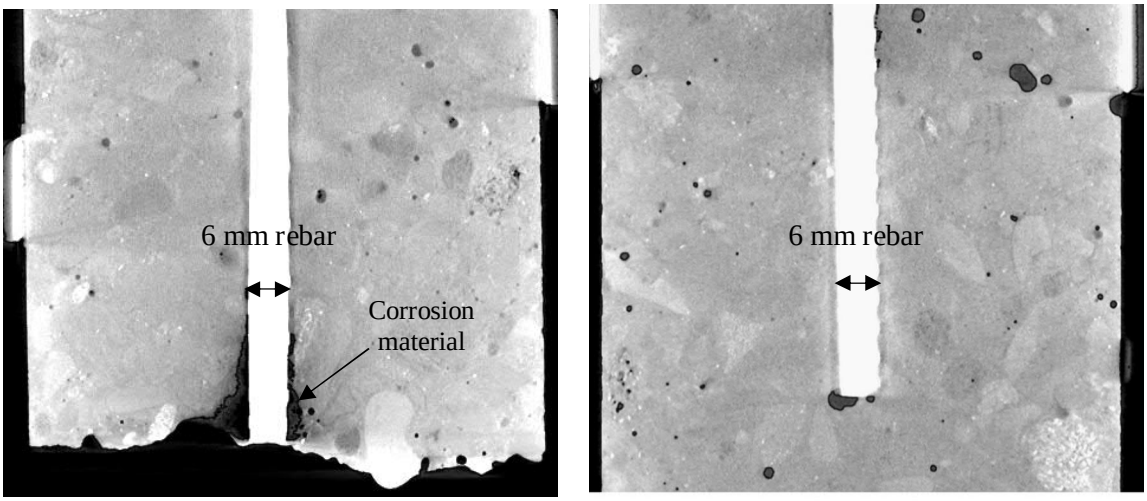

a) Corrosion on cracked side b) Corrosion on non-cracked side

Figure 6.24. Chloride induced corrosion under cyclic loading (sample E)

The crack surfaces of cyclically loaded samples were covered by some white material as well as the corrosion products. This phenomenon was not observed in other loading conditions. The surface was scratched to gather some powder and conduct X-Ray Diffraction (XRD) analysis. Figure 6.25 shows the white material on cracked surface of sample E. The highest peak of XRD spectrum was detected as Sepiolite (known as $Mg_4Si_6O_{15}(OH)_2 \cdot 6H_2O$). The other peaks were Magnetite Fe_3O_4, Maghemite (Fe_2O_3, γ-Fe_2O_3), Magnesioferrite $Mg(Fe^{3+})_2O_4$, and Brucite $Mg(OH)_2$. These corrosion products were also observed by Jaffer and Hansson (2009) on walls of macro crack of ordinary concrete under cyclic loading.

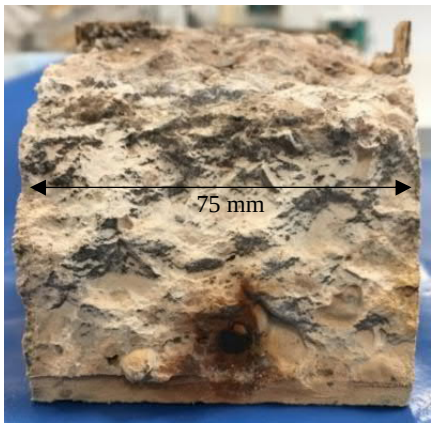

Figure 6.25. White material on the cracked surface of cyclically loaded sample E

6.10. UPV MEASUREMENTS UNDER VARIOUS LOADING CONDITIONS

UPV measurements conducted at least once in a month for all samples. The range of pulse velocity for all samples in all loading conditions were between 2.8 and 3.1 km/s and there was no pattern of pulse velocity reduction over the period of test. UPV is known as a practical method for assessing damage in concrete. However, there are some limitations to the application of this method, which may be the reason for not observing any real damage evolution in the current samples using UPV. A 54 kHz transducer with 50 mm diameter was used for the measurements. The minimum size of defect that the UPV equipment can detect is dependent on the transducers diameter. Moreover, the concrete samples were not dry, so the voids and the major crack could be always filled with water. Compression waves (the wave type used for these measurements) travel in water, so any clear velocity reduction was not observed in wet and damaged concrete.

Indirect UPV measurements are not reliable since the surface zone of concrete affects the results. Figure 6.26 shows the indirect UPV configuration for these samples. The pulse was probably passing through the compression part which was not affected by loading. Bungey and Millard (2010) have thoroughly reviewed the UPV method for concrete and asserted that pulse velocity can be effective if the member is experiencing at least 50% of the crushing strength, and it is not sensitive to early cracking. The compression parts of these samples were experiencing 6.87 MPa stress at the highest load, which is just 10% of crushing strength.

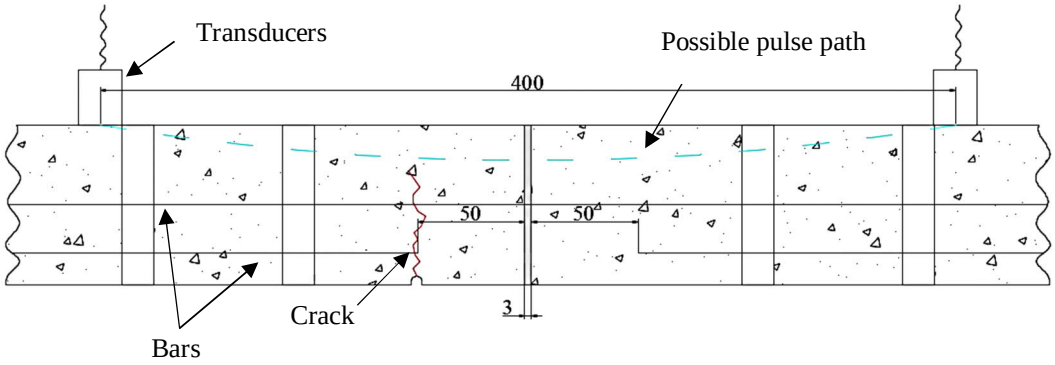

Figure 6.26. UPV configuration and possible pulse path

6.11. ZONE 1:CRACKED SIDE: KEY OBSERVATIONS AND POSSIBLE THEORETICAL EXPLANATIONS

Comparison of three main regions of interest are summarized here. Three main regions were zone 1: cracked concrete, zone 2: epoxy layer, and zone 3: body of concrete. The beams were under various loading conditions (No load, Sustained load, and Cyclic load). Figure 6.27 shows the summary of observations on cracked side and the effect of loading type on the evolution of damage, the void increase, the chloride ingress and the corrosion.

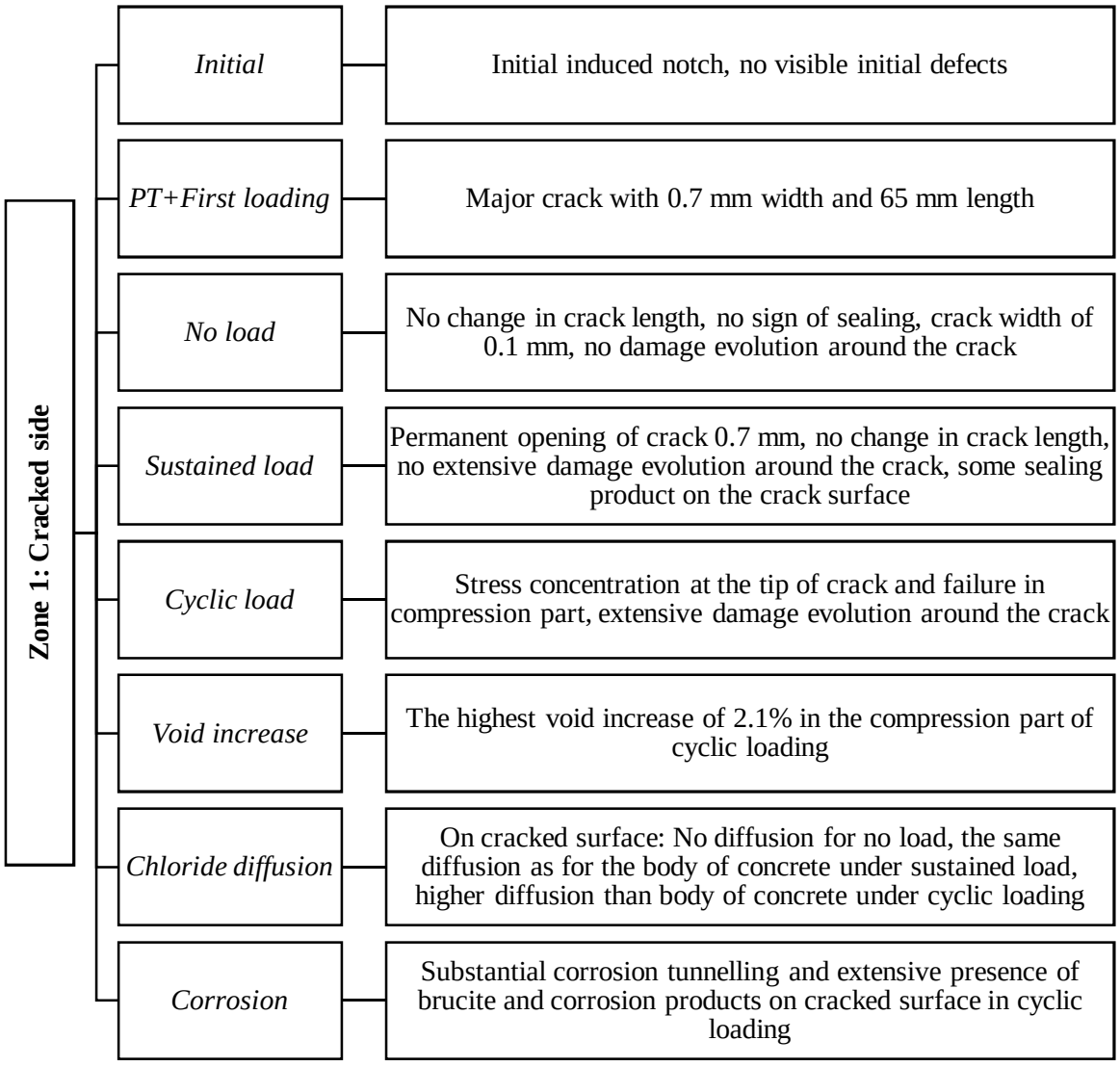

Figure 6.27. Summary of the key observations for zone 1: cracked side under various loading conditions

The stress analysis of cracked area is very complex because there is a nonlinear zone at the tip of the crack. The fracture zone of metal shows yielding and hardening plasticity behaviour, which leads to tearing, but this zone is much larger for concrete and there is no significant plastic flow. Figure 6.28 shows this fracture zone in metal and concrete schematically. The shape and size of the fracture process zone depends on the size of the sample and the aggregate size. For the sample of current

project, with 10 mm aggregate size, the fracture process zone could be more than 250 mm (Gdoutos, 2005). This means that the whole top part of the sample on the cracked side was the fracture process zone. Micro cracking, separation of interface of cement matrix and branching are the mechanisms involved in crack growth in this area and softening behaviour is observed (Gdoutos, 2005).

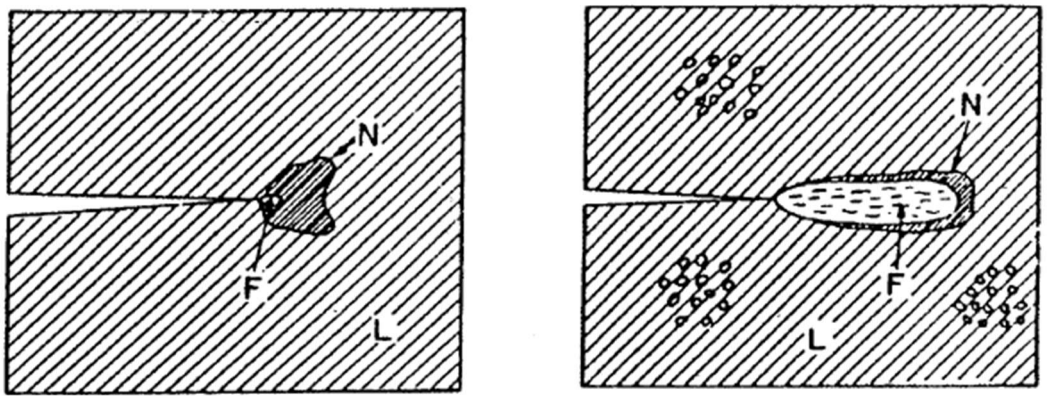

a) Metal (ductile materials) b) Concrete (quasi-brittle material)

Figure 6.28. Difference of the fracture process zone in metals and concrete (Bažant, 2002)

On the other hand, due to loss of post tensioning over the time, the neutral axes moved up which led to larger tensile area and longer crack. Therefore, the failure observed in the case of cyclic loading was compression failure at the top due to shrinking of the compression part and movement of neutral axes to a higher level.

It should also be mentioned that the presence of water has some significant effect on crack growth and the failure of cyclically loaded samples. When the pores of concrete are already filled with water, it does not let the water to move to the adjacent pores so the absorbed water can cause high pressure due to capillary action and increase the stress intensity at the micro cracks at the tip of the major crack (Bazant and Prat, 1988). Therefore, the fracture resistance of wet concrete becomes less than that of dry concrete. This can be one of the reasons for failure of the compression part of the cyclically loaded sample after 10^6 cycles while depending on the ratio of maximum stress to strength (σ_{max}/f_c=0.687/60= 0.11 in the compression area) and the ratio of minimum stress to maximum stress ($\sigma_{min}/\sigma_{max}$=0 for this configuration), the concrete was expected to resist around 10^7 cycles under compression, according to ACI Committee 215R-74 (1997) (see Figure 2.27).

Another important feature of this zone is chloride diffusion and corrosion progress through the cracked surface. A permanent crack smaller than 0.1 mm under No load condition did not provide a proper path for penetration and chloride ingress. A larger crack width like 0.7 mm under sustained load condition showed the same diffusion property as the body of concrete. However, the same crack width under cyclic loading condition led to higher chloride ingress in the cracked surface and corrosion tunnelling in the bar. This is in line with the research of Otieno et al. (2010) who showed that crack reopening can lead to a higher corrosion rate due to weakening and separation of the bond

between aggregate and cement paste under dynamic loading. Moreover, as Jaffer and Hansson (2008) explained, the crack opening and closing can lead to flowing of subsequent corrosion products to the branched cracks and cause more pressure and micro cracking and finally more chloride diffusion.

Most of the literature are focused on macro crack length and width. Although the crack length can be important for macro scale deformation and strength of concrete, micro crack growth is important for durability aspects as can be seen in the result of the current experiment. Therefore, there is a need for further work on considering the effect of micro crack growth on diffusion under cyclic loading.

6.12. ZONE 2: EPOXY LAYER: KEY OBSERVATIONS AND POSSIBLE THEORETICAL EXPLANATIONS

Figure 6.29 shows the summary of observations in the jointed area. The damage evolution was observed in the jointed area especially under cyclic loading condition. However, explaining the reason for this phenomenon is not easy and only some possible speculations are given in this section.

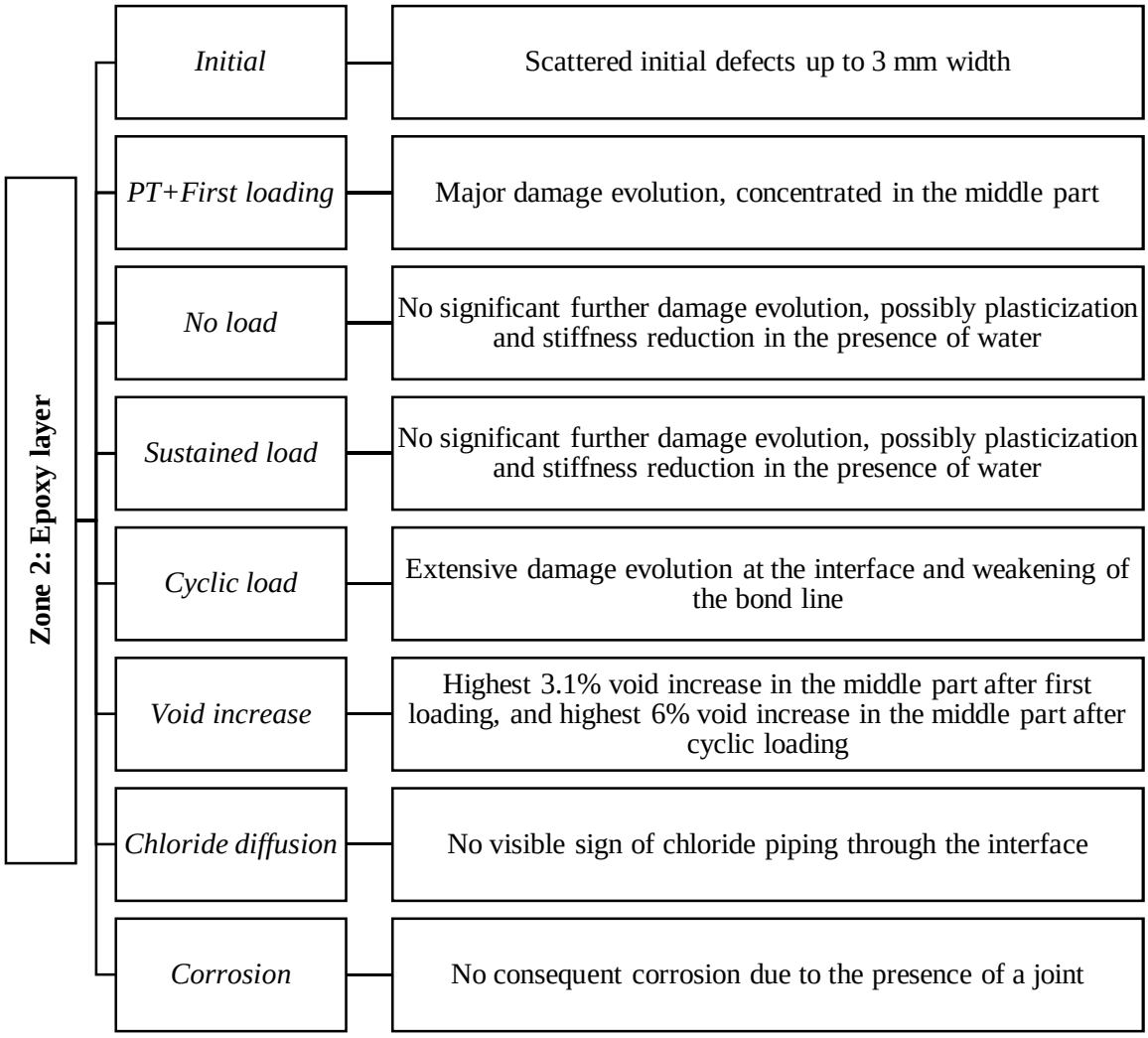

Figure 6.29. Summary of the key observations for zone 2: epoxy layer under various loading conditions

The main question that arises from the observations is the concentration of voids/micro cracks in the middle part of the epoxy, while based on the linear stress analysis, the middle part is not experiencing the highest applied tensile load. Hence, a step-by-step stress analysis and possible effects on the epoxy layer are discussed here.

6.12.1. Low workability and initial defects

The fresh epoxy is not very workable and does not flow easily (Epoxy B: 4000 mm^2 squeezability at 15 °C at 15 kg according to manufacturer data sheet). Total percentage coverage cannot be assured even though a compression force is applied at the time of curing. The lack of workability can lead to the occurrence of defects, especially in the middle part, where there is no proper access to control the coverage. When the external load is applied, the initial defects can cause localized stress concentration at the tip of the defects and cause micro cracking around the defected area.

6.12.2. Insufficient mixing and initial defects

Improper mixing of resin and hardener, incorrect ratio of resin and hardener and inconsistent distribution of the filler cause irregular hardening and shrinkage rate. The differential shrinkage within the layer can cause micro cracking and initial defects.

6.12.3. Constraint shrinkage and initial defects

Another cause of initial defects within the epoxy layer can be constraint shrinkage. During the curing period and the chemical reactions, the epoxy may shrink (for example, epoxy B shrinkage=0.04 % according to the manufacturer's data sheet). Concrete was oven dried (at 30^{o}C) for a month and had already experienced its full anticipated drying shrinkage. The epoxy was the only material to experience volume changes while the concrete was constraining it. If the epoxy is geometrically constrained during the curing period, residual stresses can develop in the epoxy layer and defects can form within the layer (Merzlyakov et al., 2006). This phenomenon can be more intense in the middle part of the epoxy due to the higher degree of constraint.

6.12.4. Thermosetting resins and residual stresses

Epoxies are highly exothermic, i.e. heat develops during curing time after mixing the resin with catalyst/curing agent/hardener (Guo, 2012). Epoxies go through three main stages to reach their final strength. First, the resin is liquid and after mixing with hardener it is still liquid until a certain time depending on the type of hardener. This period is normally called pot life and is specified by the manufacturer. However, mixing a huge volume of resin with hardener can reduce this pot life due to higher retained heat in the large mass of material and the resulting faster exothermal reaction. The second stage is the irreversible reaction transition from liquid to solid and is called gelation. In this stage, curing starts, and the epoxy is not workable anymore and the reaction produces heat. Finally, at the last stage called verification, it becomes solid. The chemical reaction during this curing process produces heat. The thicker the epoxy layer, the higher the heat production (Ratna, 2009).

The result of this study showed that the first mechanical loading was the main cause of extensive damage in the epoxy layer. This damage was especially distinct in the middle part of epoxy. Since the edges of the epoxy layer were exposed, the residual stresses/strains formed after plastic deformations of the material reaching equilibrium were not significant there. However, these residual tensile stresses were very intense at the middle part of the epoxy layer. Compression force due to post tension (PT) was constant all along the epoxy layer. The applied moment caused compression above the neutral axis and tension under it. However, the presence of the major crack on the side of joint changes the stress path. The stresses distributed from the tip of crack diagonally. Therefore, both the applied stress and the residual tensile stresses were concentrated in the middle part. The final state of stress showed the highest tension in the middle part of the epoxy resulting cracking in the middle part right after the first loading.

Moreover, epoxies can be very sensitive to temperature changes (Epoxy B has a thermal expansion coefficient of $W=2.5\times10^{-5}$ per °C, temperature range -20 °C to +40 °C, according to the manufacturer's data sheet). The laboratory temperature was constant during curing and the testing period, but expansion due to thermal changes should be considered as a potential cause of cracking within the epoxy in other circumstances.

6.12.5. Applied post tensioning and Poisson ratio effect

Another reason of extensive cracking in the middle part of epoxy after the first loading can be simply related to the applied compression with post tensioning and the Poisson effect in the epoxy layer. Unfortunately, the manufacturer has not reported the Poisson ratio of the epoxy, but potentially the horizontal pressure can cause the volume change in the epoxy layer. This volume change is constrained especially in the middle part that may lead to cracking.

6.12.6. Fracture behaviour of epoxy

Since the initial cracks exist in the middle part of epoxy, it is expected that the cracks propagate in the middle part after the loading and exposure time. Stress intensity in the middle part due to the presence of cracks has led to extensive crack propagation especially in sample F which has been under cyclic loading. Therefore, it is important to understand the fracture behaviour of epoxies in order to be able to explain the observations. The epoxy adhesive itself is very brittle. The manufacturers add fillers in to the epoxy in order to enhance the fracture property of the epoxy. The toughening mechanisms and cracking vary for different types of filler and stress condition that the material experiences during its service life. Unfortunately, the manufacturer did not supply the toughening mechanism of epoxy B. According to the evidences and observations in this project, two types of toughening method are most possible:

6.12.6.1. Nano fillers (inorganic clay minerals or graphene)

EDX analysis of epoxy B (Figure 5.22 (c)) showed that beside carbon (C) and oxygen (O) there are other major elements like calcium (Ca), silicium (Si), and aluminium (Al) in the epoxy composition. SEM analysis of epoxy B (Figure 5.22 (d)) also showed a very rough surface. Another example of SEM of epoxy B can be seen in Figure 6.30. These evidences are in line with Zotti et al. (2016) explanations about nano-filler modified epoxies by inorganic clay minerals or graphene. This type of filler can enhance mechanical properties (as epoxy B is a high strength epoxy), and depending on the percentage of filler content, the surface can become rougher (see Figure 6.31). This method is one of the most recent methods for epoxy toughening and it is highly possible that epoxy B is also made with the same method. The major fracture behaviour of this type of epoxy is crack deflection (see Figure 6.32). De-bonding of nano-clay or shear banding (local plastic deformation) are also possible scenarios for nano-composite epoxies. It is difficult to say which one of these behaviours are exactly happening in the case of this project.

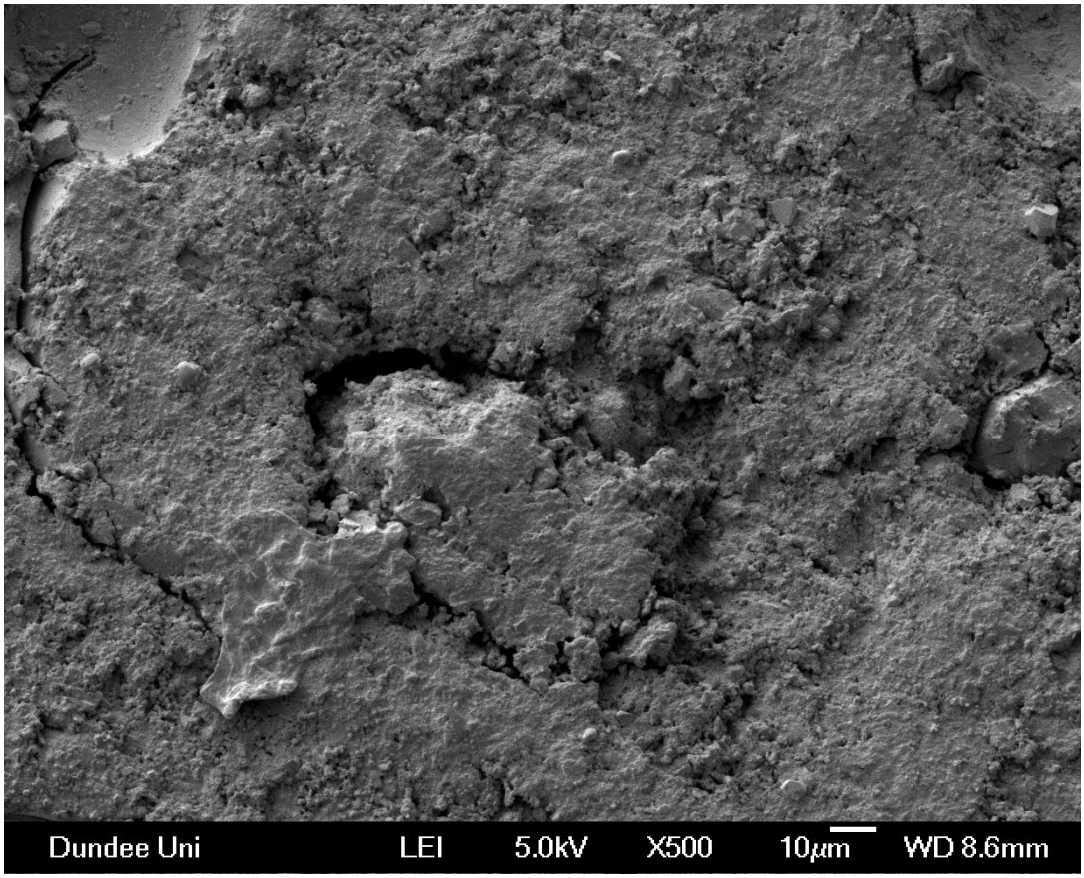

Figure 6.30. SEM image of epoxy B

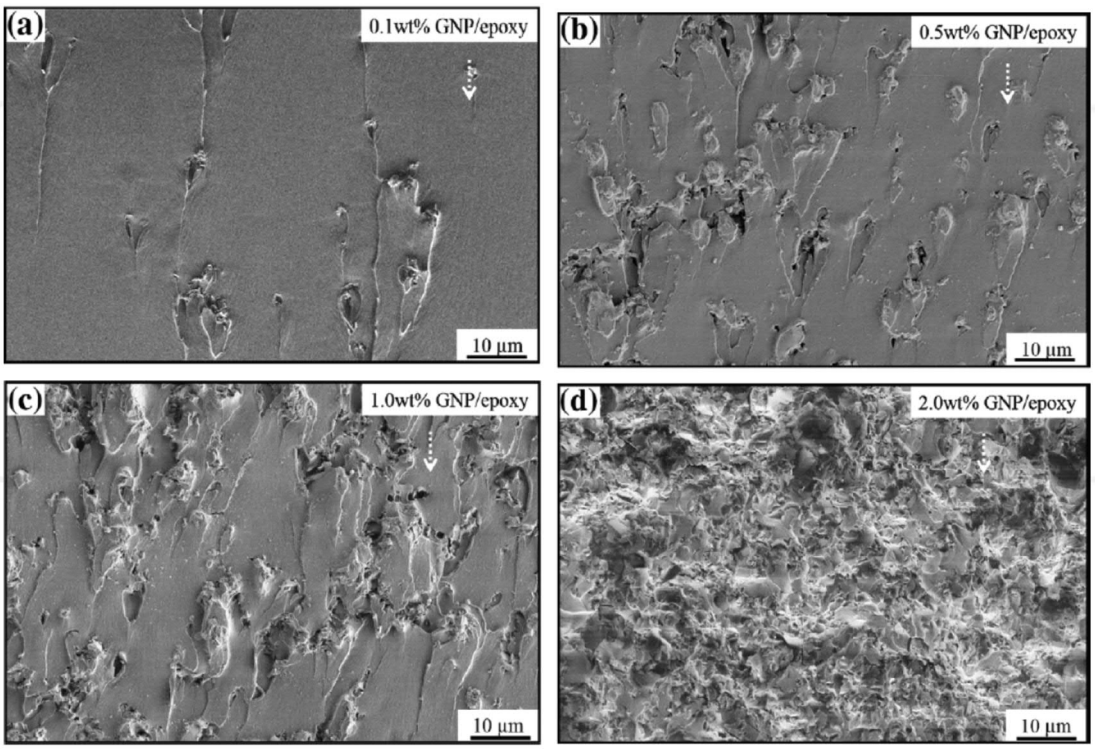

Figure 6.31. SEM images of fracture surfaces as weight % of filler

A) 0.1 wt%, b) 0.5 wt%, c) 1.0 wt%, and D) 2.0 wt%

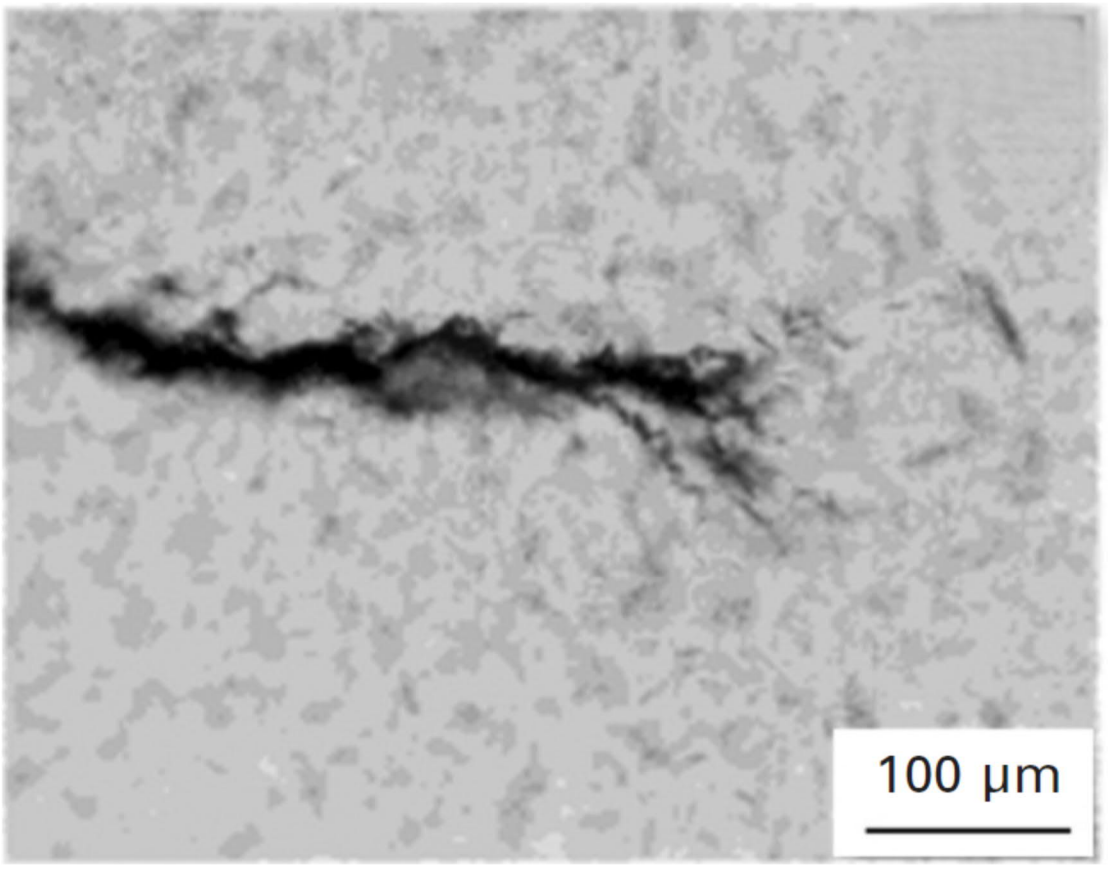

Figure 6.32. Crack deflection of epoxies with nano-composite filler (Guo, 2012)

6.12.6.2. Rubber toughened epoxy

A close look at CT-scan images, which are presented in the current chapter, does not show interconnected cracks within the epoxy layer. The damage looks like voids that are scattered around the initial defects. This raises the possibility of considering epoxy B as rubber toughened epoxy. Rubber toughening of epoxy is another common method for enhancing toughness of epoxy which shows similar toughening behaviour. This method is much older than the nano-composite toughening method and less possible for epoxy B.

6.12.7. Coupled effect of moisture and loading

The literature review showed that moisture can cause plasticization, reduction of bond strength , and change of failure mode in epoxy bonded concrete e.g. (Frigione et al., 2006, Lau and Büyüköztürk, 2010). However, the author could not find any data for coupled effect of mechanical stress and moisture on epoxy bonded concrete. The most related work can be Tuakta and Büyüköztürk (2011a) who examined the simultaneous effect of moisture diffusion and sustained load on bonded FRP to concrete. They observed pre-mature failure of the system, the deflection suddenly increased at the early stages of loading due to early micro-cracking in epoxy. At high stress intensity, the deflections were not significant, and they failed by creep fracture, but the sustained load with low stress intensity did not show any significant difference with no-load samples. The result of current project is in line with their observation about sudden cracking of the epoxy layer, but the sustained load did not cause any creep fracture in the bond line. Actually, the bond line seemed intact after three months of sustained load with high stress intensity. Although the plasticization (weakening of adhesive forces) has definitely happened in the epoxy layer, this effect is limited and has not led to premature failure. The manufacturer of epoxy B has provided the data related to the effect of water on reduction of fracture energy, which seems significant (see Figure 6.33). However, the diffusion coefficient of epoxies are very small (for example 4×10^{-13} according to Crocombe et al. (2006)) and the middle part of epoxy which is cracked is protected by the healthy outer part of epoxy layer so there can be no significant capillary suction either. Therefore, water may have not reached the very inner part of epoxy in this experimental programme. The limited plasticization can be due to stiffness reduction of the outer part of epoxy. Although the sample size in this project is very small, in a full-scale structure there will be bigger surfaces of epoxy exposed to water that can lead to greater weakening of the adhesive bond.

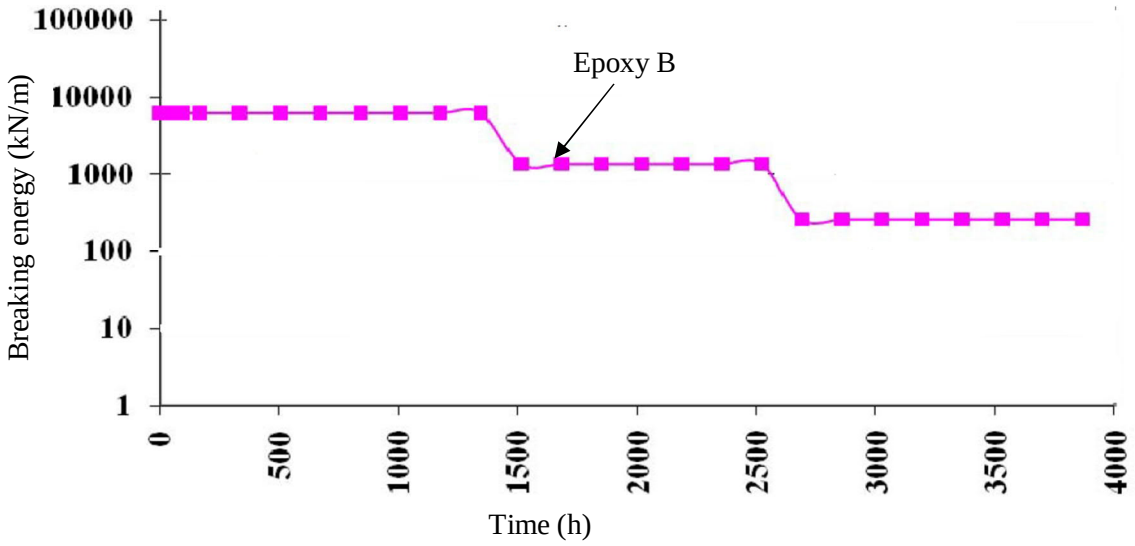

Figure 6.33. Fracture energy reduction of epoxy B during humid environment supplied by the manufacturer

On the other hand, the adhesive layer has been very much affected under the cyclic loading. Even the failure mode was changing after cycles of loading and cyclic wetting and drying exposure. It is difficult to say which one of moisture or cyclic loading effect has been dominant. Since there is no sign of chloride penetration around the joint, no water has really piped up through the bond. This means that it is more reasonable to say that mechanical effect (fatigue) has been more effective in damage evolution and weakening of the interface rather than the effect of moisture (plasticization).

6.13. ZONE 3: BODY OF CONCRETE: KEY OBSERVATIONS AND POSSIBLE THEORETICAL EXPLANATIONS

Figure 6.34 shows the summary of observations in the body of concrete at the healthy side. Overall, it can be seen that this part is almost intact and there is no considerable damage evolution.

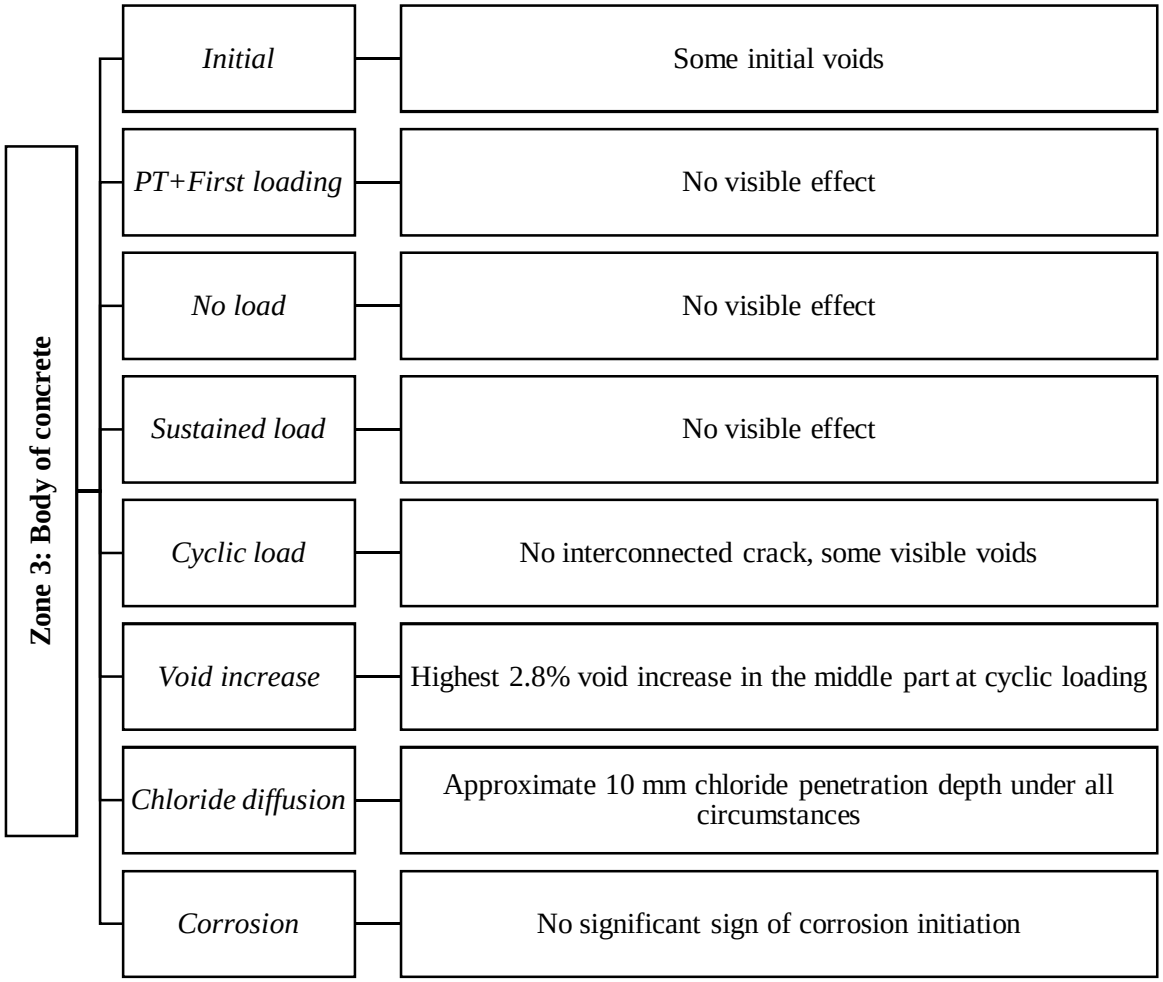

Figure 6.34. Summary of the key observations for zone 3: body of concrete under various loading conditions

There can be two reasons for good performance of un-cracked side of sample:

1. Epoxy with lower stiffness and the cracked side of concrete are sacrificial. This means that all stresses have piled up in the areas with lower stiffness or the areas with initial defects. Therefore, the elastic body of concrete has remained intact.
2. This post-tensioned concrete has a very good fatigue performance and one million cycles of loading does not affect this concrete mix significantly.

6.14. CONCLUSIONS

Considering the gap of knowledge in the coupled effect of stress and chloride ingress in epoxy bonded concrete, this chapter presented the observations and possible theoretical explanations of the experimental programme for epoxy bonded concrete under various loading conditions in seawater salt solution environment.

The problem of initial defects and early propagation of cracking in the epoxy layer was observed under all loading conditions. The first mechanical effect caused the main crack propagation in the epoxy layer. Then, the cracks in the epoxy layer did not propagate further under static and sustained load conditions. Cyclic loading caused extensive crack propagation in the epoxy ayer. Moreover, the cracks propagate into the bond line under cyclic loading.

No load and sustained load condition showed very similar behaviour, but the damage evolved more substantially in cyclically loaded samples. The cyclic loading led to crack opening and failure of the beam after one million cycles. The cracked part of concrete may have acted as the sacrificial area, so the stresses concentrated at the tip of the crack. Therefore, the other areas of the concrete remained intact under different loading conditions. If the major crack did not exist, the epoxy layer had the potential to fail earlier than concrete under cyclic loading.

Chloride ingress and water penetration, which were originally one the main concerns of the bonded system, did not progress at the interface of concrete and epoxy. The chloride ingress was also not affected by the state of loading except the chloride penetration in the major crack surface, which was highly accelerated by cyclic loading.

Overall, considering the typical industrial epoxy used in major constructions, the meso/micro assessment of the epoxy bonded concrete in this project revealed that mechanical effects are more dominant in crack evolution of this system. There are also some molecular changes in the bond line due to the presence of water. Therefore, the stiffness reduction of the beams can be related to post tensioning losses as well as plasticization of the epoxy and weakening of the bond line. This plasticization effect cannot be quantified with the methods used in this project.

7. OVER ALL CONCLUSIONS, COMPARISON OF THE RESULTS WITH THE AVAILABLE DATA, AND RECOMMENDATIONS

7.1. INTRODUCTION

The demand for cost reduction of WECs has stimulated the option of using concrete as the main structural material. Flat-face epoxy bonded concrete is one of the fastest and cheapest construction options. However, there are insufficient precedents and evidence to assure the performance of this system in the marine environment. There is a need to analyse the macro and micro mechanical behaviour of epoxy bonded concrete under various loading conditions in seawater salt solutions.

The current study used an experimental approach to assess the mechanical and durability performance of the joints. Developing reliable numerical models was not appropriate at this stage due to a lack of micro mechanical understanding and input parameters for the model. This project considered the variables affecting the static mechanical strength and the durability of the joints in addition to coupled environmental actions and mechanical load. Given the complexity of multi variant effects on the behaviour of joints, several test methods were developed, and others modified to evaluate a specific feature.

Extensive detailed conclusions were presented at the end of each chapter. This chapter draws on a summary of conclusions considering the main variables of each phase. It also underlines the practical implications arising from those results and available standards or guidance. More recommendations are also discussed for improving the innovative testing methodologies. Eventually, the main areas of concern are highlighted, and further areas for research are identified.

7.2. SUMMARY OF OVER ALL CONCLUSIONS BASED ON THE TESTED VARIABLES IN EACH PHASE

The research program set series of the most important testing variables for each phase of the project. Summary of the conclusions according to these tested variables are presented here.

Figure 7.1 and Figure 7.2 summarize the main conclusions drawn from the result of Phase I: Part 1 and Part 2. Shear/compression, tension, and torsion tests were conducted for epoxy bonded concrete to concrete in Part 1, while Part 2 assessed the shear capacity of epoxy-bonded concrete to steel.

Figure 7.3 and Figure 7.4 summarize the findings from the developed prototype in Phase II: Part 1, and chloride and water penetration testing of the jointed samples in Phase II: Part 2.

Phase III examined simultaneous effect of loading and exposure under cycles of wetting and drying in the artificial seawater salt solution. The main conclusions drawn from this innovative test set up are presented in Figure 7.5.

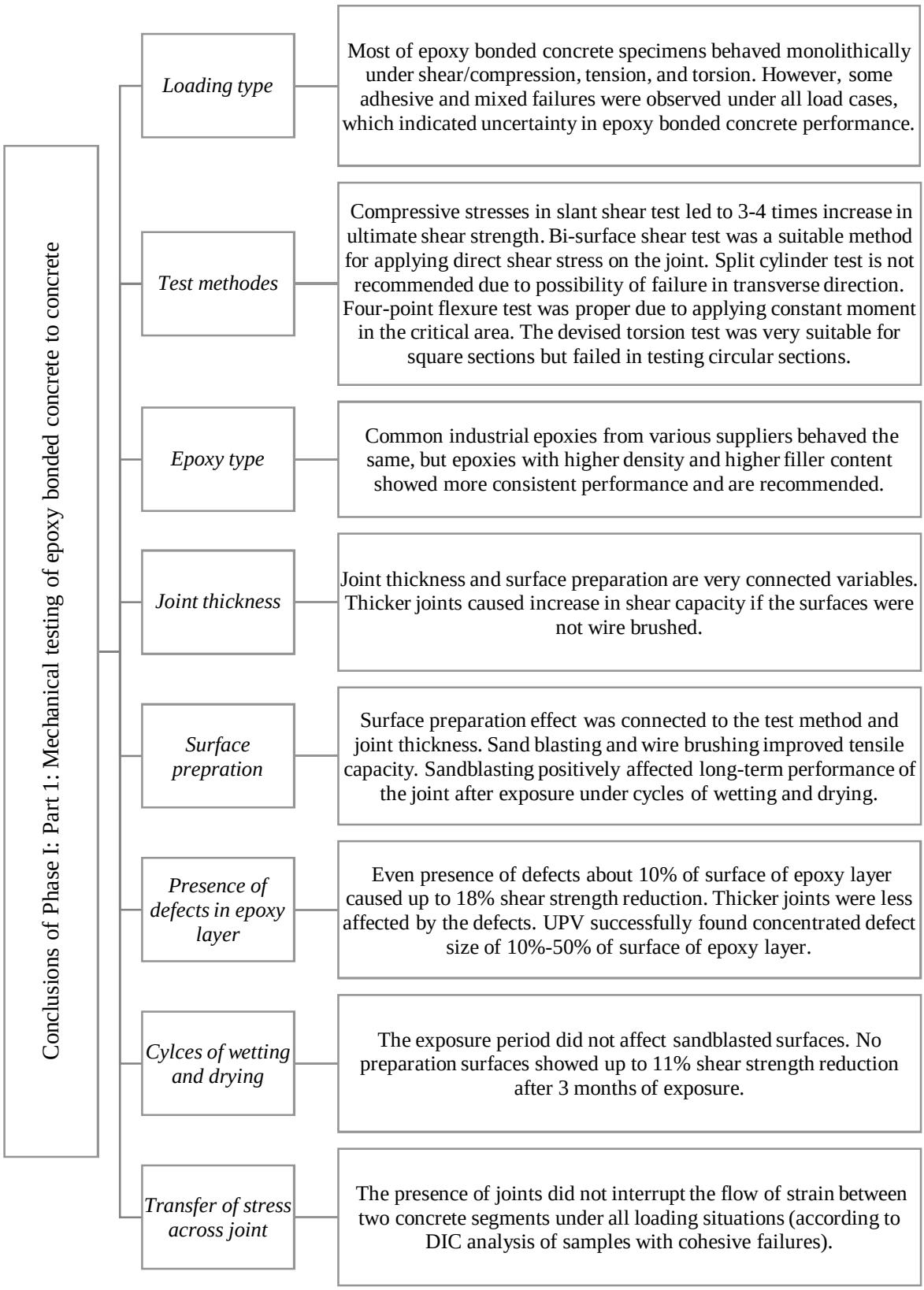

Figure 7.1. Main conclusions according to the main features of Phase I: Part 1: Mechanical testing of epoxy bonded concrete to concrete

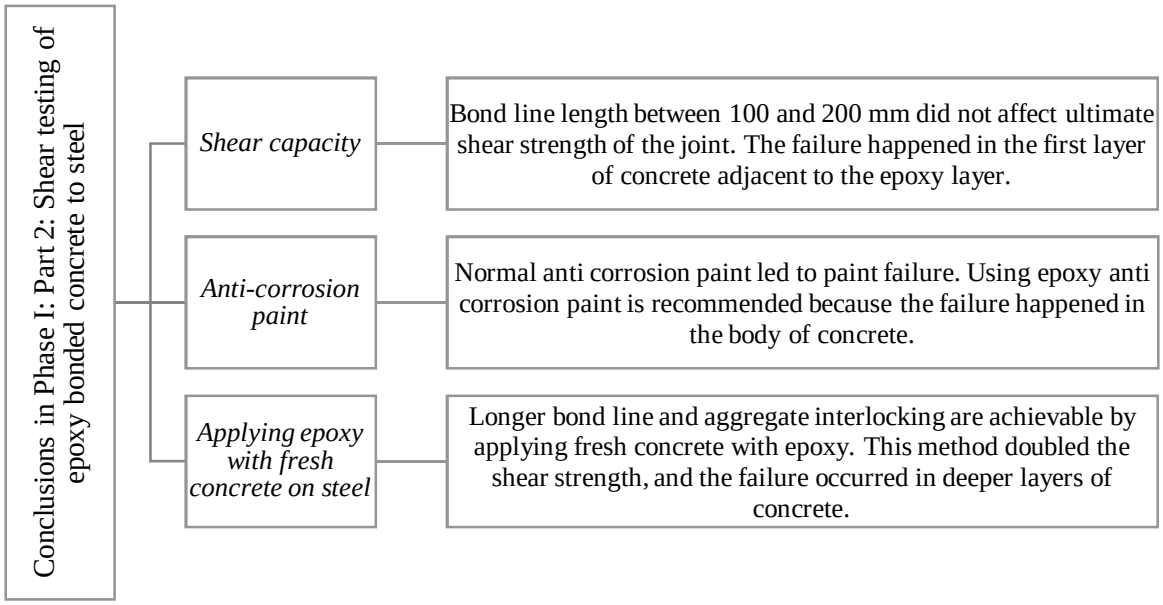

Figure 7.2. Main conclusions according to the main variables in Phase I: Part 2: Shear testing of epoxy bonded concrete to steel

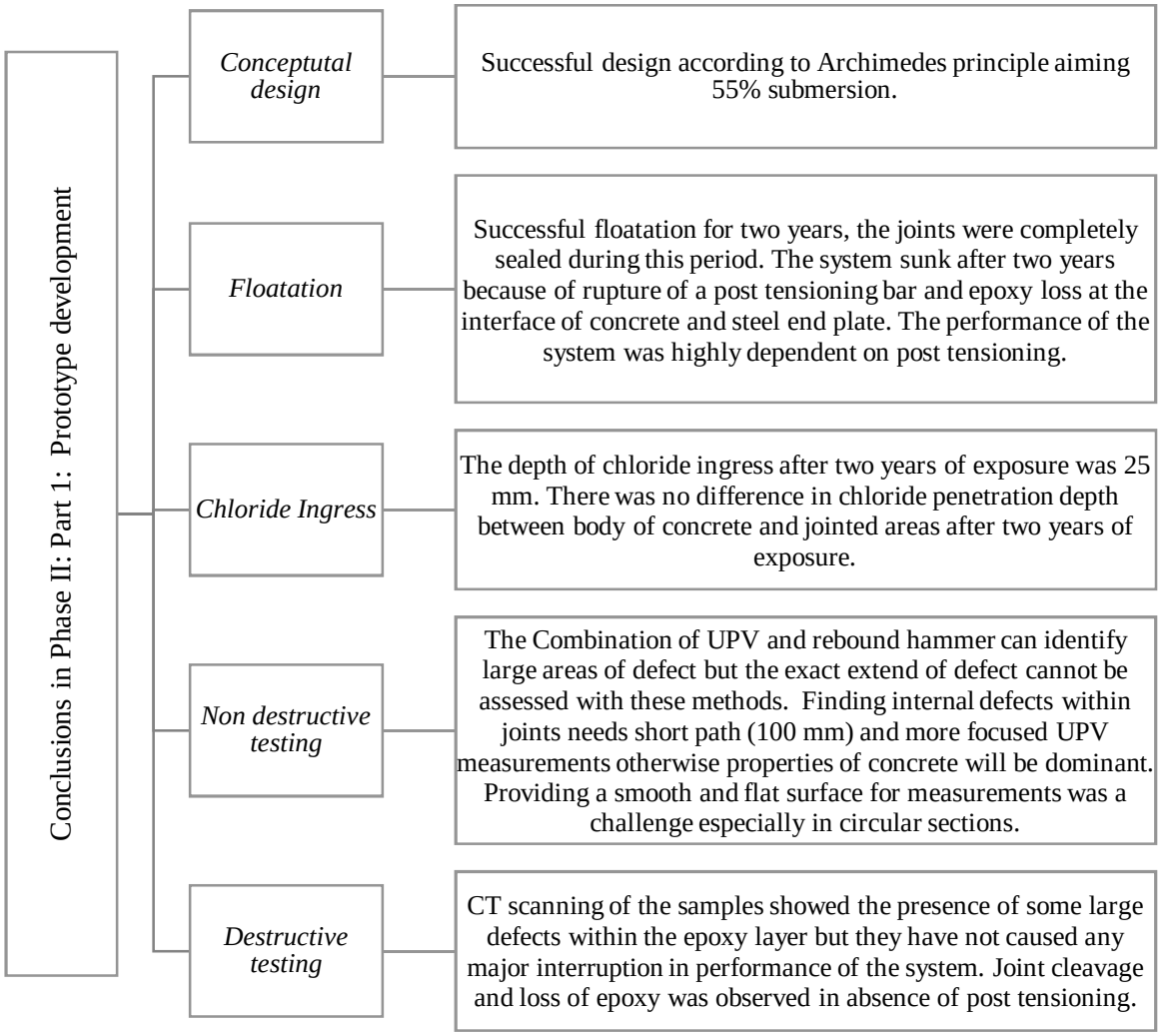

Figure 7.3. Main conclusions of Phase II: Part 1: Prototype development

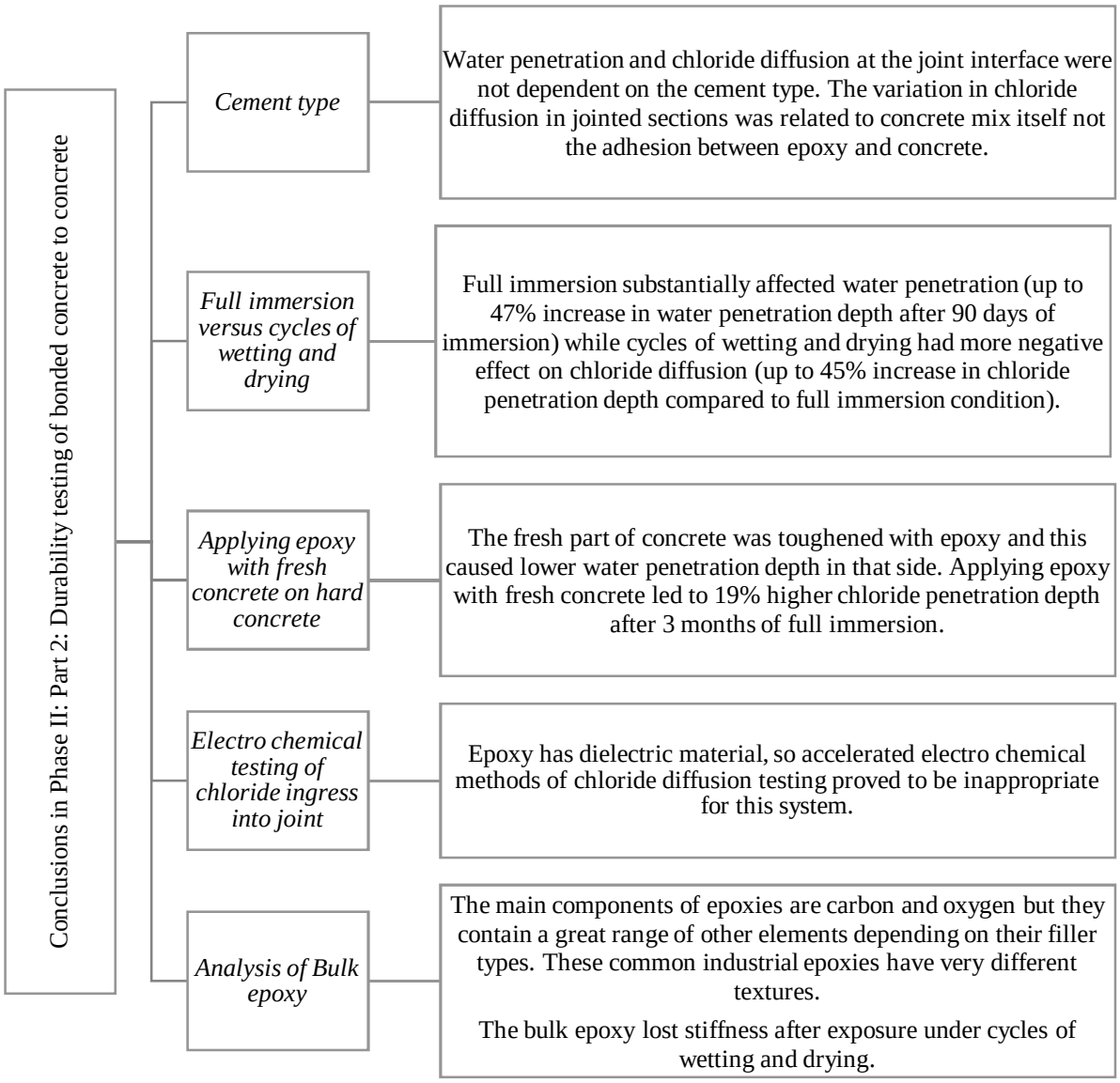

Figure 7.4. Main conclusions according to the main variables in Phase II: Part 2: Durability testing of bonded concrete to concrete

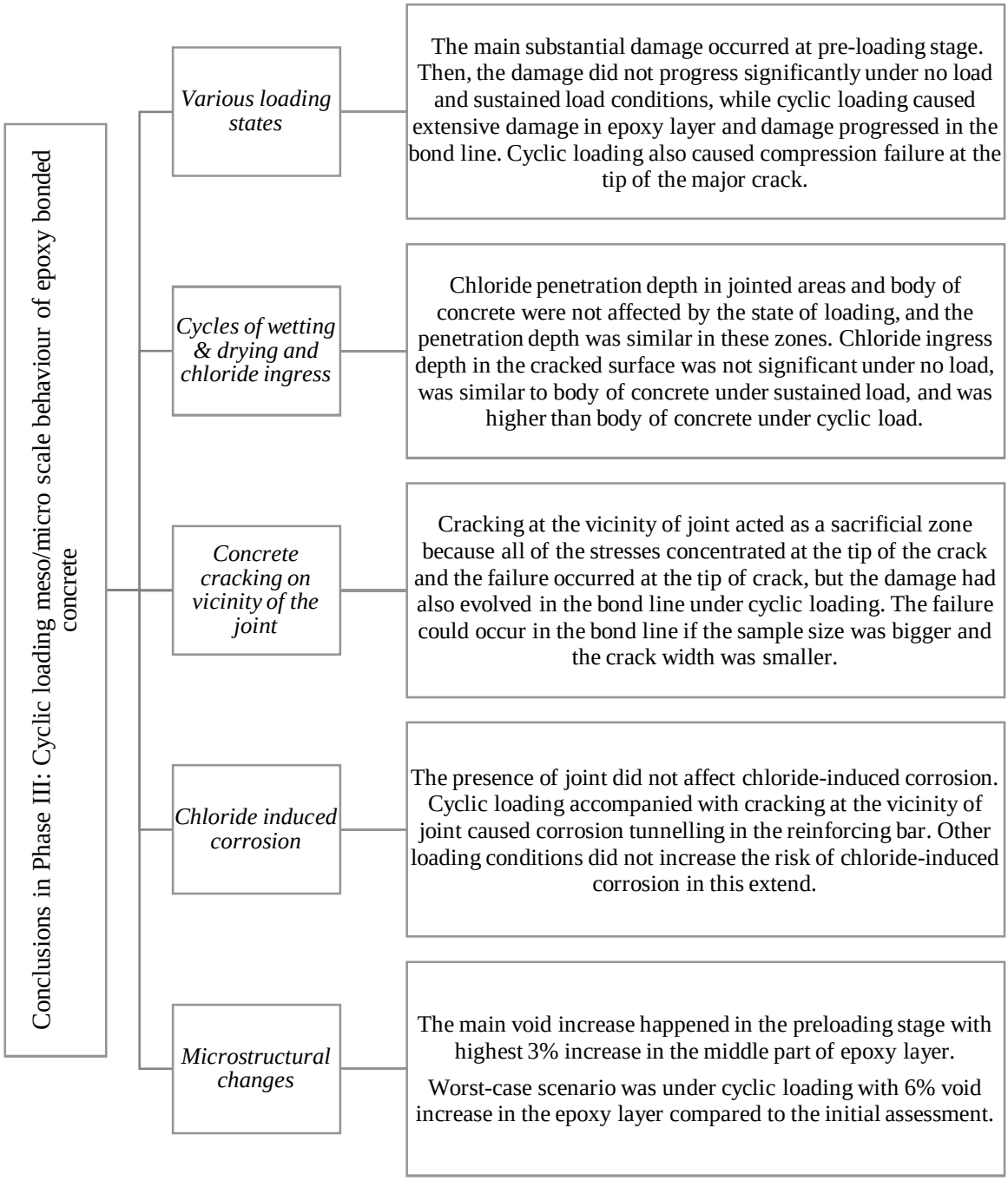

Figure 7.5. Main conclusions according to the main aspects of Phase III: Cyclic loading meso/micro scale behavior of epoxy bonded concrete

7.3. ORIGINS OF UNCERTAINTY IN THE RESULTS

The results of the experimental program showed some uncertainties and discrepancies throughout the project. For example, the failure modes of the joints varied for the samples with similar characteristics like epoxy type, join thickness, surface preparation and concrete mix. Even some detailed data given by one of the suppliers revealed the same extent of uncertainty in the failure modes and the results. For instance, testing epoxy B, after short storage in humid environment led to 60% adhesive failure and 40% cohesive failure according to data given by the manufacturer. Therefore, some possible roots of this uncertainty in the results are explained in this section.

7.3.1. Workmanship faults

Every concrete construction is very dependent on the quality of the workmanship. The samples of this project were prepared with precision, in addition, the samples with obvious defects were excluded from the results. However, the lab experience in this project showed that jointing concrete segments with epoxy was a very challenging process. Especially using spacers for adjusting the joint thickness and keeping samples aligned during curing time were not easy. There are possibilities of movements of segments during three days of curing due to ambient vibrations or creep. Batch size and proper mixing are also crucial factors. Larger batches of epoxies are very difficult to mix and also produce more heat and have shorter pot life. These small irregulates and varying batch sizes could potentially cause variations in the test results.

7.3.2. Low workability of the epoxies

The problem of the low workability and low spread ability of the epoxies were discussed extensively in Chapter 6. Low workability of the epoxies can lead to inconsistencies in the epoxy layer and consequent variations in test results. These defects are not easily detectable at the time of application.

7.3.3. Presence of the residual stresses

Presence of defects in the epoxy layer due to residual thermal or constraint shrinkage stresses were also discussed in chapter 6. All these sources of defects contribute in changes of failure modes.

7.3.4. Load eccentricities, stress concentration at the edges, and dependency on the shape and size of samples

There have been a considerable number of tests on bonded concrete since 1960, however, the results have been considerably inconsistent. CEB-FIP (2012) attributes this problem to the edge zone effect and dependency of the results on the geometry and scale of the test samples.

Moreover, DIC analysis in the current project showed different stress distribution for the same test set up. For example, Figure 7 shows two bi-surface shear tests. In the first test, the stresses are localized on the edges caused by small eccentricities in loading or local heterogeneity of concrete (see red areas in Figure 7 (a)). The second test however shows that the shear stress distributes evenly all along the bond line (see red areas in Figure 7 (b)) i.e. there is no local effect.

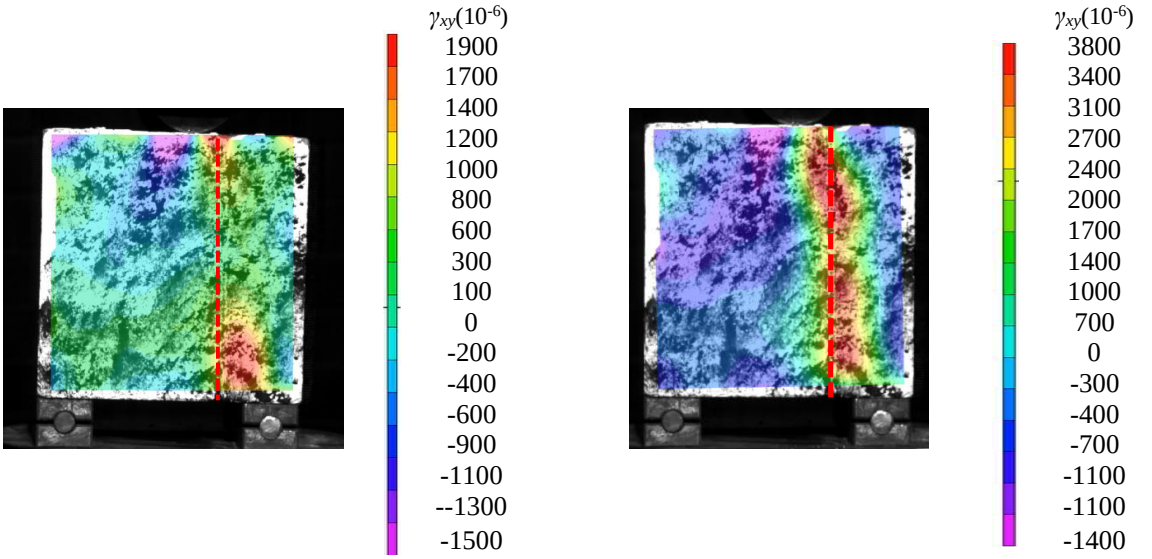

Figure 7. Stress distribution of Bi-surface shear test using DIC

7.4. SUGGESTIONS FOR IMPROVING THE TEST METHODS

The testing methods were generally successful with respect to the main objective of each phase. However, some minor issues appeared in conducting the tests which are explained here.

Regarding Phase I, all the macro mechanical testing seems suit to the purpose except for the split cylinder and circular torsion tests. The split cylinder test showed a high number of transverse cracking due to small movements of the cylinder and consequent inconsistent distribution of the load along the cylinder. Circular torsion test was not successful because of slip of the sample in the frame. Fabrication of a circular frame is needed to assure the stability of the sample during the test. Overall, the most important challenges in conducting all the macro mechanical tests were to avoid load eccentricities and precise positioning of the segments at the time of epoxy application.

In Phase II, typical assessment and durability testing procedures of concrete were suitable in case of epoxy bonded concrete. The only issues were provoked with UPV and electro chemical chloride diffusion tests. The prototype was not a thick piece of concrete (25 mm wall thickness) and UPV measurements ideally needed higher frequency transducers rather than usual 54 kHz transducers. Electro chemical chloride diffusion test also proved inappropriate for epoxy bonded concrete. Epoxy has dielectric properties that repel the chloride ions in an electric field.

Phase III assessed three different stress zones of bonded post tensioned concrete beams. The number of variables for an individual test was very high, so it was difficult to draw clear and quantitative conclusions. Although the test gave a qualitative insight in to the potential behaviour of the composite

segments in the marine environment, it was not possible to distinguish what the main influencing factors were that led to the crack propagation and stiffness reduction in the beam. Any further testing needs to reduce the number of variables, for example by applying a lower stress range and preventing major cracking next to the joint. Thus, the focus can be on the joint only.

Moreover, the cyclic loading rig needed a load cell and LVDT to record the applied load and the deformation during the testing period. The post tension losses also needed to be recorded precisely. Unfortunately, the glued studs for the post tensioning measurements came off during exposure to the seawater salt solution. Welded studs on the bars may resist better in the humid environment. The combination of a load cell, a LVDT and measurements of post tension losses could provide a reasoning for the stiffness reduction in the beams.

7.5. COMPARISON OF THE RESULTS TO THE AVAILABLE GUIDANCE AND DATA

The literature review showed the deficiency of available guidance, codes, or data for designing epoxy bonded concrete especially in the marine environment and under cyclic loading. This section looks at those limited available data and models in order to check and compare compatibility of the results of this project with them. Moreover, the areas where the results are contributing in enhancing the knowledge and understanding of epoxy bonded concrete are highlighted.

7.5.1. Estimating the ultimate strength of epoxy bonded concrete to concrete

BE EN 1504-4 (2004a) provides the basic requirements for acceptable performance of bonded concrete. However, the scope of this code does not cover specialised applications and circumstances such as extreme environmental conditions. Table 7-1 presents some examples of the required properties of bulk epoxy. These values should be compared with epoxy properties in Table 3-7 and Table 3-8. The other related characteristics of the bonded concrete which are tested in this project are mentioned at the end of this table. The suitability of application is not met with these epoxies because of showing various failure modes.

Table 7-1. Comparison of the results to BE EN 1504-4 (2004a), requirements for acceptable performance of epoxy bonded concrete to concrete

Performance characteristics	Test method	Requirements	Pass/fail/ no data	Comments
Modulus of elasticity	EN ISO 178	≥2000 N/mm^2	Pass/ no data	All the common epoxies for structures pass the criteria. the supplier should give this data.
Compressive strength	EN 12190	≥30 N/mm^2	Pass/ no data	All the epoxies in this project pass the criteria, but there is no data for epoxy F.
Coefficient of thermal expansion	EN 1770	≤ 100x10^{-6} per °C	Pass/ no data	Suppliers of epoxy C, D, E, and F do not provide the data.
Total shrinkage	EN 12617-1	≤0.1%	Pass/ no data	Suppliers of epoxy C, D, E, and F do not present the data.
Suitability for application	EN 12615 (Slant shear test)	≥6 N/mm^2 The fracture should be in concrete	Fail	All epoxies meet the strength requirements but all of them show various failure modes.
Durability (thermal and moisture)	EN 13733	The shear strength after exposure should not be less than the original condition	Fail	The samples with no surface preparation showed lower shear strength than the original condition. (The durability test condition in the current project was not the same as EN 13733.)

Even if all of the samples pass the above criteria i.e. they all fail in the body of the concrete, the question of exact resistance of epoxy-bonded concrete still exists. CEB-FIP (2012) presents a formula for calculating adhesion interlock of joints between concrete cast at different times (Equation 2.4). It is useful to check if this equation applies to the case of flat-face epoxy bonded concrete where the only related contributing parameter in shear resistance of the joint is the adhesion interlock.

Considering the mean tensile strength of the concrete used in this project, the joint shear resistance can be calculated as 1.76 MPa. All samples with sand blasted surfaces in the current project showed higher shear resistance than 1.76 MPa. Therefore, using this formula for epoxy-bonded concrete

seems slightly conservative, but it can be acceptable because all the samples have met this minimum value.

$$\tau_u = \tau_a = c_a f_{ct} = 0.4 \times 4.4 = 1.76\ MPa$$

Equation 7.1 (CEB-FIP, 2012)

$\tau_{u:}$ Ultimate shear resistance of interface

τ_a : Adhesion interlock

c_a: Roughness coefficient (Table 2-2), this value is 0.4 for sandblasted surfaces

f_{ct} : CEB-FIP (2012) states the mean value of the characteristic tensile strength of a 60 MPa concrete is f_{ctm} = 4.4 MPa, with lower and upper bound values, (5% and 95% fractiles) equal to 3.1 MPa ($f_{ct,min}$) and 5.7 MPa ($f_{ct,max}$).

The author could not find any other formulation for calculating tensile and torsional capacity of epoxy bonded concrete. Tensile and torsional resistance of the joints should not be considered equal to non-jointed concrete because some cases of failures with stress levels lower than the control samples were observed. Considering sandblasted surfaces, minimum average tensile and torsional resistance of the epoxy bonded concrete in this project were 2.5 MPa and 4.10 MPa respectively.

7.5.2. Estimating ultimate shear capacity of epoxy bonded concrete to steel

BE EN 1504-4 (2004a) does not provide any exact criteria and requirements for bonded concrete to steel. This standard includes the test methods and acceptance thresholds for bonded steel plate to steel, which is not the concern of the current study. On the other hand, the literature showed an extensive number of studies and guidance on calculating optimum bond line length and shear capacity of retrofitting plates. However, practical questions, like the effect of anti-corrosion paint and applying fresh concrete with epoxy on the plate, were not addressed.

The results of two different shear tests on the current project revealed that the anchorage length between 100 and 200 mm does not make any difference to the final shear resistance of the composite, so this length of bond line can be considered as the optimum range. This is in line with Barnes and Mays (2001) suggestions on the bond line length. The average shear capacity of epoxy bonded plates in both shear tests were 1.75 MPa with failure at the thin layer of concrete adjacent to the joint, but Barnes and Mays (2001) push out results showed average of 5.5 MPa shear resistance and the same type of failure. However, the results are not directly comparable because there are differences in concrete mixes, plate and epoxy thicknesses, and surface preparation methods.

The push out test indicated that normal anti-corrosion paint caused premature failure in the anti-corrosion paint. Therefore, it is important to use epoxy based anti-corrosion paints to get the same results as the pure steel surfaces with failure in the body of concrete.

The results of double lap shear tests showed that applying fresh concrete with epoxy on the plate can double shear resistance by providing aggregate interlock and longer bond line. However, the manufacturer's data sheets generally advise application of epoxies on dry surfaces, which is in line with Çolak et al. (2009) conclusions on the negative effect of saturated concrete interfaces on failure and strength. While the same negative effect on the ultimate strength of the joint was not observed in this project, it showed up by formation of voids in the epoxy layer after 3 months of immersion in the seawater salt solution.

7.5.3. Effect of humidity on the ultimate strength of epoxy bonded concrete

The data available on the precise effect of humidity on the ultimate strength of epoxy-bonded concrete is diverse. For example, Frigione et al. (2006) reported 30% strength reduction after one month immersion, while Lau and Büyüköztürk (2010) observed a change in failure mode after this period. Considering the results of the current project, the effect of humidity on bond strength appeared to be linked to the surface preparation, i.e. the same immediate trend of strength reduction was not observed for sandblasted surfaces after 3 months of exposure. Moreover, the bulk epoxy tensile testing showed 13% stiffness reduction of the epoxy after 3 months exposure under cycles of wetting and drying.

The manufacturer of epoxy B provided the results of fracture energy testing of the product after 160 days of storage in a humid environment (Figure 6.33). Their report indicated a 90% reduction in fracture energy at the end of this period. This is in contrast with Tuakta and Büyüköztürk (2011b) findings that the reduction of the fracture energy can reach an asymptotic value which does not progress afterward .

Overall, the epoxy becomes softer after extended periods of exposure, but this effect can vary for different epoxies in accordance with the manufactures data sheets. In addition, it does not necessarily mean that the bond strength reduces with the same trend as the stiffness reduction. The bond showed acceptable performance with good surface preparation in the time-scale of this project. Therefore, Lau (2012)'s simple recommendations for considering 50% to 60 % of the bond capacity for design in the humid environment does not seem valid.

7.5.4. Static water penetration and chloride ingress through the joints

Categorizing concrete quality according to its chloride diffusion coefficient and depth of water penetration is a very controversial topic. However, The Concrete Society (2008) attempted to draw a conclusion on concrete quality based on the typical results obtained from various permeability tests.

Table 7-2 shows the general comments about level of permeability, absorption and chloride diffusion of concrete. The current project results are compared against these general comments in Table 7-3.

Water penetration was high for bonded concrete after 3 months of exposure under full immersion or cycles of wetting and drying in seawater salt solution. It means that the epoxy bond weakens under the exposure conditions. Hence, the water with 500±50 kPa pressure can penetrate deeper at the joint interface after the exposure period. The increase in water penetration depth is only related to the epoxy layer because aging of concrete in water should improve concrete permeability and lead to lower water or chloride penetration depth. The period of exposure in the current project was short and more tests are required to predict the final depth of water penetration of bonded concrete during its service life.

Results from chloride analysis with $AgNO_3$ spray and chloride profiling did not highlight any concern. No visual excess chloride penetration at the joint interface was observed in all conditions. The diffusion coefficients were also in the low or average range (see Table 7-3). The differences in average chloride penetration in the current project are related to differences in concrete mixes and exposure conditions and not the epoxy layer. However, if the pressure causes deeper water penetration at the interface, the water can transfer chloride at the interface and then chloride ingress is a point of concern as well.

Likewise, assessment of the prototype confirmed negligible effect of presence of the joints on chloride ingress depth and highlighted the detrimental effect of water, combined with loading, on weakening the joint, which led to failure of the epoxy bond of the steel plates.

Table 7-2. General comment about concrete permeability/absorption/diffusion (The Concrete Society, 2008)

Test method	Units	Concrete permeability/absorption/diffusion		
		low	Average	high
Water penetration BS EN 12390-8	mm	<8	8-20	>20
ISAT 10min	ml/m^2/s	<0.25	0.25-0.50	>0.50
30 min		<0.17	0.17-0.35	<0.35
60 min		<0.10	0.10-0.20	<0.20
Apparent chloride diffusion coefficient	m^2/s	$<1\times10^{-12}$	1×10^{-12}-5×10^{-12}	$>5\times10^{-12}$

Chloride diffusion coefficient of bulk epoxy is approximately 1.2 ×10-12 m^2/s (The Concrete Society, 2008)

Table 7-3. Comparison of the results with The Concrete Society (2008)'s general comments on permeability/absorption/diffusion of concrete

Test method	Exposure condition	CEM III/A (50% GGBS)		100% CEMI
		Hard/hard	Hard/fresh	Hard/hard
Water penetration BS EN 12390-8	No exposure	19 mm average	-	-
	Full immersion	28 mm High	-	-
	Cycles of wetting &drying	24 mm High	25 mm High	24 mm High
ISAT 10min 30 min 60 min	No exposure	0.10 low 0.06 low 0.05 low	-	-
Apparent chloride diffusion coefficient	Full immersion	0.58×10^{-12} Low	-	-
	Cycles of wetting &drying	4.31×10^{-12} Average	-	-

7.5.5. Performance of epoxy bonded concrete under cyclic loading

There are no direct guidelines in the codes for epoxy bonded concrete under cyclic loading. The only specific recommendation is from CEB-FIP (2012) which suggests considering 40% of the static resistance for fatigue resistance of the joints. It is not possible to exactly confirm or accept this recommendation based on the results of this project. However, the extensive crack propagation in the epoxy layer under cyclic loading does not support this simplified approach.

The guidance for the fatigue life of a concrete structure can be used as a point of comparison for this composite. DNV-OS-C502 (2010) offshore concrete structures design guidelines gives Equation 7.2 for the fatigue life of concrete structures. After 3 months of loading, each beam of this project experienced about one million cycles. One of the beams failed after this number of loading cycles. Table 7-4 shows the calculated number of cycles for the compression side (farthest from neutral axes at top of the beam).

$$\log_{10} N = C_1 \frac{1 - \frac{\sigma_{max}}{C_5 f_{rd}}}{1 - \frac{\sigma_{min}}{C_5 f_{rd}}}$$

Equation 7.2 DNV-OS-C502 (2010)

C1: Related to the exposure situation, 8 for structures in water (see Table 2-5)

C5: 1 for concrete

σ_{max}: Maximum stress during cycles

σ_{min}: Minimum stress during cycles

f_{rd}: Static strength

Table 7-4. Expected number of resisting loading cycles of the beams according to DNV-OS-C502 (2010)

Position	Minimum stress (MPa)	Maximum stress (MPa)	Static strength (MPa)	Number of cycles predicted by Equation 7.2	Pass/Fail
Compression part	1.18	6.87	60	10^7	Fail [(1)]

[(1)]The tested beam failed after one million cycles

According to Table 7-4, the compression part of the beam was expected to tolerate at least 10^7 number of cycles while it failed at 10^6 number of cycles. This premature failure of the beam in the compression section is related to the presence of a crack. This major crack plays a key role under cyclic loading. Therefore, the unreinforced critical area around the joint remains as a point of concern specially under cyclic loading.

7.5.6. Mechanical loading and chloride ingress in epoxy bonded concrete

RILEM technical committee 246 (Yao et al., 2017) has recently published a test methodology to assess durability of concrete under the simultaneous effect of environmental actions and mechanical loads. This technical report implies that the state of loading can affect the chloride diffusion coefficient. However, the results of Phase III showed that the depth of chloride ingress identified by colourimetry was not significantly affected by the loading state. It is only the internal surface of the crack which showed significantly higher depth of chloride ingress under cyclic loading.

7.6. MAIN AREAS OF CONCERN AND RECOMMENDATIONS FOR FURTHER RESEARCH

This project looked at the practical challenges of using epoxy bonded concrete in the marine environment. It has proved that there are numerous interconnected variables affecting the mechanical and durability performance of this composite system. Straightforward solutions were found for some of the issues based on the results. For instance, the effect of anti-corrosion paint on the failure mode and the consequent recommendation of using epoxy anti-corrosion paint. However, addressing many other issues were not so simple. From the conclusions of the current study, several doubts arise about

the reliability of epoxy bonded concrete as the main structural element for a concrete WEC. The following points are the main areas of concern and recommendations for further research.

7.6.1. Presence of defects in epoxy layer

The problem of defects and their damaging effect came up in all Phases of the project. Defects can cause change of failure mode, high water/chloride ingress, and extensive localised cracking under first mechanical loads. Further research in this area could consider the following issues:

7.6.1.1. Construction challenges

Working with epoxies proved to be challenging. Batch size and proper mixing should be carefully considered. New epoxy application methods should be devised to assure consistent and defect free spreading of epoxy.

7.6.1.2. Quality assurance testing

Combination of UPV and rebound hammer was effective to identify the defect zones in the prototype. However, careful consideration is required to adjust the proper distance between the transducers and direction of measurements. There is a need to find more reliable methods and standardize them, specifically for epoxy bonded concrete.

7.6.1.3. Scale effect

Localised stress concentration around the defects is affected by size of the specimens. Numerous large-scale tests are required to evaluate the effect of these small size voids on the global response of the structure.

7.6.2. Performance of epoxy bonded concrete in humid environment

Despite the agreement of the results with the literature review on the negative effect of humidity on fracture toughness of the epoxy bond, the author is not convinced that there is an asymptotic value for stiffness reduction beyond where no reduction takes place. The manufacturer should supply adequate data for each epoxy type regarding the exact effect of humidity on the properties of the epoxy. There is also a need for exact formulation and service life modelling of the bonded system in the marine environment.

7.6.3. Importance of post tensioning in the reliable performance of epoxy bonded concrete

Wave energy producers like Albatern ltd. can use small floating concrete structures which are simply glued together by epoxy. Post tensioning is an expensive and highly precise process, so it is not justifiable for these small units. Moreton (1981) was sure about the monolithic behaviour of the joints even in the absence of any compression. Conversely, Hewson (2003) asserted the necessity of at least 1.5 MPa compression at all times on the joint to assure monolithic behaviour in shear. There is an evidence in the current project which conforms to Hewson (2003) suggestions. Firstly, the increase in shear capacity of the epoxy bonded concrete by 3-4 times in slant shear test which involves

compression. Secondly, failure of the post-tensioning bar of the prototype led to cracking and loss of epoxy, the end plates were also kept in place by post tensioning. Therefore, the author does not advise epoxy bonded concrete without post tensioning even for small unit WECs.

7.6.4. Waves and significant water penetration through the joint

A floating WEC will always be under wave loading or hydrostatic pressure. The results showed that the water can penetrates deeply through the jointed sections. The penetration depth also increases with aging of the epoxy layer in the humid environment. This water penetration depth is a very concerning issue in designing a concrete WEC. Further research is required to assess the phenomenon at a longer period of exposure to the marine environment.

7.6.5. Extensive crack propagation in the epoxy layer under cyclic loading

The results of the cyclic loading test brought up a serious concern regarding extensive crack propagation in the epoxy layer. There is also a shift from cracking at the middle of the epoxy layer to the bond line under cyclic loading. There should be specific data available regarding each epoxy's fracture characteristics, effect of humidity and fatigue resistance. This data should be supplied by the epoxy manufacturer and further research is required to identify design guidance for this aspect of epoxy bonded concrete in the marine environment.

7.6.6. Cracking adjacent to the joint and chloride induced corrosion in the cracked surface under cyclic loading

The major crack always occurs in the critical unreinforced area adjacent to the joint (assuming a defect free joint and monolithic behaviour). This major crack does not arise any concern under the static and sustained load condition, but it leads to significant chloride diffusion at the cracked surface under cyclic loading. The high chloride ingress depth at the cracked surface causes tunnelling corrosion at the end of the reinforcing bar. Therefore, the design should avoid the possibility of any cracking in the critical area adjacent to the joint.

8. REFERENCES

AASHTO 89 -AMERICAN ASSOCIATION OF STATE HIGHWAY AND TRANSPORTATION OFFICIALS 1989. *Guide Specifications for Design and Construction of Segmental Concrete Bridges Interim Specifications 1990 –1999.*

ABU-TAIR, A., LAVERY, D., NADJAI, A., RIGDEN, S. & AHMED, T. 2000. A new method for evaluating the surface roughness of concrete cut for repair or strengthening. *Construction and building materials,* 14**,** 171-176.

ABU-TAIR, A., RIGDEN, S. & BURLEY, E. 1996. Testing the bond between repair materials and concrete substrate. *ACI Materials Journal,* 93**,** 553-558.

ACI-ASCE COMMITTEE 445 2013. 445.1R-12 Report on Torsion in Structural Concrete. 92.

ACI COMMITTEE 215R-74 1997. Considerations for design of concrete structures subjected to fatigue loading. *Journal Proceedings,* 71.

ACI COMMITTEE 357 2010. Report on floating and float-in concrete structures. American Concrete Institute.

ADAMS, R. D. & PEPPIATT, N. A. 1974. Stress analysis of adhesive bonded lap joints. *Strain analysis 9,* 185-196.

AHMED, T. M. A., BURLEY, E. & RIGDEN, S. R. 1999. The effect of alkali ;silica reaction on the fatigue behaviour of plain concrete tested in compression, indirect tension and flexure. *Magazine of Concrete Research,* 51**,** 375-390.

AHN, W. & REDDY, D. 2001. Galvanostatic testing for the durability of marine concrete under fatigue loading. *Cement and Concrete Research,* 31**,** 343-349.

ALLICHE, A. & FRANGOIS, D. 1992. Damage of Concrete in Fatigue. *Journal of Engineering Mechanics,* 118**,** 2176-2190.

ARYA, C. & WOOD, L. A. 1995. The relevance of cracking in concrete to corrosion of reinforcement. *CS-TR--44.*

ASTM INTERNATIONAL 2013. ASTM C805 M Standard test method for rebound number of hardened concrete. Conshohocken, PA.

ASTM INTERNATIONAL 2014. ASTM D638 Standard test method for tensile properties of plastics. West Conshohocken,PA: ASTM International.

ASTM INTERNATIONAL 2015a. ASTM C876 Standard test method for corrosion potentials of uncoated reinforcing steel in concrete. West Conshohocken, PA: ASTM International.

ASTM INTERNATIONAL 2015b. ASTM D907 Standard terminology of adhesives. West Conshohocken,PA: ASTM International.

BARNES, R. A. & MAYS, G. C. 2001. The transfer of stress through a steel to concrete adhesive bond. *International journal of adhesion and adhesives,* 21**,** 495-502.

BAROGHEL-BOUNY, V., BELIN, P., MAULTZSCH, M. & HENRY, D. 2007. AgNO3 spray tests: advantages, weaknesses, and various applications to quantify chloride ingress into concrete. Part 1: Non-steady-state diffusion tests and exposure to natural conditions. *Materials and structures,* 40**,** 759-781.

BAŽANT, Z. P. 2002. Concrete fracture models: testing and practice. *Engineering Fracture Mechanics,* 69**,** 165-205.

BAZANT, Z. P. & PRAT, P. C. 1988. Effect of temperature and humidity on fracture energy of concrete. *ACI Materials Journal,* 85**,** 262-271.

BENZARTI, K., CHATAIGNER, S., QUIERTANT, M., MARTY, C. & AUBAGNAC, C. 2011. Accelerated ageing behaviour of the adhesive bond between concrete specimens and CFRP overlays. *Construction and building materials,* 25**,** 523-538.

BIZINDAVYI, L. & NEALE, K. 1999. Transfer lengths and bond strengths for composites bonded to concrete. *Journal of composites for construction,* 3**,** 153-160.

BLAGOJEVIC, A., FENNIS-HUIJBEN, S. & WALRAVEN, J. C. Impact of cracks on chloride-induced corrosion and durability of reinforced concrete structures-a literature review. V International PhD Student Workshop on Durability of Reinforced Concrete: From Composition to Service Life Design. VTT Technology 65, 2012. VTT Technical Research Center.

BONALDO, E., BARROS, J. A. & LOURENÇO, P. B. 2005. Bond characterization between concrete substrate and repairing SFRC using pull-off testing. *International journal of adhesion and adhesives,* 25**,** 463-474.

BORDES, M., DAVIES, P., COGNARD, J. Y., SOHIER, L., SAUVANT-MOYNOT, V. & GALY, J. 2009. Prediction of long term strength of adhesively bonded steel/epoxy joints in sea water. *International Journal of Adhesion and Adhesives,* 29**,** 595-608.

BOWDITCH, M. R. 1996. The durability of adhesive joints in the presence of water. *International Journal of Adhesion and Adhesives,* 16**,** 73-79.

BOYLE, M. 2001. Epoxy resins. *Materials Park, OH: ASM International***,** 78-89.

BRITISH STANDARDS INSTITUTION 1996. BS 1881-208 Testing concrete. Recommendations for the determination of the initial surface absorption of concrete. London: BSI.

BRITISH STANDARDS INSTITUTION 1999. BS EN 12615 Products and systems for the protection and repair of concrete structures. Test methods. Determination of slant shear strength. London: BSI.

BRITISH STANDARDS INSTITUTION 2002a. BS EN 1008 Mixing water for concrete. Specification for sampling, testing and assessing the suitability of water, including water recovered from processes in the concrete industry, as mixing water for concrete. London: BSI.

BRITISH STANDARDS INSTITUTION 2002b. BS EN 12390-3 Testing hardened concrete – Part 3:Compressive strength of test specimens. London: BSI.

BRITISH STANDARDS INSTITUTION 2004a. BS EN 1504-4 Products and systems for the protection and repair of concrete structures - Definitions, requirements, quality control and evaluation of conformity. Structural bonding. London: BSI.

BRITISH STANDARDS INSTITUTION 2004b. BS EN 1992-1, Eurocode 2: Design of concrete structures. London: BSI.

BRITISH STANDARDS INSTITUTION 2004c. BS EN 1994-1-1 Eurocode 4. Design of composite steel and concrete structures. General rules and rules for buildings. london: BSI.

BRITISH STANDARDS INSTITUTION 2004d. BS EN 12504-4 Testing concrete in structures. Determination of ultrasonic pulse velocity. London: BSI.

BRITISH STANDARDS INSTITUTION 2006. BS EN 15167-1 Ground granulated blast furnace slag for use in concrete, mortar and grout. Definitions, specifications and conformity criteria. London: BSI.

BRITISH STANDARDS INSTITUTION 2009a. BS EN 934-2 Admixtures for concrete, mortar and grout.Concrete admixtures – Definitions, requirements, conformity, marking and labelling. London: BSI.

BRITISH STANDARDS INSTITUTION 2009b. BS EN 12350-2 Testing fresh concrete – Part 2: Slump test. London: BSI.

BRITISH STANDARDS INSTITUTION 2009c. BS EN 12350-6 Testing fresh concrete – Part 6: Density. London: BSI.

BRITISH STANDARDS INSTITUTION 2009d. BS EN 12390-5 Testing hardened concrete. Flexural strength of test specimens. London: BSI.

BRITISH STANDARDS INSTITUTION 2009e. BS EN 12390-6 Testing hardened concrete. Tensile splitting strength of test specimens. London: BSI.

BRITISH STANDARDS INSTITUTION 2009f. BS EN 12390-8 Testing hardened concrete. Depth of penetration of water under pressure. London: BSI.

BRITISH STANDARDS INSTITUTION 2010. TDD CEN/TS 12390-11 Testing hardened concrete - Part 11: Determination of the chloride resistance of concrete, unidirectional diffusion. London: BSI.

BRITISH STANDARDS INSTITUTION 2011. BS EN 197-1 Cement. composition, specifications and conformity criteria for common cements. London: BSI.

BRITISH STANDARDS INSTITUTION 2013a. BS 1881-125 Testing concrete, Methods for mixing and sampling fresh concrete in the laboratory. London: BSI.

BRITISH STANDARDS INSTITUTION 2013b. BS 6349 Maritime structures. London: BSI.

BRITISH STANDARDS INSTITUTION 2013c. BS EN 1097-6 Tests for mechanical and physical properties of aggregates. Determination of particle density and water absorption. London: BSI.

BRITISH STANDARDS INSTITUTION 2015a. BS 8500-1 Concrete – Complementary British Standard to BS EN 206. Part 1: Method of specifying and guidance for the specifier. London: BSI.

BRITISH STANDARDS INSTITUTION 2015b. BS 8500-2 Concrete – Complementary British Standard to BS EN 206. Part 2: Specification for constituent materials and concrete. London: BSI.

BROUGHTON, W. 1999. Report No 19 Combined cyclic loading and hostile environments *NPL Report CMMT (A).*

BROUGHTON, W., CROCKER, L. & GOWER, M. 2007. Design and Testing of Bonded and Bolted Joints. *NPL Manual.* NPL

BROUGHTON, W. & MERA, R. 1999. Environmental degradation of adhesive joints, accelerated testing. *NPL Report CMMT (A)*, 197.

BUNGEY, J. H. & MILLARD, S. G. 2010. *Testing of Concrete in Structures, Third Edition,* CRC Press.

BÜYÜKÖZTÜRK, O., BUEHLER, M. J., LAU, D. & TUAKTA, C. 2011. Structural solution using molecular dynamics: Fundamentals and a case study of epoxy-silica interface. *International Journal of Solids and Structures,* 48**,** 2131-2140.

BÜYÜKÖZTÜRK, O., LAU, D. & TUAKTA, C. Durability and long-term performance modeling of frp-concrete systems. The 6th International Conference on FRP Composites in Civil Engineering-CICE2012, 2012.

CASTELLOTE, M. & ANDRADE, C. 2006. Round-Robin test on methods for determining chloride transport parameters in concrete. *Materials and Structures,* 39**,** 955-990.

CASTELLOTE, M., ANDRADE, C. & ALONSO, C. 2001. Measurement of the steady and non-steady-state chloride diffusion coefficients in a migration test by means of monitoring the conductivity in the anolyte chamber. Comparison with natural diffusion tests. *Cement and Concrete Research,* 31**,** 1411-1420.

CEB-FIP 2012. fib Bulletin 55: Model Code 2010 – Final draft. *vol.1*. Lausanne, Switzerland: Comité Euro-International du Béton.

CHEN, J. & TENG, J. 2001. Anchorage Strength Models for FRP and Steel Plates Bonded to Concrete. *Journal of Structural Engineering,* 127**,** 784-791.

ÇOLAK, A., ÇOŞGUN, T. & BAKıRCı, A. E. 2009. Effects of environmental factors on the adhesion and durability characteristics of epoxy-bonded concrete prisms. *Construction and Building Materials,* 23**,** 758-767.

COMITÉ EURO-INTERNATIONAL DU BÉTON 2012. CEB-FIP. fib Bulletin 55: Model Code 2010 – Final draft, Vol. 1. Lausanne,Switzerland.

CORRELATEDSOLUTIONS.COM. 2015. *Correlated Solutions* [Online]. [Accessed February 2015].

CROCOMBE, A. D., HUA, Y. X., LOH, W. K., WAHAB, M. A. & ASHCROFT, I. A. 2006. Predicting the residual strength for environmentally degraded adhesive lap joints. *International Journal of Adhesion and Adhesives,* 26**,** 325-336.

CZARNECKI, L., GARBACZ, A. & KRYSTOSIAK, M. 2006. On the ultrasonic assessment of adhesion between polymer coating and concrete substrate. *Cement and Concrete Composites,* 28**,** 360-369.

DA SILVA, L. F., CARBAS, R., CRITCHLOW, G. W., FIGUEIREDO, M. & BROWN, K. 2009. Effect of material, geometry, surface treatment and environment on the shear strength of single lap joints. *International Journal of Adhesion and Adhesives,* 29**,** 621-632.

DE GOEIJ, W., VAN TOOREN, M. & BEUKERS, A. 1999. Composite adhesive joints under cyclic loading. *Materials & design,* 20**,** 213-221.

DEEPRASERTWONG, K. & LEUNG, Y. 1994. A full scale- destructive test of a precast segmental box girder bridge with dry joints and external tendons. *Proceedings of the ICE-Structures and Buildings,* 104**,** 297-315.

DEHGHANI, H. & FADAEE, M. J. 2014. Probabilistic assessment of torsion in concrete beams externally strengthened with CFRP composites. *Materials and Structures,* 47**,** 885-894.

DEREWONKO, A., GODZIMIRSKI, J., KOSIUCZENKO, K., NIEZGODA, T. & KICZKO, A. 2008. Strength assessment of adhesive-bonded joints. *Computational materials science,* 43**,** 157-164.

DET NORSKE VERIT 2010. DNV-OS-C502 Offshore concrete structures DNV.

ESKANDARIAN, M., AZARI, S., PAPINI, M., SCHROEDER, J., FAULKNER, D. & SPELT, J. 2006. The effect of substrate material on the quasi-static measurement of critical energy release rate in adhesive joints.

ESPELID, B. & NILSEN, N. 1998. Field Study of the Corrosion Behavior on Dynamically Loaded Marine Concrete Sructures. *Special Publication,* 109.

FOSSA, K., KREINER, A. & MOKSNES, J. 2008. Slip forming of advanced concrete structures. *Walravan and Stoelhorst (eds) 2008 Taylorand Francis Group***,** 831-836.

FRANCOIS, R. & MASO, J. 1988. Effect of damage in reinforced concrete on carbonation or chloride penetration. *Cement and Concrete Research,* 18**,** 961-970.

FRIGIONE, M., AIELLO, M. & NADDEO, C. 2006. Water effects on the bond strength of concrete/concrete adhesive joints. *Construction and building materials,* 20**,** 957-970.

GARBACZ, A., GÓRKA, M. & COURARD, L. 2005. Effect of concrete surface treatment on adhesion in repair systems. *Magazine of Concrete Research,* 57**,** 49-60.

GDOUTOS, E. 2005. Fracture Mechanics: An Introduction, 2nd edn.(Vol. 123 of Solid Mechanics and Its Applications). Springer, Dordrecht.

GERWICK, C. 1999. *Construction of marine and offshore structures*, CRC Press.

GLEDHILL, R. & KINLOCH, A. 1974. Environmental failure of structural adhesive joints. *The journal of adhesion,* 6**,** 315-330.

GLEICH, D. M. 2002. *Stress analysis of structural bonded joints*, TU Delft, Delft University of Technology.

GU, P. & BEAUDOIN, J. J. 1998. *Obtaining effective half-cell potential measurements in reinforced concrete structures*, Institute for Research in Construction, National Research Council of Canada Ottawa.

GUO, Q. 2012. *Thermosets : structure, properties and applications*, Cambridge, UK ; Philadelphia, PA, Cambridge, UK ; Philadelphia, PA : Woodhead Publishing.

HARTSHORN, S. R. 2012. *Structural Adhesives: Chemistry and Technology*, Springer US.

HELLAND, S., AARSTEIN, R. & MAAGE, M. 2010. In-field performance of North Sea offshore platforms with regard to chloride resistance. *Structural Concrete,* 11**,** 15-24.

HEWLETT, P. C. 2001. *Lea's chemistry of cement and concrete*, Oxford, UK, Elsevier Ltd.

HEWSON, N. R. 2003. *Prestressed concrete bridges: design and construction*, Thomas Telford.

IAEA 2002. *guide book on non destructive testing of concrete structures*, Vienna, Austria, The International Atomic Energy Agency.

JACKSON, N. & DHIR, R. 1997. *Civil Engineering Materials*, Palgrave Macmillan.

JAFFER, S. J. & HANSSON, C. M. 2008. The influence of cracks on chloride-induced corrosion of steel in ordinary Portland cement and high performance concretes subjected to different loading conditions. *Corrosion Science,* 50**,** 3343-3355.

JAFFER, S. J. & HANSSON, C. M. 2009. Chloride-induced corrosion products of steel in cracked-concrete subjected to different loading conditions. *Cement and Concrete Research,* 39**,** 116-125.

JENG, C.-H., CHIU, H.-J. & PENG, S.-F. 2013. A new apparatus and method for torsion test of large-size reinforced concrete beams. *Journal of Testing and Evaluation,* 42**,** 1-15.

JÚLIO, E., BRANCO, F. & SILVA, V. 2005. Concrete-to-concrete bond strength: influence of an epoxy-based bonding agent on a roughened substrate surface. *Magazine of concrete research,* 57**,** 463-468.

KARAYANNIS, C. G. & CHALIORIS, C. E. 2013. Design of partially prestressed concrete beams based on the cracking control provisions. *Engineering Structures,* 48**,** 402-416.

KHOSRAVI, N., BARKER, L., O'DONOGHUE, V., BENZIE, J., NEWLANDS, M. & JONES, R. Use of concrete as the primary construction material for the pelamis wave energy converter. Renewable Energies Offshore - 1st International Conference on Renewable Energies Offshore, RENEW 2014, 2015. 305-312.

KNOX, E. M. & COWLING, M. J. 2000. Durability aspects of adhesively bonded thick adherend lap shear joints. *International Journal of Adhesion and Adhesives,* 20**,** 323-331.

KOSEKI, K. & BREEN, J. E. 1983. Exploratory study of shear strength of joints for precast segmental bridges. Center for Transportation Research, : The University of Texas at Austin, .

KÜTER, A., GEIKER, M. R., OLESEN, J. F., STANG, H., DAUBERSCHMIDT, C. & RAUPACH, M. Chloride ingress in concrete cracks under cyclic loading. 3rd International Conference on Construction Materials, 2005. The University of British Columbia.

LAU, D. 2012. Moisture-induced Debonding in Concrete-epoxy Interface. *HKIE Transactions,* 19**,** 33-38.

LAU, D. & BÜYÜKÖZTÜRK, O. 2010. Fracture characterization of concrete/epoxy interface affected by moisture. *Mechanics of Materials,* 42**,** 1031-1042.

LEGER, R., ROY, A. & GRANDIDIER, J. C. 2010. Non-classical water diffusion in an industrial adhesive. *International Journal of Adhesion and Adhesives,* 30**,** 744-753.

LENSCHOW, R. 1980. Long term random dynamic loading of concrete structures. *Matériaux et Construction,* 13**,** 274-278.

LU, X. Z., TENG, J. G., YE, L. P. & JIANG, J. J. 2005. Bond–slip models for FRP sheets/plates bonded to concrete. *Engineering Structures,* 27**,** 920-937.

MEGALLY, S., SEIBLE, F., GARG, M. & DOWELL, R. K. 2002. Seismic performance of precast segmental bridge superstructures with internally bonded prestressing tendons. *PCI journal,* 47**,** 40-56.

MEHTA, P. K. 2002. *Concrete in the marine environment,* CRC Press.

MEHTA, P. K. & MONTEIRO, P. J. M. 2006. *Concrete Microstructure properties and materials,* Berkely, McGraw-Hill.

MERZLYAKOV, M., MCKENNA, G. B. & SIMON, S. L. 2006. Cure-induced and thermal stresses in a constrained epoxy resin. *Composites Part A: Applied Science and Manufacturing,* 37**,** 585-591.

MOMAYEZ, A., EHSANI, M. R., RAMEZANIANPOUR, A. A. & RAJAIE, H. 2005. Comparison of methods for evaluating bond strength between concrete substrate and repair materials. *Cement and Concrete Research,* 35**,** 748-757.

MORETON, A. Epoxy glue joints in precast concrete segmental bridge construction ICE Proceedings, 1981. Thomas Telford, 163-177.

MOSLEY, W. H., BUNGEY, J. H. & HULSE, R. 2012. *Reinforced Concrete Design to Eurocode 2,* Palgrave Macmillan.

NAWY, E. G. 2008. *Concrete construction engineering handbook,* CRC press.

NEVILLE, A. M. 2011. *Properties of Concrete , 5th edition,* Edinburgh, Pearson.

NISHIZAKI, I. & KATO, Y. 2011. Durability of the adhesive bond between continuous fibre sheet reinforcements and concrete in an outdoor environment. *Construction and Building Materials,* 25**,** 515-522.

NT BUILD 443 1994. Concrete, hardened: accelerated chloride penetration.

NT BUILD 492 1999. Concrete, mortar and cement based repair materials: chloride migration coefficient from non-steady state migration experiments.

OHLSSON, U., DAERGA, P. A. & ELFGREN, L. 1990. Fracture energy and fatigue strength of unreinforced concrete beams at normal and low temperatures. *Engineering Fracture Mechanics,* 35**,** 195-203.

OTIENO, M. B., ALEXANDER, M. G. & BEUSHAUSEN, H.-D. 2010. Corrosion in cracked and uncracked concrete – influence of crack width, concrete quality and crack reopening. *Magazine of Concrete Research,* 62**,** 393-404.

PELAMIS WAVE POWER 2013. Feasibility report on construction of P2e machines from precast structural concrete Commercially Confidential

PÉREZ FERNÁNDEZ, R. & LAMAS PARDO, M. 2013. Offshore concrete structures. *Ocean Engineering,* 58**,** 304-316.

POPINEAU, S., RONDEAU-MOURO, C., SULPICE-GAILLET, C. & SHANAHAN, M. E. R. 2005. Free/bound water absorption in an epoxy adhesive. *Polymer,* 46**,** 10733-10740.

POWSNER, R. A., PALMER, M. R. & POWSNER, E. R. 2013. X-ray Computed Tomography. *Essentials of Nuclear Medicine Physics and Instrumentation, Third Edition***,** 119-128.

RANDL, N. 2013. Design recommendations for interface shear transfer in fib Model Code 2010. *Structural Concrete,* 14**,** 230-241.

RATNA, D. 2009. *Handbook of Thermoset Resins,* Shawbury, Shrewsbury, Shropshire, Rapra Technology Ltd.

ROMBACH, G. 2002. Precast segmental box girder bridges with external prestressing-design and construction. *INSA Rennes Technical University, Hamburg-Harburg, Germany*.

ROMBACH, G. A. Dry joint behavior of hollow box girder segmental bridges. FIP Symposium "Segmental Construction in Concrete", New Delhi, 2004.

ROY, A., GONTCHAROVA-BENARD, E., GACOUGNOLLE, J.-L. & DAVIES, P. 2000. Hygrothermal effects on failure mechanisms of composite/steel bonded joints. *ASTM special technical publication,* 1357**,** 353-371.

SAIBABU, S., SRINIVAS, V., SASMAL, S., LAKSHMANAN, N. & IYER, N. R. 2013. Performance evaluation of dry and epoxy jointed segmental prestressed box girders under monotonic and cyclic loading. *Construction and Building Materials,* 38**,** 931-940.

SAKATA, Y. & OHTSU, M. 1997. Spectral response and acoustic emission of reinforced concrete members under fatigue bending. *Journal of acoustic emission.*

SANTOS, D. S., SANTOS, P. M. & DIAS-DA-COSTA, D. 2012. Effect of surface preparation and bonding agent on the concrete-to-concrete interface strength. *Construction and Building Materials,* 37**,** 102-110.

SANTOS, P. M. & JULIO, E. N. 2007. Correlation between concrete-to-concrete bond strength and the roughness of the substrate surface. *Construction and Building Materials,* 21**,** 1688-1695.

SANTOS, P. M. & JÚLIO, E. N. 2013. A state-of-the-art review on roughness quantification methods for concrete surfaces. *Construction and Building Materials,* 38**,** 912-923.

SANTOS, P. M. & JÚLIO, E. N. 2014. Interface shear transfer on composite concrete members. *ACI Structural Journal,* 111**,** 113.

SANTOS, P. M. D. & JÚLIO, E. N. B. S. 2011. Factors affecting bond between new and old concrete. *ACI Materials Journal,* 108**,** 449-456.

SI LARBI, A., FERRIER, E. & HAMELIN, P. 2009. Concrete to steel lap joint failure criteria under combined shear and peeling stress. *Journal of Constructional Steel Research,* 65**,** 386-394.

SI LARBI, A., FERRIER, E., JURKIEWIEZ, B. & HAMELIN, P. 2007. Static behaviour of steel concrete beam connected by bonding. *Engineering Structures,* 29**,** 1034-1042.

SUBRAMANIAM, K. V. & SHAH, S. P. 2003. Biaxial tension fatigue response of concrete. *Cement and Concrete Composites,* 25**,** 617-623.

TADA, H., PARIS, P. C. & IRWIN, G. R. 1973. The stress analysis of cracks. *Del Research Corp, Hellertown PA.*

TAYEH, B. A., BAKAR, B. A., JOHARI, M. M. & VOO, Y. L. 2012. Mechanical and permeability properties of the interface between normal concrete substrate and ultra high performance fiber concrete overlay. *Construction and Building Materials,* 36**,** 538-548.

THE CONCRETE SOCIETY 2008. Technical Report 31: Permeability Testing of Site Concrete. . UK: The Concrete Society.

THE CONCRETE SOCIETY 2009. Technical Report 69 :Repair of concrete structures with reference to BS EN 1504. UK: The Concrete Society.

THE CONCRETE SOCIETY 2010. Technical Report 72: Durable post-tensioned concrete structures UK: The Concrete Society.

TORRENTI, J. M., PIJAUDIER-CABOT, G. & REYNOUARD, J.-M. 2010. *Mechanical behaviour of concrete,* Great Britain, WILEY.

TOUTANJI, H. & ORTIZ, G. 2001. The effect of surface preparation on the bond interface between FRP sheets and concrete members. *Composite structures,* 53**,** 457-462.

TUAKTA, C. & BÜYÜKÖZTÜRK, O. 2011a. Conceptual model for prediction of FRP-concrete bond strength under moisture cycles. *Journal of Composites for Construction,* 15**,** 743-756.

TUAKTA, C. & BÜYÜKÖZTÜRK, O. 2011b. Deterioration of FRP/concrete bond system under variable moisture conditions quantified by fracture mechanics. *Composites Part B: Engineering,* 42**,** 145-154.

TURMO, J., RAMOS, G. & APARICIO, A. C. 2006. Shear strength of dry joints of concrete panels with and without steel fibres: Application to precast segmental bridges. *Engineering Structures,* 28**,** 23-33.

VENUGOPAL, V. & NEMALIDINNE, R. 2015. Wave resource assessment for Scottish waters using a large scale North Atlantic spectral wave model. *Renewable Energy,* 76**,** 503-525.

VOLKERSEN, O. 1938. Die Nietkraftverteilung in zugbeanspruchten Nietverbindungen mit konstanten Laschenquerschnitten. *Luftfahrtforschung,* 15**,** 41-47.

WAAGAARD, K. 1982. Fatigue strength evaluation of offshore concrete structures. *ACI Special Publication,* 75.

WANG, C. & WANG, B. 2014. *Large Floating Structures: Technological Advances,* Springer.

YAO, J., TENG, J. G. & CHEN, J. F. 2005. Experimental study on FRP-to-concrete bonded joints. *Composites Part B: Engineering,* 36**,** 99-113.

YAO, Y., WANG, L., WITTMANN, F. H., DE BELIE, N., SCHLANGEN, E., GEHLEN, C., WANG, Z., ALAVA, H. E., CAO, Y. & YUNUS, B. M. 2017. Recommendation of RILEM TC 246-TDC: test methods to determine durability of concrete under combined environmental actions and mechanical load. *Materials and Structures,* 50**,** 155.

ZHANG, B. 1998. Relationship Between Pore Structure and Mechanical Properties of Ordinary Concrete Under Bending Fatigue. *Cement and Concrete Research,* 28**,** 699-711.

ZHAO, Y., REN, H., DAI, H. & JIN, W. 2011. Composition and expansion coefficient of rust based on X-ray diffraction and thermal analysis. *Corrosion Science,* 53**,** 1646-1658.

ZOTTI, A., ZUPPOLINI, S., ZARRELLI, M. & BORRIELLO, A. 2016. Fracture Toughening Mechanisms in Epoxy Adhesives. *Adhesives-Applications and Properties.* InTech.

APPENDIX A

LVDT and load cell calibration method

High magnification extensometer calibrator was used for calibration four LVDTs (see Figure A.1). One complete revolution of the thimble indicates 0.5 mm movement. One major division on the extensometer shows 0.01 mm and the minor division indicate 0.002 mm. Each LVDT was aligned straight to the head of extensometer. The small movements of the extensometer were pressing the LVDT's head. Both the movement and change in the voltage were recorded at each step. The voltage range of LVDTs was between -2.5 V to 2.5 V and it was recorded by a data logger. Therefore, the movements were continued to reach this voltage range. Figure A.2 shows the relationship between the voltage and extensometer movement readings. The slope of this line was used as the calibration factor for each LVDT.

Figure A.1. Extensometer calibrator used for calibration of the LVDT

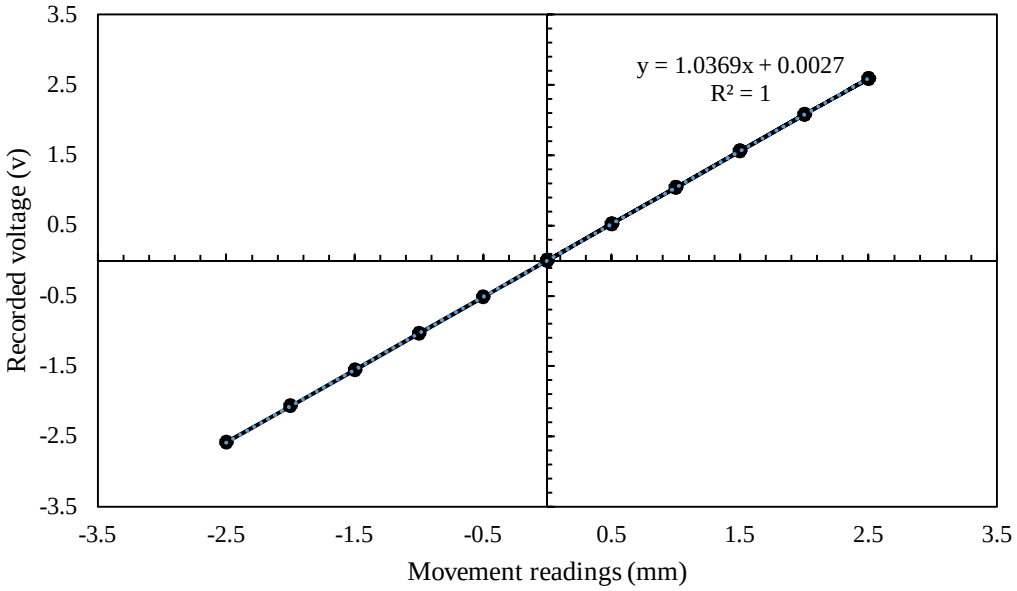

Figure A.2. An example of calibration graph of LVDT

The load cell was calibrated by recording the applied load versus the voltage changes. The voltage was recorded by a data logger as well. The relationship between applied load and the voltage changes can be seen in Figure A.3. The slope of this line was used as the calibration factor.

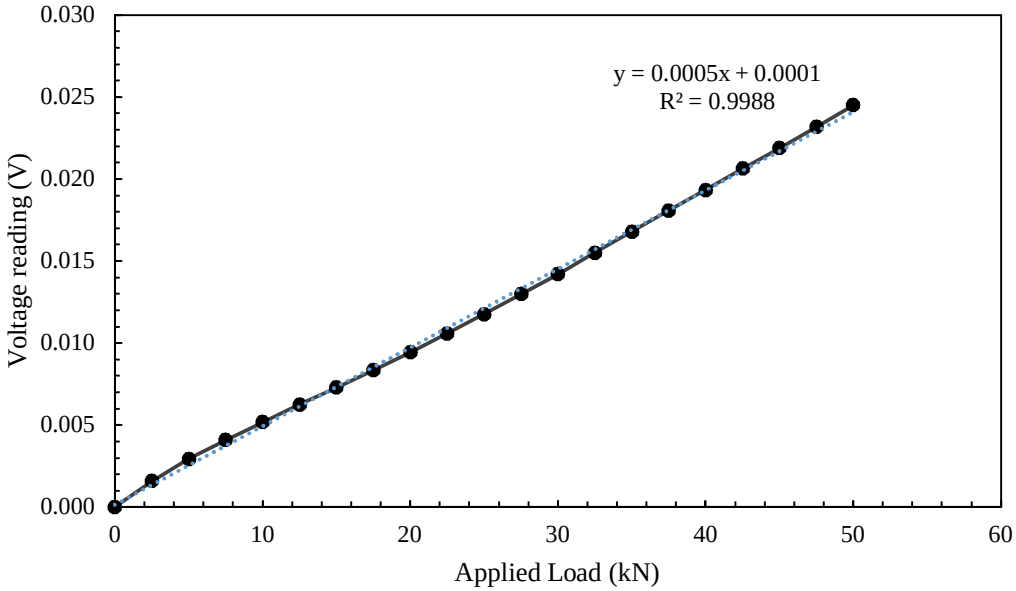

Figure A.2. Calibration of Load cell based on applied load and voltage reading

APPENDIX B

Acid soluble chloride titration method

Almost 5 gr of concrete sample was required for conducting this procedure. The concrete powder was collected by grinding off material in layers. The weight of the samples for each layer was measured. The acid soluble procedure was conducted by mixing 100 mm distilled water with the powder of concrete and adding 10 ml of 5 M nitric acid (HNO_3). The boiled mix was placed on a hotplate magnetic stirrer for 3-5 minutes (see Figure B.1). The solution should be cooled in room temperature.

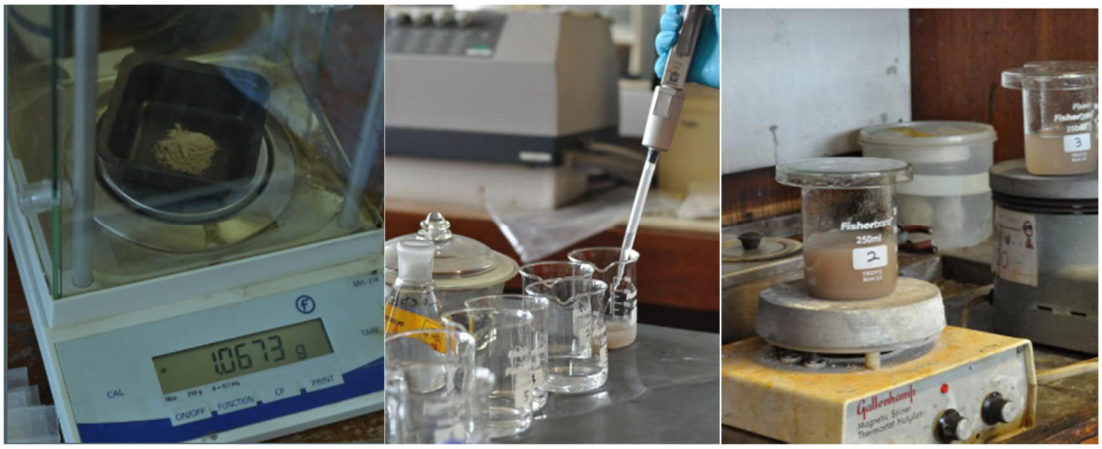

Figure B.1. Acid soluble process using 5 M HNO_3

Metrohm 719 DMS Titrino was used to conduct the titration process. The instrument can measure the absolute Cl^- content of the sample. This result should be divided by the volume of the sample to give the mg/l or ppm concentration for the chloride ions. During this process, $AgNO_3$ solution reacts with the sample and form AgCl. The potential of this solution was monitored during the process of adding $AgNO_3$. The titration finishes when all the Cl^- ions have been matched by Ag^+ ions.

The values of non-steady state diffusion coefficient (D_{nss}) and surface chloride content (C_s) can be calculated by curve fitting of the chloride profile to Equation B.1. This can be done based on principles of the least squares.

$$C(x,t) = C_s - (C_s - C_i)\text{erf}\left(\frac{x}{\sqrt{4\,D_{nssd}\,t}}\right)$$

Equation B.1. (NT BUILD 443, 1994)

D_{nss}: Apparent non-steady state diffusion coefficient, m^2/s

x: Average depth, m

t: Immersion duration, s

C(x,t): Chloride content at each depth , mass% of sample

C_s: Surface chloride content, mass% of sample

erf: Error function